The Role of the Runx2/CBFβ complex in Breast Cancer

A thesis submitted to the University of Manchester for the degree of

Doctor of Philosophy

In the Faculty of Life Sciences

2013

Rahna Ayub

Contents

Contents 2
List of Figures 6
List of Tables 8
Abstract 9
Declaration 10
Copyright Statement 10
Acknowledgements 11
List of Abbreviations 12
1.0 Introduction 15
1.1. Introduction 16
1.2. The mammary gland 17
1.2.1. Developmental stages of embryonic mammary glands 19
1.2.2. Developmental stages of adult mammary glands 22
1.2.3. Factors involved in embryonic mammary gland development 25
1.2.4. Factors involved in adult mammary gland development 26
1.3. Breast cancer 31
1.3.1. Bone Remodelling and Breast cancer 33
1.4. Runx family transcription factors 36
1.4.1. Runt/CBFβ Heterodimerisation 39
1.4.2. Runx1 (AML1/ CBFA2/ PEPBP2αB) 42
1.4.3. Runx3 (AML2/ CBFA3/ PEBP2αC) 42
1.5. Runx2 43
1.5.1. The role of Runx2 in skeletal development 43
1.5.2. The role of Runx2 in human disease 46
1.5.3. Post translational modification and regulation of Runx2 function 47
1.5.4. Repression of Runx2 activity 50
1.6. Runx2 and Normal Breast development 51
1.7. Runx2, Breast Cancer and Bone Metastasis 54
1.8. CBFβ 55
1.8.1. Role of CBFβ 58
1.8.2. CBFβ in disease 59
1.8.3. CBFβ in breast cancer and invasion 60

1.9. Project Aims 61
2.0 Materials and Methods 63
2.1. Antibodies and Reagents 64
2.2. Cell Lines 64
2.3. Stimulation of lactation from HC11 cells 65
2.4. Thawing cells 65
2.5. Freezing cells 66
2.6. Generation of a stable cell line 66
2.7. Whole cell extraction 67
2.8. Nuclear and Cytoplasmic extraction 67
2.9. Sodium dodecyl sulphate - polyacrylamide gel electrophoresis (SDS-PAGE) 68
2.10. Western Blot analysis 68
2.11. Immunocytochemistry of monolayer cells 69
2.12. Microscopy of fluorescence for cells grown in monolayer 70
2.13. 3D Cell Culture 70
2.14. Indirect Immunofluorescence staining of cells cultured in matrigel 71
2.15. Microscopy of cells grown in three dimension 71
2.16. Transient transfection of siRNA for protein knockdown 72
2.17. 2D RNA extraction 73
2.18. 3D RNA extraction 74
2.19. Real-time reverse transcription-PCR 75
2.20. Data analysis of RT-PCR using 2-ΔΔCT method 77
2.21. cRNA Microarrays 77
2.21.1. Preparation of RNA for microarray analysis 77
2.21.2. Affymetrix microarray procedure 78
2.21.3. Statistical analysis of microarray data 79
2.22. Electrophoretic Mobility Shift Assay (EMSA) 80
2.22.1. Generation of double stranded oligonucleotides 80
2.22.2. Radiolabeling oligonucleotides 81
2.22.3. Electrophoretic Mobility Shift Assay 81
3.0 Runx2 is expressed throughout acini formation in HC11 cells 83
3.1. Introduction 84

3.2. Expression and localisation of Runx2/CBFβ in normal mammary epithelial cells 85

3.3. 3D acini model using HC11 cells 90

3.4. The development of 3D acini in vitro 94

3.5. Immunofluorescence confirms localisation of Runx2 96

3.6. Nuclear Runx2 expression is present throughout acini development 99

3.7. Runx2 in hormonal induction of gene expression in mammary acini structures 101

3.8. The effect of lactogenic hormones on β-casein expression in Runx2 depleted HC11 cells. 104

3.9. Discussion 107

3.9.1. Runx2 and CBFβ are expressed in normal breast epithelial cells 107

3.9.2. HC11 cells form 3D acini structures when cultured in basement membrane matrix 108

3.9.3. Runx2 localisation is nuclear throughout acini development 109

3.9.4. siRNA treatment prevents production of milk protein β-casein in HC11 cells 111

4.0 Knockdown of CBFβ in MDA-MB-231 cells results in MET 114

4.1. Introduction 115

4.2. CBFβ knockdown in metastatic breast cancer cells results in an altered morphology 116

4.2.1. MDA-MB-231 cells knocked down for CBFβ show an altered morphology in 2D cell culture 116

4.2.2. CBFβ knockdown causes a more pronounced change in morphology when grown in 3DMatrigel cell culture system 120

4.2.3. shCBFβ MDA-MB-231 cells form solid and hollow clusters in 3D cell culture 122

4.2.4. CBFβ knockdown in MDA-MB-231 cells allows acini formation when grown in 3D 124

4.3. Re-expression of CBFβ prevents cluster and acini formation 127

4.3.1. Generation of a hormone inducible CBFβ-ER stable cell line using MDA-MB-231 cells knocked down for CBFβ 129

4.3.2. 4OH-Tamoxifen induces nuclear translocation of CBFβ 131

4.3.3. CBFβ-ER induction with 4OH rescues Runx2 target gene expression 133

4.3.4. Induction of CBFβ-ER prevents clustering and acini formation 136

4.4. Knockdown of CBFβ results in Mesenchyme to Epithelial Transition..... 142

4.5. Discussion 145

4.5.1. CBFβ knockdown in metastatic breast cancer cells causes formation of acini structures in 3D cell culture..... 145

4.5.2. Rescue of CBFβ causes a reversion to a stellate formation 147

4.5.3. CBFβ is involved in EMT 148

5.0 Identification of Runx2/CBFβ target involved in breast cancer remodelling of bone using cells grown in 3D..... 150

5.1. Introduction 151

5.2. Microarray analysis of MDA-MB-231 cells knocked down for CBFβ and grown in a 3D matrigel system 152

5.3. DAVID analysis of 3D and 2D microarray data 155

5.4. Common genes are affected by CBFβ knockdown in 2D and 3D MDA-MB-231 cells 158

5.5. Validation of microarray genes by RT-PCR 164

5.6. IL11 is a potential target gene of Runx2/CBFβ 168

5.6.1. Runx2 binds to the IL11 promoter 168

5.7. Discussion 178

5.7.1. Metastatic breast cancer cells express different genes when grown in matrigel.....178

5.7.2. Comparison of 2D and 3D MDA-MB-231 shCBFβ cells..... 179

5.7.3. Knock down of CBFβ in 2D and 3D cells yields common genes in microarray analysis 180

6.0 General discussion 182

6.1. Project aims 183

6.2. Developing a 3D matrigel cell culture system 186

6.3. Knockdown of CBFβ in metastatic breast cancer cells results in a mesenchymal-epithelial transition (MET) 188

6.4. Further work taking shCBFβ cells from the *in vitro* 3D system to *in vivo* 190

6.5. Disrupting CBFβ interaction with Runx2 as a possible therapeutic target 192

6.6. Potential roles of Runx1 and Runx3..... 193

References 195

Appendix 210

Number of words: 53820

List of Figures

Fig. 1.1.Structure of mammary glands. 18

Fig. 1.2. The developmental stages of embryonic mammary gland 21

Fig. 1.3. The developmental stages of the mammary gland..... 24

Fig. 1.4. Progression of mammary gland development is regulated by different transcription factors..... 30

Fig. 1.5. Breast cancer cells increase bone resorption 35

Fig. 1.6. Structure of the Runx family proteins..... 37

Fig. 1.7. Runx2/ CBFβ heterodimerisation 41

Fig. 1.8. Knockdown of Runx2 in mice prevents bone formation..... 43

Fig.1.9. Osteoblastigenesis is regulated by Runx2 but also involves other transcription factors..... 44

Fig. 1.10. Activators and repressors of Runx2..... 49

Fig. 1.11. Genomic structure of CBFβ isoforms and protein structure of CBFβ..... 57

Fig. 3.1. HC11 cells express both Runx2 and CBFβ protein. 87

Fig. 3.2. In HC11 cells, Runx2 is nuclear and CBFβ is localised in both the nucleus and cytoplasm..... 89

Fig. 3.3. Mouse mammary epithelial (HC11) cells form acini when grown in a 3D matrigel system. 93

Fig. 3.4. Stages of acini development in a 3D matrigel system 95

Fig. 3.5. Runx2 expression detected using Antibody ab54868 gave specific staining. 97

Fig. 3.6. Secondary antibody staining shows no specific staining..... 98

Fig. 3.7. Runx2 expression is nuclear throughout acini development. 100

Fig. 3.8. siRNA knockdown of Runx2 in mouse mammary epithelial (HC11) cells and establishing β casein mRNA detection at different time points. 103

Fig. 3.9. siRNA transfection disrupts β-casein stimulation by prolactin and dexamethasone. 106

Fig. 4.1. Verification of CBFβ knockdown in breast cancer cells and comparison of growth in 2D. 119

Fig. 4.2. Knockdown of CBFβ in metastatic breast cancer cells causes a change in morphology in 3D culture. 121

Fig. 4.3. Breast cancer cells with reduced CBFβ form clusters and hollow lumen structures when grown in 3D. 123

Fig. 4.4. Breast cancer cells depleted of CBFβ form acini structures. 126

Fig. 4.5. Using a 4OH tamoxifen inducible system to activate CBFβ translocation. 128

Fig. 4.6. Generation of a stable cell line with mouse CBFβ-ER expression. 130

Fig. 4.7. Validation of Flag-CBFβ-ER plasmid expression and induction using 4OH-Tamoxifen. 132

Fig. 4.8. CBFβ-ER is functionally active following 4OH-Tamoxifen induction. ... 135

Fig. 4.9. Re-expression of CBFβ causes reversion to the invasive phenotype in 3D. 137

Fig. 4.10. Induction of CBFβ-ER in the shCBFβ cells significantly changes the morphology of structures when grown in 3D 140

Fig. 4.11. Induction of CBFβ-ER in shCBFβ knockdown cells rescues the invasive phenotype seen in 3D culture following 14 days growth. 141

Fig. 4.12. MET markers following CBFβ knockdown in breast cancer cells in 3D RNA extraction. 144

Fig.5. 1. Microarray analysis of MDA-MB-231 cells knocked down for CBFβ and grown in 3D. 154

Fig. 5.2. DAVID analysis identifies genes involved in bone development and cell movement 156

Fig. 5.3. DAVID analysis of 2D microarray identifies genes involved in cell migration. 157

Fig. 5.4. Heat map showing the expression profile of MDA-MB-231 cells knocked down for CBFβ and compared in a 2D and a 3D environment. 159

Fig. 5.5. MDA MB 231 cells knocked down for CBFβ have common genes when grown in a 2D and a 3D environment. 161

Fig. 5.6. Validation of some common genes found between the 2D and 3D microarrays following CBFβ knockdown in metastatic breast cancer cells. 166

Fig. 5.7. IL11 promoter sequence highlighting possible Runx sites. DNA 169

Fig. 5.8. Runx2 binds to IL11 promoter site 1 in UMR106 cells. 172

Fig. 5.9. Runx2 binds to IL11 promoter site 2. 174

Fig. 5.10. Runx2 binds to IL11 promoter site 3. 177

List of Tables

Table 1.1. The pathological stages of Breast Cancer 32

Table 2.1. Primers designed for RT-PCR 76

Table 2.2. Oligonucleotides used for EMSA probes..... 80

Table 5.1. List of the common genes between 2D and 3D shCBFβ MDA MB 231 cells. 163

Table 5.2. Correlation of microarray and RT-PCR experiments for validation of CBFβ genes in 2D and 3D growth 167

Table 6.1. Comparison of different 3D cell culture methods available 187

Abstract

The University of Manchester Rahna Ayub
PhD in Molecular Cancer Studies September 2013
Thesis Title: The Role of the Runx2/CBFβ complex in Breast Cancer

Breast cancers frequently metastasise to the skeleton where they cause osteolytic bone destruction. Effective treatment of bone metastasis remains a considerable clinical challenge. In the UK around 70% of the 12,000 patients that die from breast cancer annually have bone metastasis. Whilst existing therapies provide some pain relief, by limiting the tumour-mediated bone degradation, bone metastases are presently incurable. There is therefore an urgent need to develop therapies to prevent bone metastatic breast cancer. The transcription factor complex Runx2/CBFβ is a key regulator of bone development and is aberrantly expressed in breast cancer, leading to up-regulation of bone metastasis-associated genes. Previous work has demonstrated that Runx2/CBFβ determines the invasive phenotype of metastatic breast cancer cells and is required for the expression of metastatic genes. The Runx2/CBFβ complex also has a role in normal breast gene expression, activating expression of the milk protein β-casein in response to hormones. However, little is known about the normal role of Runx2/CBFβ in breast cells.

The overarching aim of this project was to determine the role of Runx2/CBFβ in metastasis and identify the target genes that determine the metastatic phenotype. In order to understand the role of Runx2/CBFβ in breast cancer, initial experiments were performed to determine the role of Runx2/CBFβ in normal breast cells. A 3D culture system was established to examine the role of Runx2/CBFβ in regulating gene expression in non-cancerous differentiated epithelial breast cells. Attempts were also made to determine the Runx2/CBFβ target genes after lactogenic hormone stimulation. Unfortunately siRNA knockdown of Runx2 was incompatible with hormonal stimulation. However, 3D cell culture of normal mammary gland cell line HC11 showed Runx2 was expressed throughout the development of mammary acini structures. In addition the expression of CBFβ was confirmed in these cells.

Having established the 3D culture system, experiments were subsequently performed to examine the role of CBFβ in the metastatic breast cancer cell line MDA-MB-231. These experiments demonstrated that depletion of CBFβ has a remarkable effect on the phenotype of the cells, leading to the development of mammary acini structures normally formed by non-cancerous breast cancer cell lines. Thus, depletion of CBFβ results in a reversion to an epithelial phenotype, suggesting that CBFβ is required to maintain the epithelial to mesenchymal transition (EMT). RT-PCR analysis also revealed changes in the expression of EMT marker genes. We also demonstrated that the EMT reversion could be rescued by re-expressing an inducible form of CBFβ. These data suggest that CBFβ is required to maintain the mesenchymal phenotype of metastatic breast cancer cells.

Finally, a microarray analysis of MDA-MB-231 cells was performed to identify Runx2/CBFβ target genes that might contribute to the mesenchymal phenotype. Cells depleted of CBFβ and grown in 3D revealed reduced expression of IL11. This is known to be involved in bone remodelling. Inspection of the IL11 promoter revealed potential DNA binding sites which confirmed binding to Runx2 using EMSA.

Declaration

No portion of the work referred to in the thesis has been submitted in support of an application for another degree or qualification of this or any other university or other institute of learning;

Copyright Statement

i. The author of this thesis (including any appendices and/or schedules to this thesis) owns certain copyright or related rights in it (the "Copyright") and s/he has given The University of Manchester certain rights to use such Copyright, including for administrative purposes.

ii. Copies of this thesis, either in full or in extracts and whether in hard or electronic copy, may be made **only** in accordance with the Copyright, Designs and Patents Act 1988 (as amended) and regulations issued under it or, where appropriate, in accordance with licensing agreements which the University has from time to time. This page must form part of any such copies made.

iii. The ownership of certain Copyright, patents, designs, trade marks and other intellectual property (the "Intellectual Property") and any reproductions of copyright works in the thesis, for example graphs and tables ("Reproductions"), which may be described in this thesis, may not be owned by the author and may be owned by third parties. Such Intellectual Property and Reproductions cannot and must not be made available for use without the prior written permission of the owner(s) of the relevant Intellectual Property and/or Reproductions.

iv. Further information on the conditions under which disclosure, publication and commercialisation of this thesis, the Copyright and any Intellectual Property and/or Reproductions described in it may take place is available in the University IP Policy (see http://www.campus.manchester.ac.uk/medialibrary/policies/intellectual-property.pdf), in any relevant Thesis restriction declarations deposited in the University Library, The University Library's regulations (see http://www.manchester.ac.uk/library/aboutus/regulations) and in The University's policy on presentation of Theses

Acknowledgements

Firstly I would like to express my gratitude to my supervisor Dr. Paul Shore, for his support and guidance throughout the PhD. I am particularly grateful for the many discussions, the encouragement, the responsibility and the freedom to follow my own path in my research. In addition, I would like to thank my advisor, Dr. Cathy Tournier, for her advice and insights into my work during our meetings. I am also grateful to BBSRC and the University of Manchester fund for their financial support during my studies.

To my colleagues and friends, a very special thank you for all the support and guidance. In particular, to Elisa Aguilar Martinez, Karen Susan Palmer, Cesar Lopez Camacho, Daniel Mendoza-Villanueva, Ling-I Su, Daniel Wratting, Tom Wood and Yanin Na. You all made this experience very enjoyable and I wouldn't be the person I am today without you.

To my amazing family, I can't express enough how much I have appreciated your support, love and encouragement. To my Dad who taught me from a young age that anything can be achieved if you try hard enough and who has been my strength. To my Mum, who has been my role model. To my three sisters who have been my will power and who always know how to make me smile. Thank you all.

List of Abbreviations

2D	Two Dimensional
3D	Three Dimensional
AML	Acute Myeloid Leukemia
BP	Base Pairs
BMP	Bone Morphogenetic Proteins
BSA	Bovine serum, Albumin
BSP	Bone Sialoprotein
CBFβ	Core Binding Factor β
CCD	Cleidocranial Dysplasia
cDNA	Complementary DNA
DAPI	4', 6-diamidino-2-phenylindole
dATP	Deoxyadenosine-5’-triphophate
DAVID	Database for Annotation, Visualisation and Integrated Discovery
DNA	Deoxyribonucleic acid
DBD	DNA Binding Domain
DMEM	Dulbecco’s Modified Eagle’s Medium
DMSO	Dimethyl Sulfoxide
DNA	Deoxyribonucleic Acid
dNTP	Deoxynucleotide-5’-triphosphate
DTT	Dithiothreitol
E	Embryonic Day
EDTA	Ethylene Diamine Tetra-acetic Acid
EGF	Epidermal Growth Factor
EGTA	Ethylene glycol tetra-acetic acid
EMSA	Electrophoretic Mobility Shift Assay
FBS	Fetal Bovine Serum

FGF	Fibroblast Growth Factor
GAPDH	Glyceraldehyde 3-phosphate dehydrogenase
GFP	Green Flourescent Protein
HAT	Histone acetyl transferase
HDAC	Histone deacetylase
HEPES	N-2-Hydroxyethylpiperazine-N'-ethanesulfonic acid
HI	Heat inactivated
Hr	Hour
IF	Immunofluorescence
IGF	Insulin-like Growth Factor
kDa	KiloDalton
MAPK	Mitogen- Activated Protein Kinase
Mins	Minutes
mM	milli Molar
MMP	Matrix metalloproteinase
mRNA	messenger Ribonucleic acid
NLS	Nuclear Localisation Signal
NMTS	Nuclear Matrix Targeting Signal
NP-40	Nonidet P-40
NS	Non-Specific
OC	Osteocalcin
OPN	Osteopontin
PAGE	Polyacrylamide gel electrophoresis
PBS	Phosphate Buffered Saline
PCR	Polymerase Chain Reaction
PFA	Paraformaldehyde
PI3K	Phosphoinositide
PMSF	Phenylmethanesulphonyl fluoride
Prlr	Prolactin Receptor

PS	Penicillin/Streptomycin
PTH	Parathyroid Hormone
PTHrP	Parathyroid hormone related peptide
QA	Glutamine/Alanine
RANK	Receptor Activator of NFκB
RANKL	RANK Ligand
RD	Runt Domain
RNA	Ribonucleic acid
RPM	Revolutions per minute
RPMI	Roswell Park Memorial Institute
RT-PCR	Reverse Transcriptase- Polymerase Chain Reaction
Runx	Runt-related
SD	Standard Deviation
SDS	Sodium dodecyl sulphate
shRNA	short hairpin RNA
siRNA	small interfering RNA
TEMED	N,N,N',N'-tetramethylaethyl-enediamine
TBS	Tris Buffered Saline
TBST	Tris Buffered Saline-Tween
TBE	Tris Borate EDTA
TE	Tris EDTA
TEB	Terminal End Bud
TGFβ	Transforming growth factor β
WT	Wild Type

1.0 Introduction

1.1. Introduction

In the UK 12,000 patients that die from breast cancer annually have bone metastasis. How breast cancer spreads so readily to the skeleton is not fully understood, and there are currently no treatments that specifically prevent breast cancers from spreading to bone. There is therefore an urgent need to identify the key molecules involved in breast cancer bone metastasis in order to develop successful therapies for these patients.

It is well established that breast cancer cells preferentially invade and grow as secondary tumours in bone where they induce local bone degradation (Akhtari et al., 2008; Chen et al., 2010; Patel et al., 2011; Zhang et al., 2010). *In vitro*, breast cancer cells inhibit osteoblast differentiation while concurrently enhancing osteoclast differentiation (Barnes et al., 2004). Thus, metastatic breast cancer cells direct the activity of bone cells. However, the molecular mechanisms that determine the ability of breast cancer cells to form bone metastases are poorly understood.

The transcription factor Runx2 is a key regulator of bone development and is aberrantly expressed in breast cancer cells, leading to up-regulation of bone metastasis-associated genes (Karsenty, 2008; Lau et al., 2006; Pratap et al., 2005). Runx2 forms a regulatory complex with its co-activator, CBFβ. Previous work from our laboratory has demonstrated that Runx2/CBFβ regulates genes associated with metastasis in breast cancer and that both components of the complex are required for metastatic breast cancer cells to migrate (Mendoza-Villanueva et al., 2010; Mendoza-Villanueva et al., 2011). The overall aim of this project was to establish how Runx2/CBFβ determines the ability of metastatic breast cancer cells to migrate.

1.2. The mammary gland

The function of the mammary gland is to produce milk to feed offspring. Humans have two complex mammary glands; one in each breast. Each mammary gland is made up of many alveoli, which are hollow cavities (Fig. 1.1). These alveoli are lined with mammary epithelial cells which are able to secrete milk proteins. Outside these are myoepithelial cells which contain α-smooth muscle actin and so are able to contract. Upon suckling of the breast nipple, the hormone oxytocin is released from the pituitary gland and acts on the myoepithelial cells causing them to contract. This squeezes the milk into the alveoli. The alveoli are joined in groups to form lobules, each of which has a lactiferous duct that drains the milk out of the nipple (Fig. 1.1) (Weigelt and Bissell, 2008). The developmental stages in the mammary gland are conserved between mammals. Therefore, much of the research conducted on the mammary gland has been conducted in mice. For this reason, the next sections will detail both human and mice mammary glands.

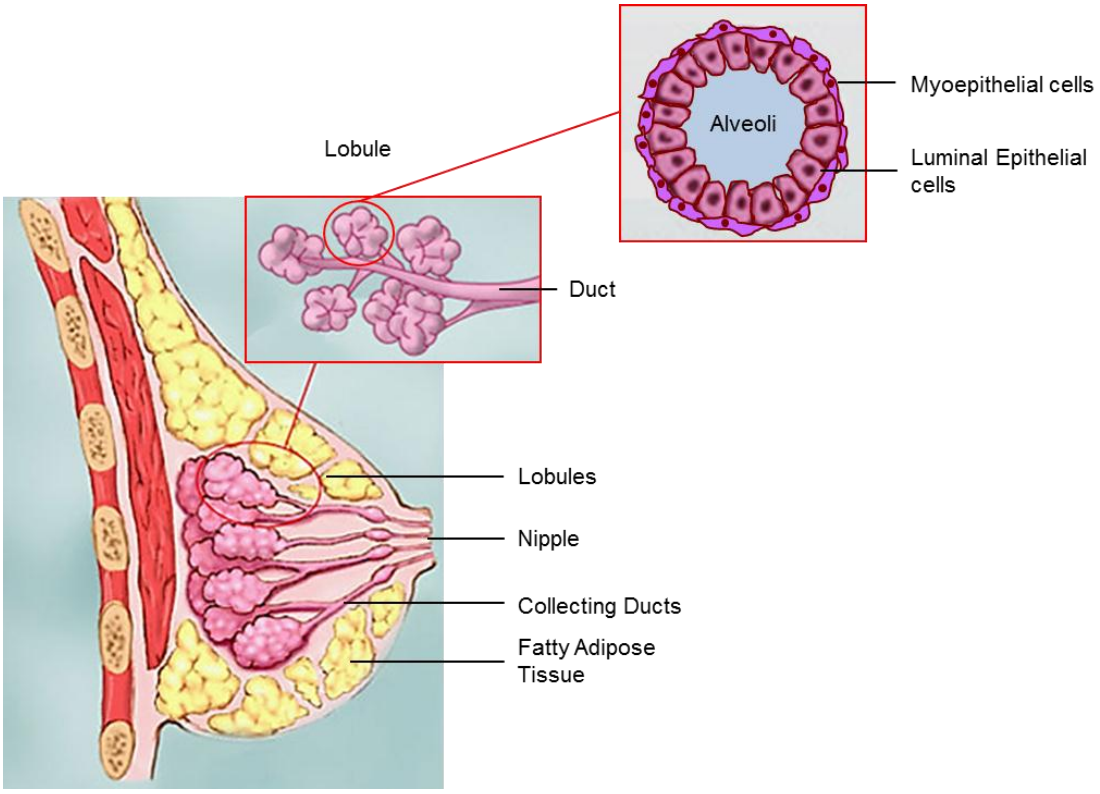

Fig. 1.1.Structure of mammary glands. The mammary gland is made up of many alveoli which are lined with milk secreting epithelial cells. These alveoli join to form lobules. The milk is squeezed out of the mammary epithelial cells by the myoepithelial cells and expelled out through the lactiferous duct which leads to the nipple. (Adapted from www.breastcancer.org).

1.2.1. Developmental stages of embryonic mammary glands

While humans have two complex mammary glands, mice have ten simple mammary glands called fat pads. These are located just below the skin in pairs along two mammary lines. Three of these pairs are thoracic and two pairs are inguinal. At the end of each fat pad is a nipple which is connected to the primary epithelial duct in order for lactation to occur (Russo and Russo, 1996). There are three main stages of mammary development; embryonic, pubertal and adult. These initial stages of embryonic mammary development will be described briefly.

The mouse mammary glands begin to develop before birth from embryonic day (E) 10.5 with the formation of milk lines, which are a single line of mammary cells (Fig. 1.2A). These epidermal cells become columnar and multi-layered. At E11.5 these cells migrate to form the 5 pairs of lens shaped placodes which are numbered 1 to 5 from the thoracic to inguinal regions respectively (Fig. 1.2B) (Veltmaat et al., 2004). Between E12.5 and E14, the cells of the placodes invaginate into the mesenchyme below. This forms a mammary bud. By E15.5 proliferation of the mammary epithelial cells leads to ductal branching. A cord of cells develops from the initial placode to a secondary fat pad structure. From this time there is branching and slow growth which results in formation of a ductal lumen and a nipple structure. By birth a nipple sheath forms and the 5 pairs of mammary placodes become mammary fat pads. Another growth spurt does not commence again until puberty (Fig. 1.2C) (Cowin and Wysolmerski, 2010; Watson and Khaled, 2008).

After birth, when the mouse is approximately 3 weeks old, the ovaries begin to secrete hormones. The hormones secreted induce the formation of terminal end buds (TEBs) at the ends of the duct structures. These are club-shaped structures that form

at the tips of the growing ducts. A cap of cells at the leading edge of the TEBs drives proliferation of the growing ducts into the underlying fat pads. This growth is regulated by the surrounding stroma. The TEB cap cells differentiate into myoepithelial cells and will form the outer bilayer of cells which surround an inner luminal cell layer. The tubular cells of the ducts form the luminal cells. These will produce the alveoli structures of the mammary gland. Secondary ducts grow laterally from the primary ducts branching like the roots of a tree (Macias and Hinck, 2012).

From this time, up until the mouse is between 10-12 weeks, there is growth and branching of the ducts. At the end of puberty, the branching ducts will occupy 60% of the fatty stroma (Cowin and Wysolmerski, 2010). With each menstrual cycle, tertiary branching occurs, but further differentiation does not occur until pregnancy. This stage is termed the virgin state of mammary gland development. Once the mammary glands have reached this stage, there are four main stages of adult mammary development; virgin, pregnancy, lactation and involution (Hassiotou and Geddes, 2013; Hennighausen and Robinson, 2005; Richert et al., 2000).

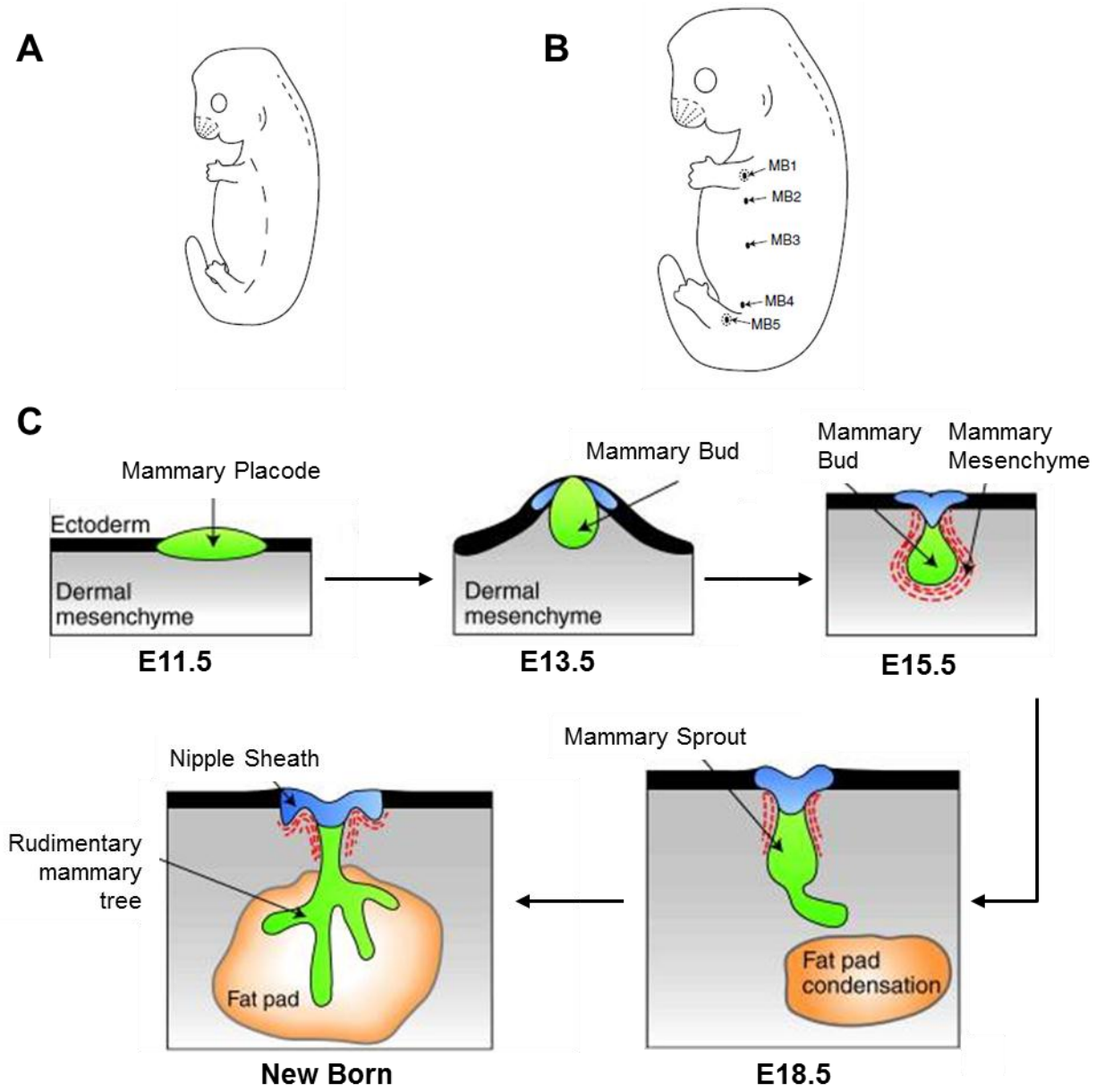

Fig. 1.2. The developmental stages of embryonic mammary gland. (A) The development of the embryonic mammary glands begins with the milk line. (B) 5 pairs of placodes form along the milk line. (C) Diagram showing the development of the mammary placodes to mammary buds modified from (Cowin and Wysolmerski, 2010; Watson and Khaled, 2008).

1.2.2. Developmental stages of adult mammary glands

The virgin state begins when the mice reach puberty and the mammary glands begin to lengthen and form branches and alveolar buds. This proliferation is a result of hormones secreted during puberty. While there is further branching with each menstrual cycle due to the release of hormones, this growth is relatively minimal compared to the pubertal stage. A further growth spurt only occurs when the next stage of mammary gland development is triggered, pregnancy (Hassiotou and Geddes, 2013).

During the pregnancy stage, the mammary glands undergo complete remodelling maturing into a functional milk-secreting organ. This maturation is directly regulated by hormones and growth factors. The initial phase of pregnancy involves cellular proliferation. This induces the formation of new ducts as well as elongation of existing ducts through mitotic activity at the TEBs. Spherical structures called alveoli are then formed at the TEBs. These have an inner epithelial layer that encapsulates a lumen and an outer layer made of myoepithelial cells. The myoepithelial cells differentiate to have smooth-muscle properties. In the second and third trimesters of pregnancy, prolactin levels gradually increase causing the alveolar cells to differentiate to allow for milk secretion (Watson and Khaled, 2008).

After parturition the third stage of mammary gland development, lactation, begins. At this stage the inner epithelial cells of the alveoli produce milk proteins. The milk is secreted into the alveoli lumen by contraction of the outer smooth muscle layer in response to suckling of the nipple. The milk is then expelled through the nipple to feed the offspring (Hughes and Watson, 2012).

The final stage of the cycle is when the new born is weaned from the milk. This step induces involution which consists of apoptosis of mammary epithelia cells. Involution is only reversible during the first two days of weaning. However, if the mammary gland is not re-stimulated within this time then the mammary glands can no longer lactate and reverts back to the state of a virgin mammary gland within approximately two weeks (Watson and Khaled, 2008).

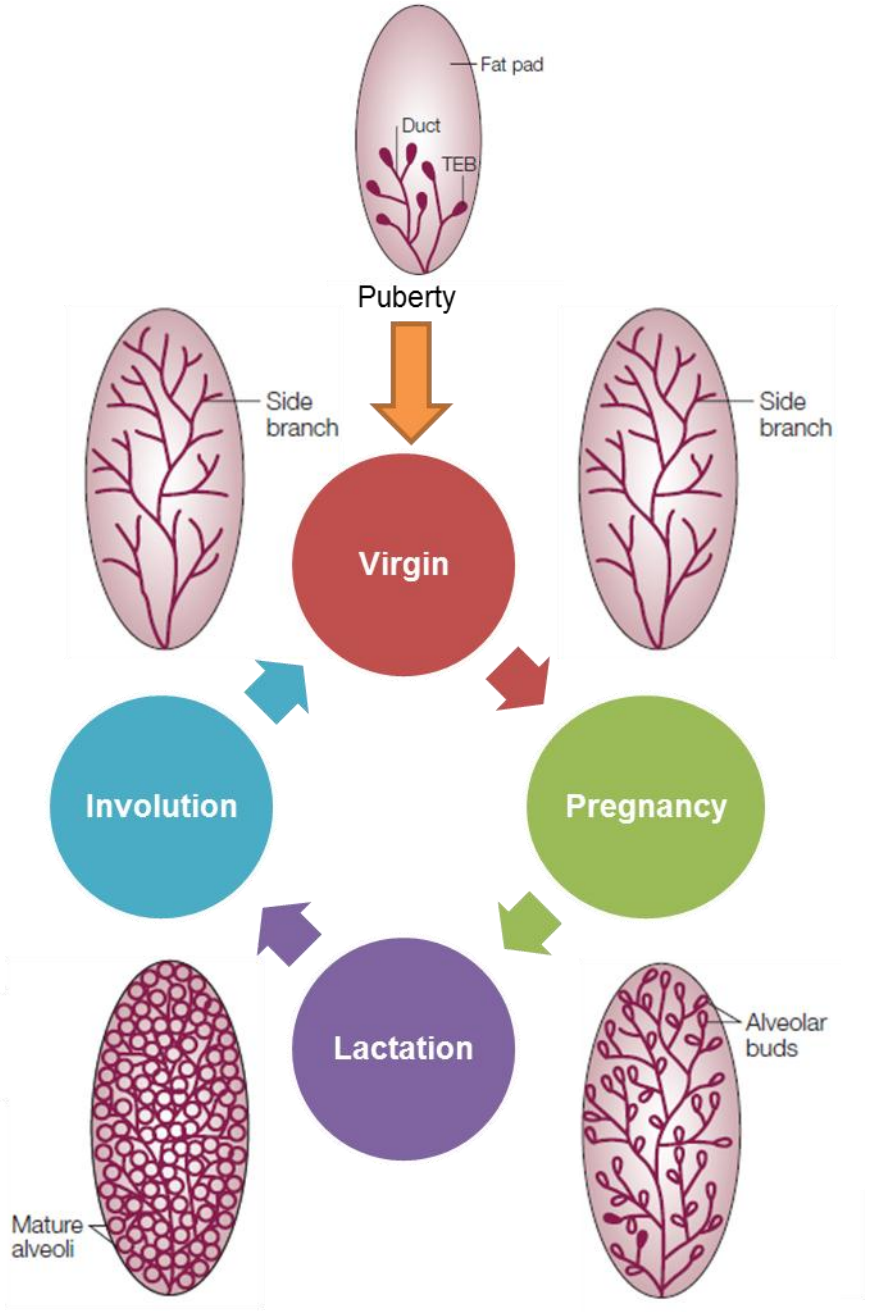

Fig. 1.3. The developmental stages of the mammary gland. The development of the mammary glands begins with the growth of terminal end buds (TEBs). The four main states of the adult mammary gland are the virgin stage, pregnancy, lactation and involution. With pregnancy there is extensive differentiation and proliferation (modified from Hennighausen and Robinson, 2005).

1.2.3. Factors involved in embryonic mammary gland development

Considering the mammary gland has many stages of development with multiple cell types differentiating, it can be expected that mammary gland development involves regulation by different transcription factors and requires different cofactors (Cowin and Wysolmerski, 2010). At the embryonic stage of mammary development, wingless-related MMTV (murine mammary tumour virus) integration site (Wnt) signalling is essential for the formation of the mammary milk lines. If this pathway is inhibited by Dickkopf1 (DKK1), formation of the mammary buds is abolished (Veltmaat et al., 2004).Wnt10b expression in the milk line suggests the canonical Wnt/β-catenin signalling pathway is activated (Chu et al., 2004; Macias and Hinck, 2012). Wnt ligands bind to the cell surface receptor frizzled (FZD) and its coreceptor LDL receptor related protein 5/6 (LRP5/6). This leads to activation of dishevelled protein (DSH) which in turn inhibits the complex glycogen synthase kinase 3β (GSK3β), Axin and adenomatous polyposis coli (APC). When active, GSK3β phosphorylates β-catenin which targets β-catenin for degradation by proteasomes. However, inhibition of GSK3β by the Wnt signalling pathway prevents this phosphorylation and as a result β-catenin is not degraded. β-catenin accumulates in the cytoplasm and then translocates into the nucleus. Here it binds and activates a T-cell factor (TCF)/lymphoid enhancer binding factor 1 (LEF1) transcription family member (Jamieson et al., 2012). This transcription factor then binds to the promoter of its target genes and results in cell proliferation and differentiation (Cowin and Wysolmerski, 2010; Gehrke et al., 2009). This wnt signalling pathway is important throughout the mammary gland development.

At the placode stage of mammary bud development wnt signalling is still an important factor. The transcription factor T-box 3 (Tbx3) expression regulates wnt signalling and is itself controlled by fibroblast growth factors (FGFs) that are released from somites under the mesenchyme of the milk line (Macias and Hinck, 2012). The bone morphogenetic protein 4 (BMP4) is also expressed at this stage and may control Tbx3 expression (Cho et al., 2006).

Development of the mammary bud and rudimentary ducts require signalling by the parathyroid hormone related protein (PTHrP). This is produced by the mammary epithelium itself and acts through the G-coupled protein receptor, PTH receptor (PTH1R). Knockout studies of PTHrP showed that mammary placodes developed but no branching occurred and nipple sheaths were not formed. Therefore PTHrP is required for ductal branching (Foley et al., 2001; Wysolmerski et al., 1995). Taken together, these factors regulate the development of mammary buds, resulting in the formation of a nipple sheath and a rudimentary ductal system.

1.2.4. Factors involved in adult mammary gland development

At birth, while the mammary glands are rudimentary, they are competent to produce milk given the correct hormonal signals (Macias and Hinck, 2012). This highlights the importance of the various hormonal signals received at each point in mammary gland development. Therefore, some of the major factors involved will be described.

The neonatal to pubertal period of mammary gland development is a slow process, with little proliferation occurring. However, the hormonal signals received during puberty induce immense cell proliferation and ductal branching. Growth hormone

(GH) released from the pituitary gland binds to GH receptors (GHR) (Howard et al., 1996). This induces the production of Insulin-like growth factor 1 (Igf1) both locally in the mammary stromal fibroblasts and from the liver. Igf1 induces mammary epithelial cells to proliferate, resulting in ductal growth (Brisken and O'Malley, 2010). Another hormone, estrogen, is produced by the ovaries and is a membrane soluble ligand which binds to the estrogen receptor (ERα). This induces cell growth and maintenance of the alveolar cells. This is supported by mice models lacking the Estrogen Receptor-α (ERα) which do not have ductal outgrowth in later stages and are also infertile (Korach et al., 1996). Amphiregulin (AREG), a member of the epidermal growth factor (EGF) family, is released in response to ERα and generates the production of further growth factors (McCave et al., 2010). This surge of multiple growth factors results in mammary cells proliferating and differentiating until the adult stage of mammary gland development is reached. During puberty, estrogen levels rise first and progesterone becomes a major factor in later development. This is because estrogen induces expression of progesterone receptors (PR) preparing the cells for the progesterone response in later stages (Brisken and O'Malley, 2010).

At the virgin stage of mammary development, the transcription factor CCAAT/enhancer binding protein β (CEBPβ) regulates alveolar lumen development and ERα regulates branching of the ducts (Feng et al., 2007; Watson and Khaled, 2008). This stage of development is about maintenance of the alveoli and ductal system, with only small growth cycles in keeping with the menstrual cycle (Macias and Hinck, 2012).

During pregnancy, the mammary gland once again undergoes extensive proliferation and differentiation. This is triggered by hormones such as prolactin which is secreted

by the pituitary gland and stimulates the ovaries to secrete progesterone. Progesterone binds to the progesterone receptor (PR) which dimerises and moves into the nucleus initiating the transcription of Wnt and receptor activator of nuclear factor (NF)-κB ligand (RANKL) (Oakes et al., 2006). Wnt4, 5b and 6 are all downstream targets of PR and follow the canonical wnt signalling pathway, as described earlier, to initiate target genes which stimulate side branching and alveolar development (Incassati et al., 2010). RANKL binds to its receptor, RANK, which results in NFκB activation. This then moves into the nucleus and activates transcription of cyclin D1 which increases proliferation (Oakes et al., 2006). Prolactin also binds to its own receptor, prolactin receptor (Prlr) (Fig. 1.4). This binding is particularly important in the lactation stage of the mammary gland development.

After parturition the lactation stage begins which involves the expression and secretion of milk proteins. Prolactin binds to its receptor Prlr, which then dimerises and leads to phosphorylation of the associated Janus kinase (Jak2). This causes phosphorylation of specific residues on the Prlr recruiting Stat5. Jak2 phosphorylates Stat5 which subsequently forms a homodimer. This Stat5 homodimer translocates to the nucleus where it can bind to the promoter region of genes and activates transcription. Downstream targets of this pathway include α-casein, β-casein and whey acidic protein (WAP) (Fig. 1.4.). These are milk proteins that are secreted by the mammary epithelial cells (Hughes and Watson, 2012).

The final stage, of the mammary gland development is involution. This stage has a down-regulation of Stat5 and an up-regulation of Stat3 which remains up-regulated for the first 10 days of involution (Hughes and Watson, 2012). Involution is initiated from a prolonged period of not expelling milk from the breast. This causes build-up

of milk proteins in the mammary gland and activation of Leukemia inhibitory factor (LIF). LIF binds to the receptor complex LIF receptor (LIFR) and GP130 (Kritikou et al., 2003). This binding recruits Jak and subsequently Stat3 as described in the previous Jak/Stat pathway. Stat3 dimerises and translocates to the nucleus where it initiates transcription of Stat3, CEBPδ and IGFBP5. These result in apoptosis and so the mammary gland begins to regress back towards its pre-pregnancy state (Hughes and Watson, 2012; Watson and Khaled, 2008). This activity of different transcription factors through different stages is an important factor to consider as Runx2 expression may change throughout the different stages of development.

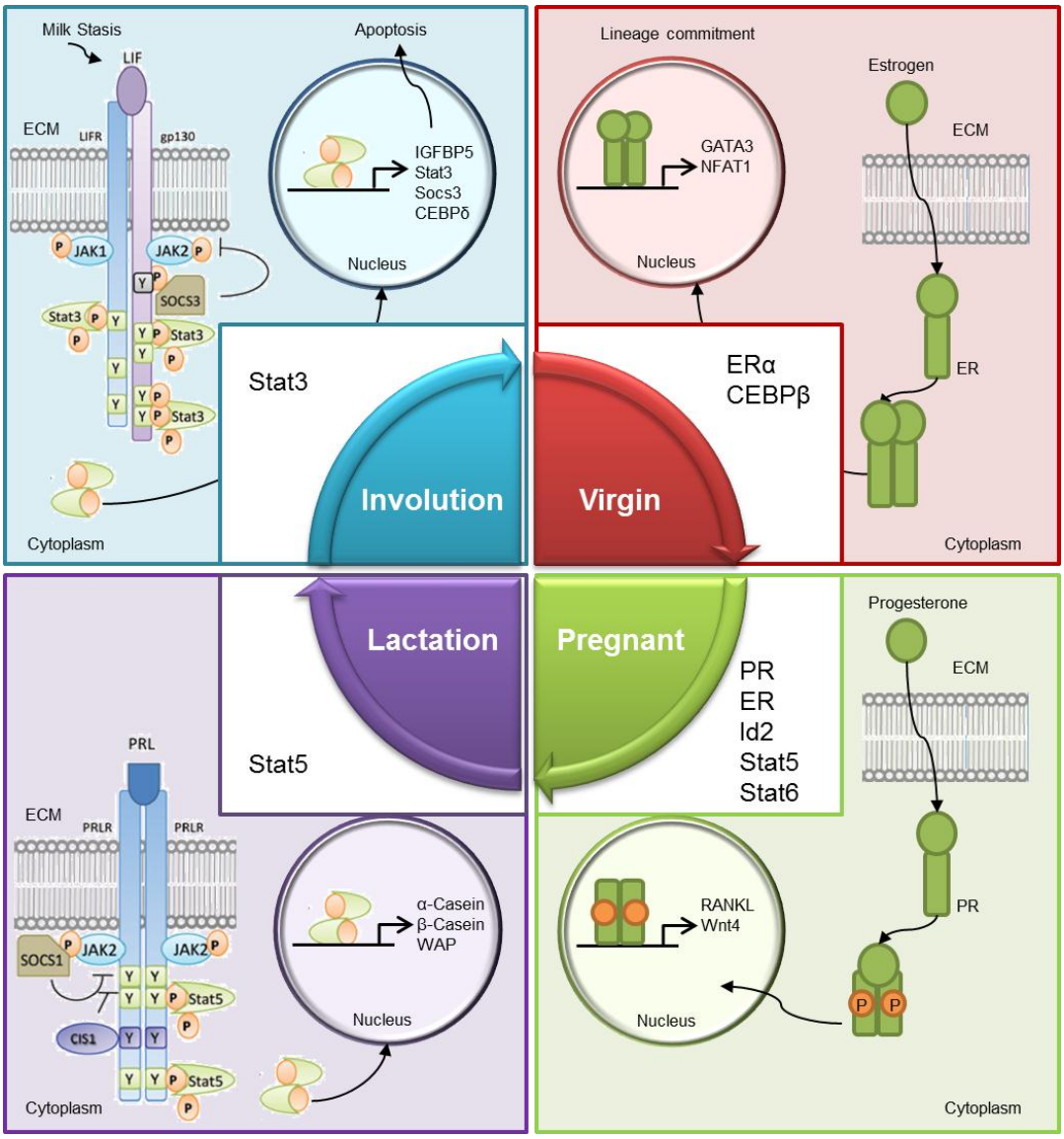

Fig. 1.4. Progression of mammary gland development is regulated by different transcription factors. The different stages of mammary development involve different transcription factors. The four main stages of adult mammary gland development are shown. For simplicity only one known pathway for each stage is shown schematically (Adapted from Hughes and Watson, 2012).

1.3. Breast cancer

Breast cancer occurs when the growth of cells in the mammary gland becomes disrupted leading to tumour formation. There are various types of breast cancer. Ductal Carcinoma In Situ (DCIS), is abnormal growth of the cells lining the ducts. Lobular Carcinoma In Situ (LCIS) is abnormal cells in lobules of the breast. This type is not usually invasive. Paget disease is abnormality of the nipple only. In early stages of tumour development the tumours can be treated in various ways including surgery. Consequently patients have a chance to go into remission and have an increased survival rate. In contrast, patients who are in the advanced stages of breast cancer cannot be cured. The clinical stages of breast cancer depends on the size of the tumour, whether the cancer cells have spread from the breast into lymph nodes and whether they have metastasised to other areas of the body (Lakhani et al., 2006). These stages are shown in table 1.

In advanced cancers the breast cancer cells are able to metastasise out of the breast and migrate to different parts of the body. For this to occur, the breast cancer cells must adapt invasive capabilities and enter the blood vessels or the lymphatic system to travel around the body. The cancer cells must then exit the vessels and enter new organs. Breast cancer cells can migrate to many different organs, such as the lungs, liver, brain and bone. The metastasis of breast cancers to bone was first shown by Stephen Paget in 1889 (Paget, 1989). Since then, there have been many more studies that show the metastasis of breast cancer to bone occurs in an estimated 85% of cases (Coleman, 2001; Lipton et al., 2009; Yin et al., 2005). Paget proposed a ‘seed and soil’ hypothesis to explain this. The cancer cells (seeds) can only grow in a nutritious environment (soil) to thrive and grow (Paget, 1889). This suggests that metastasis of

cancers to bone is a regulated event rather than a random event. Therefore it is likely that the bone microenvironment is conducive to the growth of breast cancer cells which have metastasised.

Stage	Description
0	• Formation of abnormal cells in the breast • Ductal, lobular Carcinoma in Situ or Pagets disease
IA	• Tumour is 2 cm or smaller • Cancer remains in breast
IB	• Small clusters of breast cancer cells have moved to lymph nodes (between 0.2 mm and 2 mm) and EITHER • No tumour is found within the breast OR • The tumour is 2 cm or smaller
IIA	• No tumour is found in the breast or tumour is 2 cm or less. Cancer is found in lymph nodes OR • Tumour is between 2 cm and 5 cm and has not moved lymph nodes
IIB	• Tumour is between 2 - 5 cm and has spread to 1-3 lymph nodes OR • Tumour is over 5 cm and has not moved lymph nodes
IIIA	• No tumour is found in the breast OR tumour may be of any size and found in 4-9 lymph nodes • Tumour is over 5 cm and small clusters of breast cancer cells (0.2 mm – 2 mm) are found in lymph nodes
IIIB	• Tumour may be any size AND the cancer has spread to the chest wall AND/OR to the skin of the breast which causes swelling or an ulcer (Inflammatory breast cancer) • The tumour has spread to lymph nodes
IIIC	• No tumour found in the breast OR any size tumour in breast and has spread to skin causing swelling or ulceration AND/OR spread to chest wall AND • Tumour spread to 10 or more lymph nodes
IV	• Breast cancer has spread to other organs of the body e.g. Brain, lungs, liver, kidney and bone

Table 1.1. The pathological stages of Breast Cancer. A table showing the various clinical stages of breast cancer progression. (Adapted from National Cancer Institute, 2012).

1.3.1. Bone Remodelling and Breast cancer

In the late stage of breast cancer, the cancer metastasises out of the breast and can colonise other areas of the body. Once this occurs, the cancers become incurable. This metastasis could be to brain, liver or lungs but in 85% of cases, this metastasis occurs to bone. For this reason, the bone microenvironment and how breast cancers affect the bone will be discussed.

The skeleton has flat bones, such as the skull, and long bones, such as the tibia, femur and humerus (Dhurjati et al., 2008). The bone microenvironment itself consists of two parts. The outer layer can be described as a harsh environment for cell growth as it is a densely mineralised tissue. The inner layer is the bone marrow which contains stem cells for the production of blood and immune cells. It is this inner bone marrow of long bones to which metastatic breast cancer cells colonise. Once penetrated the mineralised bone provides the breast cancer cells with a rich source of growth factors allowing growth and sustenance of the breast cancer cells at the expense of disruption of bone physiology as well as haematopoiesis (Dhurjati et al., 2008).

Under normal conditions the skeleton undergoes bone remodelling, which is a process in which the bone is actively undergoing a process of breaking down (resorption) and rebuilding (Fig. 1.5A; Proff and Romer, 2009). However, breast cancer cells are able to cause an increase in bone resorption which means the mineralised bone matrix is broken down to release the minerals and calcium held within it. With this increased bone resorption osteolytic lesions are formed. This degradation of the bone in around the tumour leads to bone fracture, nerve compression and hypercalcaemia due to the increase in blood calcium (Akhtari et al., 2008).

Breast cancer cells achieve this increase in resorption by releasing factors that can act either directly on the cells that cause bone resorption (osteoclasts) or indirectly by acting on the cells that usually rebuild bone (osteoblasts) (Fig. 1.5B). For example, breast cancer cells secrete Parathyroid hormone related peptide (PTHrP) which acts on osteoblast cells causing them to release RANKL. This binds to RANK receptors on osteoclast precursor cells and causes them to undergo differentiation into mature osteoclast cells which cause bone resorption (Guise et al., 1996; Thomas et al., 1999). Macrophage colony-stimulating factor (M-CSF) is also released from the osteoblast cells in response to PTHrP and leads to increased osteoclast differentiation (Mancino et al., 2001). After the osteoclasts break down the bone matrix, TGFβ is released and is part of an important positive feedback loop for further PTHrP to be released from the breast cancer cells (Yin et al., 1999).

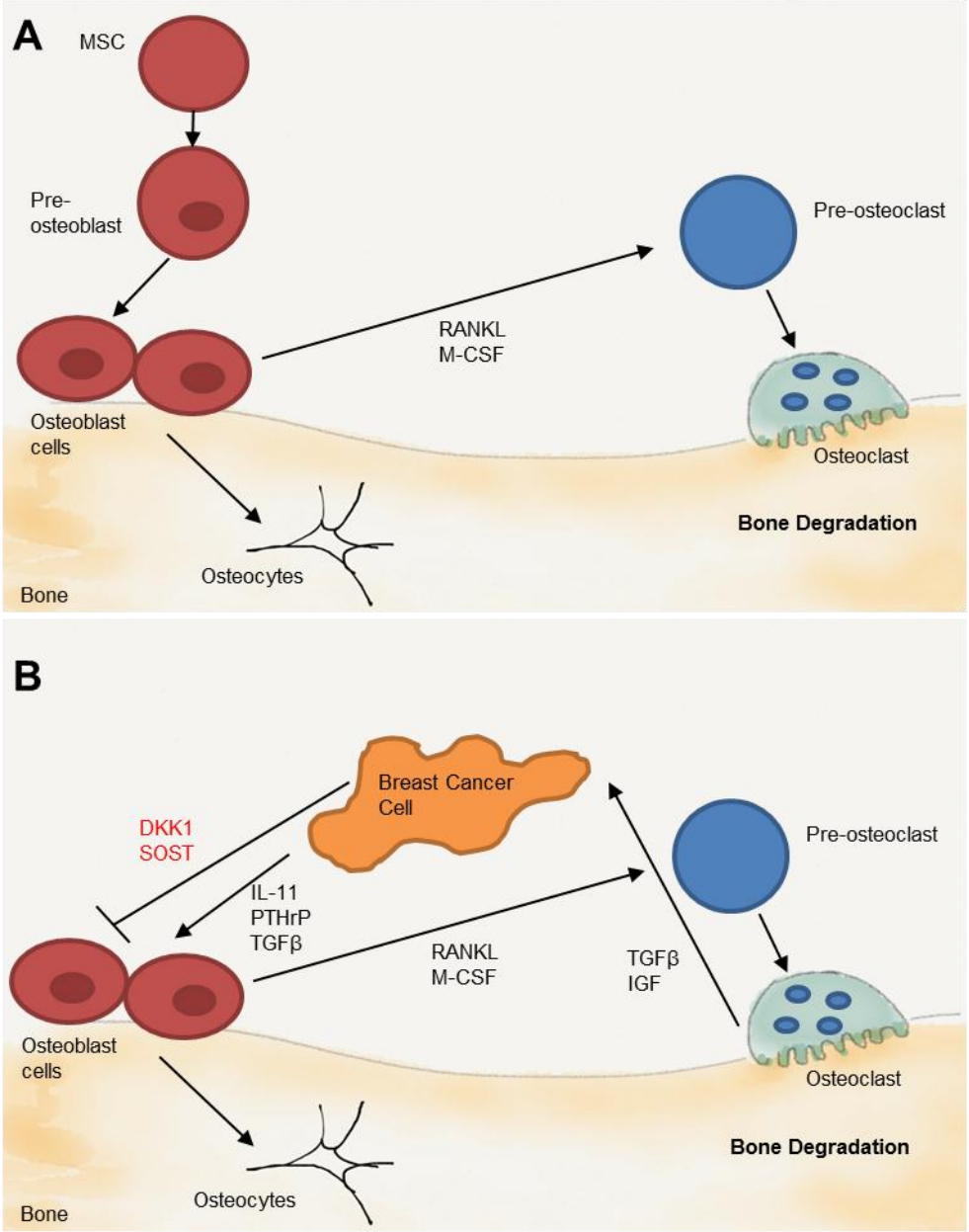

Fig. 1.5. Breast cancer cells increase bone resorption. (A) Diagram of bone remodelling in normal bone. Osteoblasts are differentiated from mesenchymal stem cells (MSC) and form bone. Differentiated osteoclasts degrade bone. (B) Diagram of bone remodelling following breast cancer metastasis to bone. Breast cancer cells secrete factors such as PTHrP, TGFβ and IL-11 that cause osteoblast cells to release RANKL and M-CSF. These act on osteoclast progenitor cells and cause them to differentiate into mature multinucleated osteoclast cells. This leads to increased bone resorption and the release of growth factors from the bone matrix. One such factor is TGFβ which acts on breast cancer cells to release more PTHrP and thus forms a positive feedback loop.

While the breakdown and recovery of bone is controlled as described above, the initial formation of bone is under the regulation of the transcription factor Runx2. Runx2 is also expressed in the mammary gland epithelium and overexpressed in metastatic breast cancers (Ferrari et al., 2013). These observations have led to the hypothesis that Runx2 contributes to the expression of genes in breast cancer cells that confers upon them the ability to colonise bone and direct the activity of the osteoblasts and osteoclasts to degrade bone. The following sections will provide further detail on the Runx2 family and the role of Runx2 in bone in both health and disease and review the evidence for the proposed role of Runx2 in breast cancers.

1.4. Runx family transcription factors

The Runt-related (Runx) transcription factors contain a highly conserved region known as the Runt Domain (Braun and Woollard, 2009; Coffman et al., 1996; Robertson et al., 2006). This is a 128 amino acid motif located towards the N-terminus. This domain is named after the gene *runt* which was first discovered in Drosophila melanogaster. There are three main members of the mammalian Runt family; Runx1 (AML1/ CBFA2/ PEBP2αB), Runx2 (AML3/ CBFA1/ PEBP2αA/ Osf2) and Runx3 (AML2/ CBFA3/ PEBP2αC) (Levanon et al., 1994). The domain structure of these Runx proteins is shown in Fig 1.6.

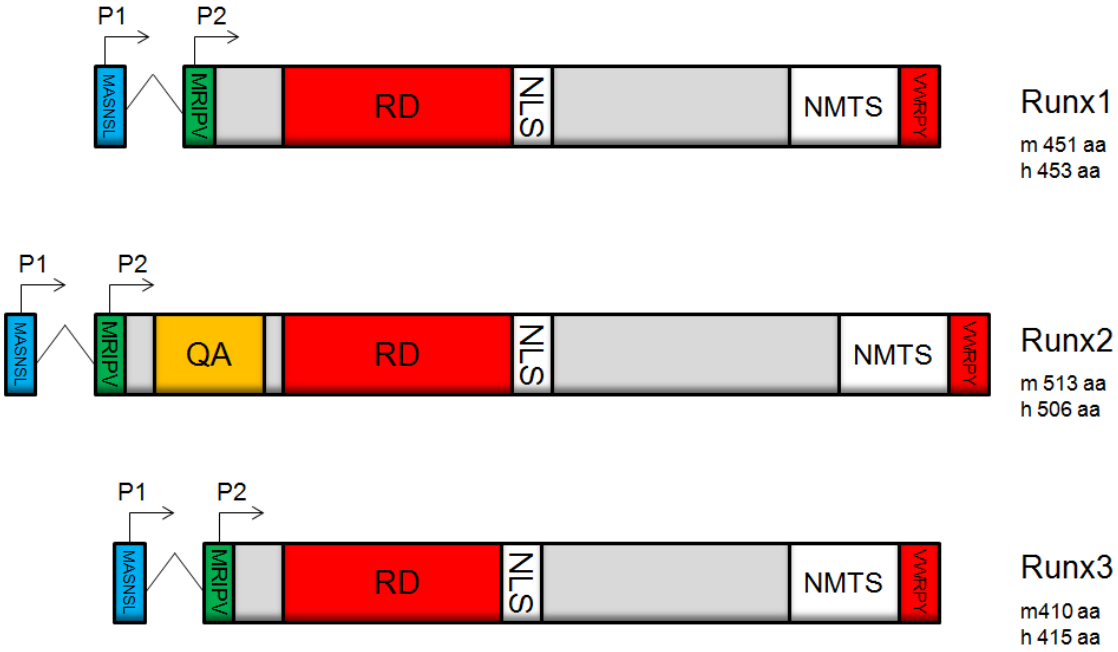

Fig. 1.6. Structure of the Runx family proteins. The Runt domain (RD) and the C-terminal VWRPY sequence is highlighted in red. These areas are homologous between all three proteins. The nuclear localisation signal (NLS) and the nuclear matrix-targeting signal (NMTS) are also shown. Runx2 contains a unique QA (glutamine/alanine) domain. There are two promoters which give rise to two main isoforms beginning with MASNS or MRIPV.

All three mammalian Runx genes have two promoters. The two promoters are P1, which is the distal, and P2, which is proximal. These promoters give rise to the two major Runx isoforms which are type II and begin with the amino acid sequence MASNS and type I, beginning with MRIPV respectively (Banerjee et al., 2001; Ducy et al., 1997). With alternate splicing at least 12 different isoforms can be created for Runx2 (Levanon and Groner, 2004; Stock and Otto, 2005).

The C-terminal end of the runt protein is also conserved and in most species ends with the amino acid sequence VWPRY. The only exception is the *run* gene in C. elegans which ends IWRPF (Coffman, 2003). Once the Runx2 protein has been produced it is localised to the nucleus and to sub nuclear foci within the nucleus (Zaidi et al., 2001). This localisation is directed by two domains within the Runx2 protein. The first is the nuclear localisation signal (NLS) and the second is the nuclear matrix targeting signal (NMTS). The NLS is 9 amino acids in length and is located at the carboxyl terminal immediately after the Runt domain (Kanno et al., 1998a). The NMTS is 31 amino acids long and is located further towards the carboxyl end of the protein and is responsible for localisation of Runx2 to sub nuclear foci (Zeng et al., 1998; Zeng et al., 1997). Runx2 is unique in comparison to other Runx family members in that it also has a QA (Glutamine/Alanine) domain which plays a role in the transactivation of Runx2 (Thirunavukkarasu et al., 1998).

The Runt domain contains the DNA binding domain (DBD) and is where the Runx proteins can bind DNA containing the consensus sequence 5'-PuACCPuCA-3'or the complementary sequence 5'-TGPyGGTPy-3' (Hart and Foroni, 2002; Kamachi et al., 1990; Schroeder et al., 2005). However, this Runt domain also allows protein-protein interactions and is required for heterodimerisation with CBFβ (Ito, 2004; Kanno et al., 1998). The importance of this interaction is described below.

1.4.1. Runt/CBFβ Heterodimerisation

All Runx proteins are heterodimeric with the Runx protein forming the α-subunit and CBFβ forming the β-subunit. The Runt domain is made up of 12 β strands that form an S-type immunoglobin fold (Bartfeld et al., 2002). CBFβ does not interact with the DNA itself but instead it binds to the Runx protein causing a change in conformation at loop 11from being closed to open. This change in conformation is known as the S-switch (Backstrom et al., 2002; Bartfeld et al., 2002).

Structural studies have shown that the Runx/CBFβ interaction occurs between the N-terminal 141 amino acids of CBFβ and the Runt domain (Huang et al., 2001). CBFβ binds to the Runt domain at a site away from the DNA binding interface. At the Runx/CBFβ interface, the exposed β sheet region of Runx Runt domain, which is composed of β5, β10 and β11 intervenes into the space between β3 and β5 of CBFβ, which form the edges of a β sheet and thereby stabilizes the two subunits (Tahirov et al., 2001).

The Runx/CBFβ interface extends linearly from the DNA and can be divided into two predominantly hydrophilic interaction areas, one proximal to DNA (Area I) and one distal (Area II), with an intervening hydrophobic area (Fig. 1.7). Area I consists of β5, L5, and β10 of Runx and β1, L1, L2, and β3 of CBFβ (Fig. 1.7). A hydrogen bonding network is formed in this area between the backbones and side chains of Ala107, Tyr113, and Ser114 of Runx and the side chains of Asn63, Arg33, and Lys28 of CBFβ; the phenol ring of Tyr113 also makes van der Waals contacts with Thr30 and Val58 of CBFβ. In addition, the side chain of Thr149 of Runx is hydrogen bonded to the backbone of Asn63 of CBFβ. Area I extends to the central hydrophobic region situated between β5, β10, L10, β11, and L11 of Runx and β2, β3, and L5 of CBFβ, where Met106, Thr151, Phe153, Val159, and H163 of Runx and

Phe17, Asn63 (methylene part), Leu64, and Ser65 (methylene part) of CBFβ are involved in van der Waals contacts (Tahirov et al., 2001).

Area II consists of L1, L10, and β11 of RUNX and the N terminus, α1, β3, β5, and L5 of CBFβ. This area contains a short, intermolecular, parallel β sheet, composed of β11 of Runx and β5 of CBFβ, with hydrogen bonds between the backbones of Pro157 and Val159 of Runx and Ile102 and Asn104 of CBFβ. The hydrogen bonding network in the area around the parallel β sheet extends between the backbone and side chain of Thr161 of Runx and the side chain of Asn104 of CBFβ. The parallel β sheet is also stabilized by van der Waals contacts between Pro156 and Gln158 (methylene part) of Runx and Ile102 of CBFβ on one side, and between Pro157 and Val159 of Runx and Gln67 (methylene part), Met101, Leu103, and Leu64 of CBFβ on the other side, a network of van der Waals contacts that extends all the way to the central hydrophobic region. Near this site, the side chain of Asn69 and backbone of Asp66 of Runx are hydrogen bonded to the backbone of Pro2 and side chain of Lys11 of CBFβ, respectively, and Pro68 of Runx makes a van der Waals contact with Val5 of CBFβ, stabilizing the N-terminal regions of both subunits (Tahirov et al., 2001). Consequently, heterodimerisation leads to a more stable conformation by enhancing the ability of the Runt domain to bind to DNA (Tahirov et al., 2001; Tanga et al., 2000; Wang et al., 1993).

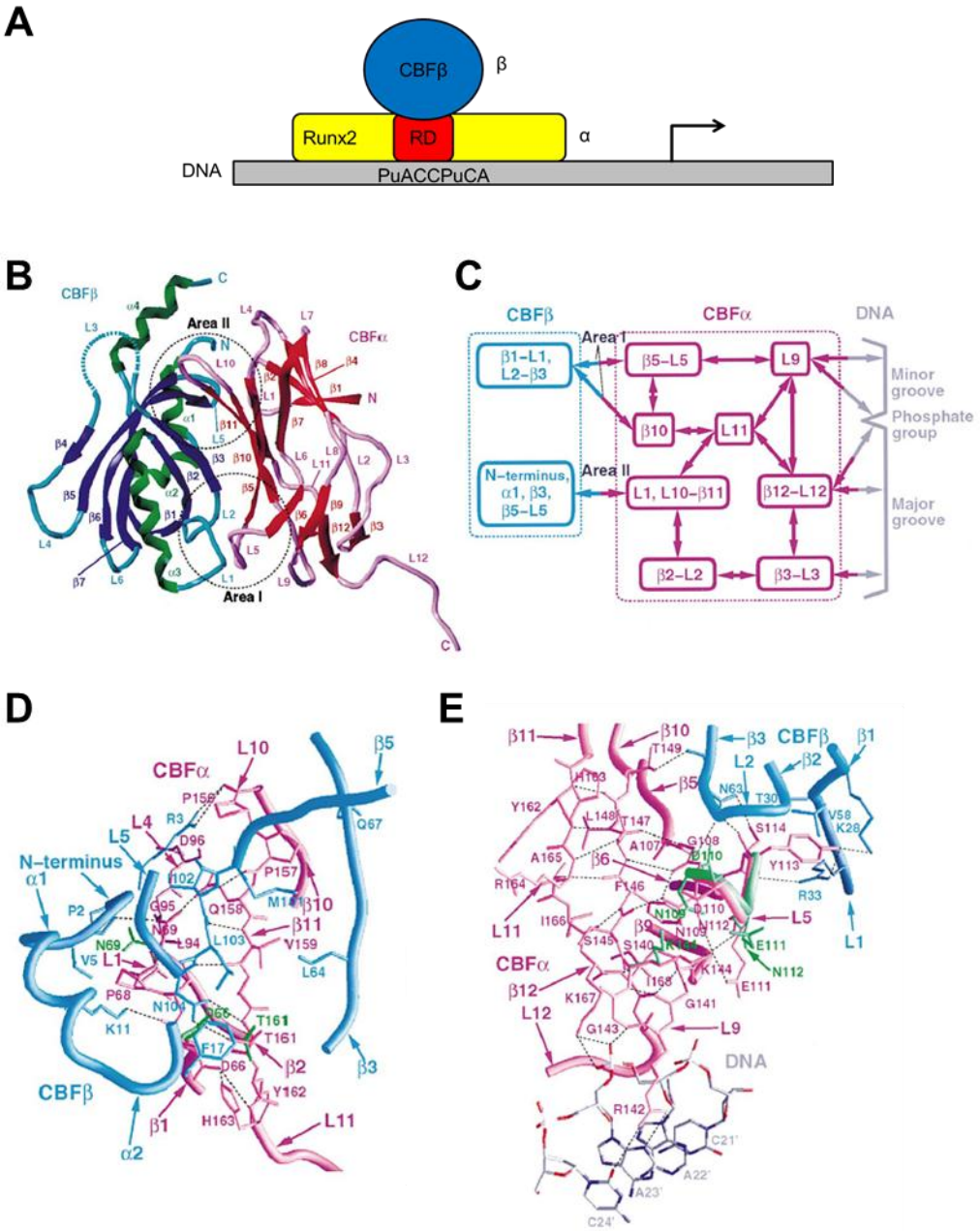

Fig. 1.7. Runx2/ CBFβ heterodimerisation. (A) A schematic diagram showing Runx2 of the Runx2/CBFβ complex binds DNA at the runt domain (RD). (B) A crystalised protein structure of Runx/CBFβ binding. (C) A schematic representation of the network between CBFβ (blue), Runx (pink) and DNA (grey). (D) and (E) Steroviews highlighting the hydrogen bonding (black dotted lines) network between Runx, CBFβ and DNA at Area II (D) and I (E). This demonstrates the change in conformation with CBFβ binding and the structure without CBFβ is shown in green. Modified from (Tahirov et al., 2001).

1.4.2. Runx1 (AML1/ CBFA2/ PEPBP2αB)

The Runx1 gene is the largest of the family and is 260 kb in size. The functional role of Runx1 became apparent after the generation of Runx1 null mice (Okuda et al., 1996; Wang et al., 1996b 1998). These studies found Runx1 to be involved in definitive haematopoiesis (North et al., 1999). In humans, mutations found in the Runx1 gene are associated with leukaemia such as acute myeloid leukaemia (AML) and acute lymphoblastic leukaemia (ALL).

1.4.3. Runx3 (AML2/ CBFA3/ PEBP2αC)

Runx3 is the smallest of the Runx family at 67 kb (Bae et al., 1995). The role of Runx3 was also found after the generation of Runx3 knockout mice. These mice have revealed a connection between Runx3 and gastric cancer (Li et al., 2002). Runx3 is also important in the central nervous system (Levanon et al., 2002; Inoue et al., 2003). In addition there is evidence for Runx3 having a role in the development of T cells. Runx3 is required for the lineage specificity of T cells through the silencing of cytotoxic thymocytes (Taniuchi et al., 2002). This regulation also involves Runx1 which is required for the repression of CD4-CD8- thymocytes (Ito, 2004; Woolf et al., 2003).

1.5. Runx2

1.5.1. The role of Runx2 in skeletal development

Runx2 is essential for the formation of the skeleton. Its role in bone formation was established through the production of Runx2 knockout (KO) mice (Komori et al., 1997; Otto et al., 1997a). Studies in these mice showed Runx2 deficiency prevents the formation of calcified bone (Fig. 1.8). Furthermore, mice with homozygous mutations died after birth as a result of respiratory failures. Heterozygous mutants showed skeletal abnormalities that are similar to those seen in humans who have Cleidocranial dysplasia (CCD) (Otto et al., 1997b). This will be discussed further in later sections. These results show that Runx2 is vital for skeletal development, as in the absence of Runx2 calcified bone is not formed.

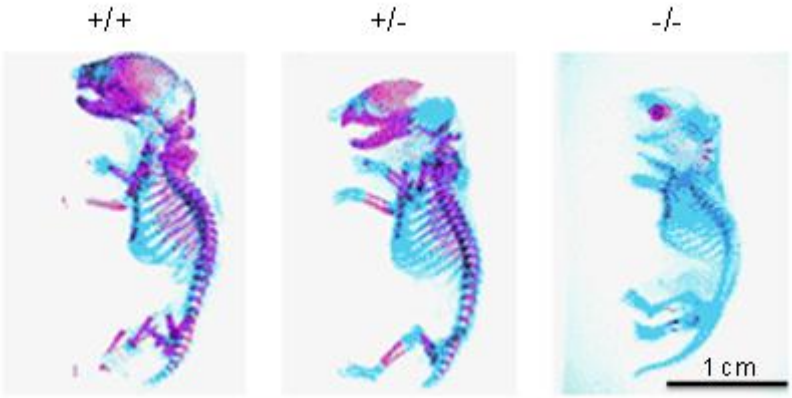

Fig. 1.8. Knockdown of Runx2 in mice prevents bone formation. Runx2 knockout mice cannot form calcified bone. A wild type (+/+) new born mouse is shown in the left panel, heterozygous (+/−) mouse shows some reduction in calcified bone (middle panel) however a mutant (−/−) mouse (right panel) shows very little calcified bone. Alizarin red staining indicates calcification and Alcian blue staining indicates cartilage. Bar 1 cm (adapted from Komori et al, 1997).

To gain an understanding of the role Runx2 has within mammary cells it is important to also understand the current roles of Runx2 within bone. There are three main cell types within the skeleton; osteoblasts, osteoclasts and chondrocytes. Both osteoblasts and osteoclasts are in bone, while chondrocytes form cartilage. Osteoclasts are of monocyte macrophage lineage and degrade bone. Osteoblasts and chondrocytes are differentiated from mesenchymal stem cells (MSC). Osteoblasts are involved in formation of bone (Fig. 1.9).

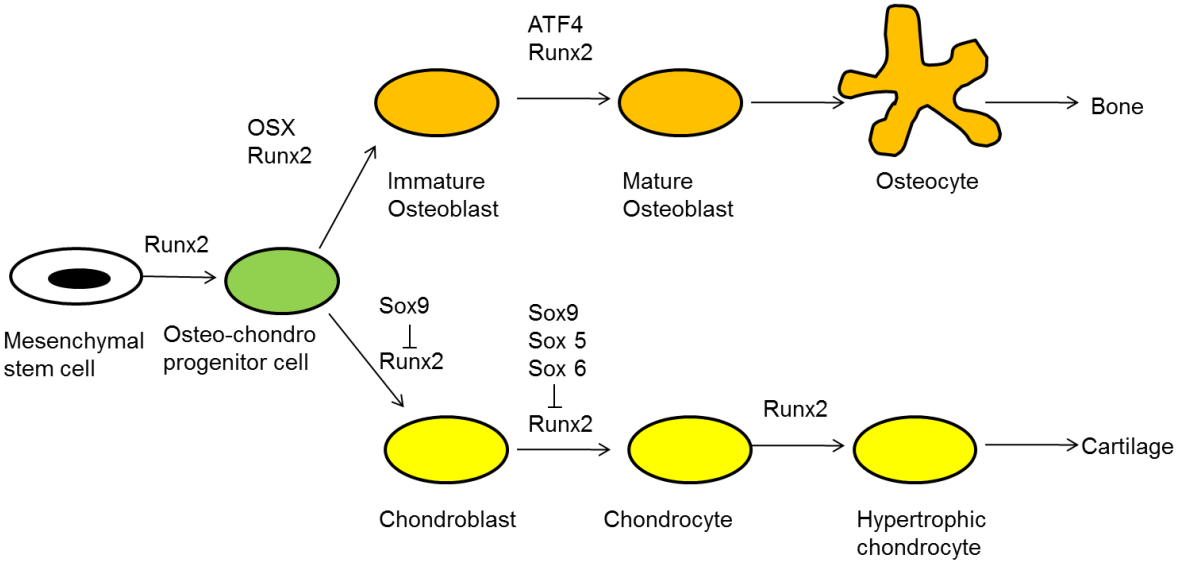

Fig.1.9. Osteoblastigenesis is regulated by Runx2 but also involves other transcription factors. Both osteoblast and chondrocytes are derived from mesenchymal stem cells which differentiate into osteo-chondro progenitor cells with the activity of Runx2. At this point the expression of Sox9 determines whether osteoblast or chondrocyte cells are formed by inhibiting Runx2.

There are multiple stages of development from MSC to osteocytes which are embedded in bone and each stage can be identified using specific markers. MSC differentiate into osteo-chondro progenitor cells which express bone matrix proteins such as osteonectin. These cells differentiate into immature osteoblast and then mature osteoblast cells which express osteopontin and osteocalcin respectively (Ducy et al., 1997; Liu et al., 2001; Geoffroy et al., 2002). Both of these bone proteins have Runx2 binding sites in the promoter and are regulated directly by Runx2 (Sato et al., 1998; Javed et al., 1999). The final stage of maturation is to osteocyte cells, which occurs after mature osteoblast cells are embedded in the bone matrix (Komori, 2006).

While Runx2 KO mice have no calcified bone, they do have very low levels of early-stage osteoprogenitor markers (osteonectin). There are no markers for immature or mature osteoblasts present in these Runx2 KO mice. This shows that Runx2 expression is essential for commitment of MSC through the osteogenic lineage (Komori et al., 1997; Otto et al., 1997a). Yet Runx2 is not sufficient to drive this differentiation. In Osterix (Osx) KO mice there is also no differentiation of osteo-chondro progenitor cells to immature osteoblast cells. However, these mice do have Runx2 expression in the mesenchymal cells, showing that Runx2 is upstream of Osx (Nakashima et al., 2002). Therefore, while Runx2 is required for MSC to differentiate into osteoprogenitor cells, both Runx2 and Osx are needed for osteo-chondro progenitor cells to differentiate into immature osteoblast cells.

Further differentiation into mature osteoblasts requires down regulation of Runx2. This down regulation occurs in conjunction with Msx2, a homeobox protein transcription factor (Shirakabe et al., 2001). If Runx2 is not down regulated in these late stages, the result is osteopenia (Liu et al., 2001). Although Runx2 is down regulated, it is still able to initiate osteocalcin transcription due to other co-factors.

ATF4, a member of the CREB family, binds to Runx2 and enhances the expression of osteocalcin (Xiao et al., 2005) (Fig. 1.9).

Runx2 does not only promote differentiation of MSCs into osteoblasts, but inhibits their differentiation into chondrocytes (Komori, 2011). For cartilage development, the transcription factor sex determining region (SRY)-box 9 (Sox9) is required for chondrocytes differentiation from the osteochondro-progenitor cells (Bi et al., 1999). Other Sox proteins Sox5 and Sox6 are also regulators. The expression of Sox9 causes Runx2 inhibition, allowing the chondrocytes lineage progression. However, transient expression of Runx2 in pre-hypertrophic chondrocytes leads to the development of hypertrophic chondrocytes (Takeda et al., 2001).

1.5.2. The role of Runx2 in human disease

Homozygous Runx2 knockout mice do not develop calcified bone whereas mice heterozygous for Runx2 do form bone. However, bone formation in the heterozygous mice is abnormal and closely resembles the phenotype in humans with the autosomal-dominant skeletal disorder cleidocranial dysplasia (CCD). This is caused by Runx2 haploinsufficiency (Lee et al., 1997; Otto et al., 1997b). Characteristics of CCD include short stature, the absence of clavicles, Wormian bones (having additional cranial plates) and defects in teeth (Mundlos, 1999).

CCD is caused by mutations in Runx2 and has been mapped to chromosome 6p21. Many of the mutations occur in the DBD in the Runt domain of Runx2, thus showing the importance of this domain in the function of Runx2 (Otto et al., 2002). However, mutations can also occur upstream and downstream of this domain causing loss of function. Types of mutation described include deletions, translocations, missense,

non-sense and splice-site mutations (Hoeijmakers, 2001). There are many variations in which mutation can occur, however, a known frameshift mutation occurs at the carboxy-terminus of Runx2. Although the Runt domain is unaffected, the SMAD 1,2,3,5 binding domain is mutated. Also the NMTS may also be affected (Cunningham et al., 2006). Therefore, there are other areas of the Runx2 protein that are involved in Runx2 regulation.

1.5.3. Post translational modification and regulation of Runx2 function

Runx2 has both transcriptional activation and repression domains. The main activation domain is the proline-serine-threonine (PST) rich region which is situated between the NLS and NMTS (Fig. 1.10) (Kanno et al., 1998a). This domain is involved with interactions with co-activator proteins (Pelletier et al., 2002). Co-activators are proteins that are able to bind to Runx2 and promote the recruitment of RNA polymerase II. These coactivators do not bind to DNA directly but are still required for gene expression by transcriptional activation (Schroeder et al., 2005). In order for transcription of the Runx2 target gene, Runx2 needs to bind to the promoter region of the DNA sequence. This binding allows RNA polymerase to bind and initiate transcription. Some co-activators have histone acetlytransferase (HAT) activity and so can cause chromatin to relax by marking the lysine residues within histones with acetyl groups. This weakens the DNA-chromatin association and so makes DNA more accessible for transcription. Examples of co-activators that interact with Runx2 include p300, MOZ and MORF (Sierra et al., 2003a) (Pelletier et al., 2002). P300 causes Runx2 activation of the osteocalcin gene by interacting with the activation domain on Runx2 (Sierra et al., 2003b). Both MOZ and MORF are members of the MYST family of HATs. They are able to enhance Runx2 activation

of the osteocalcin promoter by interacting with the Runx2 activation domain (Pelletier et al., 2002).

Runx2 can also interact with other transcription factors in order to initiate transcription of target genes. The transcription factors enhance the activity of Runx2 by either the recruitment of co-activators or through the prevention of co-repressor binding (Schroeder et al., 2005). Transcription factors that activate gene expression include BMP-responsive Smads (such as Smad 1 and Smad 5) (Hanai et al., 1999), Ets1, (Sato et al., 1998a) androgen receptors (AR) (Ning and Robins, 1999), Oct-1 (Inman and Shore, 2005), Hes-1(McLarren et al., 2000) and CAAT enhancer binding proteins (C/EBPS) (Gutierrez et al., 2002). These proteins can interact with either the DNA binding domain or the activation domains of Runx2 (Fig. 1.10).

Phosphorylation of different serine (S) and threonine (T) residues on Runx2 by different kinases results in changes in signal pathways that effect differentiation of osteoblasts (Shui et al., 2003). Phosphorylation of S247 (S226 of human type I Runx2) resulting from stimulation by Fibroblast Growth Factor 2 (FGF2) causes increased Runx2 activity. Runx2 can also be phosphorylated as a result of the Mitogen-Activated Protein Kinase (MAPK) pathway. For example, Insulin-like growth factor 1 (IGF1) activates MAPK/ extracellular signal regulated kinase (ERK) pathway to increase Runx2 phosphorylation and increase osteoblast expression genes (Jonason et al., 2009). The stimulation of parathyroid hormone (PTH) causes protein kinase A (PKA) phosphorylation of S347 in mice (T341 in humans). This results in transactivation of Runx2 and an increase in MMP13 expression. This is particularly important during fetal bone development due to the role of MMP13 in degrading collagen (Selvamurugan et al., 2000). These results indicate the importance of Runx2 phosphorylation in relation to its activation.

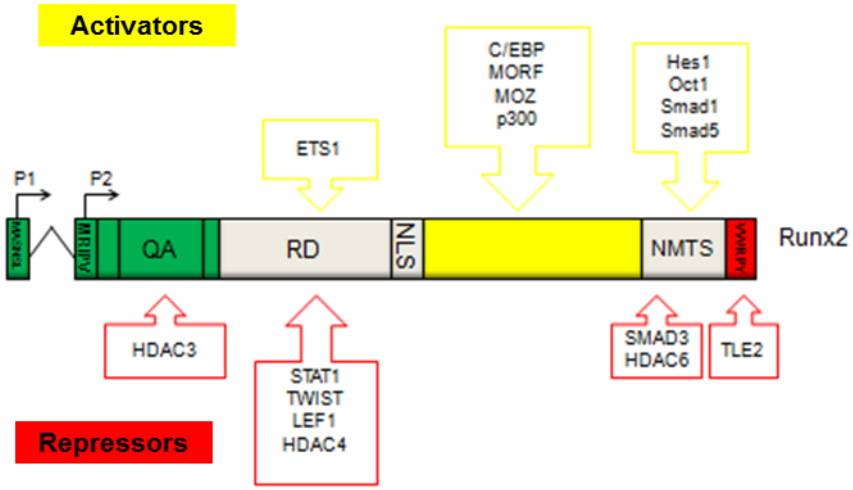

Fig. 1.10. Activators and repressors of Runx2. The activators of Runx2 expression are shown above Runx2 while the repressors are shown below. Activators include ETS1, C/EBP, MORF, MOZ, p300, Hes1, Oct1, Smad1 and Smad 5. Repressors include HDAC3, STAT1, TWIST, LEF1, HDAC4, Smad3, HDAC6 and TLE2. The arrowed boxes indicate the location of binding. The green domain represents the activation and repression domain. The yellow domain is the PST activation domain and the red domain is the repression domain. Both possible promoters have been shown. RD (Runt domain), NLS (Nuclear localisation signal), NMTS (Nuclear matrix targeting signal), QA (Glutamine/Alanine).

1.5.4. Repression of Runx2 activity

In addition to the activation domains, Runx2 also has domains that contribute greatly to the repression of Runx2 activity by mediating binding to other proteins. The amino terminus of Runx2 is involved in the regulation of Runx2 activity (Inman et al., 2005; Schroeder et al., 2004). These first 94 amino acids allow binding to HDAC3 which causes repression of Runx2 activity (Schroeder et al., 2004). At the C-terminal region of Runx2, the last five amino acids, VWRPY, are also involved in repression of Runx2. This region interacts with the transducin-like enhancer of split (TLE)/ Groucho (Grg) family members (Thirunavukkarasu et al., 1998). The NMTS region also contains a repression domain (Thirunavukkarasu et al., 1998; Westendorf et al., 2002). The RD itself is also involved in interactions with co-repressors and transcription factors that prevent the Runx2 protein from binding to DNA (Vega et al., 2004).

While co-activators cause relaxation of chromatin, co-repressors have the opposite effect and so cause chromatin to condense. This requires the recruitment of proteins with Histone deacetylase (HDAC) activity (Schroeder et al., 2004; Jensen et al., 2008). HDACs are able to deacetylate histone proteins by removing acetyl groups from lysine residues. This strengthens the bonds between DNA and chromatin thereby DNA is less accessible and results in down-regulation of transcription. Runx2 can associate with many different HDACs as shown in Fig 1.10 (Schroeder et al., 2004).

Dephosphorylation of S104 by MAP Kinase phosphatase 1 (MKP1) abolishes its ability to heterodimerise with CBFβ. This decreases its stability and so reduces Runx2 function (Kugimiya et al., 2007; Wee et al., 2002). The cell-cycle proteins

cyclin D1/CDK4 phosphorylate S472 in mice models (corresponding to S451 in human Runx2). This phosphorylation leads to ubiquitination and subsequently proteasomal degradation of Runx2 (Shen et al., 2006).

Transcription factors can also inhibit Runx2 activity. Such transcription factors include Smad3, Stat1 and Twist (Alliston et al., 2001; Kim et al., 2003; Yang et al., 2004). One way in which these transcription factors repress Runx2 is by binding to the RD. This prevents Runx2 from binding to DNA as the DNA binding domain is located within the Runt domain. The transcription factor Twist acts in this way (Bialek et al., 2004). Another method adapted by Stat1 is to sequester Runx2 in the cytoplasm (Kim et al., 2003; McCarthy et al., 2000).

1.6. Runx2 and Normal Breast development

While Runx2 is a major bone regulator, its expression has also been shown in breast. Expression in breast was first detected *in vivo* in mice embryonic mammary placodes, which are precursors to the mice mammary buds (Otto et al., 1997a). Additionally Runx2 was identified in a microarray of terminal end buds of mouse. These are involved in branching of the mammary glands (Kouros-Mehr and Werb, 2006). There is also evidence of expression of Runx2 and Runx1 mRNA in adult mice (Blyth et al., 2010; Wang et al., 2011b). Taken together, the expression of Runx2 in normal mammary gland suggests that Runx2 does have a role in breast.

The highly regenerative potential of mammary glands highlights the importance of stem cells in these tissues at both the embryonic and adult stages of mammary development (Ferrari et al., 2013). A role for Runx2 in mammary gland stem cells is emerging. Studies of Runx homologs in invertebrates such as *C. elegans*, has shown

that rnt-1 (Runx homolog) mutations results in reduced proliferation of stem cells (Wang et al., 2010).

In mammalian cells, a possible role for Runx2 in embryonic stem cells is emerging. The cell line HC11 displays self-renewal capabilities which are a key characteristic of stem cells (Williams et al., 2009). The HC11 cell line is normal breast cells taken from a mid-pregnant mouse (Danielson et al., 1984). These cells are particularly interesting as they can be stimulated to lactate and so can give an insight into two stages of development (Ball et al., 1988; Taverna et al., 1991). Research in our laboratory has shown that HC11 cells express Runx2 (Inman and Shore, 2003; 2005)

These HC11 cells are able to produce milk proteins upon stimulation with hormone and so simulate a lactating breast. One such milk protein detected is β-casein. Interestingly, this milk protein has a consensus Runx binding site to which Runx2 is able to bind. Furthermore, Runx2 binding is essential for the activation of β-casein. Runx2 is recruited to the promoter binding site by Oct-1 to which it binds and forms a complex (Inman et al., 2005). Together, this presence of Runx2 in embryonic terminal end buds, its role in HC11 cells and the *in vitro* observation that Runx2 expression decreases during the mammary differentiation process indicates a role for Runx2 in embryonic stem cells and mammary (Ferrari et al., 2013; Inman and Shore, 2003; 2006; Williams et al., 2009).

There is also evidence that Runx2 may be involved in adult stem cells. Markers for stem cells were expressed in the mammary basal population in adult mice. These stem cells were confirmed to have self-renewal capacity (Shackleton et al., 2006). The presence of these stem cells was confirmed using different known stem cell surface markers (Ferrari et al., 2013). A microarray analysis of the mouse mammary

gland showed an enrichment of Runx2 in this basal compartment (Kendrick et al., 2008). This was validated by qRT-PCR analysis which showed Runx2 expression is up regulated in the basal cell population (Molyneux et al., 2010). This shows the presence of stem cells in adult mammary gland and a potential role for Runx2 in these cells.

There are other indications of a role for Runx2 in adult mammary gland development. Osteopontin a known bone gene regulated by Runx2 in osteoblasts is also expressed in mammary epithelial cells during pregnancy and lactation (Nemir et al., 2000). Runx2 is also able to bind to the Runx2 consensus binding site in the osteopontin promoter in HC11 cells and activates its transcription (Inman and Shore, 2003). This shows that Runx2 expression is regulated and functions in a similar manner in mammary epithelial cells to that in osteoblasts.

The normal mammary cell line (MCF10A) produces the acini type structures seen in mammary glands when grown in a 3D matrigel system *in vitro* (Debnath and Brugge, 2005). A 3D matrigel system is a cell culture method that allows cells to form structures with the support of an extracellular matrix (explained in further detail in later chapters). The ability of MCF10A cells to produce these acini structures is disrupted upon over expression of Runx2 (Pratap et al., 2009). Structures formed lack polarisation and have reduced apoptosis as well as increased proliferation. This suggests that Runx2 has a role in cellular organisation.

This overexpression of Runx2 in MCF10A cells produced a phenotype that resembles breast cancer cells in 3D studies. Incidentally, a role for Runx2 in breast cancer cells is also evident.

1.7. Runx2, Breast Cancer and Bone Metastasis

Runx2 expression is not limited to normal breast. In fact the first indication that Runx2 may have a role in the body other than in bone came from its expression in breast cancer cell lines. A microarray comparing normal breast, non-invasive breast cancer and metastatic/invasive breast cancer showed that Runx2 was one of the most up regulated genes from non-invasive to invasive breast cancer (Nagaraja et al., 2006). In order for breast cancer cells to metastasise to other areas of the body, they must acquire invasive properties. An *in vitro* matrigel invasion assay showed that transient knockdown of Runx2 in a metastatic breast cancer cell line reduced invasive capacity. Conversely, ectopic expression of Runx2 in non-metastatic breast cancer cells increases invasive capacity (Pratap et al., 2005).

Genes that are known markers for metastasis include the matrix metalloproteinase (MMPs) (Johansson et al., 2000). Runx2 directly regulates the expression of MMP13 and MMP9 in metastatic breast cancer (Javed et al., 2005; Pratap et al., 2005). Together these data show that Runx2 regulates the expression of known metastatic genes suggesting a role for Runx2 in breast cancer metastasis.

Once breast cancers gain invasive properties and move out of the breast, in 85% of cases they metastasise to bone. Of these cancers that colonise bone, most cause osteolysis as described earlier. *In vivo* studies have shown that injecting metastatic breast cancer cells (MDA-MB-231) into mice limbs, caused osteolysis in 80% of cases (Barnes et al., 2004; Javed et al., 2005). However, injecting MDA-MB-231 cells containing a mutated Runx2 reduced osteolysis to 5% (Barnes et al., 2004). In addition, it is known that breast cancers produce large amounts of PTHrP which

induces osteoclasts and bone resorption. This activity is also regulated by Runx2 through binding of Indian Hedgehog (IHH) (Pratap et al., 2008).

In addition to its role in breast cancer cells as stimulator of osteoclast activity, Runx2 has also been shown to mediate the ability of breast cancer cells to inhibit osteoblast differentiation. (Mendoza-Villanueva et al., 2011). Runx2 binds to the promoter region of the wnt signalling antagonist sclerostin and induces expression. Media from MDA-MB-231 cells containing secreted sclerostin was plated onto bone marrow stromal cells (BMSCs) and this inhibited differentiation of BMSCs. However, depletion of sclerostin from the MDA-MB-231 cell media caused no inhibition of osteoblast cell differentiation when placed onto BMSCs. This demonstrated that sclerostin was directly inhibiting the differentiation of the osteoblast cells (Mendoza-Villanueva et al., 2011).

1.8. CBFβ

All Runx transcription factor proteins are heterodimers, binding to CBFβ. The CBFβ gene is located on chromosome 16q22 and contains 6 exons. These can be alternatively spliced to yield 4 protein isoforms (Huang et al., 1999). Of these 4 isoforms CBFβ (187) and CBFβ (182) differ only at the 3' end of exon 5, where exon 6 has been spliced to the end of exon 5 in the CBFβ (182) isoform (Fig. 1.11A). CBFβ (148) and CBFβ (155) are generated by splicing that skips exons 3 and 5 respectively. The isoforms CBFβ (187) and CBFβ (182) interact with Runx in a similar manner. However, CBFβ (182) is found in 2-3 fold higher abundance than CBFβ (187). CBFβ (148) and CBFβ (155) do not stably associate with Runx proteins (Adya et al., 2000).

The CBFβ subunit of the heterodimer binds Runx proteins at the Runt domain and induces a conformational change that enhances the DNA binding activity of Runx proteins. While Runx proteins can bind DNA without CBFβ, this binding affinity is very weak (Adya et al., 2000). The heterodimerisation domain for CBFβ is located at the N-terminal 141 amino acid (Fig. 1.11B) (Huang et al., 1999).

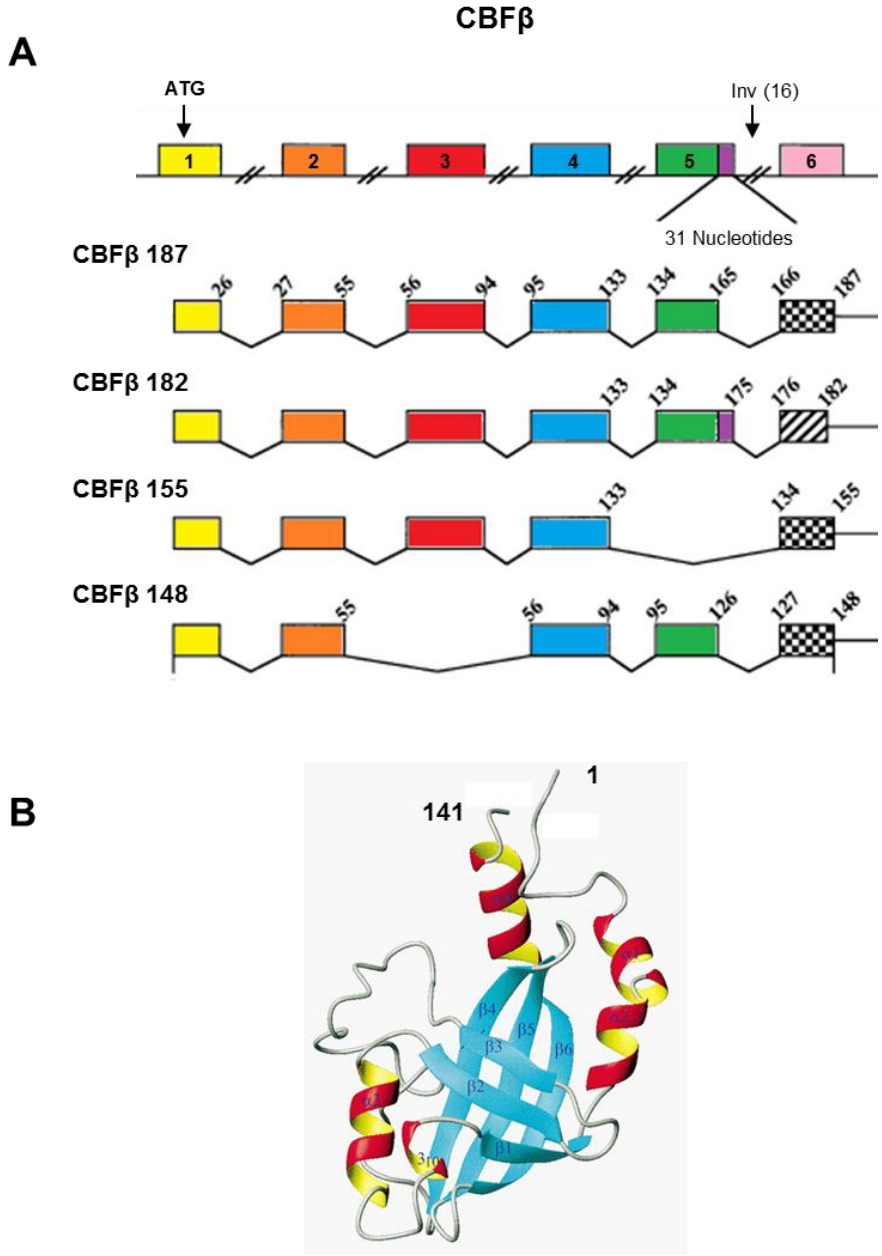

Fig. 1.11. Genomic structure of CBFβ isoforms and protein structure of CBFβ. (A) Diagram of the 4 alternative splicing products of the CBFβ gene. The 6 different exons are shown as coloured boxes. Amino acid residues from each exon are labelled. Location of almost all inv (16) breakpoints indicated by arrow (Adapted from Adya et al., 2000). (B) Ribbon representation of 141 aa CBFβ heterodimerisation domain. (Adapted from (Huang et al., 1999).

1.8.1. Role of CBFβ

The role of CBFβ was established with the aid of CBFβ knockout mice models. Mice with homozygous mutations for CBFβ died between E 11.5 and 13.5 (Sasaki et al., 1996). In addition, these mice had haemorrhaging in the central nervous system (CNS) from E 11.5 and 12.5. There is also no definitive haematopoiesis in the liver of the mice embryos (Sasaki et al., 1996; Wang et al., 1996a). These observed phenotypes in the homozygous CBFβ knockout mice resemble the same phenotype seen in Runx1 knockout mice (Wang et al., 1996b). This suggests that CBFβ is essential for haematopoiesis.

As these CBFβ knockout mice died very early in gestation, other models were needed to establish the role of CBFβ in later stages of tissue development. A CBFβ-GFP knock in mouse model was created by fusing the first 151 amino acids of CBFβ to a GFP sequence. These mice show normal haematopoietic function showing that the CBFβ-GFP construct functions in a similar manner to endogenous CBFβ. However, these mice died soon after birth which shows the GFP tag disrupted function in later stages of some tissue development (Kundu et al., 2002).

Rescue of the CBFβ knockdown mice with a CBFβ directed with a Gata1 promoter (CBFβ$^{-/-}$tg) showed rescue of hematopoiesis and no haemorrhaging (Yoshida et al., 2002). This confirms the requirement of CBFβ for hematopoiesis but in addition these mice also showed that by E 18.5 there was a severe delay in calcification. Calcification of bone is part of skeletal development and is regulated by Runx2. These CBFβ$^{-/-}$tg mice also had very low expression of osteocalcin, the marker for mature osteoblasts, while osteopontin, a marker for immature osteoblasts was still expressed in intramembranous bone. This indicates that the osteoblasts in CBFβ$^{-/-}$ tg

were immature and further shows that CBFβ is essential for bone development (Yoshida et al., 2002).

1.8.2. CBFβ in disease

AML is caused by lack of Runx1 function. This could be due to Runx1 mutation, or as is the case of the inversion mutation due to CBFβ loss of function. An inversion mutation can occur between CBFβ on chromosome 16 (16q22) and the MYH11 gene (16p13) which encodes the smooth-muscle myosin heavy chain gene (SMMHC). The resulting chimera is CBFβ-SMMHC [Inv(16)(p13q22)] (Goyama and Mulloy, 2011; Le Beau et al., 1983; Shigesada et al., 2004). In vitro studies have shown that Runx1 maintains its heterodimerisation domain and so is still functionally able to bind DNA in cells containing CBFβ-SMMHC (Liu et al., 1993). The Runx1 protein becomes sequestered in the cytoplasm of cells and so is not able to enter the nucleus to bind DNA. CBFβ-SMMHC dimerises and binds Runx1 at the first 11 amino acids of the CBFβ sequence and the SMMHC region sequesters the complex in the cytoplasm by binding to actin (Yoshida et al., 2005). Truncations of the N terminal SMMHC fragment prevent the CBFβ-SMMHC protein from binding to actin. As the CBFβ portion of these truncated proteins still binds Runx1, the entire complex is able to the move to the nucleus (Adya et al., 1998). These experiments show that CBFβ is essential for haematopoiesis and in addition that CBFβ moves into the nucleus with the aid of Runx1. Other mutations that result in AML occur in Runx1, such as the Runx1-ETO translocation mutation and the TEL-Runx1 mutation which is the most common cause of childhood AML (Yamagata et al., 2005).

The disease CCD, as mentioned earlier, is caused by mutations in Runx2. Rescue of a CBFβ knockout mouse model with CBFβ under the control of a Gata1 promoter

resulted in mice that died soon after birth due to respiratory failure and had short limbs and dwarfism. CBFβ$^{-/-}$tg mice also had absent clavicles and had only partial calcification of the frontal and parietal bones of the skull (Westendorf et al., 2002). These are traits found in CCD patients. Expression of Runx2 at both the mRNA and protein level showed Runx2 was similar in WT and CBFβ-Gata1 mice (Yoshida et al., 2002). Therefore, this suggests that Runx2/CBFβ heterodimerisation is required for normal Runx2 function. This is confirmed by evidence that patients who have a mutation in the runt domain of Runx2, causing interference between Runx2 and CBFβ, develop CCD. 63% of CCD patients have mutations in the runt domain of Runx2 (Cunningham et al., 2006).

1.8.3. CBFβ in breast cancer and invasion

While CBFβ expression is known to be ubiquitously expressed throughout different tissues, its expression in breast cancer cells was confirmed in our laboratory using metastatic breast cancer cell line MDA-MB-231 and non-metastatic breast cancer cell line MCF7. A co-immunoprecipitation experiment confirmed that the Runx2/CBFβ complex is present in MDA-MB-231 cells. It has already been established that Runx2 inhibition reduces invasive capacity (Pratap et al., 2005). Our laboratory has shown that inhibition of CBFβ by both siRNA and using a stable shRNA knockdown cell line also has a reduction in invasive capacity using a matrigel invasion assay (Mendoza-Villanueva et al., 2010).

This reduction in invasive capacity has been linked to the decrease of downstream targets of Runx2/CBFβ that are involved in cell migration such as MMP13 and MMP9 (Pratap et al., 2005; Selvamurugan et al., 2004). Other known Runx2 target

genes, OPN, OC and Galectin-3 all reduce in mRNA levels following Runx2 knockdown in MDA-MB-231 cells. However, not all these known Runx2 target genes showed a reduction in mRNA expression following CBFβ expression. Galectin-3 expression was independent of CBFβ knockdown, though ChIP analysis showed the CBFβ/Runx2 complex was recruited to the Galectin-3 promoter. This shows that not all target genes of Runx2/CBFβ require CBFβ for expression (Mendoza-Villanueva et al., 2010).

1.9. Project Aims

Given the dynamic nature of the mammary gland and the multiple stages of development, it is clear that different transcription factors are involved in the various stages. A 3D cell system allows the growth of structures found *in vivo*. In terms of mammary gland cells, these structures are acini. Runx2 expression has been identified and shown to have a role in the HC11 cell line which is a model cell line for normal mammary gland (Inman and Shore, 2003). Thus, the first aim was to create a 3-Dimensional (3D) cell culture system. This 3D model was then used to identify whether Runx2 expression changes during the formation of acini structures. In addition, considering Runx2 has been shown to bind and activate transcription of the milk protein β-casein, the dependence on Runx2 was to be determined using Runx2 knockdown studies in HC11 cells. As Runx2 acts in the form of a heterodimer, the presence of CBFβ was also established.

Understanding the regulation of normal breast development is important in order to gain a better insight into the changes that occur in breast cancer. Runx2/CBFβ has already been found to be important in breast cancer in terms of its ability to invade

the body in late stage cancers and also the bone remodelling that occurs following breast cancer metastasis to bone (Javed et al., 2005; Mendoza-Villanueva et al., 2011). There are no current treatments to cure breast cancers once they have metastasised out of the breast. Knockdown of CBFβ alone in a metastatic breast cancer cell line has resulted in reduced invasive capacity (Mendoza-Villanueva et al., 2011). Therefore, the second aim of this project was to identify the potential involvement of CBFβ in the invasion of metastatic breast cancer cells. Considering the role of Runx2/CBFβ in metastatic breast cancer and the potential of CBFβ knockdown alone on these cells, the third aim was to identify possible downstream targets of this complex using microarray analysis of cells knocked down in CBFβ. Of particular interest were genes in relation to breast cancer's ability to remodel bone once it has metastasised.

2.0 Materials and Methods

2.1. Antibodies and Reagents

Anti-Runx2/cbfa1 monoclonal mouse (D130-3; MBL, Little Balmer), mouse monoclonal antibody to Runx2 (Abcam; ab54868-100), Runx2 (M70) polyclonal rabbit (sc-10758; Santa Cruz), rabbit polyclonal antibody to Runx1/AML1 (ab23980-100; Abcam), rabbit polyclonal antibody to CBFβ (ab33516-100, Abcam), rabbit polyclonal antibody to β-Tubulin (ab6046; Abcam), rabbit polyclonal to Lamin B1 (ab16048; Abcam). Control siRNA-A (sc-37007), mouse PEBP2β siRNA (sc-37682), mouse Runx2 siRNA (sc-37146), mouse Runx1 siRNA (sc-37678) all from Santa Cruz Biotechnology.

2.2. Cell Lines

HC11 cells are a mammary epithelial cell line taken from a BALB/c mouse during the middle of its pregnancy (Danielson et al., 1984). They were cultured in Roswell Park Memorial Institute (RPMI) media containing 10% heat inactivated Fetal Bovine Serum (HI FBS; Sigma), 50 µg/ml gentamycin (Sigma), 5 µg/ml Insulin from bovine pancreas (Sigma) and 10 ng/ml epidermal growth factor (EGF) (Sigma).

HeLa cells are human cervical cancer cells and were grown in Dulbecco's modified Eagle's medium (DMEM; Gibco) supplemented with 10 % FBS and 1 % PS.

UMR106 cells are rat osteosarcoma cells and were also cultured in DMEM supplemented with 10 % FBS and 1 % PS.

MDA-MB-231 cells are human metastatic breast cancer cells. These cells stably express Green Fluorescent Protein (GFP). They were cultured in DMEM supplemented with 10 % FBS and 1 % PS, 1% non-essential amino acid, 1% L-Glutamine, 2µg/ml geneticin.

MDA-MB-231 cells stably expressing shCBFβ were grown in DMEM supplemented with 10 % FBS and 1 % PS, 1% non-essential amino acid, 1% L-Glutamine, 2μg/ml geneticin and 0.4μg/ml puromycin.

shCBFβ MDA-MB-231 cells with CBFβ-ER stable cell lines were grown in DMEM supplemented with 10% FBS and 1% PS, 1% non-essential amino acid, 1% L-Glutamine, 2μg/ml geneticin, 0.4 μg/ml puromycin and 500 μg/ml hygromycin.

MCF10A cells are non-cancerous breast cells. These cells were cultured in DMEM/F12 supplemented with 5% horse serum, 20 ng/ml EGF, 0.5 μg/ml hydrocortisone, 100 ng/ml cholera toxin, 10 μg/ml insulin and 1% PS.

All cells were kept at 37°C, 5 % CO_2 in the presence of humidity.

2.3. Stimulation of lactation from HC11 cells

HC11 cells were stimulated to lactate by growing to confluency and then treated with complete media supplemented with 10^{-6} M dexamethasone (Sigma) and 5 μg/ml Prolactin (Sigma). The treated cells were incubated at 37°C, 5 % CO_2 with humidity for 12 hrs to 5 days as indicated.

2.4. Thawing cells

Cells were taken from liquid nitrogen and thawed quickly in a 37°C water bath. They were then put into 5 ml of the required media in a small 25 cm^3 corning flask and incubated at 37°C/ 5 % CO_2 with humidity.

2.5. Freezing cells

The desired cells were split 24 hrs prior to freezing so that they would be in the growth phase of the cell cycle. Suspension cells were centrifuged for 6 mins at 1000 RPM. Adherent cells were first trypsinised for approximately 3 mins at 37°C before being centrifuged in the same manner. The supernatant was discarded and the pellet resuspended in 1 ml recovery medium (Gibco). These were first put on ice then transferred to -20°C and to -80°C the following day. Cells were later stored in to liquid nitrogen.

2.6. Generation of a stable cell line

The stable cell line MDA-MB-231 had previously been created (Mendoza-Villanueva et al., 2010). These cells were transfected with a pcDNA3.1/Hygro plasmid containing a mouse Flag-CBFβ-ER construct or the empty pcDNA3.1/Hygro plasmid. Transfected cells were treated with the addition of 500 μg/ml hygromycin (Sigma) into the media and the selection process last for 10 days. Single colonies of surviving cells were then picked and plated into a 96 well plate. Final clones were then assessed for the expression of the construct using western blot analysis with both anti-flag and anti-CBFβ antibodies.

The shCBFβ MDA-MB-231 Flag-CBFβ-ER stable cell line is an inducible system. The ER tag sequesters the complex in the cytoplasm. Nuclear translocation was induced with 0.1 μM 4-OH Tamoxifen with incubation at 37°C/5% CO_2 and humidity.

2.7. Whole cell extraction

In order to obtain protein samples for western blot analysis, whole cell extractions were carried out using cells grown in either 10 cm petri dishes or 6 well plates (Corning) as required. Cells were washed three times with phosphate buffered saline (PBS; Gibco) and then lysed with the addition of 1x laemmli buffer (0.625 M Tris-HCl (pH 6.8), 50% glycerol, 10% SDS, 10% ß-mercaptoethanol, 0.05% bromophenol blue) and collected using a cell scraper. Samples were then boiled at 95°C for 5 mins to denature proteins before use in further experiments.

2.8. Nuclear and Cytoplasmic extraction

Nuclear and cytoplasmic extracts were prepared by first collecting cells into a pellet through trypsinisation and washing twice with PBS. The pelleted cells were then resuspended in 400 µl of ice cold Buffer A (10 mM HEPES pH 7.9, 10 mM KCl, 0.1 mM EDTA, 0.1 mM EGTA, 1 mM DTT, 0.5 mM PMSF) with the addition of complete mini-EDTA-free protease inhibitor cocktail (Roche). This was incubated at 4°C for 15 mins to allow the cells to swell. Cells were lysed with the addition of 10% Nonidet NP-40 (Fluka) with a vigorous vortex for 10 secs. After centrifuging at 4°C, 14 000 RPM for 30 secs, the supernatant containing the cytoplasmic extract was removed and stored at -80°C. Any further contamination of cytoplasmic content was removed by washing the pellet with buffer A two times. The pellet was then resuspended in ice cold Buffer B (20 mM HEPES pH 7.9, 0.4 M NaCl, 1 mM EDTA, 1 mM EGTA, 1 mM DTT, and 1 mM PMSF) containing protease inhibitors and vortexed vigorously for 45 mins at 4°C. The nuclear debris was pelleted by centrifuging at 14 000 RPM at 4°C for 5 mins and the supernatant containing the nuclear extracts was removed and frozen at -80°C.

2.9. Sodium dodecyl sulphate - polyacrylamide gel electrophoresis (SDS-PAGE)

The samples for whole cell extraction and the nuclear and cytoplasmic extracts were then used for protein expression analysis using SDS-PAGE. For the nuclear and cytoplasmic extracts, the protein samples were denatured by mixing protein sample at a ratio of 4:1 with a 5x loading buffer (0.625M Tris-Cl (pH 6.8), 50% glycerol, 10% SDS, 10% ß-mercaptoethanol, 0.05% bromophenol blue) and heating at 95°C for 5 mins. The Pageruler prestained protein ladder plus (Fermentas) was used as a molecular marker. The samples were run on a12% SDS gel at 250 volts immersed in 1 X Tris/Glycine/SDS Running Buffer for 35 mins.

To visualize protein bands, the gels were stained with coomassie brilliant blue R250 (0.2% Coomassie Blue, 7.5% glacial acetic acid, 50% ethanol) and then destained with destaining solution (5% ethanol, 7.5% glacial acetic acid). Gels were dried for 40 mins at 80°C using a gel dryer.

2.10. Western Blot analysis

The protein resolved by SDS-PAGE were transferred onto a nitrocellulose membranes (Whatman) soaked in transfer buffer (250 mM Tris, 190 mM Glycine, 20% methanol and 1% SDS) using a semidry transfer machine BlotterTM (Bio-Rad) set at 12 V for 75 mins. The membrane was blocked in 5 % milk (Marvel) in Tris Buffered saline with 0.1 % Tween-20 (TBS-T; Sigma). Following 1 hr incubation at room temperature, the membrane was probed with the required antibody for either 1-2 hrs at room temp, or overnight at 4°C, with gentle agitation. The antibodies Anti-Runx2/cbfa1 monoclonal mouse (D130-3) (MBL), rabbit polyclonal antibody to

Runx1/AML1 (ab23980-100; Abcam) and rabbit polyclonal antibody to CBFβ (ab33516-100, Abcam) were all used in a 1:500 dilution and were incubated for either 2 hrs or overnight. The rabbit polyclonal antibody to β-Tubulin (ab6046; Abcam) and rabbit polyclonal to Lamin B1 (ab16048; Abcam) were used in a 2:3000 dilution and were only incubated for 1 hr at room temp. All antibodies were diluted in 5% (w/v) milk in TBST.

After three 10 min washes in TBST, the membranes were incubated for 1 hr with the secondary antibody at room temp. Secondary antibodies used were either goat anti-mouse IgG or goat anti-rabbit IgG, which are conjugated with horseradish peroxidase (Pierce) and used to probe the blot in a 1:500 dilution. The membranes were washed a further three times for 10 mins each, then treated with Supersignal West Dura Extended Duration Substrate (Pierce) following manufacturer recommendations. The signal was detected using a Bio-Rad Fluor-S multi-imager (Biorad) and images manipulated using Quantity One software to detect the signal.

2.11. Immunocytochemistry of monolayer cells

Cells were grown on coverslips in 24 well plates and washed twice with pre-warmed phosphate buffered saline (PBS), fixed for 20 mins at room temp using 4 % paraformaldehyde (PFA; Biorad). Cells were permeabilised with 0.1 % triton for 15 mins at room temp then washed twice in PBS and blocked using 1 % Bovine Serum Albumin (BSA) in PBS for 1 hr at room temp. Relevant primary antibody was diluted in 1 % BSA and cells were either left for overnight incubation at 4°C or incubation for 1 hr at room temp. After washing three times for 5 mins each at room temp with gentle agitation, the cells were incubated with the secondary antibody which was either Alexa flour anti-mouse or anti-rabbit antibody (Invitrogen) and

used in a 1:250 dilution for 1 hr at room temp. The cells were washed three times for 5 mins in PBS and once in dH_2O for 5 mins to remove any excess PBS. Coverslips were then mounted onto glass slides using Prolong Antifade Reagent with DAPI (Molecular probes) and left to dry overnight at room temperature before being stored at 4^oC.

2.12. Microscopy of fluorescence for cells grown in monolayer

Images were taken using an Olympus BX51 upright microscope on a 60x/ 1.40 UPlanApo objective with oil immersion and captured using a Coolsnap ES camera (Photometrics) through MetaVue Software (Molecular Devices). Specific band pass filter sets for DAPI, FITC and Texas red were used to prevent bleed through from one channel to the next. Images were then processed and analysed using ImageJ (http://rsb.info.nih.gov/ij).

2.13. 3D Cell Culture

HC11 cells were grown in three-dimension (3D) on a thin layer of the reconstituted basement membrane Growth Factor Reduced Matrigel (BD Biosciences; BD No. 354230). This was pre-cooled overnight at 4^oC in order to liquefy and spread evenly onto the base of 35 mm Glass Bottom dishes (MatTek corporation, MA, USA). Cells were seeded at 40 000 cells/ ml in RPMI medium containing 10% Heat-inactivated FBS, 50 µg/ ml gentamycin, 5 µg/ml Insulin, 10 ng/ ml EGF and 2% matrigel for HC11 cells. MDA-MB-231 cells were seeded at 25 000 cells/ml in DMEM media containing 10% FBS, 1% PS, 1% L-Glutamine, 1% non-essential amino acid. Cells were incubated in a 5% CO_2 incubator at 37 °C in the presence of humidity. The cell media was changed with 2% matrigel every 4 days.

2.14. Indirect Immunofluorescence staining of cells cultured in matrigel

To prepare the 3D cell cultures for immunofluorescent imaging, the medium was removed from the cells and immediately replaced with 2% PFA to fix the cells. These were incubated at room temp for 20 mins. The cells were permeabilised using 0.5% Triton X-100 (Sigma) in PBS and placed at $4^{o}C$ for 10 mins. Following this the cells were rinsed three times for 10 mins at room temp using a 100 mM Glycine in PBS solution. A 1 hr incubation in a blocking solution named immunofluorescence (IF) Buffer (PBS, 0.1% BSA, 0.2% Triton X-100, 0.05% Tween-20) took place at room temp. The cells were then incubated with the desired primary antibodies overnight at $4^{o}C$ using a dilution of 1:250

After three 20 min washes in IF buffer the cells were incubated with the secondary antibodies used at 1:250 for 1 hr at room temp. The cells washed a final three times for 20 mins each with IF buffer and once with water for 5 mins before mounting with Prolong Antifade Reagent (Molecular Probes) with DAPI staining of nuclei. The samples were left to dry at room temp overnight and then stored for a maximum of 1 week at $4^{o}C$.

2.15. Microscopy of cells grown in three dimension

Due to the glass bottom dishes being used, only inverted microscopes could be used for fluorescent imaging. Two inverted microscopes have been used, the first was a delta vision microscope and the second was an inverted confocal microscope. Images were acquired on a Delta Vision RT (Applied Precision) restoration microscope using a 60x/ 1.40 Plan Apo objective with oil immersion and the Sedat filter set

Chroma 86000. The images were collected using a Coolsnap HQ (Photometrics) camera with a Z optical spacing of 0.2µm. Raw images were then deconvolved using the Softworx software and maximum intensity projections of these deconvolved images are shown in the results. Alternatively, images were collected on a Leica TCS SP5 AOBS inverted confocal using a 63x/ 0.6-1.40 HCX PL Apo objective and 2x confocal zoom. The confocal settings were as follows, pinhole 1 airy unit, scan speed 1000Hz unidirectional, format 1024 x 1024. Images were collected using the following detection mirror settings; FITC 494-530nm*;* Texas red 602-665nm*;* Cy5 640-690nm using the 488nm (20%), 594nm (100%) and 633nm (100%) laser lines respectively. When it was not possible to eliminate cross-talk between channels, the images were collected sequentially. When acquiring 3D optical stacks the confocal software was used to determine the optimal number of Z sections. Only the maximum intensity projections of these 3D stacks are shown in the results. Images were viewed on LAS AF Lite software and exported as TIFF files to be analysed using ImageJ.

2.16. Transient transfection of siRNA for protein knockdown

HC11 cells were grown in either 6 well plates or 10 cm petri dishes for the purpose of protein knockdown using siRNA. Mouse Runx2 siRNA (sc-37146) was used for knockdown of Runx2, mouse PEBP2β siRNA (sc-37682) for CBFβ knockdown and mouse Runx1 siRNA (sc-37678) for Runx1 knockdown. A control siRNA-A (sc-37007) was used as a control for transfection using siRNA. For transfections in a 6 well plate, cells were seeded at 2 x 10^5 cells per well in 2ml of RPMI supplemented with 10% HI FBS, 5 µg/ml Insulin and 10 ng/ml EGF but no antibiotics. This was incubated for 18 hrs at 37° C and 5% CO_2 to reach 60-80% confluency. A solution

containing 6-8 µl of the siRNA duplex diluted in 100 µl of the transfection medium OptiMEM (Gibco) was prepared. A second solution containing 6-7 µl of the transfection reagent Oligofectamine (Invitrogen) was diluted in 100 µl of OptiMEM. These two solutions were mixed by pipetting the diluted siRNA into the diluted Oligofectamine reagent and incubated at room temp for 30 mins. The cells were washed with PBS and immediately a further 800 µl of OptiMEM was added to the solutions and overlaid gently onto the cells. The cells were incubated at 37° C at 5% CO_2 for 5 hrs before 1 ml of growth medium containing 20% HI FBS, 10 µg/ml Insulin and 20 ng/ml EGF was gently added to each well to give an overall 1x normal growth medium concentration.

For transfections in a 10 cm petri dish cells were seeded at 500 000 cells per petri dish in antibiotic-free media and incubated for 37° C and 5% CO_2. 33 µl of siRNA was diluted in 1225 µl of OptiMEM and 28 µl of Oligofectamine was diluted in 88 µl OptiMEM or as indicated. The two solutions were mixed as described previously and the cells were washed with warm PBS. 3 ml OptiMEM was overlaid onto the cells before the addition of the diluted siRNA/ Oligofectamine mix. The cells were incubated for 5 hrs 37° C and 5% CO_2 before the transfection mixture was mixed with 5 ml 2x growth media. In both cases the media was changed to 1x normal growth media after 24 hours.

2.17. 2D RNA extraction

Cells were pelleted in PBS and the RNA was extracted using a RNeasy mini kit (Qiagen) following the manufacturer's instructions. 10 µl of β-mercaptoethanol was added to 1 ml of the lysis buffer RLT. Each pellet was resuspended in 350 µl of this lysis buffer and equal volume of 70 % ethanol. The cell lysate was transferred into

Qiagen RNeasy mini spin columns and centrifuged at 12 000 RPM for 1 mins. The column was washed using 700 µl of buffer RW1 and then twice with 500 µl of Buffer RPE (wash buffer with ethanol). The RNA was eluted twice with 15 µl of RNase-free water each time to give a total volume of 30 µl of RNA sample.

2.18. 3D RNA extraction

6-well plates were lined with 500µl of 100% Matrigel per well and cells were seeded at 100 000 cells/ml per well in 2% Matrigel with 2 ml media per well for a period of 4 days. The cells were extracted from the Matrigel following the protocol as described by Lee at al. (Lee et al., 2007). The media was removed from the matrigel and was gently rinsed using PBS to remove residual media. 3 volumes of ice cold PBS-EDTA (5 mM Ethylene diamine tetra-acetic acid (EDTA), 1mM $NaVO_4$, 1.5 mM NaF in PBS) were added to each well and scraped to detach the matrigel containing cells. Three wells were combined to produce enough cells for one RNA extraction sample. Following 30 mins incubation at 4^oC with gentle rocking the cells were transferred into tubes and shaking resumed for 30 mins. Once all the matrigel was dissolved, samples were centrifuged at 3000 RPM for 2 mins at 4 ^oC. The supernatant was removed and the cells rinsed with a further 2 volumes of PBS-EDTA. Cells were centrifuged at 3000 RPM for 5 mins at 4 ^oC to pellet. Once the supernatant was removed, the cell pellet was treated to RNA extraction following the RNeasy mini kit (Qiagen) manufacturer's instructions.

2.19. Real-time reverse transcription-PCR

The expression levels of β-casein mRNA were analysed after stimulation of HC11 cells to lactate. Expression levels of Runx2, CBFβ, Runx1, IL11 and SOST were also analysed. RNA levels were measured using QuantiTect SYBR Green RT-PCR Kit (204243; Qiagen). The Biorad RT PCR machine (CFX-96 termocycler) was set to the following protocol; 30 mins at 50°C, 15 mins at 95°C, then 39 cycles of 15 sec at 94°C, 30 sec at 51°C, 30 sec at 72°C and finally 5 sec at 65°C. The following primers were used for polymerase chain reaction (PCR) amplification:

Primer Name	Forward primer (5'-3')	Reverse primer (5'-3')	Origin
GAPDH	GCACAGTCAAGGCCGAGAA	GCCTTCTCCATGGTGGTGA	M
RPLO	GGCGACCTGGAAGTCCAA	CCATCAGCACCACAGCCTT	H
β-casein	CTGTATCCTCTGAGACTGAT	GATGCTGGAGTGAACTTTAG	M
Runx2	AAATGCCTCCGCTGTTATGAA	GCTCCGGCCCACAAATCT	M
Runx2	AGCCCTCGGAGAGGTACCA	CGGAGCTCAGCAGAATAATTTTC	H
CBFβ	GTATGGGTTGCCTGGAGTTTGA	GTCTTCTTGCCTCCATTTCCTC	M
CBFβ	CTTAGAAAGAGAAGCAGGCGGAA	AACTCCAGACAGCCCATACCA	H
Runx1	TTGTCGGGCGGAGCGGTAGA	CTGGCACGGCCGGGTGAAAT	H
IL11	ACTTCCACCTCAGGACATCG	GGTGGTTAAAAGGACAGGCA	H
SOST	CCTCCTGAGAACAACCAGACC	TGTCAGGAAGCGGGTGTAGTG	H
MMP13	AAATTATGGAGGAGATGCCCATT	TCCTTGGAGTGGTCAAGACCTAA	H
Cytokeratin 7	CCGCCTCCCAGACATCTTTGAG	CCACATCCTTCTTCAGCACCAC	H
Snail	CCCCAATCGGAAGCCTAACT	GCTGGAAGGTAAACTCTGGATTAG	H
Slug	TTCGGACCCACACATTACCT	GCAGTGAGGGCAAGAAAAAG	H
Fibronectin	GAATAATCAGAAGAGCGAGCC	ACTCAGAAGTGTCCTGGAATG	H
Vimentin	AGCAGG AGTCCACTGAGTACCG	GTGACGAGCCATTTCCTCCTTC	H
Integrin α5β6	CTACCTGTGGTGACCCCTGTAAC	GCTTGGCCAGCTGCTGAC	H
MMP9	ACCACAACATCACCTATTGGATC	ACCAAACTGGATGACGATGTCT	H
Occludin	GAATTCAAACCGAATCATTG	ACTGAACCTGACCGTACATGAAGAAT TTCATCTTCTGG	H
Desmoplakin	GAAATATCTGGCAAACGAGACA	GCCAGCTGGAGCTCATAATC	H
E-Cadherin	ACAGCCCCGCCTTATGATT	TCGGAACCGCTTCCTTCA	H

Table 2.1. Primers designed for RT-PCR

M= Mouse. H=Human

2.20. Data analysis of RT-PCR using 2-ΔΔCT method

Quantitative Real Time PCR was performed on the cDNA synthesised and the data was analysed using the equation as described by Livak et al. (Livak and Schmittgen, 2001). The mRNA expression from the endogenous RPLO or GAPDH genes was used to normalise for differences in the amount of total RNA for each sample. All values were expressed relative to the RPLO expression in terms of fold increase or decrease. Each sample was expressed as the cycle threshold (C_T) which is the cycle number at which each PCR reaction reached a predetermined fluorescence threshold, set within the linear range of all reactions. The mean value of three replicates for each sample was calculated and expressed as the C_T. The gene expression of each sample was then calculated using the difference (ΔC_T) between the C_T value of the target gene sample and the mean C_T value of the endogenous control (RPLO or GAPDH). Relative expression was calculated as the difference ($\Delta\Delta C_T$) between the ΔC_T values of the test and control samples. The relative expression of the genes of interest was calculated and expressed as $2^{-\Delta\Delta CT}$. Data presented are presented as mean ± standard deviation (S.D.). Significant statistical differences were evaluated using Students T-test where differences of $P<0.05$ were considered statistically significant.

2.21. cRNA Microarrays

2.21.1. Preparation of RNA for microarray analysis

For microarray analysis, MDA-MB-231 cells stably knocked down for CBFβ using shRNA and a control stable MDA-MB-231 cell line transfected shNS (non-specific) were used (Mendoza-Villanueva, 2010; Mendoza-Villanueva et al., 2011). These cells were grown in a 3D matrigel system as previously described. Cells were

extracted from the matrigel (Lee et al., 2007). The RNA was then extracted from the cells using RNeasy Mini kit (Qiagen) according to the manufacturer's instructions. To confirm there was no DNA contamination, the RNA extracted was resolved on a 1% agarose gel at 90 V for 30 mins in 1x tris acetate, EDTA (TAE) buffer (40 mM tris acetate, 1 mM EDTA). The DNA was stained with ethidium bromide and visualized under an ultraviolet source.

2.21.2. Affymetrix microarray procedure

The microarray experiments were conducted by the microarray facility. The quality and size distribution of the RNA was assessed with the RNA Nano Lab on a Chip Kit (Agilent Technologies). First-strand cDNA was synthesised using 3µg of the supplied RNA with superscript II reverse transcriptase primed by a poly (T) oligomer (Invitrogen). Second strand cDNA synthesis was followed by an *in vitro* transcription reaction in which biotinylated CTP and UTP were incorporated into the generated transcripts. The products were fragmented to 200 nucleotides or less and 15 µg of the fragmented product was used to prepare 300 µl hybridisation cocktail [100 mM MES, 1M NaCl, 20 mM EDTA, 0.01% Tween-20, 0.1 mg/ml *Homo Sapien* DNA and 0.5 mg/ml acetylated BSA]. The cocktails were heated to 95°C and hybridised onto the Affymetrix GeneChip® Human Genome U133 Plus 2.0 Array (Affymetrix Inc, Cat. No. 900466) for 16 hours at 45°C. After hybridisation, arrays were washed at low (6x SSPE) and high (100 mM MES, 0.1 M NaCl) stringency and stained with streptavidin-phycoerythrin. Fluorescence was amplified by adding biotinylated anti-strepavidin and an additional aliquot of strepavidin-phycoerythrin stain. The GeneChip® Scanner 3000 7G (Affymetrix, Santa Clara CA) was used to

obtain intensity signal and quality data of the scanned arrays. Each microarray experiment was repeated as biological replicates for statistical robustness.

2.21.3. Statistical analysis of microarray data

Technical quality control was performed with dChip (V2005) using default settings (www.dchip.org) (Li and Wong). Background correction, quantile normalisation and gene expression analysis were performed using RMA in bioconductor (Bolstad et al., 2003). To establish relationships and compare variability between samples, principal components analysis (PCA) was used since this method is able to reduce the effective dimensionality of complex gene-expression space without significant loss of information (Quackenbush, 2001). PCA was performed with Partek Genomics Solution (version 6.5, Copyright 2010, Partek Inc., St. Charles, MO, USA). Two differential expression tests were performed of shNS MDA-MB-231 cells versus shNS MDA-MB-231 (one for each background), using Limma using the functions lmFit and eBayes (Smyth, 2004). Gene lists of differentially expressed genes were controlled for false discovery rate (fdr) errors using the method of QVALUE (Storey and Tibshirani, 2003).

In order to produce a heat map comparing 2D and 3D microarrays, a gene list of differentially expressed genes (971 probesets) was created by filtering for probesets with a q-value less than 0.05 and fold change greater than 2 in either test. This data set was segregated into 8 clusters based on similarity of expression profile across the dataset using a k-means clustering algorithm. Clustering was performed on the means of each sample group (log 2) that had been z-transformed (for each probeset the mean set to zero, standard deviation to 1). K-means clustering was done on the basis of similarity of profiles (Manhattan Distance) across the dataset using the

"Super Grouper" plugin of maxdView software (available from http://bioinf.man.ac.uk/microarray/maxd/)).

2.22. Electrophoretic Mobility Shift Assay (EMSA)

2.22.1. Generation of double stranded oligonucleotides

The generation of double stranded oligonucleotides for the desired sequences under investigation required the production of two complementary single-stranded oligonucleotides. These sequences were designed with an additional CAGT sequence at each 5' end. All oligonucleotides were purchased from Eurofins MWG Operon. The DNA sequences of the oligonucleotides used was as indicated in Table 2.1. The annealing reaction consisted on 1 µg of each single-stranded oligonucleotide into a total volume of 20 µ TE buffer (10 mM Tris HCl (pH 8.0), 1 mM EDTA). The reaction mixture was heated to 100°C for 3 mins then immediately transferred into a beaker containing 1.5 L of water 80°C and left to cool to room temperature. The annealed oligonucleotides were stored at -20°C.

Name	Oligonucleotide Sequence (5'-3')
Runx IL 11 s1	Sense: CAGTAGCCGGGTGTGGTGGCGCAC Antisense: CAGTGTGCGCCACCACACCCGGCT
Runx IL 11 s1 MUT	Sense: CAGTAGCCGGGTGACTTGGCGCAC Antisense: CAGTGTGCGCCAAGTCACCCGGCT
Runx IL 11 s2	Sense: CAGTACCTCTGTGCGGTGACGTCC Antisense: CAGTGGACGTCACCGCACAGAGGT
Runx IL 11 s2 MUT	Sense: CAGTACCTCTGTGACTTGACGTCC Antisense: CAGTGGACGTCAAGTCACAGAGGT
Runx IL 11 s3	Sense: CAGTCTTGCTCTGTGGTGAATCCC Antisense: CAGTGGGATTCACCACAGAGCAAG
Runx IL 11 s3 MUT	Sense: CAGTCTTGCTCTGACTTGAATCCC Antisense: CAGTGGGATTCAAGTCAGAGCAAG

Table 2.2. Oligonucleotides used for EMSA probes

2.22.2. Radiolabeling oligonucleotides

Klenow reaction was used for [α^{32}P] deoxyadenosine Triphosphate (ATP) radioactive labelling of double stranded oligonucleotides with 5' overhangs. The Klenow reaction contained 2µl of 0.1 µg/µl of double stranded oligonucleotides, 1 µl 10 nmol/unit klenow enzyme (Roche), 1 µl 2 mM deoxynucleotide-5'-triphosphate (dNTP) without deoxyadenosine-5'-triphosphate (dATP), 2 µl radiolabelled [α^{32}P] dATP with a final volume of 10 µl using distilled water. The Klenow mixture was incubated at 37 °C for 30 mins. The radiolabelled oligonucleotides were purified, by resolving the 10 µl Klenow mixture on a 10% non-denaturing polyacrylamide gel. This was resolved using 1x Tris Borate EDTA (TBE: 45 mM tris-borate, 1 mM EDTA) running buffer run at 30 mA for 2 hours. The radiolabelled oligonucleotides were excised using ultra violet (UV) bioluminescence and the gel slice immersed in 300 µl TE buffer overnight. The 300 µl TE buffer containing double stranded oligonucleotides was mixed with 1 ml ethanol, 30 µl Miniprep III [3M potassium acetate; 11.5% acetic acid] and 1 µl 20 mg/ml glycogen. The mixture was incubated at -80 °C for 1 hour and then centrifuged at 13,000 rpm for 10 mins. The pellet was washed with 100 µl of 70% ethanol and centrifuged at 13,000 rpm for 10 mins. The pellet was air dried for 10 mins and then dissolved in 50 µl TE buffer.

2.22.3. Electrophoretic Mobility Shift Assay

Nuclear extracts for MBA-MB-231 cells were prepared as previously described. The DNA-binding affinity of Runx2 protein was examined by EMSA using [α-32P] dATP radiolabelled DNA. The binding reactions contained 2 µl DZ buffer (25 mM HEPES pH 7.9, 20% Glycerol, 2 mM $MgCl_2$, 1 mM DTT, 0.1 µM $ZnCl_2$, 0.2 mM

EDTA), 3.75 µl 4xFPF (20 µM Spermidine, 23.5 µM EDTA), 1 µl polydeoxyinosinic deoxycytidylic acid (dI/dC) (250 µg/ml), 1 µl Bovine Serum Albumin (BSA) (20 mg/ml), 1.5 µl KCl (1 M), and 4-6 µl nuclear extracts which was adjusted with distilled water to a total volume of 15 µl. The binding reactions were pre-incubated at room temperature for 20 mins. 2 µl of ^{32}P-labeled double stranded DNA was added and mixed gently. The competition assay contained 20 times more unlabelled double stranded competitor DNA. For supershift experiments, monoclonal (2 µl) anti-Runx2 antibody (MBL, Little Balmer) was added to the final mixture. 2 µl of loading dye [20% Ficoll, 0.25% xylene cyanol, 0.25% bromophenol blue, 70 mM ethylene diamine tetra-acetic acid (EDTA), 4.6 mM Tris-Cl pH 6.8] was added to each sample. The DNA-protein complexes were resolved on a 5% non-denaturing polyacrylamide gel in 1x TBE running buffer and run at 21 mA for 3-4 hours. Gels were fixed in fixing solution [70% water, 20% methanol, 10% acetic acid] for 20 mins and dried under vacuum for 1 hour at 80 °C, before being visualized on a medical X-ray film (Fujifilm) or a phosphorimager screen (Biorad).

3.0 Runx2 is expressed throughout acini formation in HC11 cells

3.1. Introduction

The fundamental function of mammary glands is to lactate following parturition, in order to feed offspring. Regulation of mammary development requires many transcription factors which have different levels of expression throughout development. Some transcription factors which have a major role in mammary gland development are key players in breast cancer (Kouros-Mehr and Werb, 2006; Pensa et al., 2009). A wider knowledge of the role of transcription factors in the normal mammary gland development will enable a better understanding of the processes that are altered when compared to breast cancer cells.

The transcription factor Runx2 contributes to breast cancer metastasis. Runx2 expression has also been detected in normal mammary gland. Expression was first detected in nascent mammary gland epithelial cells (Otto et al., 1997a). Furthermore, Runx2 was one of the transcripts enriched in a microarray study of terminal end buds (Kouros-Mehr and Werb, 2006). These are formed at the early stages of branching in the breast. Runx2 is also expressed in the non-cancerous mammary cell line, HC11, where it contributes to the expression of the milk protein β-casein, which is ordinarily produced during lactation (Inman et al., 2005).

In order to achieve the end result of expelling milk from the breast, the cells within the mammary gland must differentiate and form specific structures. These structures contain cells that either produce the milk or help expel milk. These are called acini and are made up of spherical structures with a hollow lumen (Debnath et al., 2003). Culturing cells in the usual 2D method on petri dishes does not allow these structures to be formed. One method to produce a model more representative of the structures found *in vivo* is to grow the cells in a matrix, thus enabling them to differentiate in

3D. Thus, mammary cells grown in 3D are more likely to represent cells within the mammary gland structures. To date, the role of Runx2 in differentiated mammary epithelial cells has not been established. Therefore, the experiments described in this chapter aimed to determine the role of Runx2 in mammary epithelial cells when grown in 3D cultures.

The cell line of choice was HC11 cells. These are normal mouse mammary epithelial cells that are derived from the COMMA-1D cell line which were obtained from a mid-pregnant BALB/c mouse mammary gland (Danielson et al., 1984). This particular cell line was of interest as it has retained the ability to produce milk proteins upon induction with lactogenic hormones and was therefore the most suitable cell line available to determine the role of Runx2/CBFβ in normal mammary gland function (Ball et al., 1988) (Taverna et al., 1991).

3.2. Expression and localisation of Runx2/CBFβ in normal mammary epithelial cells

In order to determine the role of Runx2/CBFβ in HC11 cells it was first necessary to characterise the expression of Runx2 during cell growth and to establish if they express CBFβ. HC11 cells are only responsive to lactogenic stimulation once in a confluent state in cell culture. Thus the milk protein β-casein is only inducible after the HC11 cells have reached 100% confluency (Ball et al., 1988; Taverna et al., 1991).

In order to establish whether Runx2 is also restricted to expression in confluent cells or whether it is expressed prior to confluency, cells were lysed at both 100% confluency and at approximately 50% confluency. Total extracts of HC11 cells were subjected to western blot analysis using anti-Runx2 monoclonal antibody which detects mouse Runx2 at 55 kDa (Fig 3.1 A). The rat osteosarcoma cells UMR106 are known to express Runx2 and so were used as a positive control for Runx2 expression (Krishnan et al., 2003). HeLa cells do not express Runx2 and were used as a negative control. β-Tubulin was used as a loading control. The protein band was detected at 55 kDa in UMR106 and HC11 cells at 50% and 100% confluency. As expected, Runx2 was not detected in HeLa cells. These results show that Runx2 is expressed in HC11 cells in both 100% confluent and 50% confluent states. This confirmed the protein expression of Runx2 in HC11 cells and additionally showed that its expression is not dependent upon the confluent state of the cells.

To establish if HC11 cells express CBFβ, total cell extracts of HeLa, HC11 100% confluent and HC11 50% confluent were subjected to western blot analysis using anti-CBFβ polyclonal antibody which detects CBFβ at 22 kDa. HeLa cells were used as positive control for CBFβ expression (Figure 3.1 B). Protein bands were detected at approximately 22 kDa in all three lanes. HC11 cells showed a double band for CBFβ. This could be due to posttranslational modification of CBFβ. These data demonstrate that CBFβ is expressed in HC11 cells.

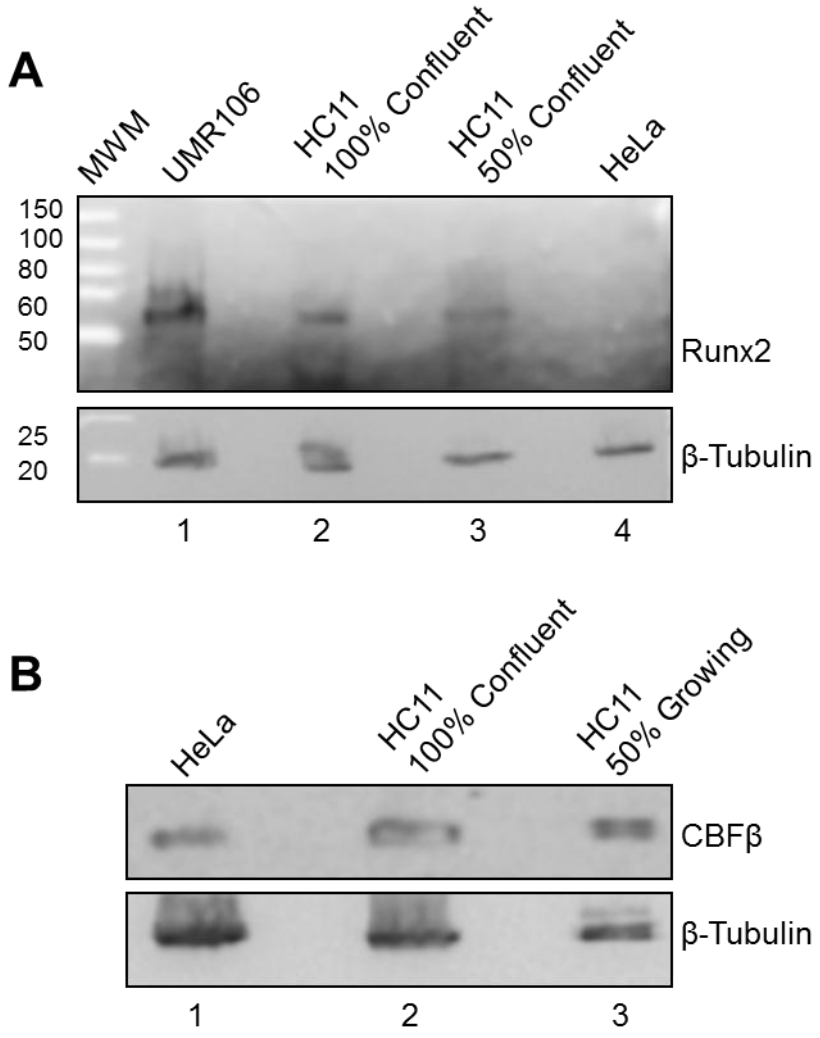

Fig. 3.1. HC11 cells express both Runx2 and CBFβ protein. (A) Western blot showing Runx2 protein expression in HC11 cells. Total cell extracts from normal mouse mammary epithelial cells (HC11) were grown to 100% confluency or approximately 50% confluency. The extracts were subjected to Western Blot analysis using anti-Runx2 monoclonal antibody (D130-3). Total cell extracts of UMR106 and HeLa cells were used as positive and negative controls respectively. (B) Western blot showing CBFβ expression in HC11 cells. Total cell extracts of mouse mammary epithelial cells, as described in (A), were subjected to Western Blot analysis with an anti-CBFβ polyclonal antibody. HeLa cells were used as a positive control for expression of CBFβ. In both (A) and (B), β-Tubulin was used as a loading control of protein into each lane.

Having confirmed the expression of Runx2 and CBFβ in HC11 cells their subcellular distribution was next examined. Nuclear and cytoplasmic fractions of cell lysates were prepared from confluent HC11 cells and subjected to western blot analysis using anti-Runx2 monoclonal antibody and anti-CBFβ polyclonal antibody. The integrity of the extracts was confirmed using antibodies for the nuclear and cytoplasmic markers Lamin B1 and β-Tubulin respectively (Goldman et al., 2005; Liu and Xu, 2006). Nuclear and cytoplasmic extracts of UMR106 cells and HeLa cells were used as positive and negative controls respectively for Runx2 expression. Runx2 was detected in nuclear extracts of UMR106 and HC11 cells but was absent from HeLa cells (Fig. 3.2). A similar analysis of CBFβ expression demonstrated that CBFβ was present in both nuclear and cytoplasmic extracts of UMR106 and HC11 cells but only in the cytoplasmic extract of HeLa cells. Together, these data demonstrate that Runx2 is nuclear and CBFβ is both cytoplasmic and nuclear in HC11 cells.

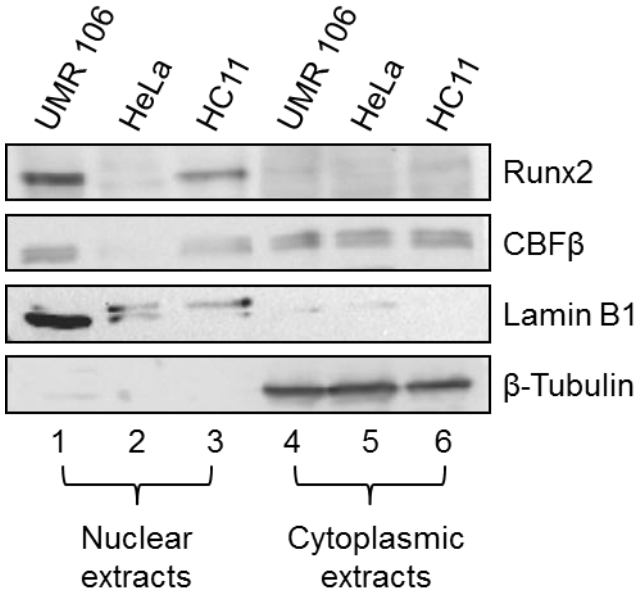

Fig. 3.2. In HC11 cells, Runx2 is nuclear and CBFβ is localised in both the nucleus and cytoplasm. Western blot of Runx2 and CBFβ protein expression after nuclear and cytoplasmic separation of HC11 cells. Nuclear and cytoplasmic extracts for normal mouse mammary epithelial cells (HC11) were subjected to western blot analysis using anti-Runx2 monoclonal antibody. UMR106 and HeLa nuclear and cytoplasmic extracts were used as positive and negative controls respectively, for Runx2 protein expression. Lamin B1 was used to confirm nuclear localisation. β-Tubulin was used to confirm cytoplasmic localisation.

3.3. 3D acini model using HC11 cells

The typical method of a monolayer cell culture technique is not representative of how the mammary epithelial cells grow naturally within the mammary gland. Having established that both Runx2 and CBFβ was present in the nucleus of confluent HC11 cells in traditional cell culture technique using cells grown in a monolayer, or 2-Dimensional (2D) cultures it was next sought to determine if this was also the case when the cells were grown in 3D cell culture.

The mammary gland is composed of many acini that are lined with milk secreting epithelial cells. These are spherical structures with a hollow lumen. The luminal epithelial cells are polarised so they have an outer basement membrane and an inner apical surface. These are defining features of acini. The hollow lumen is created as cells that do not have contact with the basement membrane undergo apoptosis (Fig. 3.3A) (Debnath et al., 2002). These structures cannot be formed in 2D culture but a 3D Matrigel system allows the growth of structures similar to those seen in mammary gland. HC11 cells have previously been grown in Matrigel and have formed acini structures (Xian et al., 2005). To confirm that HC11 cells can form acini structures 3D cultures were established using Matrigel.

Development of these acini required cells to be grown on a basement membrane preparation and can take between 10 to 21 days (Debnath et al., 2002). Therefore HC11 cells were plated onto glass bottom dishes covered with BD Matrigel Basement Membrane Matrix Growth Factor Reduced. This contains a solubilised basement membrane that contains many extracellular matrix proteins, such as laminin, collagen IV and heparin sulphate proteoglycans (Kleinman et al., 1982).

This matrigel also contains a variety of growth factors such as TGFβ and EGF (Vukicevic et al., 1992). HC11 cells were resuspended in a 2% dilution of matrigel and plated onto a layer of solidified matrigel. HC11 cells were grown in matrigel and formed 3D structures that had a spherical shape and hollow lumen (Fig. 3.3B). A distinctive feature of acini is apical-basal polarisation. The apical surface is that on the outer body, which is the inside lining of the hollow lumen. The basal surface is that on the other side away from the lumen. These polar surfaces have different protein markers. The basal surface contains laminins. Staining with anti-laminin α5 (green) showed protein localised to the outer membrane of the structure (Fig. 3.3B left panel). This indicates a basal surface.

The apical surface contains the phosphorylated proteins Ezrin/Radixin/Moesin (pERM) staining (green). Nuclei are stained using DAPI (blue). The antibody anti-pERM detects protein staining on the inner surface of the structure (Fig. 3.3B right panel). Taken together these data showed that HC11 cells formed a hollow lumen and were lined with separate basement membrane and apical surface. This indicates polarisation of the hollow lumen structure and thus confirms that HC11 cells form acini. Therefore, the basement membrane matrix provides a suitable environment for acini formation.

The acini are 3D structures with a hollow lumen rather than a cluster of cells. The images however could be interpreted as cells grown in a circular formation as opposed to a 3D structure. In order to determine whether a 3D structure with a hollow lumen has been formed images are required to be taken at different points along the z-stack. This can be achieved by using a confocal microscope. The schematic in Fig. 3.3C shows how the microscope would image the acini at different points at the z-stack to reveal a hollow lumen (Debnath et al., 2003). The images in

panel D of Fig. 3.3 have been taken using Delta vision microscopy as described in the methods. All images were of single acini taken at different points along the z-stack and correspond to the schematic diagram (Fig 3.3C). The actin cytoskeleton has been stained using Phalloidin (green) and DAPI staining (blue) was of the nuclei. Approaching from the top of the acini structure the cells form a small cluster. Moving along the z-stack through the acini reveals a wider birth of cells with a small opening in the centre of the cluster. At mid-point through the acini, the cells form a ring structure. Towards the bottom of the acini structure the cells close up once more. Thus a spherical cluster of cells has been formed in 3D with a hollow lumen within its centre.

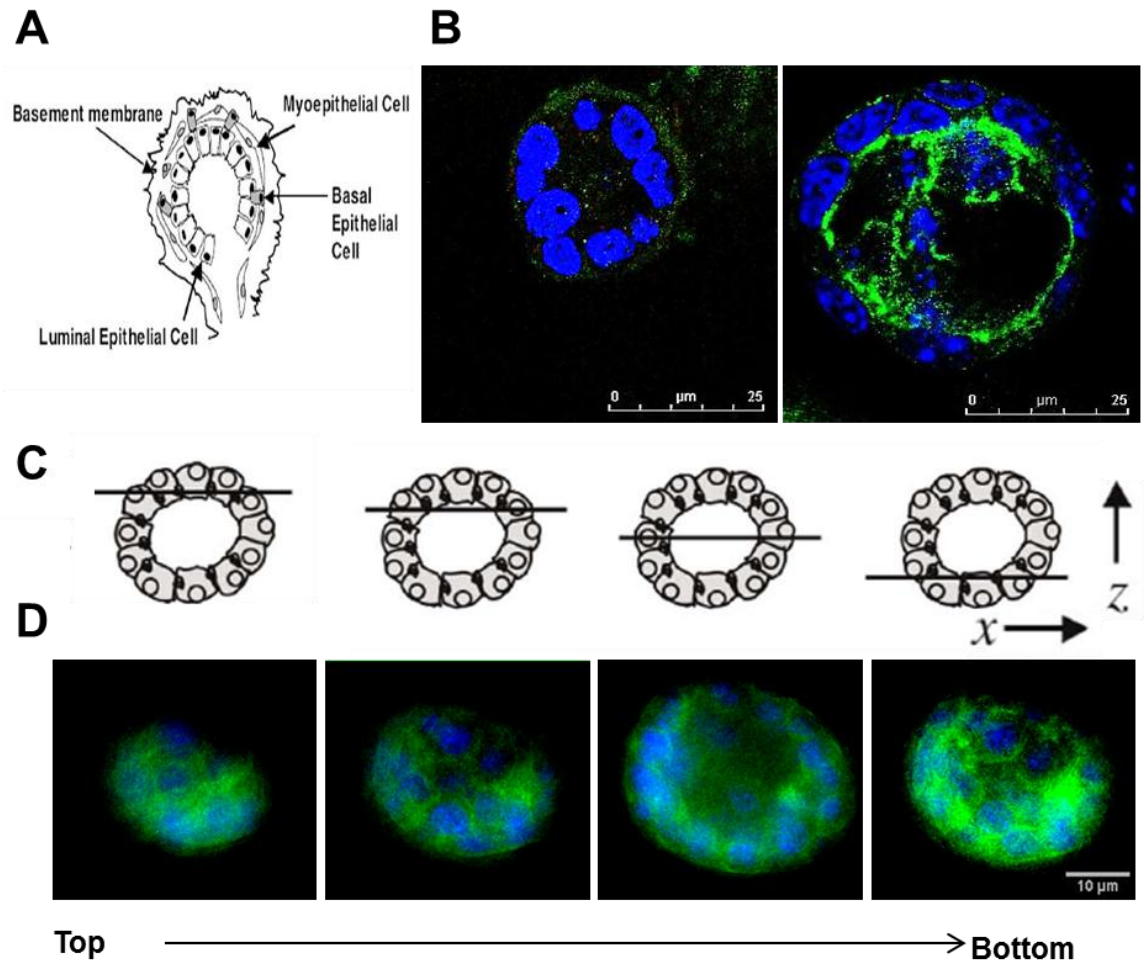

Fig. 3.3. Mouse mammary epithelial (HC11) cells form acini when grown in a 3D matrigel system. (A) Schematic diagram of acini in the mammary glands. Luminal epithelial cells are polarised around a hollow lumen and surrounded by basal epithelial and myoepithelial cells. Image adapted from (Debnath et al., 2003). (B) Immunofluorescence imaging of HC11 cells in a 3D matrigel system form polarised acini after 2 weeks growth. Left panel shows immunofluorescence microscopy of HC11 cells grown in matrigel to form 3D structures. Acini nuclei stained with DAPI (blue), basement membrane stained with laminin α5 (green). Right panel shows immunofluorescence microscopy of HC11 cells grown as in left panel. Apical surface stained with phospho Ezrin/Radixin/Moesin (pERM). Both images taken at x63 magnification with oil using Leica inverted confocal microscopy and one image from the mid-point of the z-stack is shown. (C) Schematic diagram of microscopy imaging taken at different points along the z-axis. Image adapted from (Debnath et al., 2003). (D) Delta vision images through the z-stacks of acini from top (left hand image) to bottom (right hand image) of acini. DAPI staining (blue), actin cytoskeleton stained green with Phalloidin (Invitrogen). Scale bars as indicated.

3.4. The development of 3D acini in vitro

Having shown HC11 cells can form 3D acini *in vitro*, we examined the development of these acini. In order for acini to form, a single cell suspension was required. These single cells develop into clusters and then acini. The development of the acini formation was imaged at regular intervals. The schematic diagram shown in Fig. 3.4 top panel show the development of acini in matrigel over 21 days (Debnath et al., 2003). At day 0 cells are singular and appear spherical in the matrigel. In the following days the cells proliferate and form clusters of colonies. After a week the cells reach the stage where they begin to polarise. The outer cells receive a survival signal from the surrounding basement membrane and the inner cells undergo apoptosis (programmed cell death). This eventually leaves a hollow lumen as is shown beyond day 10. Beyond day 14 the acini structures begin to form lobules. These are multi-acini structures that are bigger than individual acini and have many hollow luminal features. These are reminiscent of lobules that found within mammary glands.

HC11 cells were observed in 3D cultures at selected time points over a 21 day period. The images shown in the lower panel of Fig. 3.4 were of HC11 cells at different stages of development within the matrigel. At day 1, the cells were in single suspension. Thus the nuclear staining by DAPI was surrounded by the red Phalloidin staining of the actin cytoskeleton. By day 3, the cells formed a small cluster. At day 7, the cells began to polarise and a spherical structure developed. A hollow lumen was more pronounced by day 14. From day 14 the acini converge to form lobular structures and the image shown contained two visible hollow lumen structures.

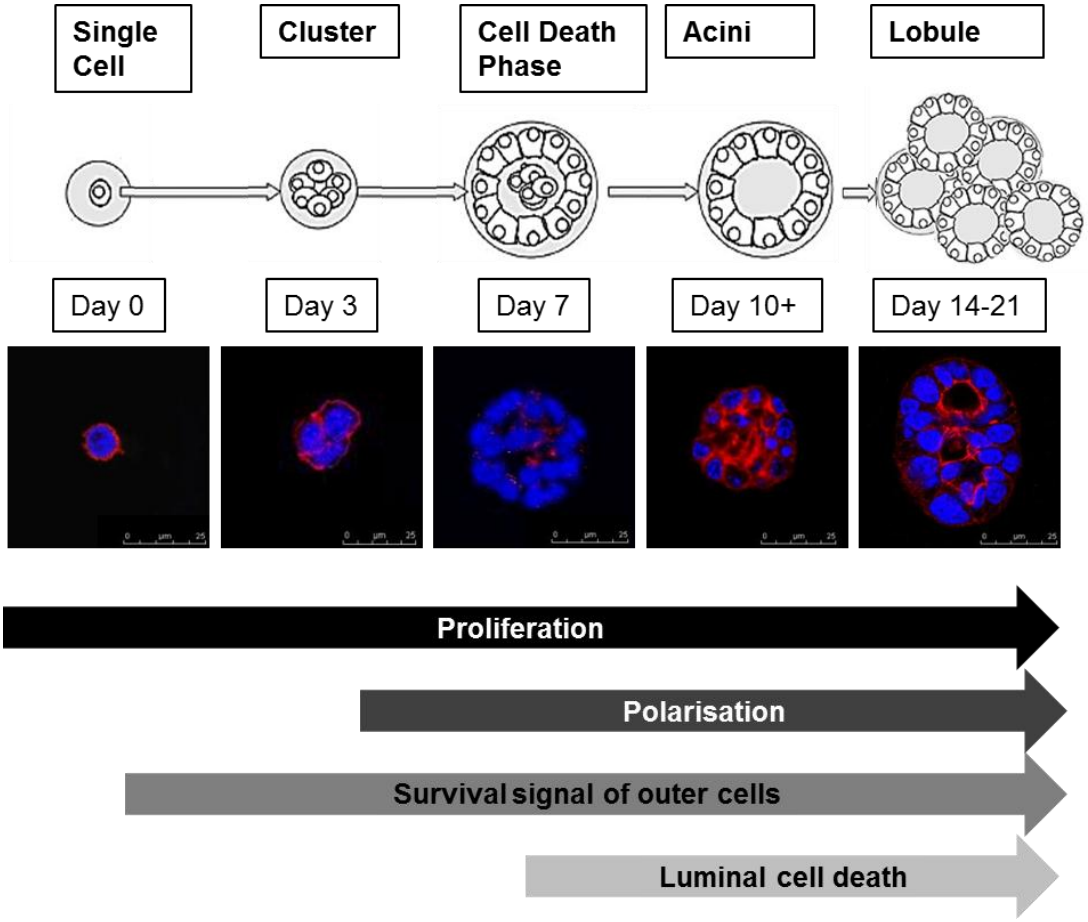

Fig. 3.4. Stages of acini development in a 3D matrigel system. Acini develop in stages within matrigel. The schematic diagram of the development stages for acini production was adapted from (Debnath et al., 2003). From left to right, the cells proliferated from single cells (Day 0) to clusters of cells (Day 3) and then polarised to form more spherical structures. Inner cells underwent apoptosis (Day 7). Acini were formed with a hollow lumen (Day 10). If incubated for longer than 10 days, lobular structures were formed (Day 14). Lower panel shows immunofluorescence images of mouse mammary epithelial (HC11) cells at different time point in acini development. Images taken using a Leica inverted confocal microscope at x63 magnification with oil. The actin cytoskeleton was stained with red Phalloidin and the DAPI staining was shown in blue. Images were taken at mid-point of the z-stack and merged using Image J. The arrows in lower section of figures indicated the time points of the different processes of acini formation. Scale bars were as indicated.

3.5. Immunofluorescence confirms localisation of Runx2

To determine the intracellular expression of Runx2 throughout the development of acini, immunofluorescence analysis was performed. In order to image Runx2 expression in HC11 cells grown in a 3D environment an antibody specific for Runx2 with little background expression was required. For this reason different antibodies targeting Runx2 expression were tested in HC11 cells grown in 2D (Fig. 3.5A). Three antibodies were used to probe for Runx2 protein in HC11 cells grown in a monolayer on coverslips. Cells were fixed and treated as described in the methods for monolayer immunofluorescence. In order to examine localisation of the Runx2 staining HC11 cells were stained for β-Tubulin and Lamin B1 for cytoplasmic and nuclear localisation respectively (Fig. 3.5B). The antibodies ab54868 and D130-3 were both monoclonal anti-mouse antibodies and were counterstained with the secondary antibody Alexa fluor 488 anti-mouse which gave fluorescence in the green spectrum. However the other three antibodies sc-10758 Runx2, β-Tubulin and Lamin B1 were all polyclonal anti-rabbit antibodies and the secondary antibody Alexa fluor 594 anti-rabbit antibody which emits red light was used. This was the only reason for the difference in colours shown in the left hand panels.

Fluorescent microscopy images showed that all three Runx2 antibodies detected Runx2 expression in the nucleus of the HC11 cells. The Runx2 antibody ab54868 showed the highest specificity for Runx2 with the least background staining in comparison to sc-10758 and D130-3. This was advantageous when investigating the subcellular localisation of Runx2 in cells grown in 3D and so was used in later experiments.

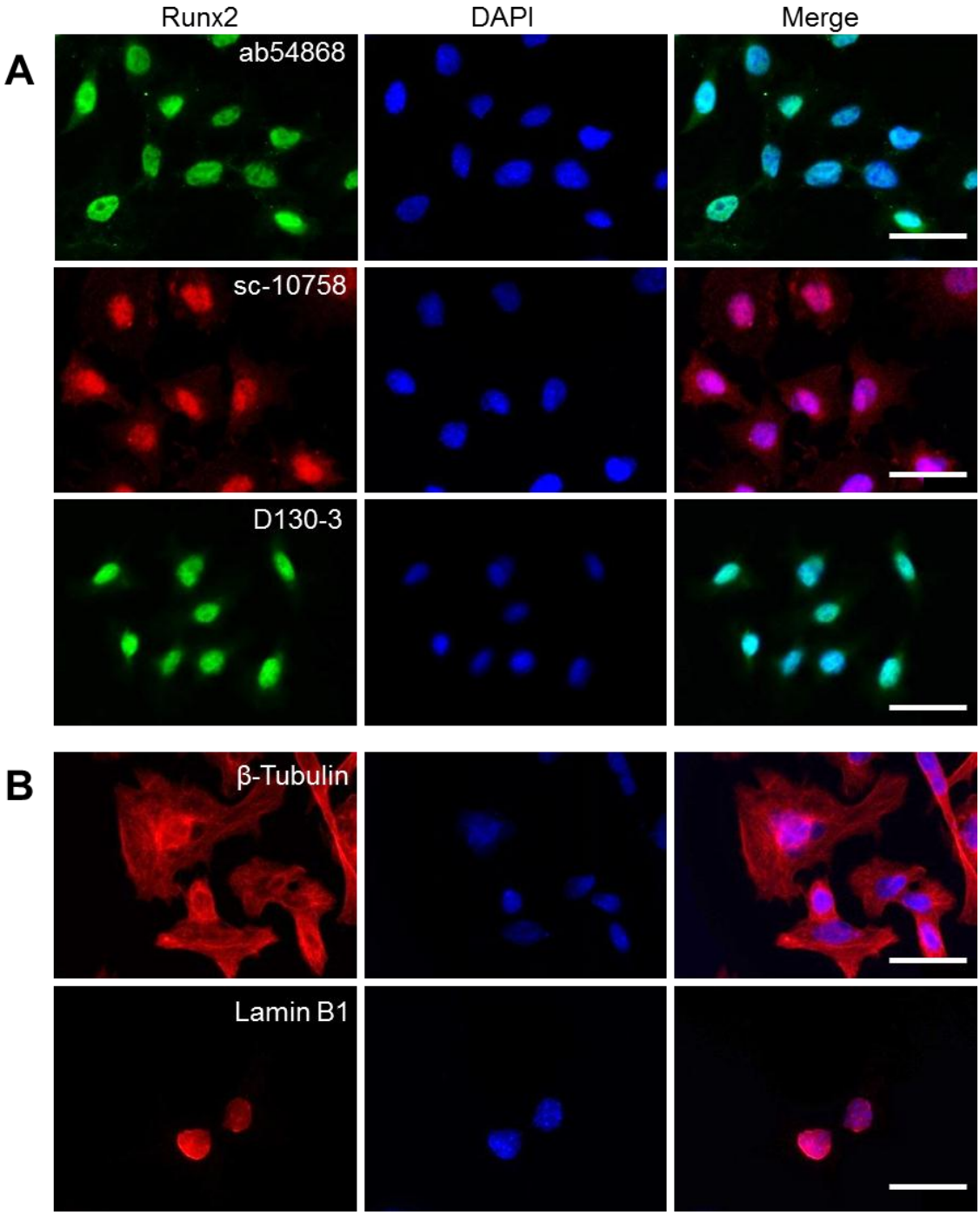

Fig. 3.5. Runx2 expression detected using Antibody ab54868 gave specific staining. (A) Immunofluorescence microscopy images of nuclear Runx2 protein expression in HC11 cells detected using different antibodies. Three different antibodies, ab54868 (Abcam), sc-10758 (santa cruz) and D130-3 (MBL) were used to detect Runx2 in HC11 cells. Left panels were Runx2 expression, middle panels were DAPI staining and right hand panels were merged images. (B) Immunofluorescence microscopy images in HC11 cells of cytoplasmic and nuclear markers. β-Tubulin (top panels) was used as a cytoplasmic marker and Lamin B1 (bottom panels) is a nuclear marker. Left panels were β-Tubulin or Lamin B1 markers, middle panels were DAPI staining and right hand panels were merged images. Images were acquired with an Olympus widefield microscope using a x60 objective with oil. Scale bars represented 50 µm.

The β-Tubulin and the Lamin-B1 staining acted as controls for antibody specificity by showing cytoplasmic and nuclear staining respectively. As an additional control for primary antibody specificity, the secondary antibodies used were stained for without the presence of a primary antibody (Fig. 3.6). The two secondary antibodies did not produce staining as seen with the Runx2 antibodies and so shows that the Runx2 antibodies were specific.

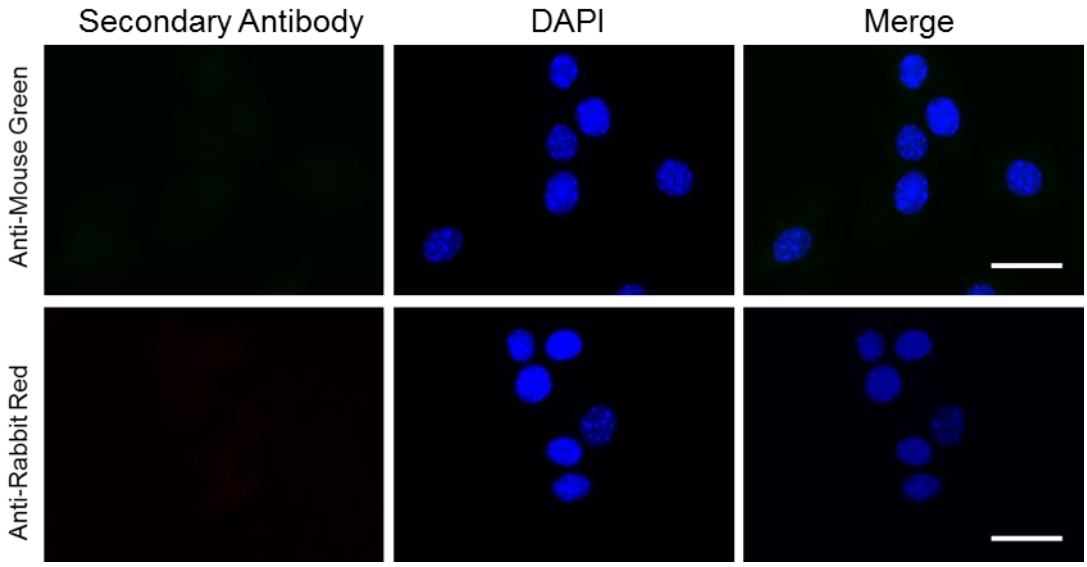

Fig. 3.6. Secondary antibody staining shows no specific staining. Immunofluorescence microscopy images of secondary antibodies only in HC11 cells detected using an anti-Mouse Green antibody and an anti-Rabbit-Red antibody. Left panels were secondary antibody expression, middle panels were DAPI staining and right hand panels were merged images. Images were acquired with an Olympus widefield microscope using a x60 objective with oil. Scale bars represented 50 µm.

3.6. Nuclear Runx2 expression is present throughout acini development

Mammary gland development requires the use of different transcription factors at different stages of development. To determine if Runx2 expression changes at different stages of acini development. immunofluorescence analysis was performed. The Runx2 antibody ab54868 (green) was used to detect Runx2 expression. Acini were also stained with Phalloidin (red) for the detection of cytoplasmic compartment. (Fig. 3.7). Significant Runx2 expression was detectable from day 1 after seeding and was maintained throughout all subsequent stages of acini development observed up to 14 days. Thus Runx2 is present within the nucleus before and after differentiation of the mammary epithelial cells.

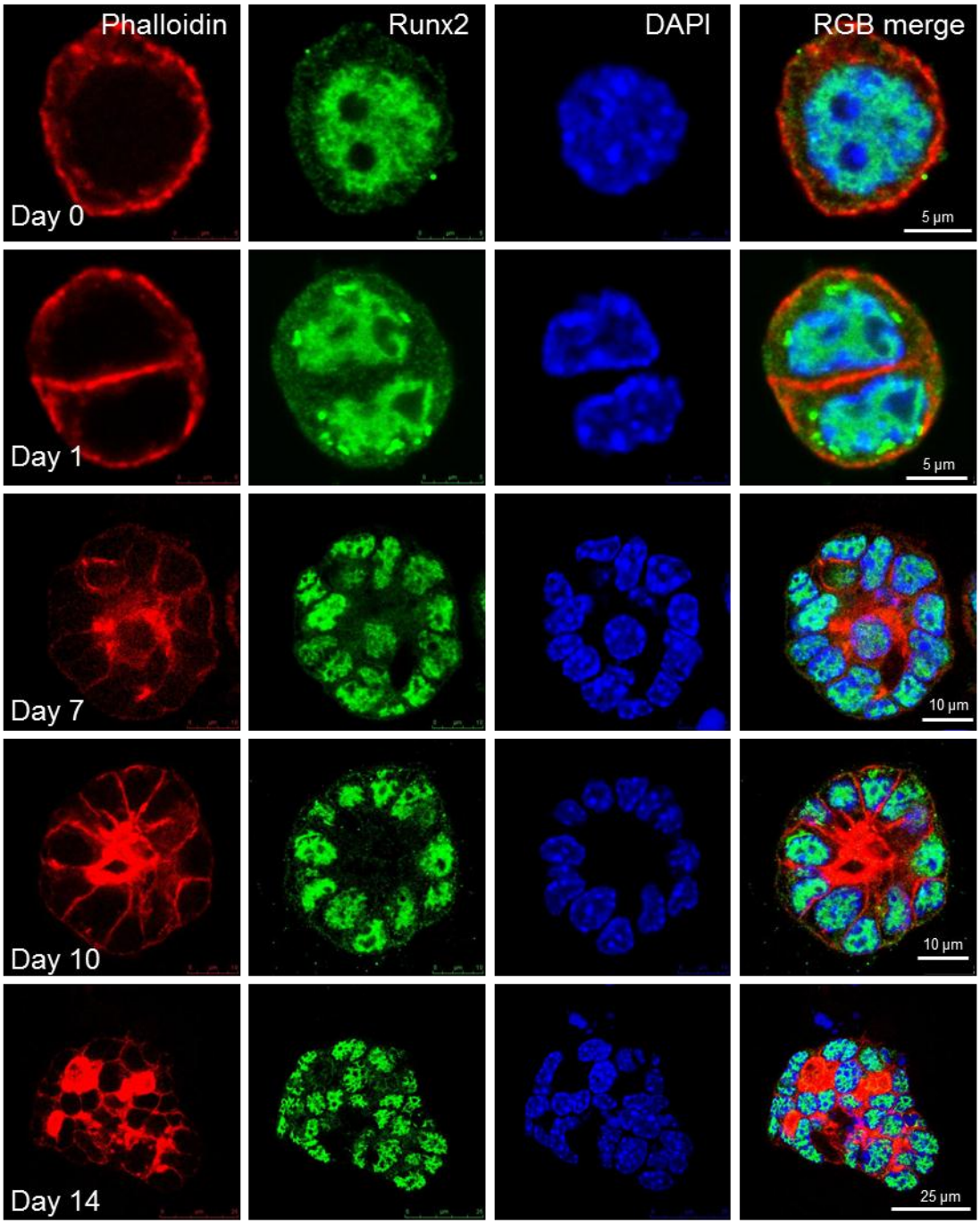

Fig. 3.7. Runx2 expression is nuclear throughout acini development. Immunofluorescence microscopy images of mouse mammary epithelial (HC11) cells incubated in matrigel to form 3D structures. HC11 cells were grown in 3D culture and were immunostained for Runx2 (Ab-54868) shown in green and phalloidin (red), for cytoplasmic detection, at different stages of development as indicated. Nuclei were stained with DAPI (blue). Equatorial cross sections shown. Images were taken using Leica inverted confocal microscopy at x63 magnification with oil and images were processed using image J. Scale bars as indicated.

3.7. Runx2 in hormonal induction of gene expression in mammary acini structures

Previous studies have already established that Runx2 is required for lactogenic hormone-induction of β-casein in 2D cultures (Inman et al., 2005). However, to date a role for Runx2 in the mammary gland *in vivo* has not been established. Therefore the aim was to establish if Runx2 was required for hormonal induction of gene expression in acini, which are more representative of mammary epithelial cells *in vivo*. The ultimate objective of these experiments was to establish a Runx2 deficient HC11 cell line to determine the role of Runx2 in hormone-induced gene expression in 3D cultures. However, as will be described here, it was discovered that transfection of control siRNAs affected hormone induction.

To obtain successful knockdown of Runx2 expression the effectiveness of siRNAs was determined in 2D cultures. HC11 cells were transfected with either a non-specific (NS) siRNA or siRNA targeted to Runx2 knockdown. As a further control untransfected HC11cells (wild type (WT)) were also used. Following a 2 day or a 3 day transfection period, whole cell extracts were subjected to western blot analysis using anti-Runx2 monoclonal antibody (Fig 3.8).

At 2 days post transfection, western blot analysis using anti-Runx2 antibody detected a band in the WT HC11 cells and those treated with NS siRNA. A weak band was seen in cells transfected with Runx2 siRNA. The same result was observed in cells 3 days post transfection. As a loading control the β-Tubulin was used. These results showed that Runx2 siRNA specifically knocked down Runx2 protein and this knockdown persists up to 3 days post transfection.

Having established that Runx2 could be efficiently knocked down the next objective was to confirm whether β-casein expression could be induced in HC11 cells by incubation with prolactin and dexamethasone (Ball et al., 1988). HC11 cells were stimulated with prolactin and dexamethasone 12, 24 and 36 hrs. These three different time points were used to determine the most suitable stimulation time in relation to the 2 to 3 day knock down of Runx2 protein by siRNA. As a control for incubation, HC11 cells were simultaneously grown in normal media (unstimulated). RNA was extracted and analysed by RT-PCR real time testing β-casein mRNA expression. GAPDH was used as a control for mRNA expression. Results showed that cells which were stimulated had an increase in β-casein mRNA production at all three time points (Fig. 3.8 B). This was significantly higher than the unstimulated HC11 cells ($n=3$, $p<0.5$). Thus, HC11 cells were successfully stimulated to express β-casein and this increase in β-casein expression was approximately 2000 fold higher after just 12 hours.

This increase in β-casein mRNA after just 12 hrs was an important factor as the siRNA transfection was transient; meaning the knockdown of Runx2 protein was time limited. This transient nature of the siRNA has previously been confirmed. Having observed Runx2 knockdown at 2 days post-transfection, the cells could then be stimulated for 12 hours. Therefore, lactogenic stimulation in the absence of Runx2 was conducted.

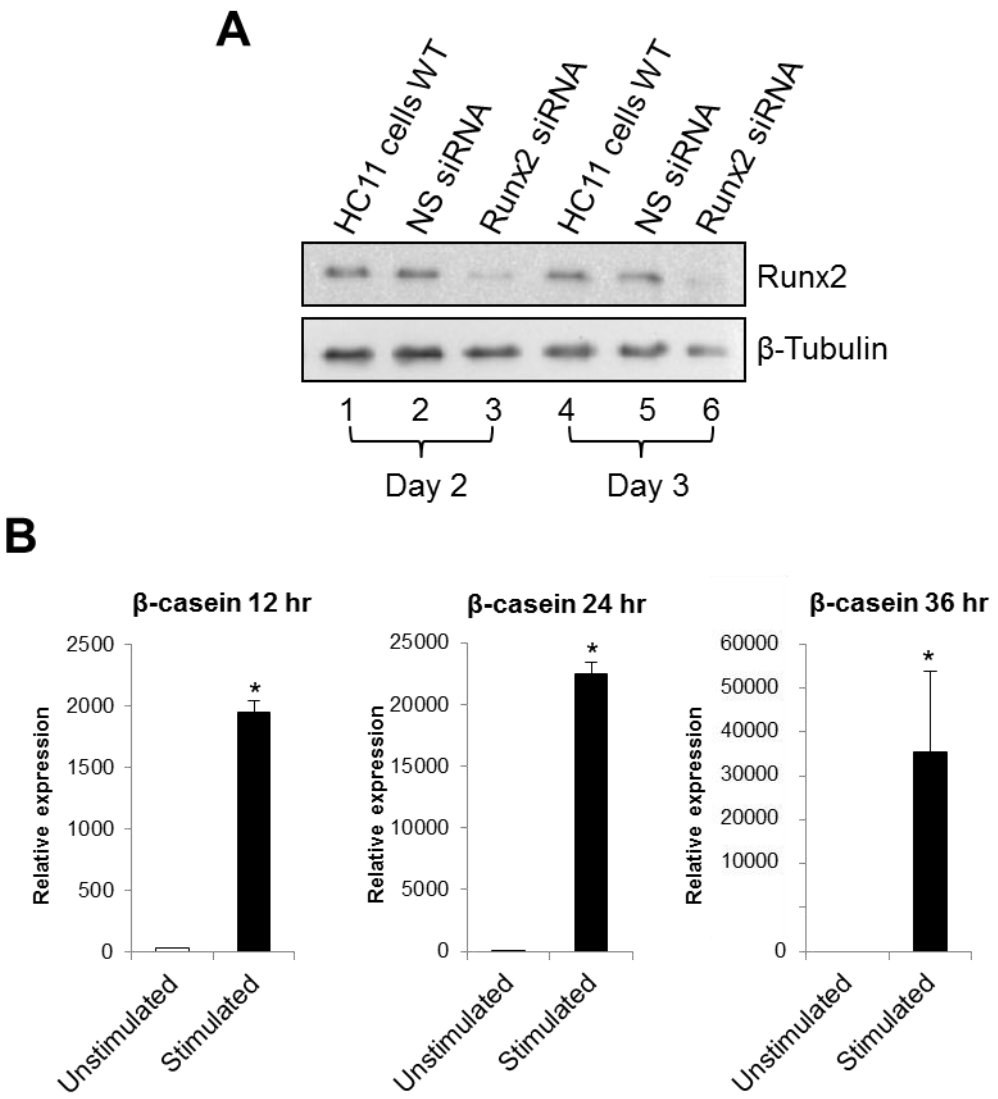

Fig. 3.8. siRNA knockdown of Runx2 in mouse mammary epithelial (HC11) cells and establishing β casein mRNA detection at different time points. (A) Western blot showing Runx2 knockdown in HC11 cells using targeted siRNA. Whole cell extracts of HC11 cells wild type (WT), HC11 cells transfected with non-specific (NS) siRNA or Runx2 siRNA to knockdown Runx2 were subjected to western blot analysis using a mono-clonal Runx2 antibody (MBL). Cells were incubated for 2 days post transfection (lanes 1-3) or 3 days post transfection (lanes 4-6). β-Tubulin was used as a loading control (bottom panel). (B) RT-PCR of β-casein mRNA expression in HC11 cells shows expression can be detected as from 12 hours post stimulation. HC11 cells were either untreated (unstimulated) or treated with prolactin and dexamethasone (stimulated). RNA extraction was carried out 12, 24 or 36 hours later, as indicated. Data represents the mean of the samples tested in triplicate for RT-PCR real time normalised against GAPDH. Error bars shown represent standard deviation. * indicates a significant difference ($n=3$, $p \leq 0.05$).

3.8. The effect of lactogenic hormones on β-casein expression in Runx2 depleted HC11 cells.

Having shown that HC11 cells can be stimulated to express milk and that Runx2 can be effectively depleted in these cells, these conditions were then combined in order to determine the effect of lactogenic hormones on the induction of β-casein in the presence and absence of Runx2. HC11 cells were transfected with NS siRNA, Runx2 siRNA or left untransfected (WT). Cells were incubated for 24 hours post transfection and then treated with prolactin and dexamethasone to induce β-casein production. 48 hours post transfection the cells were collected for RNA extraction and RT-PCR for β-casein mRNA analysis (Fig. 3.9A). WT HC11 cells treated with prolactin and dexamethasone showed a significant increase compared to unstimulated cells, which was as expected. HC11 cells transfected with NS siRNA showed no β-casein mRNA expression in either the stimulated or the unstimulated cells. HC11 cells transfected with Runx2 siRNA showed no β-casein mRNA expression in either the stimulated or the unstimulated cells. These results show that the NS siRNA was affecting the milk production capability of the HC11 cells.

Considering that the non-specific siRNA could be having an off target effect and may have been targeting an important component of the milk production process a different siRNA was used. In this case a siRNA known to target a gene sequence not present in HC11 cells was chosen. This protein was Green Flourescent Protein (GFP). Cells were transfected and treated as previously described. Results showed that WT HC11 cells treated with prolactin and dexamethasone once again showed a significant increase in β-casein expression compared to unstimulated cells. HC11 cells transfected with NS siRNA (control siRNA-A) showed no β-casein mRNA

expression in either the stimulated or the unstimulated cells. HC11 cells transfected with GFP siRNA showed no β-casein mRNA expression in either the stimulated or the unstimulated cells (Fig. 3.9B). These results showed that the siRNA transfection itself was responsible for the loss of milk production following stimulation.

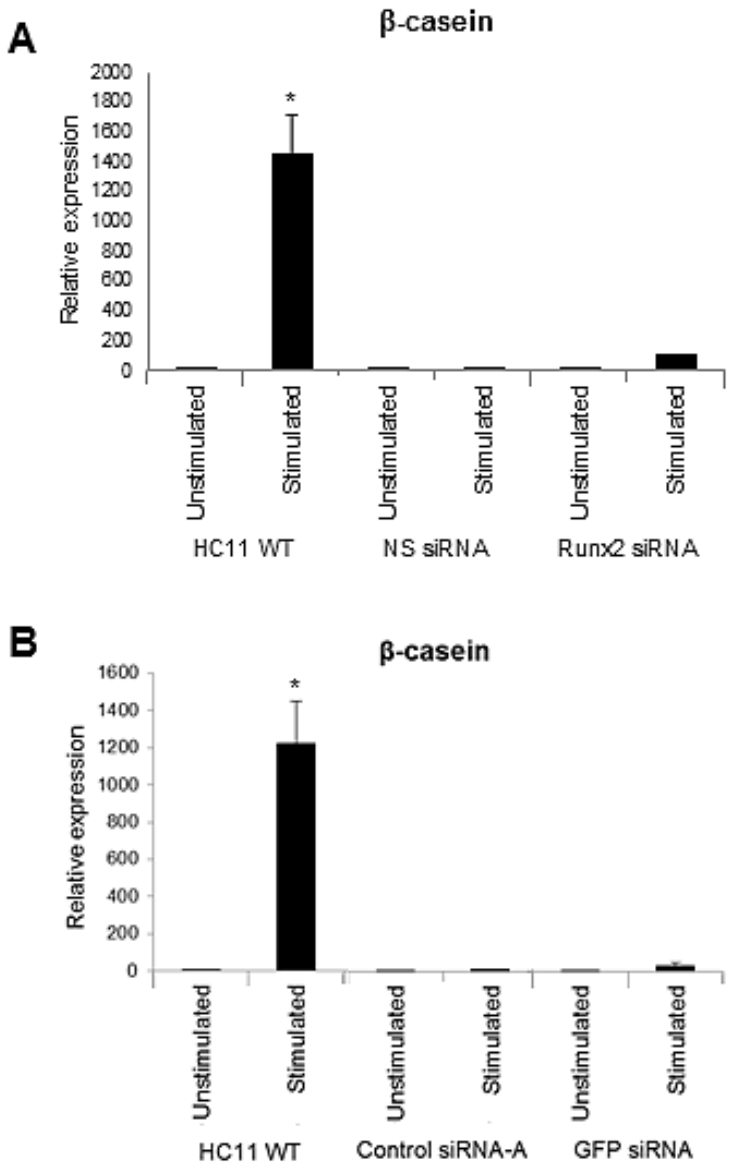

Fig. 3.9. siRNA transfection disrupts β-casein stimulation by prolactin and dexamethasone. (A) RT-PCR of mouse mammary epithelial (HC11) cells transfected with siRNA. RNA extracts for HC11 cells wild type (WT) and HC11 cells transfected with either a non-specific (NS) siRNA cells or siRNA targeted to Runx2 were either untreated (unstimulated) or treated with prolactin and dexamethasone (stimulated) for milk production. RT-PCR is of β-casein mRNA expression normalised against GAPDH. (B) RT-PCR of HC11 cells with control siRNA. Whole cell extracts for HC11 cells wild type (WT) and HC11 cells transfected with either a non-specific (control siRNA-A) siRNA cells or siRNA targeted to GFP (GFP siRNA) were either untreated (unstimulated) or treated with prolactin and dexamethasone (stimulated) for milk production. Data represent the mean of the samples tested in triplicate for RT-PCR real time. Error bars shown represent standard deviation. * indicated a significant difference ($n=3$, $p \leq 0.05$).

3.9. Discussion

The data presented in this chapter demonstrates that Runx2 protein is expressed in normal mammary epithelial cell line HC11. CBFβ protein expression is shown for the first time in HC11 cells. Runx2 expression is nuclear, while CBFβ is both nuclear and cytoplasmic. HC11 cells can be grown in 3D to form spherical acini structures. The development of these acini can be seen over a 2 week period. Staining of these acini through their development, using the previously confirmed antibody shows Runx2 is nuclear throughout development. HC11 cells can be stimulated to produce the milk protein β-casein. Runx2 protein can be knocked down in HC11 cells using siRNA. However, the use of siRNA seems to affect the ability of HC11 cells to produce β-casein.

3.9.1. Runx2 and CBFβ are expressed in normal breast epithelial cells

Runx2 was initially discovered as a regulator of bone formation and so has been broadly studied in bone cells, reviewed in (Marie, 2008). Runx2 has also been detected in nascent mammary epithelial cells (Otto et al., 1997a). The HC11 cells are a normal mouse mammary epithelial cell line (Danielson et al., 1984). This cell line has previously been used and has shown Runx2 expression (Inman and Shore, 2003). This chapter has confirmed the expression of Runx2 in HC11 cells and has now found that Runx2 is localised to the nuclear compartment of HC11 cells grown in monolayer cell culture. This nuclear localisation of Runx2 has been confirmed by using nuclear and cytoplasmic extracts of HC11 cells and additionally with immunofluorescence using three different antibodies for Runx2.

Runx proteins heterodimerise with CBFβ (Bartfeld et al., 2002). CBFβ has already been reported to be expressed ubiquitously in all tissues, but its protein expression has not been shown in HC11 cells (Komori et al., 1997). Therefore CBFβ expression in HC11 cells was tested by western blot analysis and expression was successfully detected. Furthermore, nuclear and cytoplasmic extracts of HC11 cells found CBFβ was present in both the nuclear and cytoplasmic compartments. This cytoplasmic expression is consistent with previous reports (Kanno et al., 1998b; Tanaka et al., 1997). The role of CBFβ within the cytoplasm is currently unknown although it has been elucidated that CBFβ is located in the cytoplasm and then translocates to the nucleus by Runx proteins (Adya et al., 1998). One study has shown CBFβ binds with an actin-binding protein called Filamin A which retains CBFβ within the cytoplasm (Yoshida et al., 2005).

3.9.2. HC11 cells form 3D acini structures when cultured in basement membrane matrix

With the intention of creating a more representative *in vitro* model system for cellular structure in the mammary gland, it was endeavoured to create 3D cell culture of HC11 cells. The 3D cell culture of mammary epithelial cells has previously been conducted using different cell lines such as MCF10A cells, which are normal human mammary epithelial cells, and MDA-MB-231, which are human breast tumour cells (Debnath et al., 2003) (Pratap et al., 2009). Acini have also been previously cultured using HC11 cells to study expression of fibroblast growth factor (Xian et al., 2005). This shows acini formation *in vitro* has previously been used as a model system for protein expression. Using Matrigel basement membrane matrix, HC11 cells formed

acini *in vitro* and could be identified as such by the characteristic polarisation of the cells, the formation of a hollow lumen and the presence of a basement membrane (Fig 3.3 B).

The development of these acini was imaged from the single cell stage. The cells were seen to undergo proliferation to form small clusters of cells and then larger clusters. The cells on the inner segment of the cluster underwent apoptosis and a hollow lumen structure was seen. Further growth in matrigel allowed for lobular structures to be formed.

Having successfully demonstrated acini production *in vitro*, the HC11 acini could then be tested for Runx2 expression. Runx2 has previously been detected in human mammary epithelial cells, in both normal and cancer cell lines, grown in 3D (Pratap et al., 2009). There is no published data at present on Runx2 expression in HC11 cells cultured in 3D to form acini. Various antibodies were first tested in order to confirm Runx2 could be detected specifically and with little background as it would need to be detected through matrigel in acini structures. Of the antibodies tested, the antibody ab54868 showed to be most appropriate for further use.

3.9.3. Runx2 localisation is nuclear throughout acini development

Previous studies have demonstrated the various changes that take place during acini development (Debnath et al., 2003). These changes have been demonstrated in this study and been categorised at the different stages seen as clustering, cell polarisation and formation of a hollow lumen. These stages in development of acini were then used to study Runx2 localisation through acini formation.

Runx2 is not detected in the non-transformed breast cell line, MCF10A (Pratap et al., 2009). Yet there is detection of Runx2 in HC11 cells which are from the normal breast of a pregnant mouse. This shows Runx2 expression does change in mammary development and this is expected as mammary gland requires many different transcription factors at the various stages of development (Cowin and Wysolmerski, 2010; Howlin et al., 2006; Watson and Kreuzaler, 2011). Thus, as cells in acini development undergo changes in order to form a hollow lumen, there may be changes in Runx2 expression in the development of the acini, particularly when the acini begin to polarise (Danielson et al., 1984) (Richert et al., 2000).

Using a 3D immunofluorescence technique to stain for proteins in cells embedded within the matrigel, Runx2 was stained for at various stages of acini development. At all stages tested (Day 0, 1, 7, 10, and 14) Runx2 staining was detected and this expression was localised to the nucleus of the cells in all stages. This shows that the presence of Runx2 in the mammary cells does not prevent the formation of acini. Such an expression would be necessary in both pregnant and lactating breast if Runx2 is required for milk protein regulation (Inman et al., 2005).

This expression of Runx2 in acini structures is also interesting because metastatic breast cancer cells, MDA-MB-231, have an overexpression of Runx2 and are not able to form acini type structures in a 3D matrigel system (Pratap et al., 2009). Mutation of Runx2 in MDA-MB-231 cells induces the formation of acini structures. In addition, breast cells (MCF10A) express undetectable levels of Runx2 and form acini in matrigel (Pratap et al., 2009). Ectopic expression of Runx2 in MCF10A cells disrupts formation of acini (Pratap et al., 2009). This suggests that it is the level of Runx2 expression that may be a key factor in acini development as opposed to the presence of Runx2 expression. Perhaps a threshold level exists after which point

acini development would be disrupted and this threshold may be altered at different stages of development. It would be interesting therefore to overexpress Runx2 in HC11 cells and observe whether acini development still occurs. Conversely, a stable Runx2 knock down of HC11 cells may therefore also result in a loss of acini development.

3.9.4. siRNA treatment prevents production of milk protein β-casein in HC11 cells

The research conducted in this chapter has shown HC11 grown in monolayer can be induced to produce β-casein following stimulation with prolactin and dexamethasone. There are three regulatory domains in the β-casein promoter region, named blocks A, B and C. Blocks A and B are well characterised and are both activated by Stat5 and GR. Our laboratory has shown that block C contains a Runx2 binding site and that Runx2 is recruited to this by Oct1, another transcription factor that has a DNA binding site adjacent to that of Runx2 (Inman et al., 2005). This site had already been shown to be important for β-casein activation as mutations in this site stop β-casein activation (Saito and Oka, 1996). Inman and Shore verified Runx proteins could be recruited to this β-casein promoter and in addition that it was important for β-casein activity using EMSA and luciferase. EMSA using anti-Runx2 antibody showed Runx2 binds to this site. Transfecting HC11 cells with a reporter plasmid containing either a WT β-casein Runx sequence or a mutated sequence, together with siRunx2 showed a decrease in β-casein activity (Inman et al., 2005). However, what has not previously been shown is whether knockdown of endogenous Runx2 does in fact lead to a reduction of endogenous β-casein. Therefore, the aim of

this chapter was to knockdown endogenous Runx2 using siRNA and then measure β-casein mRNA levels.

As shown in this chapter, the HC11 cells can be successfully stimulated to produce β-casein via prolactin and dexamethasone induction. The knockdown of Runx2 using targeted siRNA successfully reduced the mRNA expression of β-casein. This knockdown was still present at 48 and 72 hours post transfection, while β-casein stimulation is visible from 12 hours. Therefore, HC11 cells can be knocked down for Runx2 and then stimulated for β-casein stimulation.

When HC11 cells were transfected with siRNA targeted to Runx2, there was a decrease in β-casein mRNA activation. This is as expected as the β-casein promoter requires Runx2 binding for activation (Inman et al., 2005). However, this effect was also observed in the NS siRNA transfected cells. This is siRNA that is not targeted to any protein sequence. However, following transfection with NS siRNA there was no β-casein activation in either hormone unstimulated or stimulated HC11 cells. Some NS siRNA's have been known to have off target effects (Jackson and Linsley, 2004). For this reason, a new control NS siRNA which had a different sequence and a GFP containing plasmid was transfected. Both of these control siRNA showed a loss of β-casein mRNA up-regulation following hormone stimulation. This suggests that the loss of β-casein up-regulation is not due to the sequence for which the siRNA is targeted but due to the transfection procedure itself. For this reason a different transfection reagent was used, however the outcome was the same (data not shown). In addition, due to the negative effects of siRNA, a stable cell line for HC11 cells with Runx2 knockdown was created using shRNA Lentiviral infection. While this stable cell line did show Runx2 knockdown initially, the expression of Runx2 was rescued endogenously within a few passages and so the cell line could not be used to

experiment with (data not shown). The same result was seen in another cell line conducted by another PhD student.

It was therefore decided not to further pursue this line of research. Yet there were many points of interest within this chapter. In terms of technique, the 3D cell culture method was optimized and shown to be a useful tool.

4.0 Knockdown of CBFβ in MDA-MB-231 cells results in MET

4.1. Introduction

Breast cancer, the most common cancer in women worldwide, cannot be cured when it progresses to advanced stages. This is because last stage breast cancers metastasise out of the breast. In 85% of cases, this metastasis occurs to bone (Coleman, 2001; Paget, 1889). The mechanism for this preferential metastasis of breast cancers to bone is not currently understood. However, one theory for this is that the bone microenvironment provides an ideal source of nutrition for colonisation and proliferation.

In order to metastasise, breast cancer cells must undergo changes to gain properties such as invasiveness and loss of cell-cell adhesion. Genes known to be required for invasion of cells are MMP9 and MMP13 (Johansson et al., 2000). These are downstream targets of the Runx2/CBFβ complex (Hess et al., 2001; Javed et al., 2005; Pratap et al., 2005). Thus, this indicated a role for Runx2/CBFβ in metastatic breast cancer cell invasion and is confirmed by knockdown studies of Runx2 which resulted in a reduction of invasive capacity of the metastatic breast cancer cell line MDA-MB-231 (Mendoza-Villanueva et al., 2010; Pratap et al., 2005).

Preventing breast cancer cells from moving out of the breast is of great importance as it is at this stage that it can no longer be cured. Therapeutic targets are required which result in a loss of invasion. Considering Runx2 knockdown resulted in a reduction of invasion, Runx2 target genes and co-factors are of particular interest. One such target could be its heterodimeric partner, CBFβ. Knockdown of CBFβ alone in MDA-MB-231 cells also resulted in reduced invasive capacity (Mendoza-Villanueva et al., 2011). Therefore, the aim of this chapter was to identify the potential involvement of CBFβ in the invasion of metastatic breast cancer cells.

4.2. CBFβ knockdown in metastatic breast cancer cells results in an altered morphology

Runx2 requires CBFβ to achieve a greater DNA binding affinity, resulting in higher target gene expression (Adya et al., 2000). Therefore, loss of CBFβ would result in a decrease in Runx2/CBFβ target genes. This could explain why both Runx2 and CBFβ independently knocked down in MDA-MB-231 cells resulted in a loss of invasion (Mendoza-Villanueva et al., 2010). Therefore, considering that depletion of Runx2 in MDA-MB-231 cells resulted in cluster formation when grown in 3D, it was hypothesised that depletion of CBFβ in MDA-MB-231 cells would also result in similar phenotypic change when grown in 3D (Pratap et al., 2009). Having already established a 3D Matrigel model system, this was used to grow MDA-MB-231 cells and MDA-MB-231 cells knocked down for CBFβ.

4.2.1. MDA-MB-231 cells knocked down for CBFβ show an altered morphology in 2D cell culture

MDA-MB-231 cells stably knocked down for CBFβ (shCBFβ) have been previously constructed by Daniel Mendoza (Mendoza-Villanueva et al., 2010). In order to confirm the knockdown of CBFβ in these stably transfected MDA-MB-231 cells, the expression of CBFβ was tested at both the RNA and protein level (Fig. 4.1A and B). RNA extracts of MDA-MB-231 cells and cells stably transfected with either a non-specific sequence (shNS) or targeted for CBFβ knockdown (shCBFβ) were used for RT-PCR analysis using primers against human CBFβ and normalised against ribosomal protein LO (RPLO) levels (Fig 4.1A). CBFβ mRNA levels in shCBFβ MDA-MB-231 cells were significantly reduced in comparison to both the wild-type (WT) MDA-MB-231 cells and the MDA-MB-231 cells transfected with shNS. This

shows that CBFβ is significantly reduced at the RNA level in shCBFβ MDA-MB-231 cells.

In order to show that reduced mRNA expression translates to reduced protein expression, whole cell extracts of the same cells were subjected to western blot analysis using a polyclonal anti-Rabbit CBFβ antibody (Fig. 4.1B). A strong band present in both WT MDA-MB-231 cells and shNS MDA-MB-231 lanes showed CBFβ protein expression, whereas a faint band in the shCBFβ lane showed low CBFβ expression in this cell line. β-Tubulin was used as a loading control in all lanes (lower panel). This confirmed that CBFβ was significantly reduced at the protein level.

In addition to the protein knockdown, it was important to confirm that this knockdown had the predicted functional effect. In order to confirm this, a known target for Runx2/CBFβ was used, MMP13. RNA extracted from shNS and shCBFβ cells was used for RT-PCR analysis using primers against MMP13 and normalised against RPLO (Fig. 4.1C). MMP13 mRNA expression was significantly reduced in shCBFβ cells compared to CBFβ expressing shNS MDA-MB-231cells. This showed that the shCBFβ knockdown in MDA-MB-231cells had a functional effect, resulting in down-regulation of a Runx2/CBFβ target gene.

It is known that breast cancer cells undergo morphological changes which allow the cells to metastasise out of the breast (Chimge and Frenkel, 2013). Upon cell culture passage, it was observed that the MDA-MB-231 cells knocked down for CBFβ had a different structural morphology compared to WT and shNS MDA-MB-231 cells. For this reason, the WT MDA-MB-231cells were grown on coverslips, as were shNS and shCBFβ transfected cells. These were then imaged using snapshot widefield

microscopy in order to determine whether there was indeed a change in morphology following CBFβ knockdown. These cells were imaged at two time points, day 1 and day 4, to observe the cells at different stages of growth (Fig. 4.1D). There did not appear to be any change in growth rate between any of the cell lines (confirmed by a growth rate study, data not shown). However, there was a difference in the morphology of the cells. The MDA-MB-231 cells and shNS MDA-MB-231 cells appeared to have many protrusions which are common among invading cells. The shCBFβ MDA-MB-231 cells did not have these protrusions. Instead the cells packed together far more closely and formed a cobblestone confluent appearance. This observation indicated that depletion of CBFβ in MDA-MB-231 cells caused a change in cell morphology.

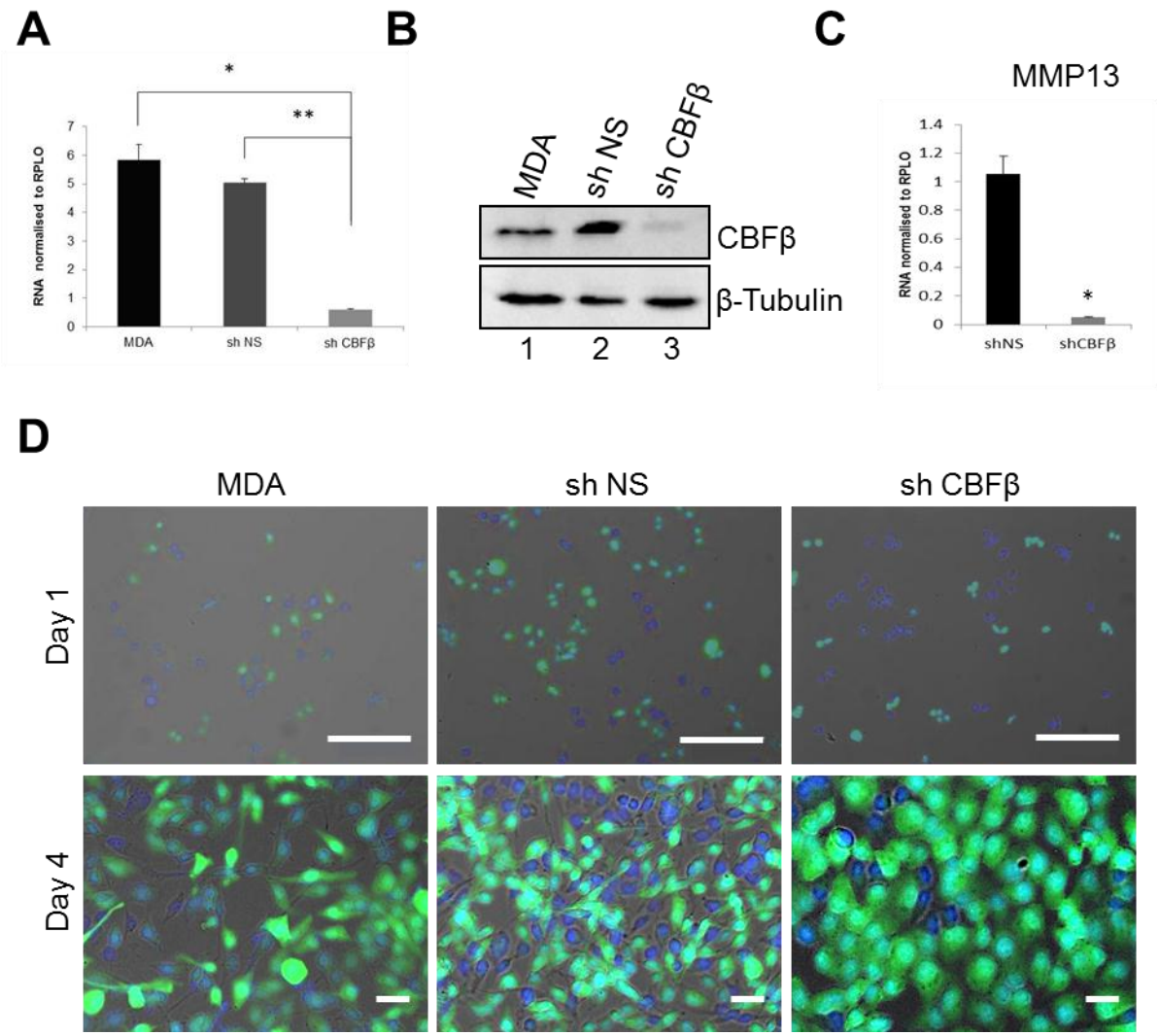

Fig. 4.1. Verification of CBFβ knockdown in breast cancer cells and comparison of growth in 2D. (A) RT-PCR of MDA-MB-231 cells had reduced CBFβ RNA expression following CBFβ knockdown. Expression of CBFβ mRNA relative to RPLO expression using RNA extracted from the same cells. Data presented as mean ± standard deviation (S.D.) (n=3). * indicates a significant difference between WT MDA-MB-231 (MDA) and shCBFβ knockdown cells. ** indicates a significant difference between shNS MDA-MB-231 cells and shCBFβ MDA-MB-231 cells using T test where $p<0.05$. (B) Western blot showing CBFβ protein knockdown in MDA-MB-231 cells. Whole cell extracts of metastatic breast cancer cells MDA-MB-231 (MDA) and stable knockdown cells using either a non-specific sequence (NS) or shCBFβ. Samples subjected to western blot analysis and with anti-CBFβ polyclonal antibody and anti-β tubulin antibody. (C) RT-PCR of MMP13 mRNA expression in MDA-MB-231 cells following CBFβ knockdown, as described in (A). (D) Immunofluorescence microscopy of MDA-MB-231 cells grown in 2D. MDA-MB-231 cells grown in 2D monolayer and fixed after Day 1 and 4. Images acquired with an Olympus widefield microscope using a x10 objective without oil. Images are merges of Dapi nuclei staining (blue), GFP expression (green) and brightfield images (grey). Scale bars represent 50 µm Day 1 and 5 µm Day 4.

4.2.2. CBFβ knockdown causes a more pronounced change in morphology when grown in 3DMatrigel cell culture system

Considering that the shCBFβ MDA-MB-231 cells grown in 2D cell culture had no protrusions, which was in contrast to the shNS and non-transfected MDA-MB-231 cells, the effect of this knockdown on 3D growth was investigated. It had already been documented that different 2D morphologies give different 3D structures (Fig. 4.2A; Bissell, 2007; Weigelt and Bissell, 2008). MDA-MB-231 cells and shNS and shCBFβ transfected MDA-MB-231 cells were plated onto matrigel as described in the previous chapter. The cells were imaged after 1 and 4 days in order to observe the growth of the cells in a 3D environment (Fig. 4.2B).

The MDA-MB-231 cells stably expressed GFP which therefore allowed the cell morphology to be detected without additional staining. At day 1, all cell types appeared to have the same spherical structure. At 4 days (bottom panel) in the matrigel the MDA-MB-231 cells had begun to invade into the matrigel and the cells had many protrusions in different directions. Comparing the structures to those in Fig. 4.2A, these cells formed 'stellate' formations. The shNS MDA-MB-231 cells had a similar morphology to the MDA-MB-231 cells.

In contrast to these structures, shCBFβ MDA-MB-231 cells formed clusters or spheres of cells (Fig. 4.2B, right panels). These structures appeared to be either 'round' or 'mass' (Fig. 4.2A, left panels). Each cluster was self-contained and there were few connections between the different cluster populations. A cluster formation is more typical of a normal breast phenotype as opposed to the breast cancer phenotype usually seen of MDA-MB-231 cells (Debnath and Brugge, 2005). Therefore, CBFβ knockdown causes a change in cellular morphology and organization in 3D culture.

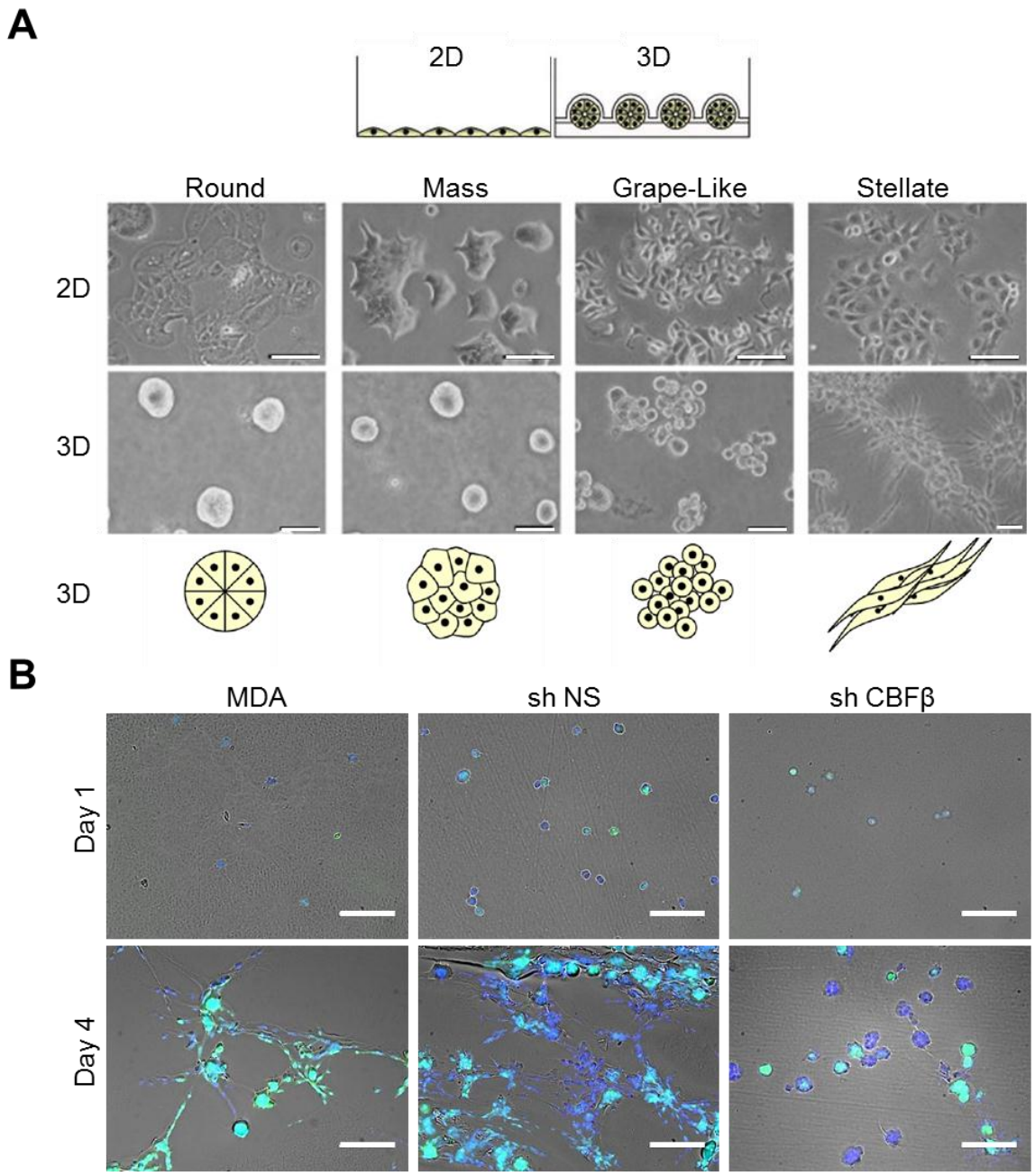

Fig. 4.2. Knockdown of CBFβ in metastatic breast cancer cells causes a change in morphology in 3D culture. (A) Different 2D arrangements give rise to different 3D structures. Adapted from Bissel et al. 2007 and Bissel et al. 2008. (B) Immunofluorescence confocal microscopy of breast cancer cells knocked down for CBFβ and grown in a 3D matrigel system. Metastatic breast cancer cells MDA-MB-231 cells (MDA), stable knocked down shCBFβ cells and non-specific stable cells (shNS) were grown in matrigel for 1 day (top panels) and 4 days (bottom panels). Cells were fixed and nuclei stained with DAPI (blue). GFP expression (green) and brightfield (grey) are also shown. Images were taken with an Olympus widefield microscope using a x10 objective without oil. Scale bar shown is 200 μm.

4.2.3. shCBFβ MDA-MB-231 cells form solid and hollow clusters in 3D cell culture

In order to determine whether the clusters seen previously (Fig. 4.2B) were compact disorganised structures, seen in 'mass' forming clusters (Fig. 4.2A) or if they were acini-like 'round' structures, the cells required growth for a longer period of time (Debnath and Brugge, 2005). Therefore, shCBFβ MDA-MB-231 cells were grown in matrigel for 14 days and imaged using confocal microscopy. This allowed imaging through the z-stack and thus identified the presence of a hollow lumen. This analysis revealed 2 different types of structures were present in the shCBFβ MDA-MB-231 cell population.

Most clusters appeared to be of a 'mass' formation. However, some clusters were spheres of 'round' cells which had a hollow lumen (Fig. 4.3A). It is worth noting however, that hollow lumen structures only made up 5% of the structures observed. The schematic diagram in Fig. 4.3B illustrates how a confocal microscope can image through the z-stack of a cluster to reveal whether this was a solid cluster of cells or whether it had a hollow lumen. Fig. 4.3C showed two of these structures. The top panel showed a solid cluster, or 'mass'. Coming from the top of this mass structure, (left) to the bottom (right) there was no void observed in the centre. In contrast to this mass image, the bottom panel of Fig. 4.3C showed a cluster with the presence of a hollow lumen. These images show that the structures created by the shCBFβ MDA-MB-231 cells grown in 3D Matrigel are a mixture of both mass clusters and round hollow luminal structures.

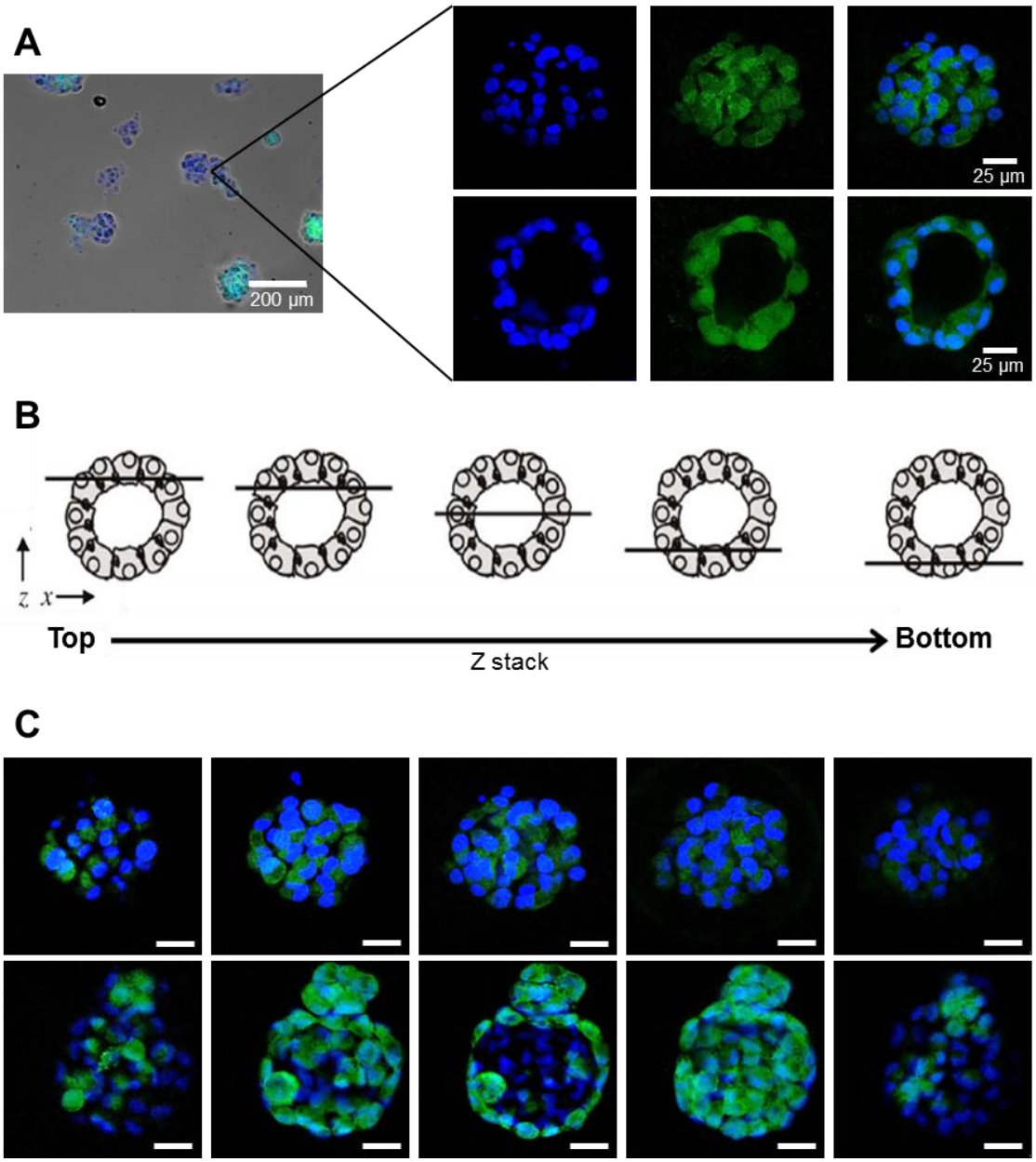

Fig. 4.3. Breast cancer cells with reduced CBFβ form clusters and hollow lumen structures when grown in 3D. (A) Immunofluorescence microscopy imaging of MDA MB 231 shCBFβ cells in matrigel. Left panel shows cluster formation of shCBFβ cells after 6 days at x10 objective using Olympus widefield microscope no oil. Right panel shows a magnified look at such clusters with x63 objective in oil using Leica SP5 inverted confocal microscope. Scale bars as indicated (B) Schematic diagram showing how a confocal microscope moves through z stack. Imaging from top to bottom of an acini type structure. (C) Immunofluorescence microscopy of shCBFβ MDA cells at different points in the Z stack of a cluster of cells. (Top panel) z stack of cells forming a cluster and (bottom panel) a hollow lumen. Cells were fixed and nuclei stained with DAPI (blue). GFP expression (green). Scale bar on confocal images represents 25 µm.

4.2.4. CBFβ knockdown in MDA-MB-231 cells allows acini formation when grown in 3D

It has previously been established that mutated Runx2 in MDA-MB-231 cells results in a more organised formation of cells in 3D culture, which resemble the acini-like structures seen in normal mammary gland cell lines (Pratap et al., 2009). Having already shown that the knockdown of CBFβ in MDA-MB-231 cells induced the formation of hollow lumen structures, it was postulated that these structures may be acini.

In order to establish whether these structures were indeed acini, the expression of known acini marker proteins was examined (Debnath et al., 2003). Acini structures polarise to form apical and basal surfaces that can be detected using different cell surface markers. pERM was used as an apical marker and integrin as a basal marker (Fig. 4.4). MCF10A cells are normal mammary epithelial cells and are known to form acini in 3D Matrigel (Debnath and Brugge, 2005). These cells were therefore used to provide a demonstration of a differentiated acini structure (Fig. 4.4A).

The outer edge of the hollow luminal structures formed by the MCF10A cells was stained with Laminin V (green). This was a marker for basement membrane and so indicated a polarisation of the structures. In addition, the cell-cell adhesion marker E-Cadherin (red) was detected between the cells to indicate the cell membranes. Therefore, this showed that the structures formed by the MCF10A cells had a hollow lumen and polarisation of cells, thus indicating that acini were indeed formed.

The MDA-MB-231 cells knocked down for CBFβ and shNS MDA-MB-231 cells were grown in Matrigel for 14 days and then stained with known acini polarisation markers, pERM and integrin (Fig. 4.4B). The top panels showed staining with pERM

in both shCBFβ and shNS MDA-MB-231 cells. In the shCBFβ MDA-MB-231 cells the anti-pERM antibody staining was predominantly detected in the inner surface of the hollow lumen (red) as shown by the arrows. In shNS MDA-MB-231 cells there were no hollow lumen structures. The cells had grown throughout the matrigel and there was no specific localisation for pERM staining. Instead it was present throughout the cells.

The bottom panel showed staining using anti-integrin α6 antibody (red) in shCBFβ and shNS cells. In shCBFβ cells that formed a hollow lumen this staining would be expected on the outside of the spherical structure. Indeed the integrin staining was visible on the outer surface of the structure. In shNS cells the integrin was not visible. Taken together this showed that there were a population of shCBFβ MDA-MB-231 cells that had formed a hollow lumen and had differentiated to form polarised cells forming distinct basal and luminal surfaces. Thus, this indicates acini formation could occur following CBFβ knockdown in MDA-MB-231 cells.

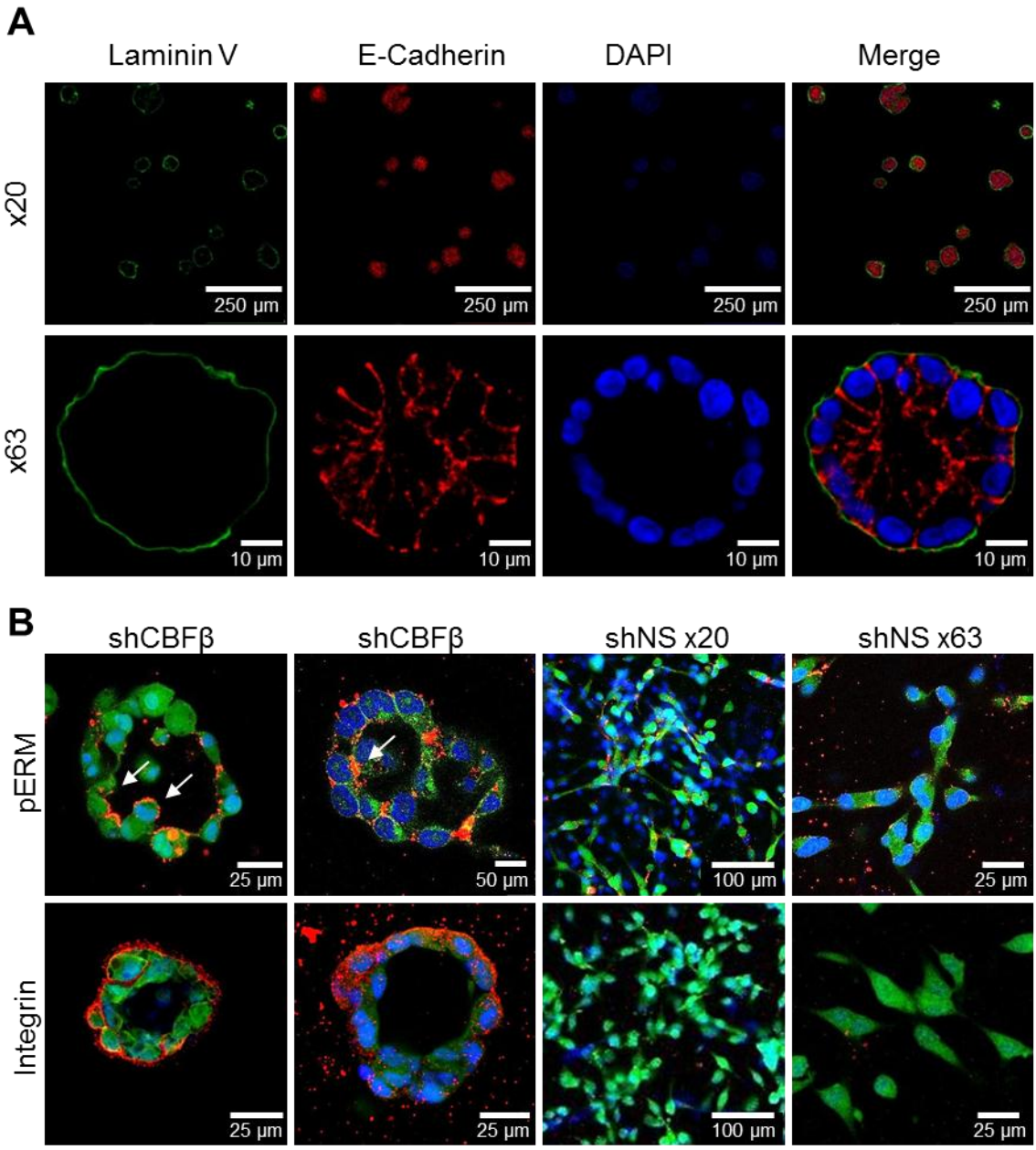

Fig. 4.4. Breast cancer cells depleted of CBFβ form acini structures. (A) Immunofluorescence microscopy imaging of MCF10A acini in 3D matrigel. Staining of basement membrane with Laminin V (green) and cell adhesion marker E-Cadherin (red). Low magnification (top panel) and high magnification (bottom panel) images shown. (B) Immunofluorescence microscopy imaging of MDA-MB-231 cells stable cells shNS (non-specific) and shCBFβ knockdown grown in 3D matrigel. MDA-MB-231 cells were grown for 14 days in matrigel and stained for apical or basement markers (Red), phospho Ezrin/Radixin/Moesin (pERM) and Integrin respectively. Images were taken using a Leica SP5 inverted confocal microscope at x 63 magnification with oil for shCBFβ images and either x63 or x20 magnification for shNS images as indicated. Cells were fixed and nuclei stained with DAPI (blue). GFP expression (green). Scale bar as indicated.

4.3. Re-expression of CBFβ prevents cluster and acini formation

The previous section showed that knockdown of CBFβ in MDA-MB-231 cells caused formation of clusters when grown in a 3D matrigel system. To demonstrate that this change in phenotype was specifically caused by depletion of CBFβ the CBFβ in depleted cells was re-expressed. In order to reintroduce CBFβ into these knockdown cells, a mouse CBFβ cDNA was used to evade the effects of the shRNA against the human CBFβ. Since the acini take 14 days to form, transient transfection was not suitable. Therefore, a stable cell line harbouring a tamoxifen-inducible CBFβ-ER fusion protein was created (Fig. 4.5A). This plasmid was created by Gillian Ran (Ran and Shore, unpublished).

The presence of the ER estrogen-binding domain fused to CBFβ sequesters CBFβ in the cytoplasm, as depicted in the schematic diagram (Fig. 4.5B). The ER sequence binds to heat shock protein 90 (HSP90) and therefore prevents CBFβ moving into the nucleus. Upon stimulation with the drug 4OH-Tamoxifen (4OH), which was able to bind to the ER domain, the HSP90 was released and the CBFβ was free to bind to Runx2 and move into the nucleus. Here the heterodimer could bind to DNA and initiate activation or repression of target genes.

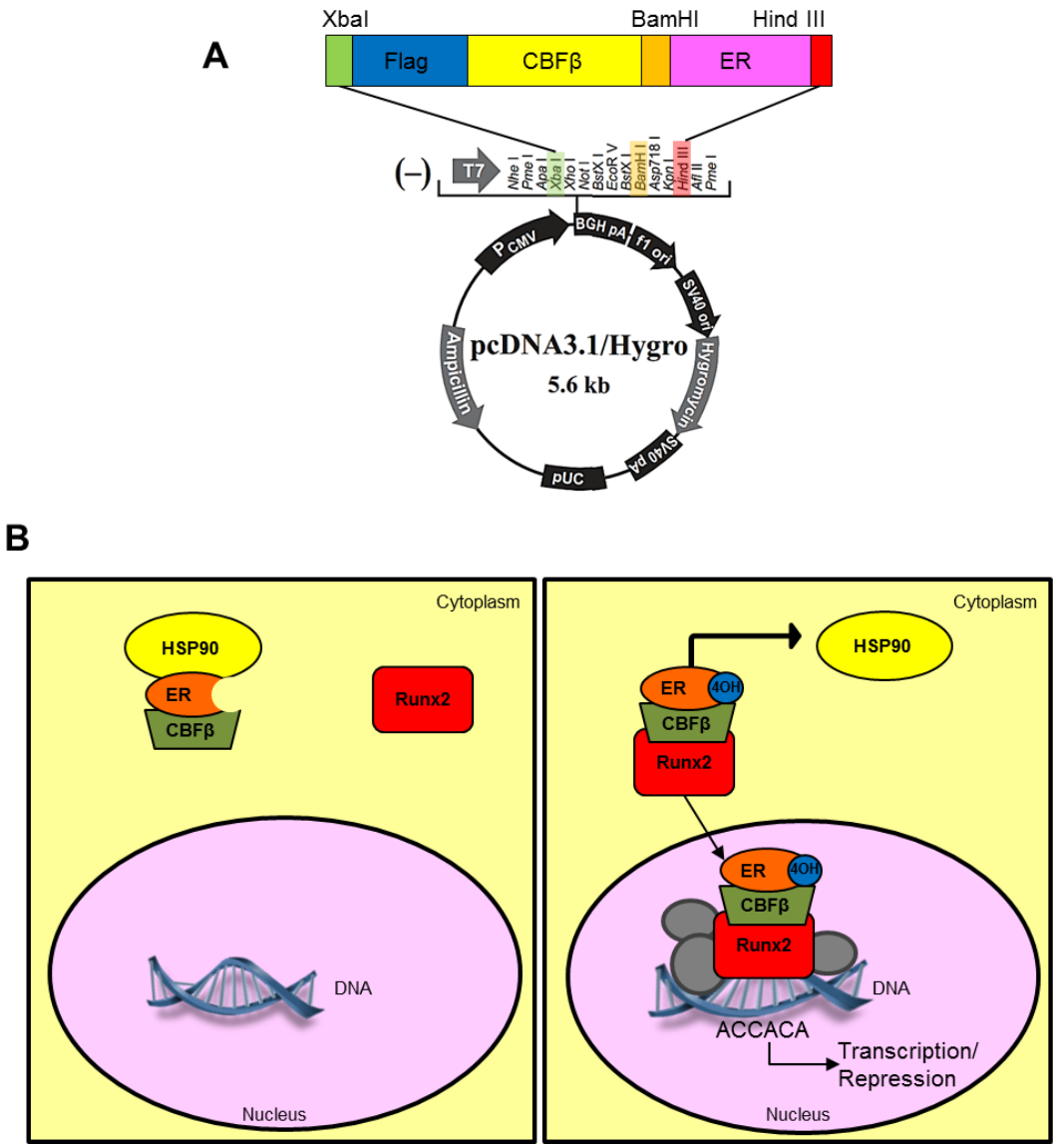

Fig. 4.5. Using a 4OH tamoxifen inducible system to activate CBFβ translocation. (A) Schematic diagram of CBFβ tagged with an estrogen receptor (ER) sequence and Flag sequence. (B) Schematic diagram of the mechanism by which 4OH-Tamoxifen (4OH) induces translocation of CBFβ-ER into the nucleus.

4.3.1. Generation of a hormone inducible CBFβ-ER stable cell line using MDA-MB-231 cells knocked down for CBFβ

The plasmid encoding CBFβ-ER was transfected into the shCBFβ MDA-MB-231cell line and stable clones were generated. Ten of these clones were subjected to western blot analysis using anti-CBFβ antibody (Fig. 4.6A). As the CBFβ was tagged with ER and Flag it had a higher molecular weight than that of endogenous CBFβ and so ran higher on the gel at approximately 100 kD. The left panel showed that clone 4 had a band at this weight. This was the only clone with this band. To confirm that this was indeed the CBFβ-ER-Flag sequence an anti-Flag antibody was also used and this showed a band in clone 4 (lane 6) as well. The loading control β-Tubulin had been used to show protein levels in all lanes. This shows a stable cell line of shCBFβ MDA-MB-231 with CBFβ-ER-Flag had been created.

In order to test that the transfection itself had no effect on further experiments, at the same time a stable cell line with the pcDNA3.1 plasmid was also created (Fig. 4.6B). This showed no CBFβ-ER presence with either the anti-CBFβ or the anti-Flag antibodies. Endogenous CBFβ was detected in WT MDA-MB-231 cells, in lane 8, using the anti-CBFβ antibody. Therefore, a stable cell line for shCBFβ MDA-MB-231 cells containing Flag-CBFβ-ER was generated.

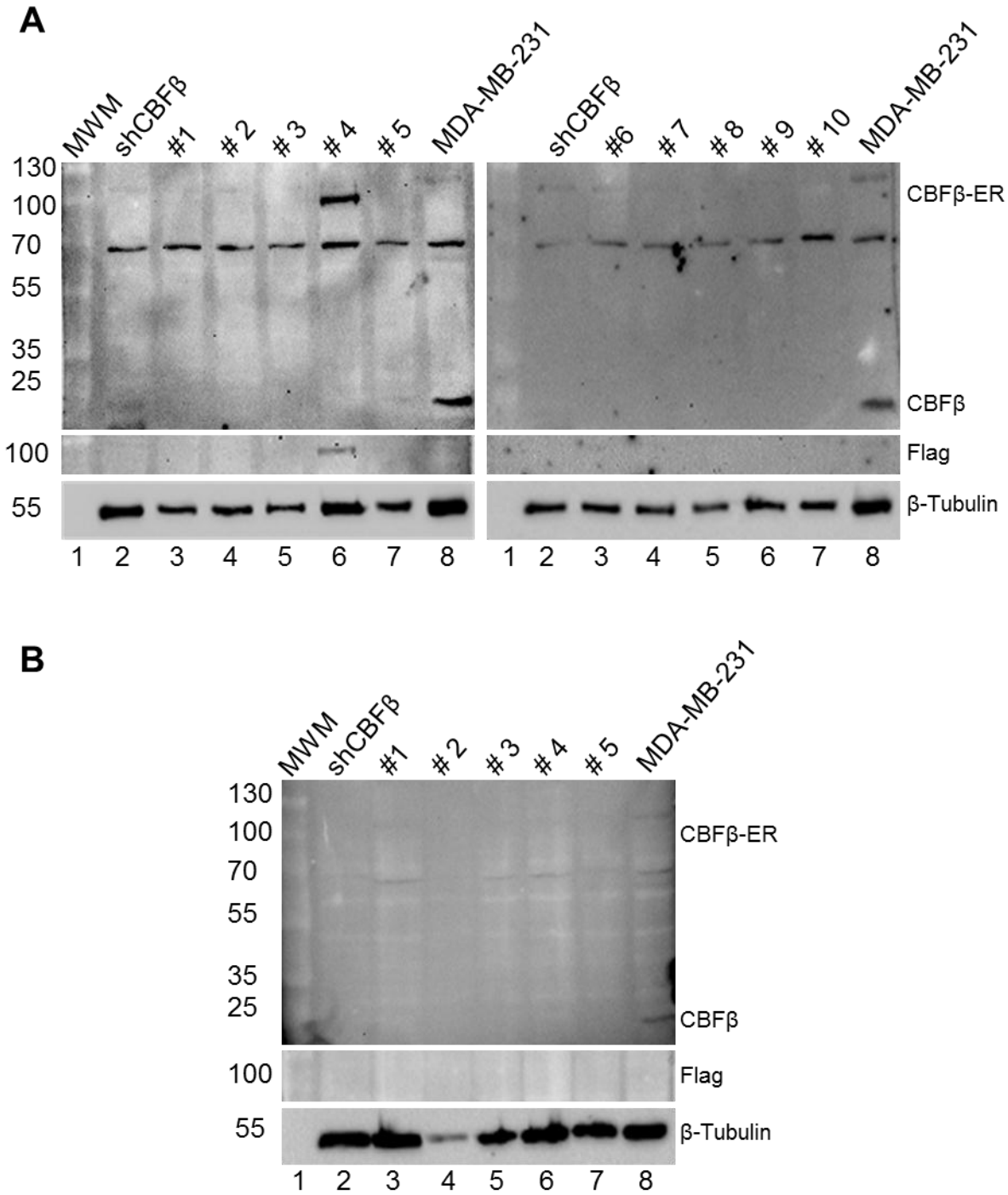

Fig. 4.6. Generation of a stable cell line with mouse CBFβ-ER expression. (A)Western blot showing mouse CBFβ-ER expression in MDA-MB-231 cells already stably knocked down for endogenous CBFβ. MDA-MB-231 shCBFβ cells were transfected with mouse CBFβ-ER and stable cell lines were grown. Total extracts from 10 clones were subjected to western blot analysis using CBFβ and flag antibodies. (B) Western blot showing MDA-MB-231 cells transfected with pcDNA3.1 plasmid. MDA shCBFβ cells were treated as described in (A). For both (A) and (B) β-Tubulin is used as a loading control, MWM indicates Molecular Weight Marker.

4.3.2. 4OH-Tamoxifen induces nuclear translocation of CBFβ

Clone 4 (Fig. 4.6A) of the shCBFβ MDA-MB-231 cells expressing Flag-CBFβ-ER, was used for subsequent experiments. For simplicity, this stable cell line was referred to as MDA-CBFβ-ER from this point. Clone 1 of the pcDNA3.1 only shCBFβ MDA-MB-231 cell line (Fig. 4.6B) was used as the control. For simplicity, this was referred to as MDA-pcDNA3.1 from this point.

The CBFβ conjugation to ER caused the complex to be sequestered in the cytoplasm (Fig. 4.5). To determine if nuclear CBFβ-ER could be induced by 4OH, MDA-CBFβ-ER cells were treated with 4OH and subjected to nuclear and cytoplasmic extraction. Fig. 4.7 shows the MDA-CBFβ-ER cell line (top) and MDA-pcDNA3.1 (bottom) treated with and without 4OH-Tamoxifen (4OH). The cytoplasmic (C) and nuclear (N) extracts were used. Lanes 1 and 2 of MDA-CBFβ-ER shows without 4OH treatment the CBFβ-ER was exclusively in the cytoplasm. In contrast, in the presence of 4OH, CBFβ-ER also accumulated in the nucleus. There was no CBFβ-ER in the control cells. Thus nuclear CBFβ-ER protein expression was induced in the MDA-CBFβ-ER cell line by the addition of 4OH.

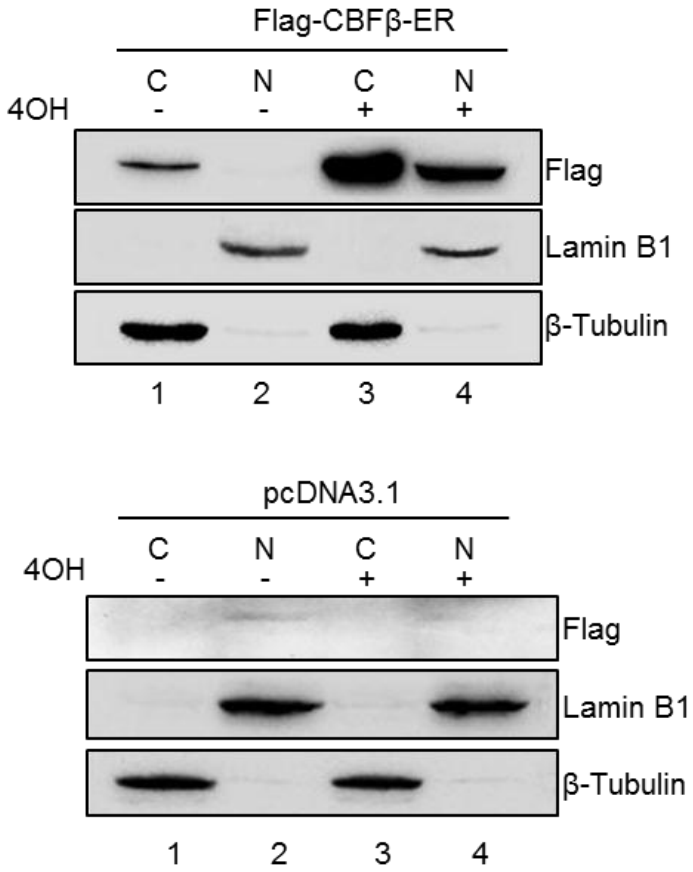

Fig. 4.7. Validation of Flag-CBFβ-ER plasmid expression and induction using 4OH-Tamoxifen. (A) Western blot analysis of MDA-MB-231 cells expressing CBFβ-ER with 4OH-Tamoxifen induction shows shuttling of CBFβ-ER into the nucleus. Top panel, the shCBFβ MDA clone 4 shown in Fig. 4.6, was treated with (+) and without (-) 4OH-Tamoxifen (4OH) and used for nuclear (N) and cytoplasmic (C) extraction. Extracts were subjected to western blot analysis using anti-flag antibody. The bottom panel shows cells transfected with pcDNA3.1 only. Lamin B1 was used as a loading control for nuclear extracts and β-Tubulin was used as a loading control for cytoplasmic extracts.

4.3.3. CBFβ-ER induction with 4OH rescues Runx2 target gene expression

Having established that nuclear CBFβ-ER protein could be induced it was next confirmed whether this protein was functionally active. The known target gene of Runx2/CBFβ, MMP13, was used to establish if it could be up-regulated in MDA-CBFβ-ER cells by 4OH treatment. MMP13 is known to be down-regulated following depletion of CBFβ (Mendoza-Villanueva et al., 2010). MMP13 expression was therefore analysed by RT-PCR in MDA-CBFβ-ER cells and MDA-pcDNA3.1 control in the presence and absence of 4OH. In the presence of 4OH, MMP13 expression increased almost 4 fold compared to the untreated cells (Fig. 4.8). In contrast, no significant change in MMP13 expression was observed in MDA-pcDNA3.1 control cells. This result suggests translocation of CBFβ-ER protein to the nucleus leads to induction of Runx2 target genes. Thus MDA-CBFβ-ER is an MDA-MB-231 cell line in which CBFβ function can be activated by incubation with 4OH.

Having so far shown that the MDA-CBFβ-ER cells successfully expressed the CBFβ-ER protein and that this protein was functionally active, the stable cells were then used in subsequent experiments. Considering that there was a difference in morphology between CBFβ expressing MDA-MB-231 cells and the CBFβ knockdown MDA-MB-231 cells in 2D cell culture (Fig. 4.1), together with the ability of MDA-CBFβ-ER cells to rescue expression of Runx2/CBFβ target genes, the cells were grown in 2D cell culture and observed for morphological differences (Fig. 4.8B).

Control MDA-pcDNA3.1 cells and MDA-CBFβ-ER cells were grown on coverslips. All cells were stained with anti-Flag antibody to detect the expression of the stably

transfected CBFβ-ER protein. MDA-pcDNA3.1 cells grown in 2D were either treated with 4OH or left untreated. In both cases, the resulting cells showed a round cobblestone appearance. In addition, as expected, there was no red anti-Flag staining to indicate the expression of the CBFβ-ER protein.

Transiently transfected MDA-CBFβ-ER cells were grown on coverslips and the media was either treated with or without 4OH. The MDA-CBFβ-ER cells grown without 4OH treatment had the same cobblestone appearance as MDA-pcDNA3.1 cells. However, these cells also showed expression of CBFβ-ER protein in the cytoplasm of the cells. In contrast to the cobblestone structures observed in all other conditions, upon 4OH induction of MDA-CBFβ-ER cells, a stellate cell structure was observed (Fig. 4.8B). In addition the CBFβ-ER protein expression was present in both the nucleus as well as the cytoplasm. This confirmed the western blot analysis (Fig. 4.7) and additionally demonstrated that nuclear expression of CBFβ-ER protein by 4OH inductions caused a change in cell structure.

Having established that nuclear induction of CBFβ-ER by 4OH resulted in a cell structure change in 2D, the cells were next grown in a 3D Matrigel system to determine whether the induction of nuclear CBFβ-ER prevented the cells from clustering and forming acini.

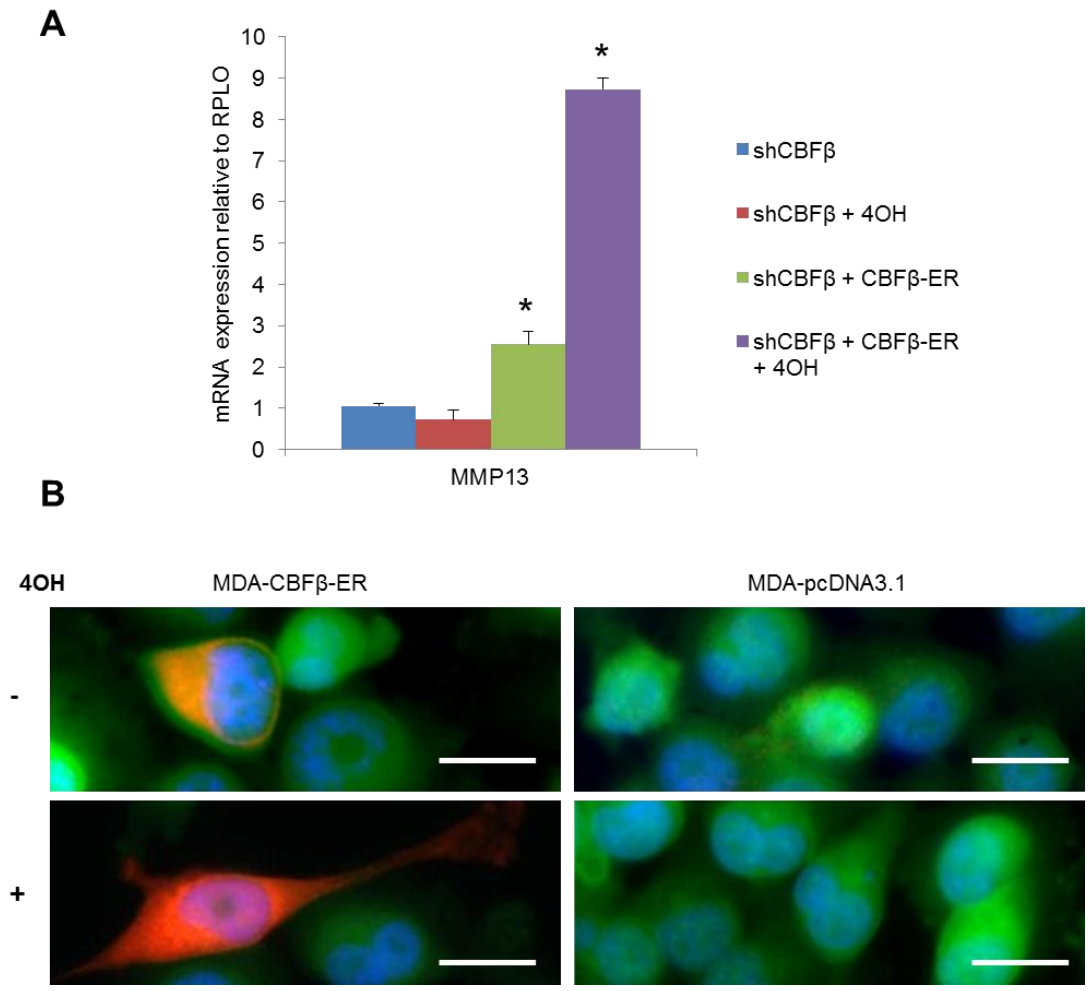

Fig. 4.8. CBFβ-ER is functionally active following 4OH-Tamoxifen induction. (A) RT-PCR using RNA from MDA-MB-231 cells showing increased expression of MMP13 with CBFβ-ER and 4OH-Tamoxifen treatment. RNA extraction of shCBFβ cells with CBFβ-ER or pcDNA3.1 only following treatment with or without 4OH-Tamoxifen (4OH TM) were subjected to RT-PCR analysis. Primers against human Runx2 and human MMP13 were used. Values were normalised against endogenous RPLO. Data presented as mean ± standard deviation (S.D.) (n=3). * indicates a significant difference using T test where $p<0.05$. (B) Immunofluorescence microscopy of shCBFβ MDA-MB-231 cells stably transfected with pcDNA3.1 or CBFβ-ER. Expression of CBFβ-ER was both in the cytoplasm and the nucleus following 4OH-Tamoxifen treatment. Cells were grown in the presence (+) or absence (-) of 4OH-Tamoxifen and then stained with anti-flag antibody (red). GFP staining is shown in green and DAPI staining in blue. Scale bars shown are 25 μm.

4.3.4. Induction of CBFβ-ER prevents clustering and acini formation

The MDA-CBFβ-ER and MDA-pcDNA3.1 stable cells were grown in matrigel for 1, 4 and 6 days. On day 0 of 3D culture, cells were either treated or untreated with 4OH. This media was changed every day. The cells were fixed at day 1, 4 and 6 as shown in Fig. 4.9. At day 1 the cells appeared to be in single cell orientation or dividing. There was no difference in cell phenotype between the MDA-CBFβ-ER cells and the control MDA-pcDNA3.1 whether they were 4OH treated or untreated.

At day 4 the cells started to form clusters. There were no stellate structured cells found in any of the cells types at this stage. All images contained cells with clusters. Therefore, there was no difference in structural phenotype between MDA-CBFβ-ER and control MDA-pcDNA3.1 cells nor between 4OH treated and untreated cells,

By day 6, in the control MDA-pcDNA3.1 cells, there were larger clusters observed. There were again only clusters seen throughout the coverslips with both 4OH treated and untreated. This was not the case in the MDA-CBFβ-ER cells. The MDA-CBFβ-ER cells had many clusters of cells in the 4OH untreated cells. In contrast, following 4OH treatment many of the clustered cells appeared to become dispersed. The cell arrangements had many protrusions that had a more stellate appearance as opposed to the spherical cells observed without 4OH treatment. Therefore, the structures seen in the 4OH treated MDA-CBFβ-ER cells were reminiscent of the WT MDA-MB-231 cell structures observed in 3D Matrigel.

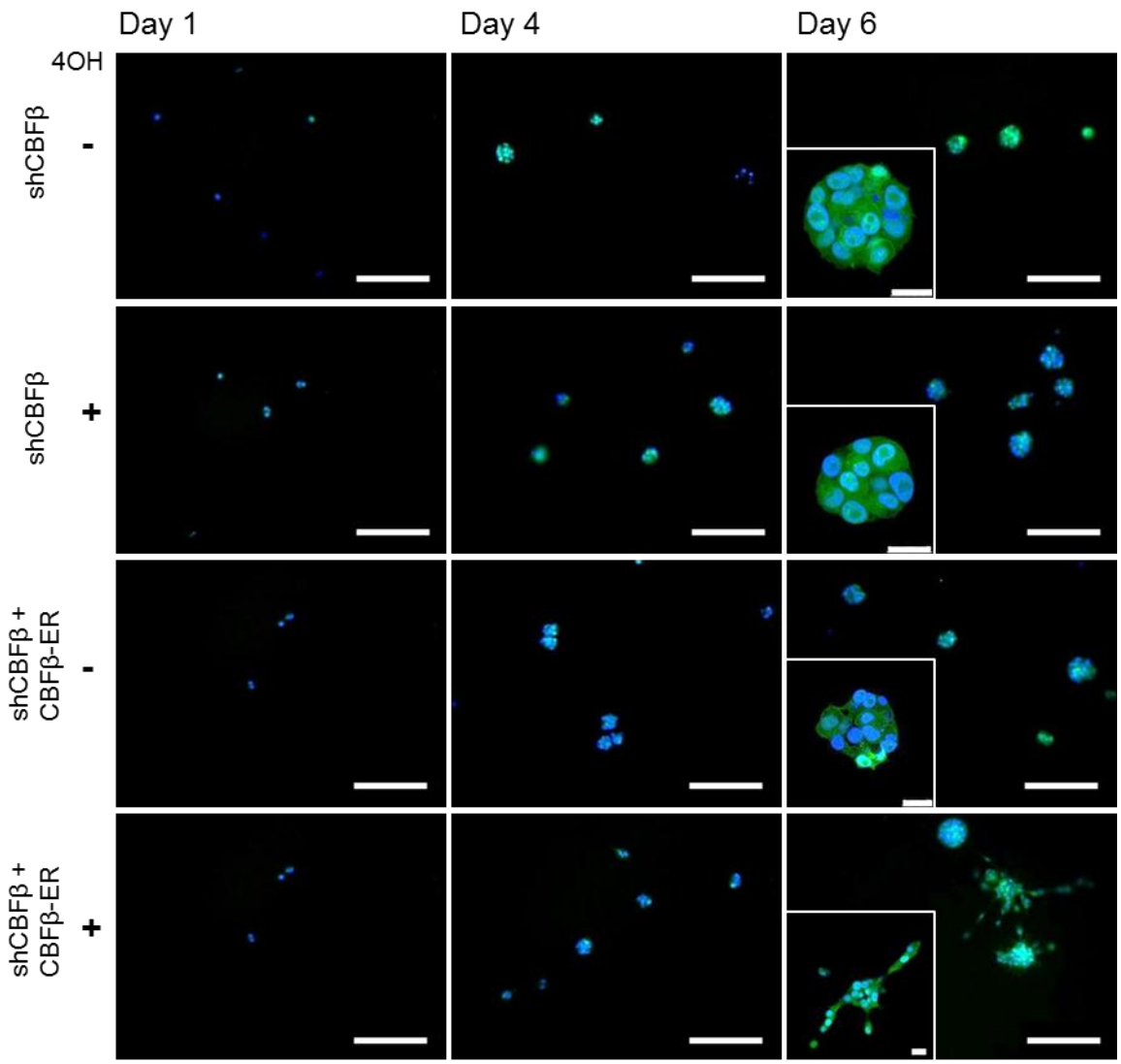

Fig. 4.9. Re-expression of CBFβ causes reversion to the invasive phenotype in 3D. Immunofluorescence microscopy of metastatic breast cancer, MDA MB 231 cells (MDA), stable knocked down shCBFβ cells and shCBFβ expressing CBFβ-ER were grown in matrigel for 1 day (left panels), 4 days (middle panels) and 6 days (right panels). Cells were grown in the presence (+) or absence (-) of 4OH-Tamoxifen. Cells were fixed and nuclei stained with DAPI (blue). GFP expression (green) is also shown. Images were taken with a Leica SP5 inverted microscope using x20 objective (inset shows x63 magnification) with oil. Scale bars shown are 25 μm.

While induction of 4OH in MDA-CBFβ-ER cells did result in many stellate structured cells, there were also compact clusters of cells. In addition, there appeared to be some stellate clusters on the untreated MDA-CBFβ-ER coverslips. In order to confirm the effects of the 4OH on MDA-CBFβ-ER cells, multiple images were taken of which three of each was shown in Fig.4.10A and B. These images were used to quantitate the changes in cell structure in response to 4OH treatment.

In order to quantify the frequency of these stellate structures, compared to rounded clusters, each treatment type was tested ie. MDA-pcDNA3.1and MDA-CBFβ-ER cells, with and without 4OH. 100 of the groups of cells were counted in each and the number of clustered versus stellate (unclustered) was recorded (Fig. 4.10C). The results showed that 99% and 100% of the MDA- pcDNA3.1 cells treated or untreated with 4OH respectively formed clusters. Therefore the 4OH had no effect on the phenotype of the MDA-pcDNA3.1 cells.

When growing the MDA-CBFβ-ER cells in 3D without 4OH treatment, 94% of the structures formed were clusters. With 4OH treatment, 70% of the structures had a stellate structure. This confirmed that with CBFβ-ER induction, the phenotype of CBFβ positive cells began to revert away from a clustered phenotype to resemble a more WT MDA-MB-231 cells structure.

Considering that knockdown of CBFβ in the original MDA-MB-231 cells resulted not only in clustered cells but structures with hollow lumens, the stable cell line MDA-CBFβ-ER were grown in the 3D matrigel system for 14 days to determine whether these too could form acini. As the MDA-pcDNA3.1 transfected cells showed no change in phenotype with or without 4OH induction, only the MDA-CBFβ-ER cells were shown (Fig. 4.11). As previously demonstrated, MDA-CBFβ-

ER cells with 4OH treatment had stellate structures. However, in contrast to the cell structures observed in the previous time points, the MDA-CBFβ-ER cells completely invaded the matrigel, mimicking that phenotype of the WT MDA-MB-231 cells (Fig. 4.11). Therefore MDA-CBFβ-ER induction causes a full reversion of the WT MDA-MB-231 phenotype after 14 days.

On the other hand, 4OH untreated MDA-CBFβ-ER cells formed large clusters of cells. Confocal microscopy of these structures did not reveal any clusters with complete hollow lumens. Some structures appeared to display the developing stages of acini progression with remnants of cell death in the centre however, even upon a longer incubation period in the Matrigel there did not appear to be any clusters with a hollow lumen (data not shown). Therefore, the MDA-CBFβ-ER stable cell line appeared to resemble a subset of the shCBFβ MDA-MB-231 cell population that was able to form clusters rather than acini structures.

Overall, the creation of the MDA-CBFβ-ER cell line allowed the rescue of endogenous CBFβ which had been knocked down using shRNA. This rescue established that it was loss of CBFβ expression that caused a change in MDA-MB-231 cell phenotype.

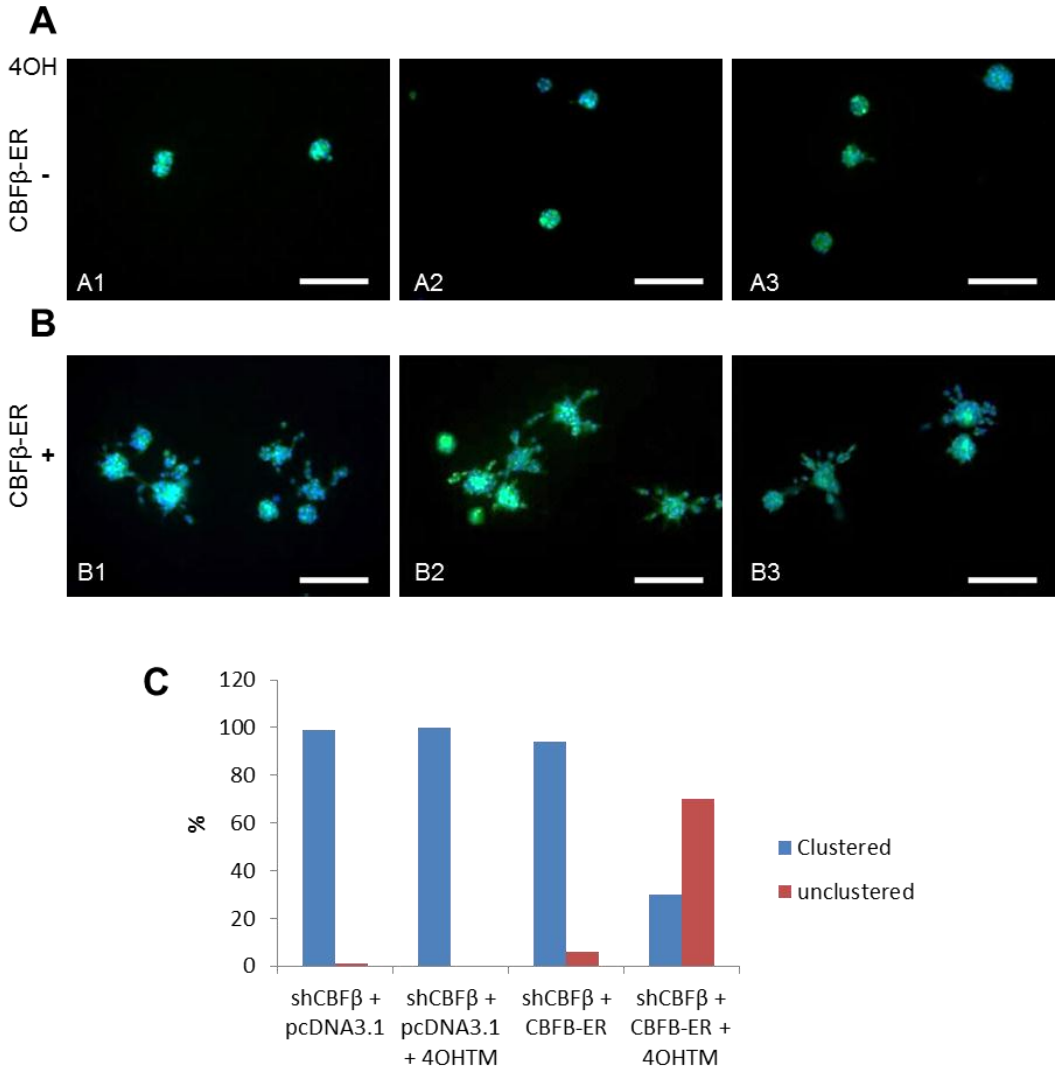

Fig. 4.10. Induction of CBFβ-ER in the shCBFβ cells significantly changes the morphology of structures when grown in 3D. (A) Immunofluorescence imaging of CBFβ-ER expression in MDA-MB-231 cells without 4OH-Tamoxifen induction shows cluster formation in 3D matrigel system. CBFβ-ER cells were grown in matrigel and imaged after 6days using a snapshot widefield microscope. (B) Immunofluorescence imaging of CBFβ-ER expression with 4OH-Tamoxifen induction shows fewer clusters and more protrusions in a 3D matrigel system. CBFβ-ER cells were grown in matrigel and imaged after 6days using a snapshot widefield microscope. (C) A quantitative analysis of clusters versus unclustered structures formed by CBFβ-ER induced cells. 100 structures in both pcDNA3.1 and CBFβ-ER stable shCBFβ cells were counted both with and without 4OH-Tamoxifen induction.

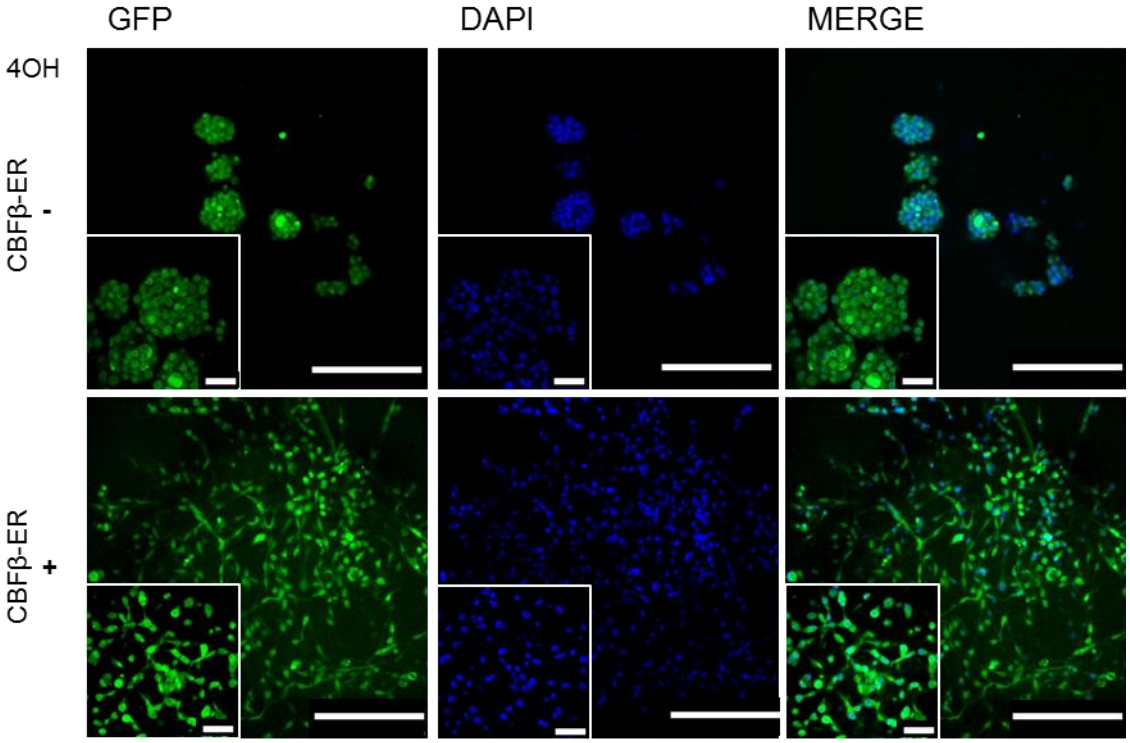

Fig. 4.11. Induction of CBFβ-ER in shCBFβ knockdown cells rescues the invasive phenotype seen in 3D culture following 14 days growth. Immunofluorescence images of metastatic breast cancer cells MDA-MB-231 cells, stable knocked down shCBFβ cells and transfected with an inducible CBFβ-ER shows a change in phenotype following 4OH-Tamoxifen induction. Cells were grown in a 3D matrigel system and either treated or untreated with 4OH for 14 days before fixed and nuclei stained with DAPI (blue). GFP expression (green) is also shown. Images were taken with an Olympus widefield microscope using a x10 objective without oil and a x60 objective with oil. Scale bar shown is 250 μm in large images and 50 μm inset.

4.4. Knockdown of CBFβ results in Mesenchyme to Epithelial Transition

The previous sections in this chapter showed that WT MDA-MB-231 cells grown in 3D Matrigel had a stellate phenotype. Previous research in our lab has shown that MDA-MB-231 cells are invasive (Mendoza-Villanueva et al., 2010). Knockdown of CBFβ in MDA-MB-231 cells changed the phenotype of these cells when grown in 3D. This knockdown resulted in clusters of cells and previous research showed this also reduced the invasive capacity of these cells (Mendoza-Villanueva et al., 2010). When grown in 3D Matrigel, the normal breast cell line MCF10A form acini (Debnath et al., 2003). Considering that MDA-MB-231 cells are mesenchymal and that MCF10A cells are epithelial, could the knockdown of CBFβ be causing a mesenchymal to epithelial transition (MET)? This question was addressed by examining expression of EMT marker proteins.

The process of MET can be determined by detecting the expression of particular markers known to be predominantly expressed in either mesenchymal cells or epithelial cells (Lee et al., 2006). For example, mesenchymal cells express genes involved in invasion such as MMP13 and MMP9. Epithelial cells express genes involved in cell-cell adhesion and polarisation such as integrins and cadherins (Creighton et al., 2013). To determine which MET genes were expressed in shCBFβ MDA-MB-231 cells, RT-PCR analysis was conducted. Considering the change in structural phenotype was more pronounced when the cells were grown in a 3D Matrigel environment, the experiment used cells grown in 3D cell culture.

MDA-MB-231 cells knocked down for CBFβ (shCBFβ) and shNS MDA-MB-231 cells were grown in 3D matrigel for 4 days. These cells then underwent 3D Matrigel

extraction and subsequently RNA extraction. This RNA was then used for RT-PCR analysis. Primers against human CBFβ were used to confirm the CBFβ mRNA knockdown. Runx2 primers were used to show there was no change in the Runx2 expression. Similarly, Runx1 was used as a control as it is known to be expressed in MDA-MB-231 cells (Fig. 4.12). All remaining genes are known MET markers (Lee et al., 2006). MMP13, Snail, Slug, Fibronectin, Vimentin and MMP9 are all known mesenchymal markers. Therefore in an MET, these genes should show a decrease in mRNA expression following CBFβ knockdown in MDA-MB-231 cells. As shown by the RT-PCR analysis, all these genes significantly reduce their mRNA expression in shCBFβ. The markers Cytokeratin 7, Occludin and E-Cadherin are all known epithelial markers. Therefore these should increase following CBFβ knockdown. As shown in the RT-PCR analysis, three of these markers showed an increase in mRNA expression in shCBFβ MDA-MB-231 cells. Integrin α5β6 and Desmoplakin showed no significant change in mRNA expression. However, the overall pattern of expression indicated an increase in cell adhesion and a decrease in cell invasive capacity. Taken together, these data suggests that knockdown of CBFβ causes MET.

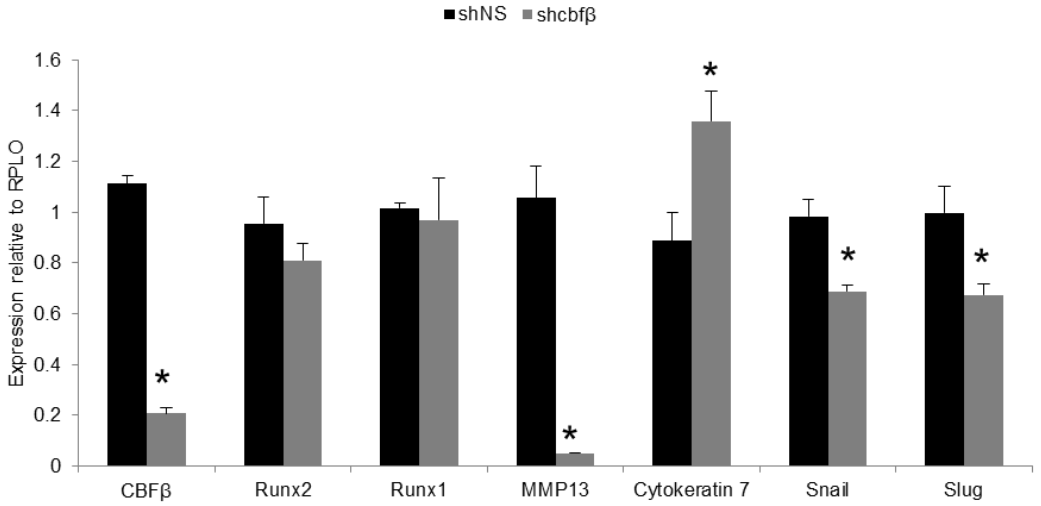

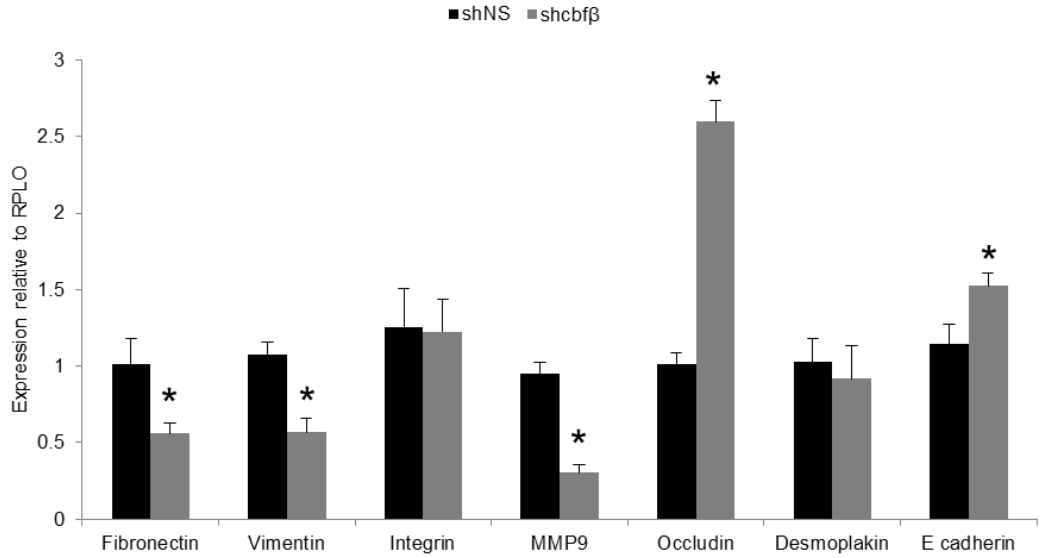

Fig. 4.12. MET markers following CBFβ knockdown in breast cancer cells in 3D RNA extraction. RT PCR of known markers for Mesenchymal- Epithelial Transition (MET). MDA-MB-231 breast cancer cells knocked down for CBFβ (shCBFβ) and a stable non-specific shRNA transfected cell line (shNS) were grown in a 3D matrigel system. Cells were extracted from the matrigel and the RNA extracted. Primers against known markers from EMT were used for RT-PCR analysis. Values were normalised against endogenous RPLO. Data presented as mean ± standard deviation (S.D.) (n=3). * indicates a significant difference using T test where $p<0.05$.

4.5. Discussion

The data presented in this chapter demonstrate that CBFβ was successfully knocked down in breast cancer cells, MDA-MB-231, and that this knockdown caused a change in morphology when grown in 2D. When grown in 3D, the shCBFβ MDA-MB-231 cells did not form a stellate arrangement, but instead formed cluster arrangements. Some of these clusters of cells had hollow lumens. When stained for apical-basal membranes, the hollow lumen structures showed some polarisation thus indicating that they were acini. A stable cell line using MDA-MB-231 cells knocked down for CBFβ was created containing a mouse Flag-CBFβ-ER sequence. This stable cell line induced CBFβ-ER protein production that was sequestered in the cytoplasm until induced by 4OH Tamoxifen allowing movement into the nucleus. CBFβ-ER induction rescued the stellate phenotype of MDA-MB-231 cells. RT-PCR analysis of shNS MDA-MB-231 cells and shCBFβ MDA-MB-231 cells revealed a decrease in mesenchymal markers and an increase in epithelial markers, thus suggesting CBFβ is involved in EMT.

4.5.1. CBFβ knockdown in metastatic breast cancer cells causes formation of acini structures in 3D cell culture

A major problem of advanced breast cancer is that it metastasises out of the breast and in 85% of cases this metastasis is to bone. Once there, many of these breast cancer cells cause bone degradation. A model cell line used to demonstrate this phenomenon was the MDA-MB-231 cells. These are metastatic breast cancer cells that have moved to the bone and are able to cause osteolytic lesions (Barnes et al., 2004). When injected into the heart of an immunocompromised mouse, these cells travel to bone and cause lesions (Sasaki et al., 1998). When Runx2 was knocked

down in these MDA-MB-231 cells, they lost their ability to invade (Barnes et al., 2004). Mendoza et al. have shown that knockdown of CBFβ in MDA-MB-231 cells also caused loss of invasion (Mendoza-Villanueva et al., 2010). Using these same MDA-MB-231 stable cells that Mendoza created, it was noticed that the shCBFβ MDA-MB-231 cells had a different morphology to the shNS MDA-MB-231 cells when grown in 2D. When grown in a 3D matrigel system, the WT MDA-MB-231 and control shNS cells spread throughout the matrigel, whereas the CBFβ knockdown cells formed clusters. Considering that cells with different 2D phenotype gave rise to very different 3D characteristics, this change in phenotype was not surprising (Bissell, 2007). In addition, this structural change in MDA-MB-231 following CBFβ knockdown was in keeping with the effects seen following Runx2 disruption in MDA-MB-231 cells (Pratap et al., 2009). Mutation of Runx2 caused MDA-MB-231 cells to form structures in 3D which resembled those seen using normal breast cells (Pratap et al., 2009).

In addition to forming clusters, after 14 days in matrigel the shCBFβ MDA-MB-231 cells started to form hollow lumen type structures resembling acini. In order for these structures to be classed as acini, they must have apical-basal polarisation. The apical membrane is the inner surface of the hollow lumen and can be stained for using pERM. The basement membrane can be stained for using integrins or laminins. The integrin staining did localise to the outer membrane of the hollow lumen structures. The pERM staining also localised to the inner surface of the acini in some structures. This suggests polarisation and so shows acini are formed.

The staining of the acini for apical-basal markers was not consistent. Only some of the integrin antibodies showed staining and there did not appear to be any staining using laminins. Furthermore, the pERM staining did not show localisation all around

the inner surface. It is also important to note that of the many cluster structures formed in the shCBFβ MDA-MB-231 cells, only 5% of the structures seen formed a hollow lumen. This suggests that while acini-type structures were being formed, knock down of CBFβ was not sufficient to fully convert the metastatic breast cancer cell phenotype back to a normal breast phenotype. Non-metastatic breast cancer cells (MCF7) form clustered cells without hollow lumens in 3D cell culture (Pinto et al., 2011). Therefore, rather than a full reversion to normal breast cells, perhaps CBFβ knockdown facilitates a reversion to a non-metastatic breast cancer state.

4.5.2. Rescue of CBFβ causes a reversion to a stellate formation

In order to show that the change in phenotype of MDA-MB-231 cells is caused by CBFβ, a rescue experiment was conducted. Under normal circumstances this rescue experiment would involve a transient transfection of CBFβ back into the MDA-MB-231 cells. This CBFβ would be mutated at the area the siRNA targets and so would not be knocked down with the endogenous CBFβ. However, this method could not be conducted as a transient transfection only lasts 2-3 days whereas the acini type structures took between 2-3 weeks to fully form. For this reason a stable cell line was created that contained a mouse CBFβ sequence and so would not be targeted by shRNA. The construct used contained an ER sequence conjugated to the C-terminal of the CBFβ sequence. This created an inducible system. Creating a stable cell line from a single cell using different colonies yielded only one clone in which CBFβ-ER was successfully expressed. Within this clone, MDA-CBFβ-ER, the CBFβ-ER construct was sequestered in the cytoplasm as demonstrated by western blot analysis of nuclear and cytoplasmic extracts. Following treatment with 4OH-Tamoxifen, CBFβ-ER protein was detected in both the cytoplasm and the nucleus. This was as

expected as the 4OH-Tamoxifen binds to the ER which released the complex from HSP90, allowing Runx2 to transport it to the nucleus (Caruso et al., 1999; Dauvois et al., 1993; Shiau et al., 1998; Yang and Li). Upon induction with 4OH-Tamoxifen there was still CBFβ present in the cytoplasm. This may have been a result of the overexpression of mouse CBFβ-ER. As CBFβ is shuttled into the nucleus by Runx2 protein, perhaps the higher amounts of CBFβ over loaded the ability for Runx2 to move the protein into the nucleus.

4.5.3. CBFβ is involved in EMT

It has previously been thought that the knock down of CBFβ prevents metastasis due to the lack of invasive capacity (Mendoza-Villanueva et al., 2010). This was backed up by the decrease in known markers of metastasis such as MMP13. However, the data in this chapter suggests that CBFβ knock down has a much broader effect on metastatic breast cancer cells. In appearance, the cells are transitioning from a mesenchymal (stellate) to an epithelial (round) phenotype following CBFβ knock down. The cells then transition back to a mesenchymal phenotype after CBFβ was reintroduced into the cell nucleus. There are known markers for mesenchymal and epithelial cells (Lee et al., 2006). RT PCR for these markers showed a decrease in mRNA of mesenchymal markers and an increase in epithelial markers following CBFβ knockdown. Thus this suggests that knockdown of CBFβ is in fact causing a transition from mesenchymal to epithelial phenotype, MET.

This transition is in keeping with data from Chimge et al. who showed that epithelial-mesenchymal transition occurs following overexpression of Runx2 in non-metastatic breast cancer cells MCF7 (Chimge et al., 2011). The role of Runx/CBFβ is further established in EMT by its role in other cancers. Malignant thyroid carcinoma cells

have an up-regulation of Runx2 compared to normal thyroid cells. Knock down of Runx2 through transient transfection led to a down regulation of known mesenchymal markers and so showed an MET (Niu et al., 2012).

It is worth noting that MDA-MB-231 cells also express Runx1 (Blyth et al., 2010). The breast cell line MCF10A cells express Runx1 and knockdown of Runx1 in these cells results in a loss of acini formation when grown in a 3D matrigel system (Wang et al., 2011a). Considering that Runx1 has previously been shown to have a role in acini formation and that Runx1 also heterodimerises with CBFβ, knockdown of CBFβ in MDA-MB-231 cells could also cause MET due to loss of Runx1 downstream target expression (Ferrari et al., 2013).

5.0 Identification of Runx2/CBFβ target involved in breast cancer remodelling of bone using cells grown in 3D

5.1. Introduction

The previous chapter showed that loss of CBFβ in metastatic breast cancer cells caused a major change in phenotype resulting in a mesenchymal to epithelial transition. Breast cancers that become metastatic must undergo an epithelial to mesenchymal transition in order to gain invasive properties and lose cell-cell contact (Creighton et al., 2013). This allows the cells to invade other regions of the body and in 85% of cases adhere to bone (Yin et al., 2005). Once at the bone breast cancer cells secrete factors that cause bone remodelling resulting in bone degradation (Chen et al., 2010). The Runx2/CBFβ complex has already been implicated in the invasion of metastatic breast cancer cells (Mendoza-Villanueva et al., 2010; Pratap et al., 2005). There is also evidence that Runx2 is involved in the bone remodelling stage once the breast cancer is at the bone. Runx2 regulates the SOST gene which produces the protein sclerostin. This inhibits differentiation of osteoblasts (Mendoza-Villanueva et al., 2011). In order to understand other roles of Runx2 in bone remodelling, further target genes need to be identified.

These MDA-MB-231 cells were particularly useful when investigating breast cancer metastasis to bone as they themselves are breast cancer cells that have colonised bone. Injection of these cells into an immunocompromised mouse heart results in bone metastasis and additionally, bone lesions are formed (Barnes et al., 2003; Selvamurugan et al., 2000). These bone lesions are considerably reduced when Runx2 is mutated (Barnes et al., 2004). Osteolytic lesions in late stage breast cancer patients are a source of immense pain and can result in fracturing. Therefore, the role of Runx2 is of great interest for possible therapeutic targets.

There were two main aims to this chapter. The first was to determine the effect of cell culture in 2D and 3D on the gene regulation of the cells. This would indicate the importance of the extracellular environment for gene regulation within breast cancer cells. The second was to identify target genes of the Runx2/CBFβ complex in order to further understand the role of this complex in breast cancer metastasis and bone remodelling.

In order to demonstrate the importance of growing cells in a 3D environment compared to a 2D environment, MDA-MB-231 cells were grown in 3D. Following growth in 3D Matrigel, the shCBFβ MDA-MB-231 cells and shNS MDA-MB-231 cells were used for microarray analysis. The data from this microarray analysis was then compared to data from a 2D microarray analysis using the same cells. This combined data was used to identify possible down-stream targets of Runx2/CBFβ.

5.2. Microarray analysis of MDA-MB-231 cells knocked down for CBFβ and grown in a 3D matrigel system

Considering there are known differences in cells grown in a 2D environment versus 3D, a microarray was conducted in which metastatic breast cancer cells, MDA-MB-231, were grown in a 3D matrigel system (Fig. 4.2A). MDA-MB-231 cells knocked down for CBFβ (shCBFβ) and MDA-MB-231 cells stably transfected with a non-specific shRNA sequence (shNS) were grown in matrigel for 4 days. This length of time had previously shown a noticeable change in phenotype (Fig. 4.1). In order to obtain the RNA needed for microarray analysis, cells were first extracted from the matrigel as described in the methods (Fig 5.1A). This was done in triplicate.

To confirm these cells had a reduction in CBFβ, the RNA was subjected to RT-PCR analysis using primers for human CBFβ and expression was normalised against RPLO expression (Fig. 5.1B). In all 3 samples the mRNA expression of CBFβ in the shCBFβ MDA-MB-231 cells was significantly reduced when compared to the shNS MDA-MB-231 cells. Having shown a significant knockdown of CBFβ, two of the shNS samples and two of the shCBFβ samples (shNS 1, shNS2, shCBFB1 and shCBFβ2) were used for microarray analysis.

The mRNA was labelled and hybridised onto the Human Genome U133 Plus 2.0 Array from Affymetrix. This was the same array that had previously been used to carry out the microarray using cells grown in 2D. This array analysed the expression level of over 38,500 human genes. As each microarray experiment was performed in duplicate a PCA statistical analysis was used.

The microarray experiments were represented in volcano plots, where each transcript was represented by a dot (Fig. 5.1C). The criteria used to determine a significant difference between the shNS and the shCBFβ samples was a fold change ≥2 and q-value ≤0.05. Q values were chosen, as opposed to the p-value, in order to get a reduced false discovery rate. The red dots represent transcripts that met this criteria and it was these transcripts that were used for further analysis. A total of 1053 transcripts were identified that met the criteria. A full list of these transcripts is shown in the appendix section of this thesis. Of these transcripts, 250 genes had been up-regulated following CBFβ knockdown and 803 were down-regulated following CBFβ knockdown (Fig. 5.1D).

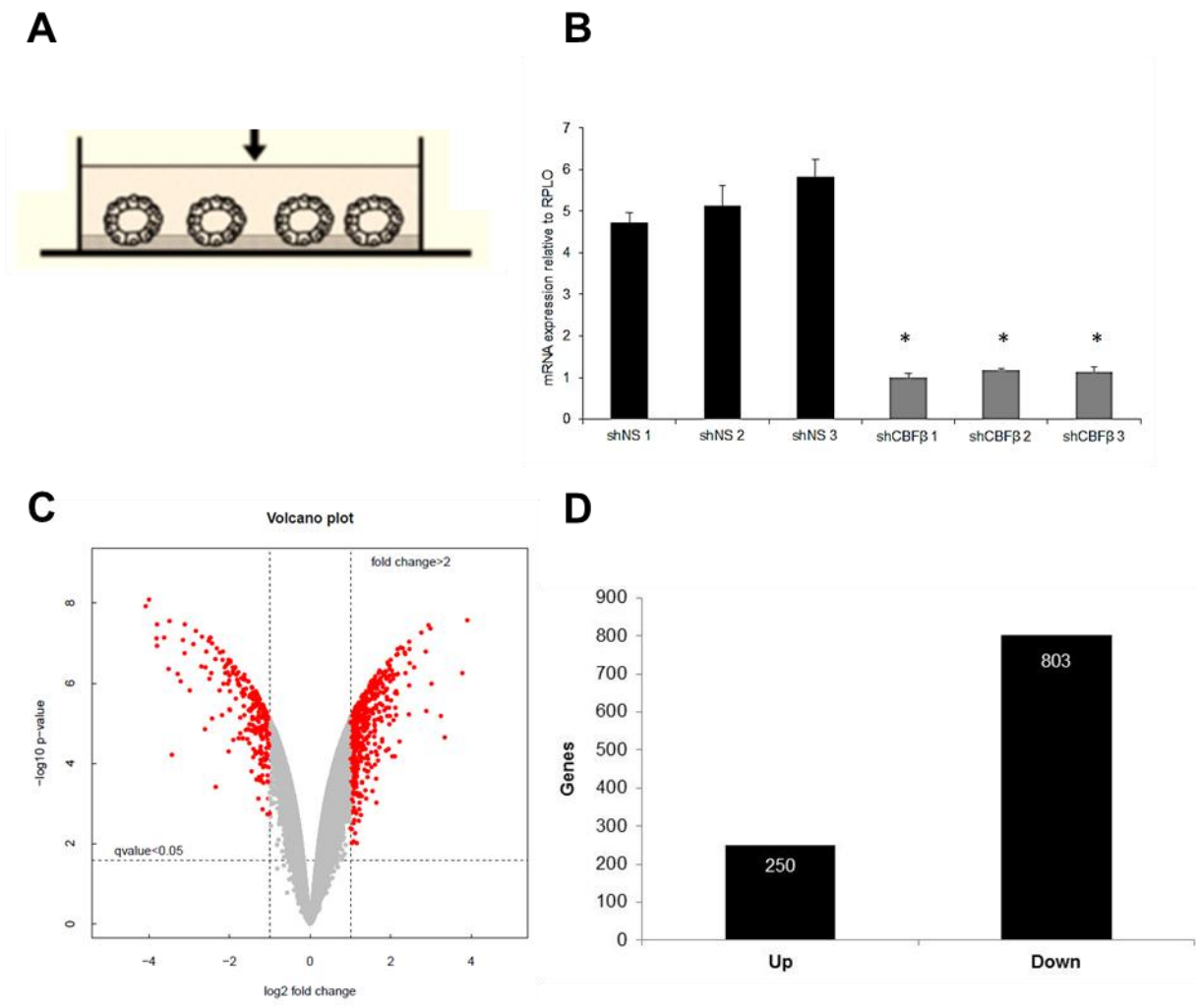

Fig.5. 1. Microarray analysis of MDA-MB-231 cells knocked down for CBFβ and grown in 3D. (A) 3D RNA extraction of MDA-MB-231 cells knocked down for CBFβ. A schematic diagram showing how MDA-MB-231 cells knocked down for CBFβ were grown in matrigel. Cells then underwent 3D RNA extraction after 4 days of growth in matrigel. (B) RT-PCR showing expression of CBFβ relative to RPLO expression using RNA extracted from the same cells. Data presented as mean ± standard deviation (S.D.) (n=3). * indicates a significant difference between shNS MDA-MB-231 and shCBFβ knockdown cells using students T test where $p<0.05$ and n=3. (C)Volcano plot of genes expressed in MDA-MB-231 cells following CBFβ knock down relative to shNS cells. The dashed vertical lines indicate a cut off of $\pm\geq 2$ fold change and the dashed horizontal line indicates a q value of ≤ 0.05. Each point indicates an individual transcript. The red points indicate the genes used for further analysis. (D) A graph representing the number of genes up and down regulated following CBFβ knock down in MDA-MB-231 cells.

5.3. DAVID analysis of 3D and 2D microarray data

Having identified the genes that met the selected criteria, the biological pathways affected were assessed. The Database for Annotation, Visualisation and Integrated Discovery (DAVID) provides functional analysis to give a better understanding of the biological meaning of a large gene data set using functional annotation (Huang da et al., 2009a; Huang da et al., 2009b). Therefore DAVID analysis was used to identify the biological processes affected by CBFβ knockdown. DAVID Functional Annotation allowed identification of groups of genes connected by known pathways. These groups were termed 'clusters'. The clusters were ranked by importance using 'Enrichment scores'. The first 8 of these clusters with the highest enrichment values have been shown (Fig. 5.2).

DAVID analysis produced dozens of clusters, each ranked by their enrichment score. The key was to select the pathways of interest. The pathways of interest for this thesis were those that related to bone remodelling and additionally those relating to to metastasis, or 'cell movement'. These pathways were seen in clusters 4, 7 and 8 in particular (Fig. 5.2).

In order to establish the extent of change in transcripts in a 3D microarray from a 2D microarray, the two microarrays were compared. Having identified these clusters of genes from the 3D microarray, a DAVID analysis of the 2D microarray genes was conducted (Fig. 5.3). The 2D data has previously been published by Daniel Mendoza and can be viewed using accession number E-MEXP-3230 (Mendoza-Villanueva et al., 2011).

National Institute of Allergy and Infectious Disease
The Database for Annotation, Visualization and Integrated Discovery

Annotation Cluster 1	Enrichment Score: 6.61		Count	P_Value	Benjamini
GOTERM_BP_FAT	vasculature development	RT	46	4.2E-9	1.4E-5
GOTERM_BP_FAT	blood vessel development	RT	44	1.8E-8	3.0E-5
GOTERM_BP_FAT	blood vessel morphogenesis	RT	36	1.5E-6	8.4E-4
GOTERM_BP_FAT	angiogenesis	RT	26	3.4E-5	7.5E-3
Annotation Cluster 2	**Enrichment Score: 4.49**		**Count**	**P_Value**	**Benjamini**
GOTERM_MF_FAT	SMAD binding	RT	15	1.6E-6	1.6E-3
GOTERM_BP_FAT	transmembrane receptor protein serine/threonine kinase signaling pathway	RT	22	7.5E-6	3.6E-3
GOTERM_BP_FAT	transforming growth factor beta receptor signaling pathway	RT	12	2.7E-3	1.4E-1
Annotation Cluster 3	**Enrichment Score: 3.81**		**Count**	**P_Value**	**Benjamini**
GOTERM_BP_FAT	response to endogenous stimulus	RT	53	1.5E-5	4.5E-3
GOTERM_BP_FAT	response to hormone stimulus	RT	49	2.0E-5	5.1E-3
GOTERM_BP_FAT	response to organic substance	RT	80	4.1E-5	8.6E-3
GOTERM_BP_FAT	response to estrogen stimulus	RT	20	1.1E-4	1.9E-2
GOTERM_BP_FAT	response to steroid hormone stimulus	RT	27	9.1E-4	8.4E-2
GOTERM_BP_FAT	response to estradiol stimulus	RT	10	1.2E-2	3.1E-1
Annotation Cluster 4	**Enrichment Score: 3.48**		**Count**	**P_Value**	**Benjamini**
GOTERM_BP_FAT	regulation of cell motion	RT	32	1.1E-5	4.8E-3
GOTERM_BP_FAT	regulation of cell migration	RT	28	4.6E-5	9.0E-3
GOTERM_BP_FAT	regulation of locomotion	RT	30	7.0E-5	1.2E-2
GOTERM_BP_FAT	positive regulation of cell motion	RT	17	1.2E-3	9.3E-2
GOTERM_BP_FAT	positive regulation of locomotion	RT	16	3.3E-3	1.6E-1
GOTERM_BP_FAT	positive regulation of cell migration	RT	14	8.9E-3	2.7E-1
Annotation Cluster 5	**Enrichment Score: 3.23**		**Count**	**P_Value**	**Benjamini**
GOTERM_BP_FAT	transmembrane receptor protein serine/threonine kinase signaling pathway	RT	22	7.5E-6	3.6E-3
KEGG_PATHWAY	TGF-beta signaling pathway	RT	16	2.6E-3	8.2E-2
GOTERM_BP_FAT	BMP signaling pathway	RT	9	1.0E-2	2.9E-1
Annotation Cluster 6	**Enrichment Score: 3.08**		**Count**	**P_Value**	**Benjamini**
GOTERM_MF_FAT	nucleoside-triphosphatase regulator activity	RT	53	2.1E-5	1.0E-2
GOTERM_MF_FAT	GTPase regulator activity	RT	52	2.3E-5	7.6E-3
GOTERM_MF_FAT	enzyme activator activity	RT	43	1.4E-4	3.4E-2
GOTERM_MF_FAT	GTPase activator activity	RT	31	3.0E-4	5.7E-2
GOTERM_MF_FAT	small GTPase regulator activity	RT	36	3.5E-4	5.5E-2
SP_PIR_KEYWORDS	GTPase activation	RT	20	1.1E-2	2.5E-1
GOTERM_BP_FAT	regulation of small GTPase mediated signal transduction	RT	27	3.0E-2	4.7E-1
GOTERM_BP_FAT	regulation of Ras protein signal transduction	RT	21	1.0E-1	7.2E-1
Annotation Cluster 7	**Enrichment Score: 2.73**		**Count**	**P_Value**	**Benjamini**
GOTERM_BP_FAT	regulation of ossification	RT	18	2.2E-5	5.3E-3
GOTERM_BP_FAT	regulation of osteoblast differentiation	RT	12	1.4E-4	2.1E-2
GOTERM_BP_FAT	positive regulation of osteoblast differentiation	RT	6	2.7E-2	4.4E-1
GOTERM_BP_FAT	formation of primary germ layer	RT	6	1.5E-1	8.0E-1
Annotation Cluster 8	**Enrichment Score: 2.65**		**Count**	**P_Value**	**Benjamini**
GOTERM_BP_FAT	ossification	RT	20	3.8E-4	5.2E-2
GOTERM_BP_FAT	bone development	RT	20	9.0E-4	8.5E-2
GOTERM_BP_FAT	osteoblast differentiation	RT	9	7.9E-3	2.6E-1
GOTERM_BP_FAT	skeletal system development	RT	35	9.4E-3	2.8E-1

Fig. 5.2. DAVID analysis identifies genes involved in bone development and cell movement. DAVID analysis was performed with the list of genes from a microarray experiment in which CBFβ was knocked down in metastatic breast cancer cells MDA-MB-231 cells grown in a 3D matrigel environment.

National Institute of Allergy and Infectious Disease
The Database for Annotation, Visualization and Integrated Discovery

Annotation Cluster 1	Enrichment Score: 2.52		Count	P_Value	Benjamini
GOTERM_CC_FAT	extracellular region part	RT	31	7.0E-6	1.6E-3
GOTERM_CC_FAT	extracellular space	RT	23	9.1E-5	6.8E-3
GOTERM_CC_FAT	extracellular region	RT	43	1.2E-3	3.7E-2
SP_PIR_KEYWORDS	signal	RT	57	3.9E-3	4.4E-1
UP_SEQ_FEATURE	signal peptide	RT	57	4.5E-3	8.8E-1
SP_PIR_KEYWORDS	glycoprotein	RT	71	5.2E-3	4.0E-1
SP_PIR_KEYWORDS	Secreted	RT	33	8.5E-3	4.0E-1
UP_SEQ_FEATURE	glycosylation site:N-linked (GlcNAc...)	RT	66	1.6E-2	9.9E-1
UP_SEQ_FEATURE	disulfide bond	RT	44	7.6E-2	1.0E0
SP_PIR_KEYWORDS	disulfide bond	RT	45	8.0E-2	6.5E-1
Annotation Cluster 2	**Enrichment Score: 2.43**		**Count**	**P_Value**	**Benjamini**
GOTERM_BP_FAT	response to estrogen stimulus	RT	8	5.3E-4	3.5E-1
GOTERM_BP_FAT	response to steroid hormone stimulus	RT	10	1.2E-3	3.8E-1
GOTERM_BP_FAT	response to hormone stimulus	RT	14	1.4E-3	3.7E-1
GOTERM_BP_FAT	response to endogenous stimulus	RT	14	3.3E-3	4.2E-1
GOTERM_BP_FAT	response to organic substance	RT	19	8.5E-3	6.3E-1
GOTERM_BP_FAT	cellular response to hormone stimulus	RT	5	1.0E-1	7.8E-1
Annotation Cluster 3	**Enrichment Score: 2.2**		**Count**	**P_Value**	**Benjamini**
GOTERM_CC_FAT	basement membrane	RT	8	7.2E-5	8.0E-3
GOTERM_CC_FAT	extracellular matrix part	RT	8	8.8E-4	3.2E-2
GOTERM_CC_FAT	extracellular matrix	RT	11	1.6E-2	3.0E-1
GOTERM_CC_FAT	proteinaceous extracellular matrix	RT	10	2.6E-2	4.1E-1
SP_PIR_KEYWORDS	extracellular matrix	RT	8	2.9E-2	4.7E-1
SP_PIR_KEYWORDS	basement membrane	RT	3	8.2E-2	6.4E-1
Annotation Cluster 4	**Enrichment Score: 2.2**		**Count**	**P_Value**	**Benjamini**
GOTERM_BP_FAT	response to wounding	RT	19	2.9E-4	3.7E-1
GOTERM_BP_FAT	inflammatory response	RT	11	1.3E-2	5.9E-1
GOTERM_BP_FAT	defense response	RT	14	7.2E-2	7.2E-1
Annotation Cluster 5	**Enrichment Score: 2.12**		**Count**	**P_Value**	**Benjamini**
GOTERM_CC_FAT	plasma membrane part	RT	48	3.3E-4	1.9E-2
GOTERM_CC_FAT	intrinsic to plasma membrane	RT	27	8.7E-3	2.2E-1
GOTERM_CC_FAT	integral to plasma membrane	RT	26	1.2E-2	2.7E-1
UP_SEQ_FEATURE	topological domain:Extracellular	RT	42	9.4E-2	1.0E0
Annotation Cluster 6	**Enrichment Score: 2.02**		**Count**	**P_Value**	**Benjamini**
GOTERM_BP_FAT	cell migration	RT	11	4.2E-3	4.6E-1
GOTERM_BP_FAT	cell motility	RT	11	8.7E-3	5.9E-1
GOTERM_BP_FAT	localization of cell	RT	11	8.7E-3	5.9E-1
GOTERM_BP_FAT	cell motion	RT	13	2.7E-2	6.2E-1
Annotation Cluster 7	**Enrichment Score: 1.84**		**Count**	**P_Value**	**Benjamini**
GOTERM_BP_FAT	wound healing	RT	10	1.1E-3	4.5E-1
GOTERM_BP_FAT	regulation of body fluid levels	RT	7	1.2E-2	6.4E-1
GOTERM_BP_FAT	blood coagulation	RT	6	1.2E-2	6.3E-1
GOTERM_BP_FAT	coagulation	RT	6	1.2E-2	6.3E-1
GOTERM_BP_FAT	hemostasis	RT	6	1.5E-2	6.0E-1
SP_PIR_KEYWORDS	blood coagulation	RT	4	1.7E-2	4.6E-1
KEGG_PATHWAY	Complement and coagulation cascades	RT	3	2.5E-1	9.4E-1
Annotation Cluster 8	**Enrichment Score: 1.75**		**Count**	**P_Value**	**Benjamini**
GOTERM_BP_FAT	apoptosis	RT	16	1.6E-2	5.8E-1
GOTERM_BP_FAT	cell death	RT	18	1.7E-2	5.9E-1
GOTERM_BP_FAT	programmed cell death	RT	16	1.8E-2	6.0E-1
GOTERM_BP_FAT	death	RT	18	1.8E-2	5.9E-1
SP_PIR_KEYWORDS	Apoptosis	RT	11	1.9E-2	4.7E-1

Fig. 5.3. DAVID analysis of 2D microarray identifies genes involved in cell migration. DAVID analysis was performed with the list of genes from a microarray experiment in which CBFβ was knocked down in metastatic breast cancer cells MDA-MB-231 cells grown in 2D.

5.4. Common genes are affected by CBFβ knockdown in 2D and 3D MDA-MB-231 cells

The individual DAVID analyses of shCBFβ cells grown in 3D and 2D showed differences in functional responses. Microarray maps provided a general view of the genes regulated showing genes that were up-regulated and down-regulated (Fig. 5.4). Therefore they were used to highlight differential gene expression. Each column represented the different conditions used, which was either shNS and shCBFβ MDA-MB-231 cells grown in 2D or in 3D cell culture. Each line of the map represents one gene. In each case the shCBFβ was compared to the shNS value and only genes with expression levels with ≥2 fold change and q value of ≤0.05 were used. Additionally the 3D values were compared to the 2D values. Genes were either up-regulated (red), down-regulated (green) or had no significant change (yellow). The genes were grouped into 8 clusters based on the similarity of expression profile across the data set. Interestingly, there were differences in gene expression profile across all 8 clusters. One example, cluster D, showed an up-regulation of genes following CBFβ knockdown in 2D but when grown in 3D these genes showed a down-regulation of expression. These results suggest a broad ranged difference in gene expression following growth of MDA-MB-231 cells in matrigel.

Having seen that there was a difference in the functional clustering between the two arrays, the genes with ≥2 fold change and q value of ≤0.05 in both the 2D and 3D microarrays were compared. The number of genes that met the criteria in the 2D microarray was 238. In the 3D microarray, 1053 genes met the criteria. Comparing these genes yielded only 34 genes that were found in both microarrays (Fig. 5.5A). This represented the subset of genes that were changed in 2D and 3D environments.

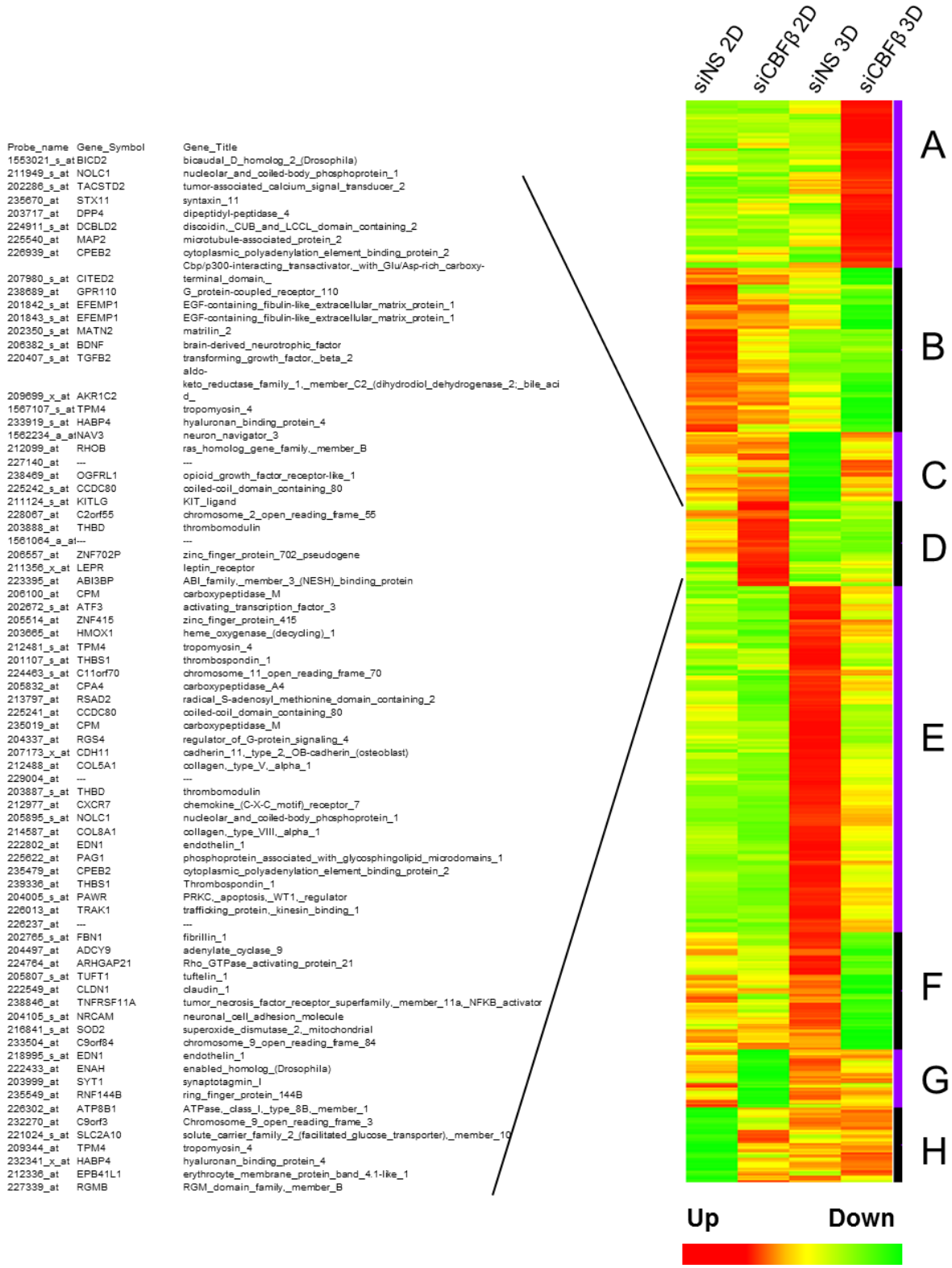

Fig. 5.4. Heat map showing the expression profile of MDA-MB-231 cells knocked down for CBFβ and compared in a 2D and a 3D environment. Clustering analysis of the genes regulated. The colour bar represents the relative abundance of each transcript and was row normalised. Red is the most abundant and green is the least. The letters on the right hand side indicate the different clusters found. The genes in group D were shown as an example of the regulated genes. Other genes within other clusters have been omitted for simplicity.

Of these 34 genes for which the expression levels changed in both 2D and in 3D cells following CBFβ knockdown, the 2D cells showed 15 genes that had been up-regulated and 19 genes down-regulated. In the 3D cells 12 genes were up-regulated and 22 genes were down-regulated (Fig. 5.5B). This showed that not all genes respond in a similar manner when grown in a 2D compared to a 3D environment.

To establish where the gene expression was similar in either environment the common genes identified in the 2D and 3D CBFβ knockdown microarrays were listed and their fold change of the expression values were listed (Table 5.1). The table showed that many of the genes do follow the same expression patterns between 2D and 3D. However, 6 of the genes showed an opposite direction of regulation in 2D compared to 3D. SPANX, TMEM45A, GRB10, CXCL1 and RASSF4 were all up-regulated following CBFβ knockdown in 2D cells, but down-regulated after CBFβ knockdown in 3D cells. IFITM1 was down-regulated in 2D cells and up-regulated in 3D cells. This shows that even those genes that are common amongst 2D and 3D cells had differing expression levels.

Amongst the common genes was the expression of CBFβ which had been knocked down by 4.4 fold in 3D cells and 9.4 fold in 2D cells. This itself acted as an intrinsic control which showed CBFβ had in fact been knocked down in the shCBFβ samples. The remaining genes had the same expression patterns yet still showed differing expression levels. For example, the expression of Hedgehog interacting protein (HHIP) was 2.6 fold up-regulated in 2D cells but was 11.2 fold up-regulated in 3D cells. Aquaporin3 (AQP3) was up-regulated by 14 fold in 3D cells, yet in 2D cells its gene expression was up-regulated by only 2.5 fold (Table 5.1).

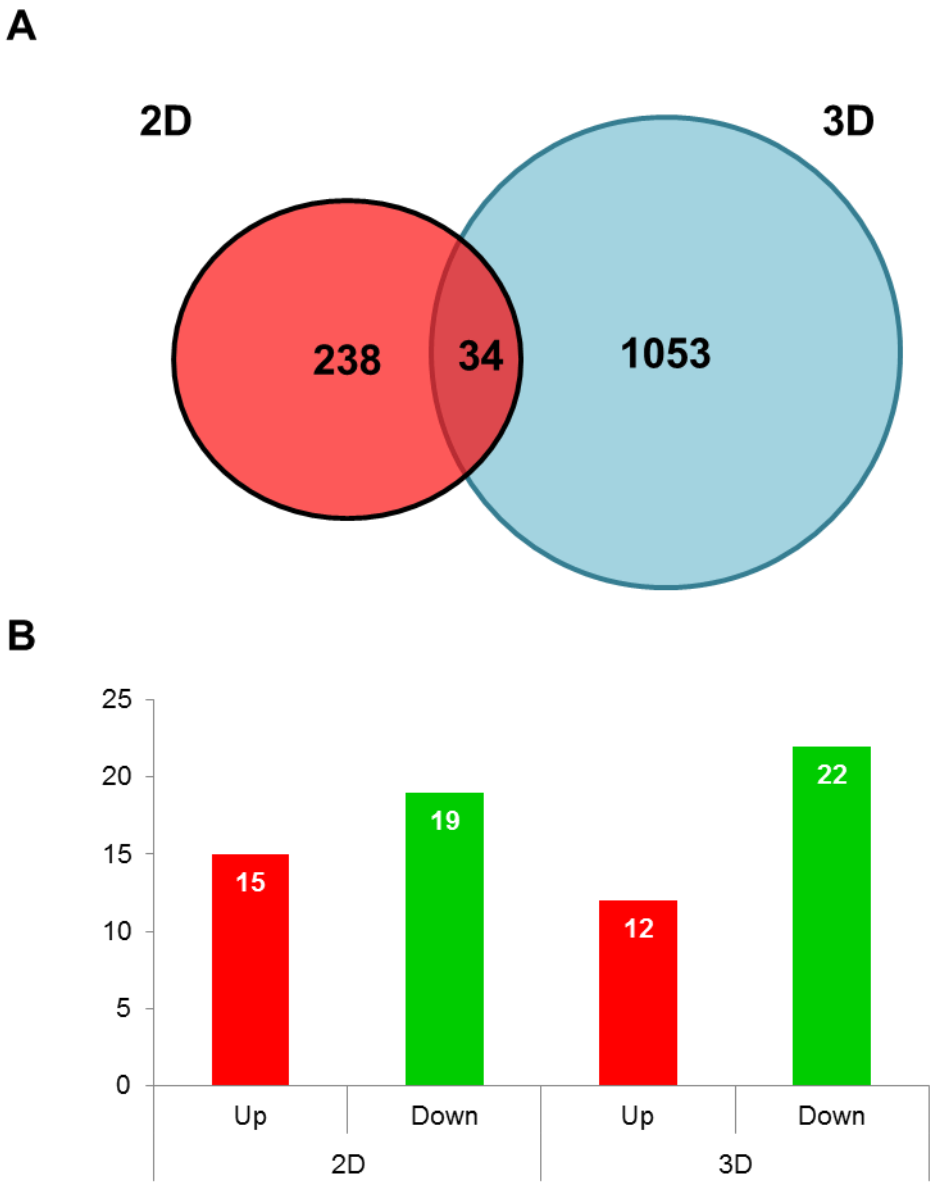

Fig. 5.5. MDA MB 231 cells knocked down for CBFβ have common genes when grown in a 2D and a 3D environment. (A) A venn diagram showing the number of genes both up and down regulated. Genes from the microarray experiment for CBFβ knockdown in MDA-MB-231 cells with a fold change ≥2 and q value ≤0.05. (B) Graph representing the number of genes Up or Down regulated in 2D or 3D cells. Only the 34 genes common to both 2D and 3D were used.

Of the common genes listed, those of particular interest were those that were related to the ability of breast cancer to remodel bone and genes that were related to cell migration. One process that had previously been studied using the 2D microarray was that of the secretory pathway (Mendoza-Villanueva et al., 2010). This cluster of genes involved production of proteins that were secreted from the cells and may be involved in the bone remodelling stage. The 34 genes listed contains multiple genes included in this pathway, such as THBS1 (Thrombospondin), KITLG (Lit Ligand), HHIP (Hedgehog Interacting Protein), CXCL1 (Chemokine (CXC motif) Ligand 1) and IL11 (Interleukin 11). Other genes of interest were ELF3 (E74 like factor 3) and BIRC3 (Baculovirus IAP repeat containing 3). The transcription factor ELF3 was chosen for its role in regulating MMP13 (Otero et al., 2012). BIRC3 was chosen due to its role in inhibiting apoptosis and so a key issue in cancer cells which proliferate uncontrollably (Saleem et al., 2013). These selected genes were used for validation using RT-PCR.

Genes	3D Fold change	2D Fold change
THBS1	2.4	4.6
ELF3	2.7	3.3
TNFSF15	6.4	2.9
KITLG	7.1	2.8
FGFBP1	4.3	2.8
SPANXB1/SPANXB2 /SPANXF1	-2.0	2.7
HHIP	11.2	2.6
TMEM45A	-3.3	2.6
HIST1H2AC	2.6	2.5
AQP3	14.0	2.5
GRB10	-2.6	2.2
OAS1	2.1	2.1
CXCL1	-15.0	2.1
GALNT5	2.4	2.0
RASSF4	-3.9	2.0
CFP	-2.2	-2.0
PLEKHH2	-2.7	-2.0
PHLDA1	-2.4	-2.0
SLC40A1	2.0	-2.0
G0S2	-3.0	-2
IFITM1	2.1	-2.1
BIRC3	-8.1	-2.2
CSF2	-10.1	-2.3
IGSF3	-2.6	-2.3
C15orf29	-2.4	-2.4
EVI2A	-4.4	-2.6
PLLP	-2.1	-2.7
SRGN	-2.7	-2.7
NUPL1	-2.0	-2.9
EVI2B	-6.8	-4.1
LAPTM5	-2.1	-4.3
CCNA1	-3.9	-5.6
IL11	-2.5	-8.3
CBFB	-4.4	-9.4

Table 5.1. List of the common genes between 2D and 3D shCBFβ MDA MB 231 cells. The common genes between the microarrays for shCBFβ MDA-MB-231cells in 2D and shCBFβ MDA-MB-231 cells in 3D are listed. Only genes which have a fold change ≥2 and q value ≤0.05 are shown.

5.5. Validation of microarray genes by RT-PCR

In order to validate the results obtained from the microarray analysis of CBFβ knockdown in 3D and 2D cell culture, RT-PCR was performed. In addition to targets found in both the 3D and 2D microarrays, three genes that were expressed in only the 3D microarray were also validated. These genes were CADM2 (Cell Adhesion Molecule 2), HPGD (Hydroxyprostaglandin) and SCIN (Scinderin). Collectively, these were chosen to further validate the 2D microarray compared to the 3D microarray as these genes were only seen in the 3D microarray. Individually, CADM2 was chosen for its role in cell polarity regulation and its tumour suppressor function (Chang et al., 2010). HPGD was chosen for its role in EMT and cell migration in breast cancer cells (Lehtinen et al., 2012). SCIN was chosen as it is a calcium regulated actin binding protein and so may be involved in both bone and breast regulation due to the requirement for calcium in bone and milk (Lejen et al., 2002).

Total mRNA was extracted from MDA-MB-231 cells stably transfected with shNS or shCBFβ grown in 3D Matrigel. Subsequently, the RNA was used for RT-PCR assays. Specific primers were designed for the ten chosen targets and used for RT-PCR (Fig. 5.6). All targets were normalised against intrinsic RPLO mRNA expression levels.

The 2D microarray potential Runx2/CBFβ target genes THBS1, KITLG, HHIP, ELF3, HPGD and SCIN all showed an increase in mRNA expression following CBFβ knockdown. BIRC3 and IL11 both showed a decrease in mRNA expression. CXCL1 and CADM2 both showed no significant change in mRNA expression. The 3D microarray showed an increase in mRNA expression of THBS1, KITLG, HHIP,

ELF3, CADM2, HPGD and SCIN. The target genes CXCL1, BIRC3 and IL11 all showed a decrease in mRNA expression (Fig. 5.6). These RT-PCR mRNA expression values were then compared to the values of the microarray (Table 5.2). If the RT-PCR matched the values seen in the microarrays, then the gene was considered to be successfully validated.

All genes tested showed similar expression patterns in 2D and 3D microarrays compared to the RT-PCR results, with CXCL1 as the exception. This gene showed an increased expression following CBFβ knockdown in the 2D microarray. However, in the RT-PCR verification, there was no significant change seen. Additionally, of the genes that did not appear in the 2D microarray data set but were found in the 3D microarray, CADM2 showed no significant change in expression in 2D and an up-regulation in expression in 3D. This corresponded to the relevant microarray data sets. On the other hand, neither HPGD nor SCIN were seen in the 2D microarray while they showed high increases in expression following CBFβ knockdown in the 3D microarray. The RT-PCR data showed that both these targets were in fact significantly changed following CBFβ knockdown. Both genes showed an up-regulation of mRNA. Taken together, these results show that there is a higher correlation between the 3D microarray data and the results obtained in the RT-PCR experiments than those between the 2D microarray and RT-PCR experiments. This data could represent potential new targets of Runx2/CBFβ.

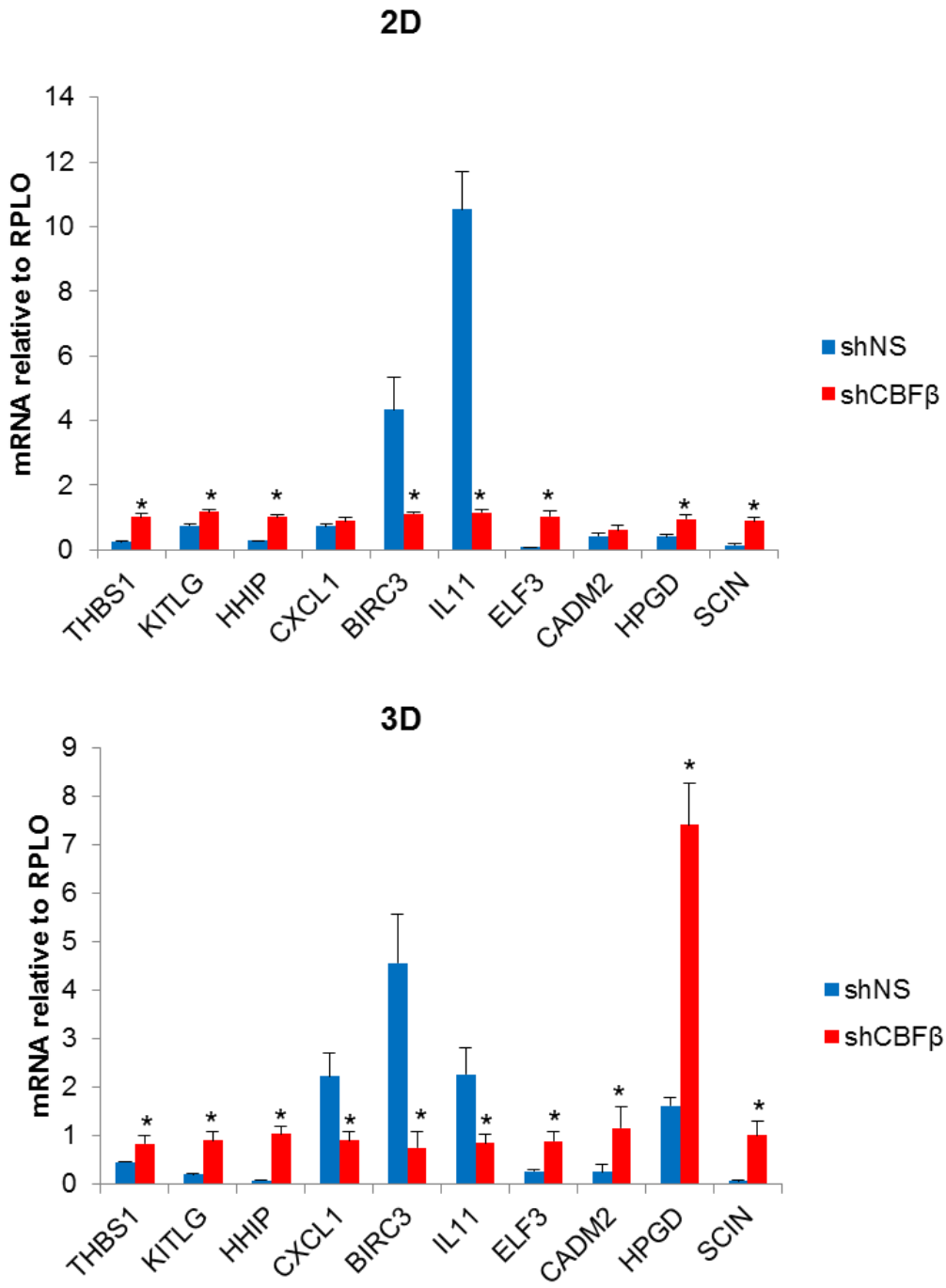

Fig. 5.6. Validation of some common genes found between the 2D and 3D microarrays following CBFβ knockdown in metastatic breast cancer cells. Ten common genes linked to bone remodelling or breast cancer metastasis were subjected to RT-PCR analysis to verify the microarray data. MDA-MB-231 cells grown in a 2D environment were subjected to RNA extraction and RT-PCR for target genes was conducted (top panel). MDA-MB-231 cells grown in a 3D environment were subjected to 3D RNA extraction and RT-PCR for target genes was conducted (bottom panel). Data are presented as mean ± standard deviation (S.D) (n=3). * Indicates a significant difference compared to shNS using the Students T-test where $P<0.05$.

Gene Name	2D Microarray Fold Change	3D Microarray Fold Change	2D RT-PCR	3D RT-PCR
THBS1	4.6	2.4	Up	Up
KITLG	2.8	7.1	Up	Up
HHIP	2.6	11.2	Up	Up
CXCL1	2.1	-14.9	NC	Down
BIRC3	-2.2	-8.1	Down	Down
IL11	-8.3	-2.5	Down	Down
ELF3	3.3	2.7	Up	Up
CADM2	~	3.1	NC	Up
HPGD	~	13.9	Up	Up
SCIN	~	16.9	Up	Up

Table 5.2. Correlation of microarray and RT-PCR experiments for validation of CBFβ genes in 2D and 3D growth. The table compares the results obtained in the microarrays for 2D and 3D shCBFβ in MDA-MB-231 cells and the RT-PCR experiments. The relevant fold changes as shown in the microarray are listed. (-) indicates down regulated gene. (~) indicates this gene was not listed in the microarray. (NC) indicates No Change in mRNA expression therefore did not yield any significant change in RT-PCR results. Up indicates a significant up regulation in mRNA expression. Down indicates a significant down regulation in mRNA expression. Statistical evaluation of significance was performed using the Students T-test where $P<0.05$ when compared to the control group.

5.6. IL11 is a potential target gene of Runx2/CBFβ

Having established that knockdown of CBFβ in MDA-MB-231 cells resulted in different gene expression in 2D and 3D matrigel the common genes were further researched. The second aim of this chapter was to identify potential target genes of the Runx2/CBFβ complex in relation to its role in bone remodelling. The IL11 transcript was found in both the 2D and 3D microarrays. IL11 is known to be produced by breast cancer cells to induce osteolysis by acting on osteoclasts (Kang et al., 2003) (Lacroix et al., 1998). For this reason, IL11 was chosen for further analysis as a potential Runx2/CBFβ target gene.

5.6.1. Runx2 binds to the IL11 promoter

Having established that knockdown of CBFβ in MDA-MB-231 cells caused a decrease in IL11 mRNA expression, the next question was whether this action could be a result of direct or indirect regulation by Runx2/CBFβ. In order for Runx2 to directly regulate IL11, there must be Runx binding sites in the promoter region of the IL11 gene. To determine if these Runx binding sites were present, the DNA sequence of human IL11 was obtained from NCBI and the region upstream of the transcription initiation site was searched for possible sites (Tang et al., 1998). Any partial Runx biding sites, which are sites which had one base pair difference were also marked (Fig. 5.7). Searching up to approximately 2000 base pairs (bps) upstream of the initiation site, there were three full Runx binding sites present. These were termed IL11 sites 1, 2 and 3. Site 1 was that closest to the transcription initiation site and site 3 was the farthest.

```
-2079 GTACCTCTGCCCCTCGCTTGCTCTGTGGTGAATCCCGGGTCTCCTCTGCCCCCATGCCTG -2020
-2019 GGGCTGGCCCACTGTGAGCCTGGGTAGGCGTCGCTGCCTCCCCCCTGGCCTGTGGGTCCC -1960
-1959 CTCCCCCCTGCACTCCTCTCCTGCCTCCACCTCTGTGCGGTGACGTCCAGGGCTCTGGCC -1900
-1899 CCGGTGGTTCTGGCCACTGTCTCCGTGTCCCCACTGTCCCGTCTTCACCCCATCTTGCTC -1840
-1839 CTGCCCCATCTCTCTCGAAGGCGACATCTTTTTCTCTGTTCCCTGATGTGTTCAGAAAAG -1780
-1779 TTAACGAGGGGAATAAGGATGGTCAGCACTGACTTTGTGCTTCACGTGAATGAGCTCGCT -1720
-1719 TTATCCTCATCGTGGCATTTAGGCGGATGAGGGTGCATCATTAACCCCCCTTCACAGATG -1660
-1659 AGGAAACTGAGGCACAGAGGGGGAGAGTCGCACATGGAGGTCTTGCCTCTATGGAGTGTC -1600
-1599 TCAGCGCCTCTTGGTCCTCAGTCTCCGTCTCTCCTCCTCCTTCCTGTCTCCACCTGCCTC -1540
-1539 TTTGAGAAAGGCTTTTCAAAAGGCCAGGCGTGGTGGTTCACACCTGTATTCCCACCACTT -1480
-1479 TGGGAGGCTGAGGCGGGAGGATGACCTGAGCTCAGGAGTTTGAGACCAGCCTGGGCAACA -1420
-1419 TGGCAAAACCCTATCTCTACTAAAAATACAAAAAATAGCCAGGCATGGTGGCGGGTGCCT -1360
-1359 GTAATCCCAGCTACTCAGGAGGCTGAGGCATGAGAATCACTTGAACCTGGGAGGCGGAGG -1300
-1299 TTACAGTGAGCTGAGATCACACCACTGCACCCCAGCCTGGGTGACACAGCGAGACTCTGT -1240
-1239 CTCAAAAAAACCAAAAACGAGGCCAGGCACGGTAGCTCACACCTGTCATCCCAGCACTTT -1180
-1179 GGGAGGCCGAGGCAGGCGGATCACGAAGTCAGGAGTTCGAGACCAGCCTGGCCAACATGG -1120
-1119 TAAGACCCCGTCTCTACTAAAAATACAAAATTAGCCGGGTGTGGTGGCGCACACCTGTAA -1060
-1059 TCCCAGCTACTTGGGAGGCTGAGGCAGGAGAATCGCTTGAACCCGGGAGGTGGAGGTTGC -1000
-999  AGTGAGCTGAGATTGTGCCATTGATCGCGCCATTGCACTCCAGCCTGGGTGACAGAGTGA -940
-939  GACTCAGTACCAAAAAACAAACAAACAAAAAACAAACAAAAAATGAGAAAGGCTTTTACT -880
-879  CTCTGCCCCCATTGCTGAGTCCCCAACATCTCAGCGTCTCTGTCTTTCTAATATCTCTGT -820
-819  CTCCCCTTTTCTGTCCCTGGGGCCTCTCCGTCCCTGTCACTCTGCCCCGTGTCTCTGTTT -760
-759  GCCTGGTGCCTTTCTTCAGCTGCGGGATCCTCTGTCTCAGAGTCTTGGTGTCTCTGTTCC -700
-699  TTTCCCCTCGGGGTCTCCCTGGGTCTCCCCAAGTCCCTCCTGCTGTCTTCCTCCCGCTCT -640
-639  CTGATCTCTGACTCCCAGAACCTCTCCCTCTGTCTCCAGGGCTGCCCCTCTGATCCTCTT -580
-579  TGCTTCTCTGGTGTGTCTCTCTGGCTGCCTCCATCTCTGTGGATCTCCATCTCCCTGTCT -520
-519  CTGTCTCAGTCTGTCCTTCACTCTGTGTGTGTGTGTGTCTCTCTCTCTCTCCTTCCCTTC -460
-459  CACTCCCTCTTCCTCCTGCCTCCACCTCTCCAGGCCCCTGTCTTGTCCCTCCGTCCGGCC -400
-399  TTTCTCTGCCTTTCCGTCCTCCTGCCTCCCCATCTCTCTCTGCTAGTCCTGGTCCAGCCG -340
-339  GACCCCCACCCACAGTCGGGCCCCAGCGCTTGAGCCTGAGTGTCTGCTCCGGCCCCTGGA -280
-279  GGTGGAGGGAGGGGACGCCAATGACCTCACCAGCCCCTCTCCGACCACCCCCCCTTTCC -220
-219  CTTTTCAACTTTTCCAACTTTTCCTTCCGTGCCCTCCTCCGAGCGCGGCGGCGTGAGCCC -160
-159  TGCAAGGCAGCCGCTCCGTCTGAATGGAAAAGGCAGGCAGGGAGGGTGAGTCAGGATGTG -100
-99   TCAGGCCGCCCTCCCCTGCCGCCTGCCCCCCGCCCGCCCGCCCCAGCCCCCTATATAACC  -40
-39   CCCCAGGCGTCCACACTCCCTCACTGCCGCGGCCCTGCTGCTCAGGGCACATGCCTCCCC  +21
```

Fig. 5.7. IL11 promoter sequence highlighting possible Runx sites. DNA sequence from +21 to -2079 bps from the start of transcription of the human Interleukin 11 (IL11) gene. Full Runx sites have been highlighted in red. Partial Runx DNA binding sites have been highlighted in blue. The transcription initiation site is shown in grey and the start of the translated IL11 sequence is in yellow.

Having established that IL11 had the potential to recruit Runx proteins to its promoter region, EMSA assays were performed to establish whether endogenous Runx2 from MDA-MB-231 cells could bind to these sites. The sites were tested individually. For each Runx site a double stranded oligonucleotide containing the Runx binding site was radiolabelled. A mutated sequence containing a three point mutation within the Runx binding site was used as competitors. Additionally a SOST oligonucleotide was used as a positive control for Runx protein binding (Mendoza-Villanueva et al., 2011).

The first site tested, Runx-IL11-site1 (s1) (Fig. 5.8A), was radiolabelled and incubated with nuclear extracts from UMR106 cells, as these cells are a positive control for Runx2 protein expression. The samples were then subjected to EMSA analysis. The radiolabelled oligonucleotide without any nuclear extract showed no retardation of complex in the gel and so all the free DNA ran through the gel and accumulated at the bottom. With addition of UMR106 nuclear extracts and an unlabelled WT competitor, there was no retardation of complex. This was expected as the WT competitor would bind most of the Runx protein. With the addition of the radiolabelled SOST oligonucleotides a complex was formed that became retarded in the gel (Fig. 5.8B, lanes 1-3). This showed that Runx protein in the UMR106 cell nuclear extract could bind to the Runx binding site on the SOST oligonucleotide. This retarded band was used as the positive control for Runx binding to the oligonucleotide.

The Runx-IL11-s1-WT oligonucleotide was radiolabelled and incubated with UMR106 nuclear extract. This produced complexes that were retarded in the gel. When a mutant competitor, which contains a 3bp mutation in the Runx binding site only, was also incubated, all other retarded complex bands were removed from the

gel leaving a single band representing Runx binding. This band was unexpectedly weaker with the addition of the competitor. The addition of a WT competitor resulted in no retardation of complex in the gel (Fig 5.8B, lanes 4-6). This showed that Runx proteins in UMR-106 cells were able to bind to the Runx binding site in the Runx-IL11-s1-WT oligonucleotide. In order to establish whether the Runx2 protein could bind to this site, anti-Runx2 antibody was incubated with a radiolabelled WT oligonucleotide and UMR106 nuclear extract. The previously retarded construct was no longer formed and instead a complex was formed which retarded higher up the gel, suggesting a higher molecular weight (Fig. 5.8B, lane 7). This was as expected if the anti-Runx2 antibody bound to the Runx2 protein/DNA complex and is termed as a 'supershift'. Thus, Runx2 can bind to the Runx-IL11-s1 in UMR106 cells.

Having shown that the Runx-IL11-s1 was able to recruit Runx2 in UMR106 cells, the experiment was repeated in order to confirm whether the same was true for MDA-MB-231 cells. Radiolabelled SOST WT oligonucleotide was incubated in the presence and absence of nuclear extract. Without nuclear extract, no bands were seen. With MDA-MB-231 cell nuclear extract there were many bands retarded in the gel. With the addition of an unlabelled WT competitor, these retarded bands did not appear (Fig. 5.8C, lane 1-3). The use of the radiolabelled Runx-IL11-s1 oligonucleotide resulted in many bands being retarded in the gel. Following incubation with a mutant competitor many of these bands were removed, however a definitive Runx/DNA band wasn't detected. With the addition of the WT competitor, all bands were removed so that there were no retarded bands. Incubation with Runx2 resulted in a supershift (Fig. 5.8C, lanes 4-7). Taken together, while Runx-IL11-s1 did have the ability to bind Runx2, as shown by the binding in UMR106 cells, it was inconclusive whether there was binding of Runx2 to this site in MDA-MB-231 cells.

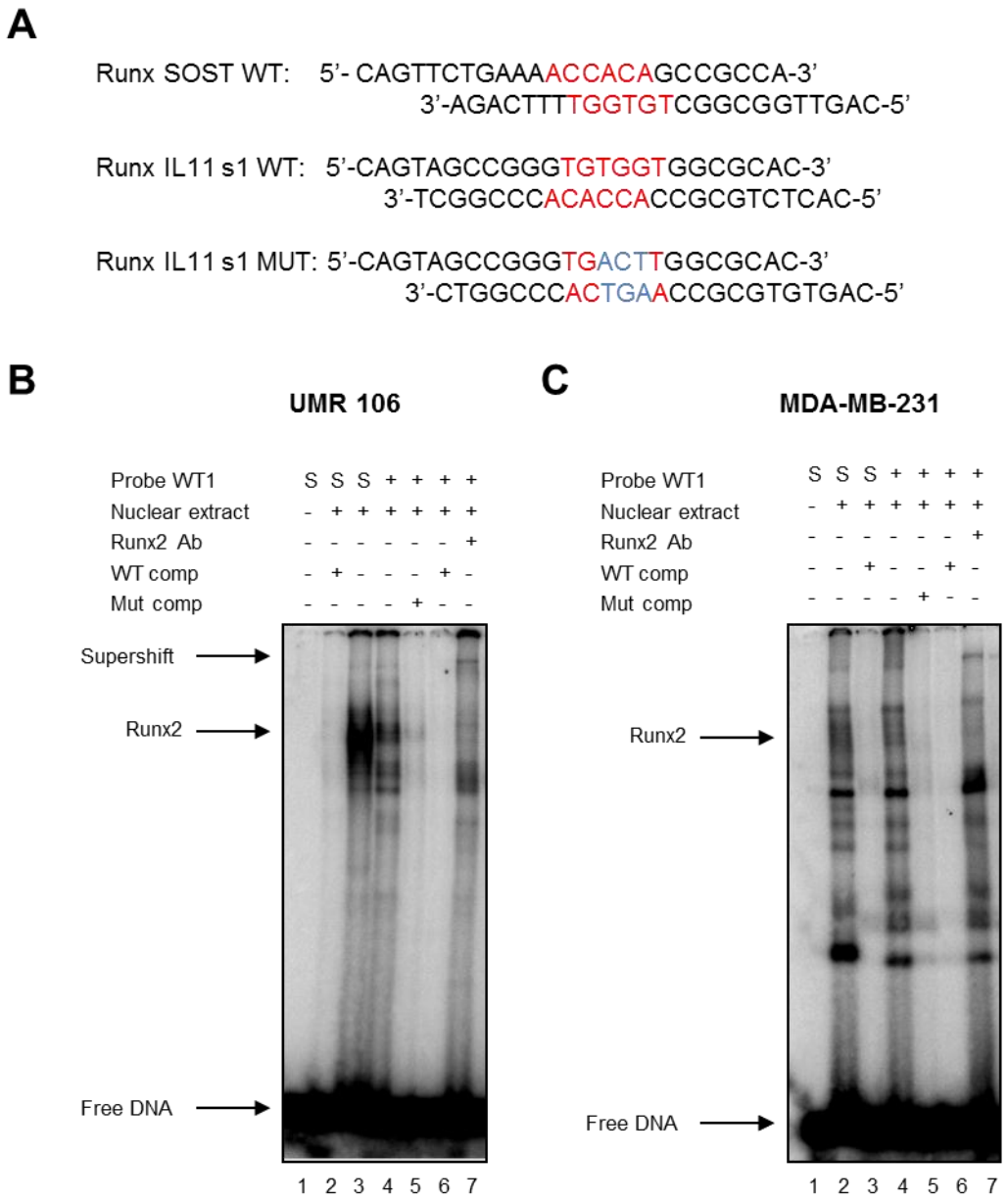

Fig. 5.8. Runx2 binds to IL11 promoter site 1 in UMR106 cells. EMSA assay demonstrating specific binding of Runx2 to IL11 promoter Runx binding site 1. (A) Diagram showing the oligonucleotides used in the EMSA experiment. Radiolabelled probes Runx IL11 s1 WT was used in experiments shown in (B) and (C). (B) EMSA assay showing Runx2 binding to IL11 promoter site 1 in UMR106 cells. Nuclear extracts from UMR106 cells were incubated with radiolabelled oligonucleotides containing the first full Runx2 binding site from the human IL11 gene promoter. (C) EMSA assay showing Runx2 binding to IL11 promoter site 1 in MDA-MB-231 cells. Nuclear extracts from MDA-MB-231 cells were incubated with radiolabelled oligonucleotides containing the first full Runx2 binding site from the human IL11 gene promoter. In both (B) and (C) competitive assays were performed with 100 fold molar excess of cold probe. SOST is used as a positive control indicated by 'S'.

The EMSA experiment was repeated using oligonucleotides created for the second full Runx binding site found in the IL11 promoter region, here termed Runx-IL11-s2-WT. A mutated form of the Runx binding site containing a 3bp mutation was also created (Fig. 5.9A). These oligonucleotides were used for EMSA assays. To determine if this site could bind Runx2, UMR106 cells were first used as a control (Fig. 5.9B). Radiolabelled SOST incubated in the presence and absence of UMR106 nuclear extract was used. Without nuclear extract, no band was seen. In contrast, with nuclear extract a single large band representing Runx2 binding is retarded in the gel. Addition of an unlabelled WT competitor eliminated this retardation (Fig. 5.9B, lanes 1-3). Thus the band for positive Runx binding to oligonucleotide was clearly distinguishable. Use of the labelled Runx IL11-s2-WT oligonucleotide also gave a large band in a similar position to that created by SOST. Addition of the unlabelled mutant competitor removed all other retarded bands except for that corresponding to Runx binding. Unexpectedly, this band was weaker than that previously seen without the mutant competitor. With incubation of a WT competitor, no bands were retarded in the gel (Fig. 5.9, lanes 4-6). A clear supershift was detected upon incubation with Runx2 antibody. The previously retarded complex was displaced to higher up in the gel (Fig. 5.9B, lane 7). This indicated that Runx2 can bind to Runx-IL11-s2-WT in UMR106 cells.

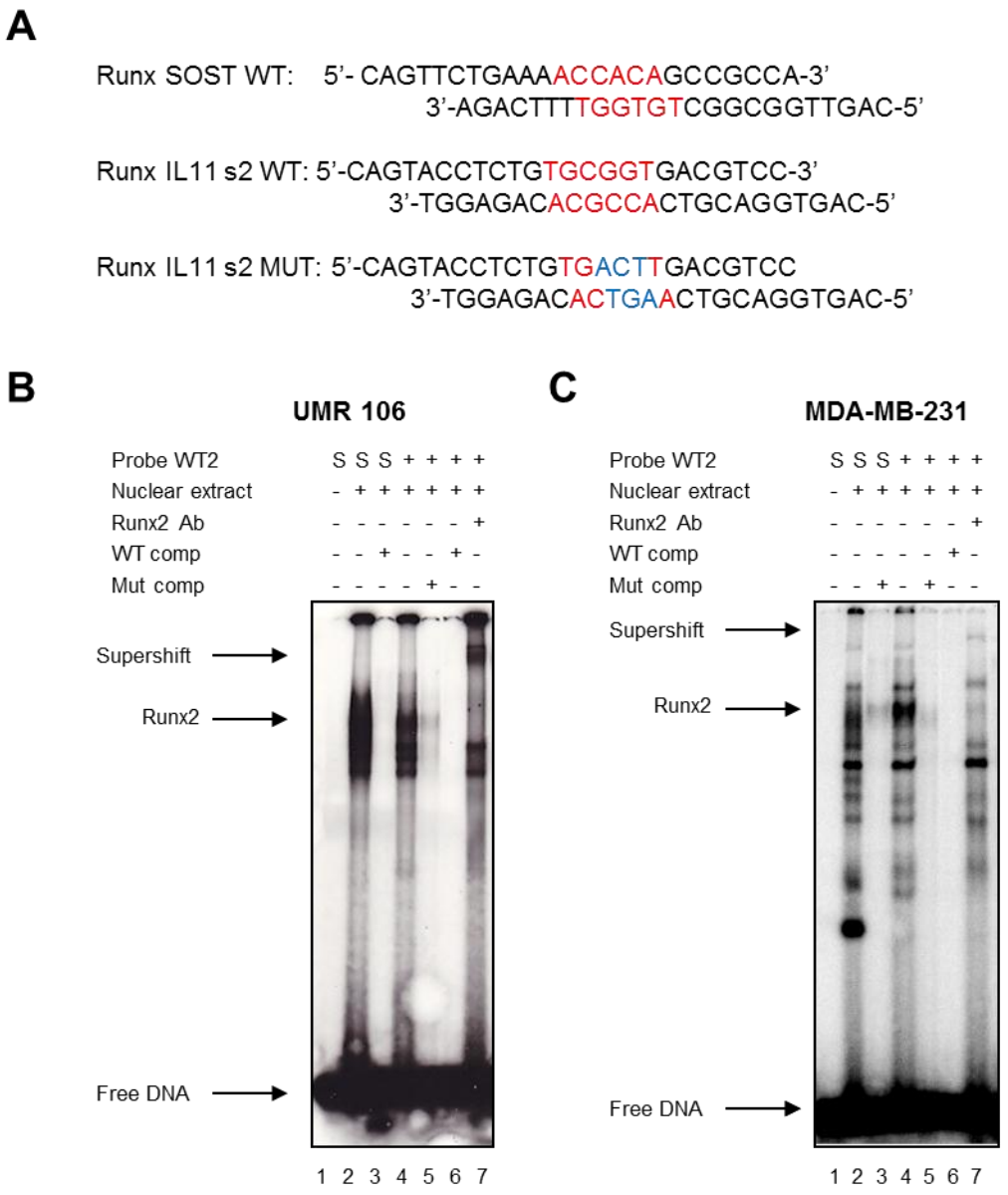

Fig. 5.9. Runx2 binds to IL11 promoter site 2. EMSA assay demonstrating specific binding of Runx2 to IL11 promoter Runx binding site 2. (A) Diagram showing the oligonucleotides used in the EMSA experiment. Radiolabelled probes Runx IL11 s2 WT was used in experiments shown in (B) and (C). (B) EMSA assay showing Runx2 binding to IL11 promoter site 2 in UMR106 cells. Nuclear extracts from UMR106 cells were incubated with radiolabelled oligonucleotides containing the second full Runx2 binding site from the human IL11 gene promoter. (C) EMSA assay showing Runx2 binding to IL11 promoter site 1 in MDA-MB-231 cells. Nuclear extracts from MDA-MB-231 cells were incubated with radiolabelled oligonucleotides containing the first full Runx2 binding site from the human IL11 gene promoter. In both (B) and (C) competitive assays were performed with 100 fold molar excess of cold probe. SOST is used as a positive control (S).

To determine whether this was the case in MDA-MB-231 cells, this EMSA was repeated in these cells (Fig. 5.9C). The incubation of SOST WT without and with nuclear extract showed an absence and retardation of bands in the gel respectively (Fig. 5.9C, lanes 1 and 2). Addition of a mutant competitor revealed a single band indicating Runx/DNA complex (Fig.5.9C, lane 3). With the radiolabelled Runx-IL11-s2-WT with nuclear extract many bands were retarded in the gel. With the addition of the mutant competitor, only a single band remained, which was no longer retarded following incubation with WT competitor (Fig.5.9C, lanes 4-6). Incubation with Runx2 antibody showed a supershift (Fig.5.9C, lane 7). This showed that Runx-IL11-s2-WT can bind Runx2 in MDA-MB-231 cells.

The third full Runx binding site found in the IL11 promoter region, termed Runx-IL11-s3-WT was also used to determine if this was also a potential Runx2 binding site. A mutated form of the Runx binding site containing a 3bp mutation was also created, Runx-IL11-s3-MUT (Fig. 5.10A). To determine if this site could bind Runx2, UMR106 cells were first used as a control (Fig. 5.10B). Radiolabelled SOST incubated in the presence and absence of UMR106 nuclear extract was used. Without nuclear extract, no band was seen, whereas with nuclear extract a single large band representing Runx2 binding was retarded in the gel. Addition of an unlabelled WT competitor eliminated this retardation of the complex (Fig. 5.10B, lanes 1-3). This retarded band represented the Runx/SOST binding which was used as the positive control. Incubation of the labelled Runx-IL11-s3-WT oligonucleotide with nuclear extract gave retardation of a complex in a similar position to that created by SOST. Addition of the unlabelled mutant competitor removed all retarded bands but one. This corresponded to the retarded band created by Runx/SOST. With incubation of a WT competitor, no bands were retarded in the gel (Fig. 5.10, lanes 4-6). A clear

Supershift was detected upon incubation with Runx2 antibody. The previously retarded complex was displaced to higher up in the gel (Fig. 5.10B, lane 7). This indicated that Runx2 can bind to Runx-IL11-s3-WT in UMR106 cells.

Once again, to determine whether this was also the case in MDA-MB-231 cells, this EMSA was repeated in these cells (Fig. 5.10C). The incubation of SOST WT without and with nuclear extract showed an absence and retardation of bands in the gel respectively (Fig. 5.10C, lanes 1 and 2). Addition of a WT competitor revealed no bands hence no retarded complexes (Fig.5.10C, lane 3). The radiolabelled Runx-IL11-s3-WT with nuclear extract resulted in many bands being retarded in the gel. However, there was no apparent band detected that would correspond to that of the Runx/DNA complex as shown by the Runx/SOST binding. With the addition of the mutant competitor, only a single band remained. This was no longer retarded following incubation with WT competitor (Fig.5.10C, lanes 4-6). Incubation with Runx2 antibody showed a supershift (Fig.5.10C, lane 7). Thus it was inconclusive as to whether Runx2 binds to the IL11 site 3 sequence in MDA-MB-231 cells.

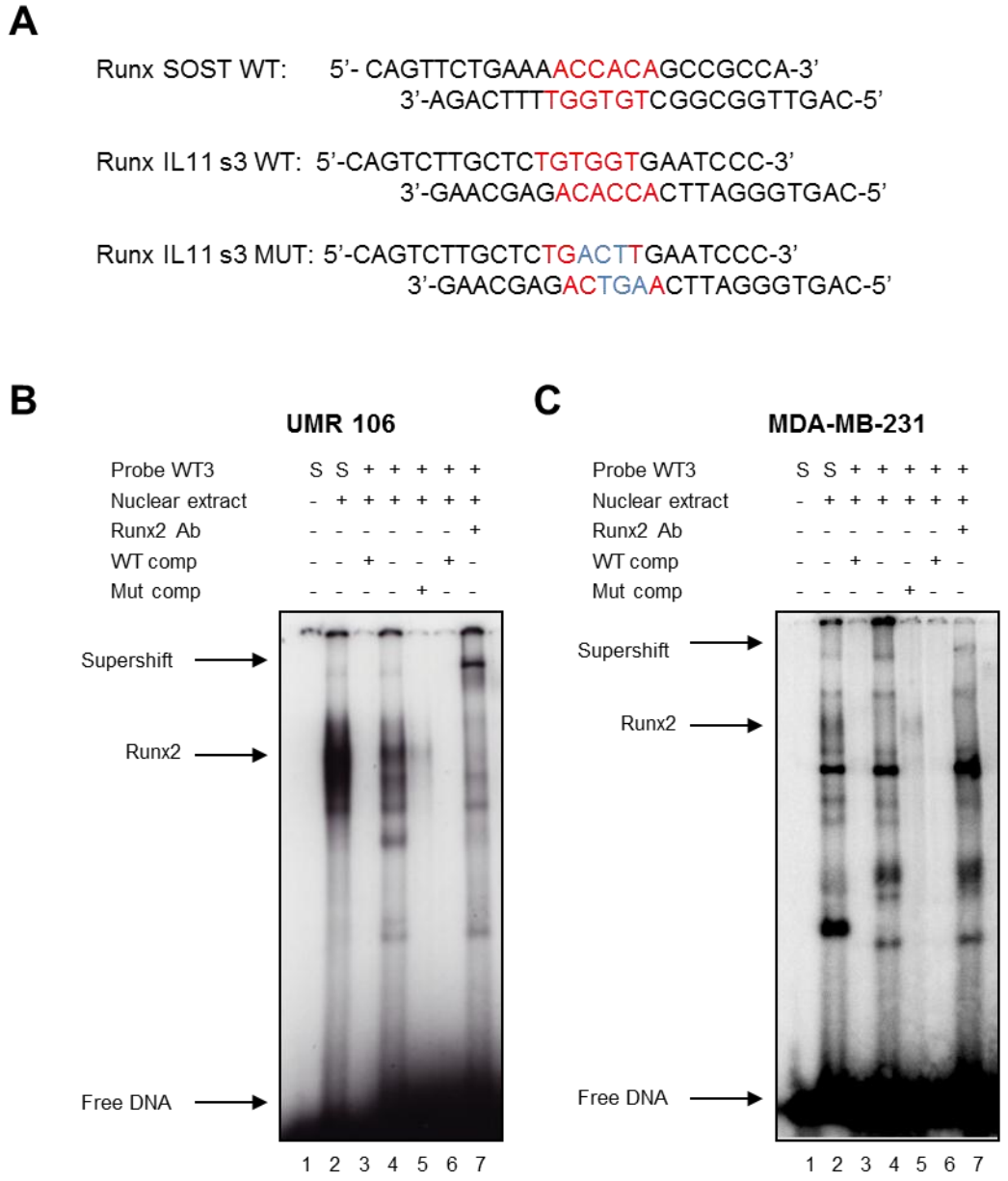

Fig. 5.10. Runx2 binds to IL11 promoter site 3. EMSA assay demonstrating specific binding of Runx2 to IL11 promoter Runx binding site 3. (A) Diagram showing the oligonucleotides used in the EMSA experiment. Radiolabelled probes Runx IL11 31 WT was used in experiments shown in (B) and (C). (B) EMSA assay showing Runx2 binding to IL11 promoter site 3 in UMR106 cells. Nuclear extracts from UMR106 cells were incubated with radiolabelled oligonucleotides containing the third full Runx2 binding site from the human IL11 gene promoter. (C) EMSA assay showing Runx2 binding to IL11 promoter site 1 in MDA-MB-231 cells. Nuclear extracts from MDA-MB-231 cells were incubated with radiolabelled oligonucleotides containing the first full Runx2 binding site from the human IL11 gene promoter. In both (B) and (C) competitive assays were performed with 100 fold molar excess of cold probe. SOST is used as a positive control (S).

5.7. Discussion

Metastatic breast cancer cells knocked down for CBFβ were grown in a 3D matrigel system and subsequently used for microarray analysis. A previous microarray analysis of these same cells grown in 2D was used to compare the change in transcripts due to the extracellular environment. Growth in matrigel resulted in a vast difference of gene regulation in MDA-MB-231 cells. Of the 2D and 3D cell, only 34 genes were common in both conditions with CBFβ knockdown. RT-PCR verified the gene expression seen in the two microarrays. IL11 was identified as a potential direct target of the Runx2/CBFβ complex. There were three potential full Runx binding sites identified. EMSA analysis confirmed Runx2 can bind all three sites in UMR106 cells but in MDA-MB-231 cells the binding of Runx2 was inconclusive.

5.7.1. Metastatic breast cancer cells express different genes when grown in matrigel

Having established in the previous chapter that CBFβ was indeed knocked down in MDA-MB-231 cells, the stable cell lines were grown in a 3D Matrigel system. The RNA extracted was used for microarray analysis. This microarray showed that over 3 times as many genes were down-regulated following CBFβ knockdown than up-regulated. Therefore, under normal cell conditions in which MDA-MB-231 cells have higher CBFβ protein levels, CBFβ would lead to an up-regulation of more genes than it would supress.

DAVID analysis grouped the genes into functional categories. Of interest was cluster 4 which included genes involved in the regulation of cell motion and cell migration. This was expected as it has previously been shown that CBFβ knockdown causes loss of invasion (Mendoza-Villanueva et al., 2011). This was linked to the fact that

the Runx2/CBFβ complex is linked to a reduction in Runx2 binding affinity and so its function (Tahirov et al., 2001). This loss of motility was seen in the previous chapter where CBFβ knockdown causes loss of protrusions in 3D cell culture.

5.7.2. Comparison of 2D and 3D MDA-MB-231 shCBFβ cells

One method to illustrate the differences between the microarrays in a visual context was to use a heat map. The heat map not only compared MDA-MB-231 cells grown in 2D with those grown in 3D Matrigel, but compared the CBFβ knockdown in 2D with 3D as well. The widespread changes in gene expression resulting from the change in extracellular environment can be seen in the heat map. The heat map does not show a single cluster which has the same pattern of gene expression between 2D and 3D cells. Cluster D shows genes in 2D are up-regulated following CBFβ knockdown, but down-regulated in a 3D environment (Fig. 5.4). This is in keeping with multiple experiments comparing cells grown in 2D and 3D. Colorectal cancer cells grown in 2D have a differing gene expression profile than those in 2D as determined by Agilent Array (Luca et al., 2013). Thyroid cells showed differing mechanisms of sodium-iodide symporter activation in 2D and 3D cell systems (Ingeson-Carlsson and Nilsson, 2013). Adipose derived stromal cells express higher levels of osteogenic differentiation in 3D cell culture (Shen et al., 2013). Therefore, this further confirms the requirement of a 3D cell culture system to provide a more representative gene expression profile.

The genes that were found in common with both 2D and 3D samples were chosen for further analysis as these genes showed that they were consistent in expression. This produced a gene list that was both manageable and also that could be investigated using both 2D and 3D cell culture. An alternative method to reduce the number of

genes to be validated would be to increase the stringency of the volcano plot. Rather than using a fold change of 2 a fold change of 5 could have been used, or a q value of 0.01 as opposed to 0.05.

5.7.3. Knock down of CBFβ in 2D and 3D cells yields common genes in microarray analysis

The second aim of this chapter was to identify further potential target genes of the Runx2/CBFβ complex in order to further understand the role this complex has in breast cancer cells and their ability to remodel bone. For this reason, the microarray data was of great use as it identified potential targets by showing the genes that change in regulation due to CBFβ knock down. It has previously been shown by a Runx2 microarray in 2D that Runx2 and CBFβ knockdown yield many of the same genes (Mendoza-Villanueva et al., 2011). This is because of the need for CBFβ to enhance the binding of Runx2 to its DNA binding site at the gene promoter.

IL11 has previously been shown to be expressed in MDA-MB-231 cells (Gupta et al., 2011). Considering IL11 has been linked to bone remodelling, and it shows a decrease in expression in both the 2D and 3D microarrays, Il11 was selected for further investigation as a possible gene target of Runx2/CBFβ (Kang et al., 2003; Mendoza-Villanueva et al., 2011). This decrease in expression following CBFβ knock down is in keeping with research in chondrocytes which showed Runx2 up-regulated IL11 expression (Enomoto et al., 2004).

Analysis of its promoter sequence showed Runx2 could potentially bind to three full sites in the first 2000 bp before the transcription initiation site. In addition there were another 10 partial Runx binding sites. Having shown that there were potential sites for Runx2 binding, the IL11 promoter regions of these sites were subjected to EMSA

analysis. EMSA analysis of these sites in UMR106 cells, which have high levels of Runx2 protein expression, showed Runx proteins could indeed bind to all three full Runx binding sites. Nuclear protein from MDA-MB-231 cells showed that the Runx2 antibody resulted in a Supershift. However, due to the reduced expression of the Runx/DNA band after the addition of the mutant competitor, together with the lack of a visible Runx/DNA band using the IL11 site 3 sequence, it is inconclusive as to whether Runx2 does indeed bind the Ill promoter region at these sites in the MDA-MB-231 cells.

In order to further confirm whether Runx2 does indeed bind to these sites, a chromatic immunoprecipitation (ChIP) experiment can be conducted. This would show whether Runx2/CBFβ complex can indeed bind to the DNA and RT-PCR analysis would show whether the IL11 promoter regions have been bound. In addition, a reporter assay experiment would show whether this Runx2/CBFβ binding to the IL11 promoter region is required for IL11 transcription.

Taken together, the data presented in this chapter has shown that 2D and 3D cell culture systems provide differing gene expression profiles. Microarray analysis has shown IL11 could be a potential target gene of Runx2/CBFβ and EMSA analysis of the possible DNA binding site regions of the IL11 promoter has shown that Runx2 can indeed bind to the IL11 promoter region.

6.0 General discussion

6.1. Project aims

The multistep process required for breast cancer cell progression has been termed the hallmarks of cancer. These hallmarks include sustaining proliferation signalling, evading growth suppressors, resisting cell death, enabling replicative immortality, inducing angiogenesis and activating invasion and metastasis (Hanahan and Weinberg, 2011). In addition to these 6 hallmarks, two enabling characteristics have been identified. These are development of genome instability and mutation and secondly tumour promoting inflammation. Two further emerging hallmarks are deregulating cellular energy metabolism and evasion if immune destruction (Hanahan and Weinberg, 2011). These hallmarks of cancer are the functional capabilities that must be acquired in order for the cancer cells to survive, proliferate, disseminate and colonise.

In terms of breast cancer progression, the normal healthy breast cells undo genomic mutations and cellular changes which transform the healthy cell into a tumour cell that continues to proliferate and resists death. Progression of these breast cancer cells to metastatic breast cancer cells involves the activation of genes required for invasion and metastasis. Finally, following dissemination to another area of the body, such as bone, the cancer cells undergo colonisation (Aguirre-Ghiso, 2007; Barkan et al., 2010).

The results chapters in this thesis loosely follows this progression from healthy breast to metastatic breast cancer cells to bone remodelling by investigating the role of Runx2/CBFβ at these various stages of breast cancer progression. It has already been established that in mammary gland, Runx2 binds to the promoter region of the

milk protein β-casein and that this binding activates β-casein transcription (Inman et al., 2005).

The first chapter intended to confirm the requirement of endogenous Runx2 in the regulation of the milk protein β-casein. While this could not be confirmed due to the siRNA affecting the cells and preventing milk production, this chapter did show that Runx2 was expressed throughout the development of acini. This is important as it shows the expression of Runx2 itself does not cause acini disruption.

Currently, it is already known that Runx2 has a role in metastatic breast cancer cells, regulating genes known to be required for invasion and metastasis, such as MMP13. CBFβ is also required for this process as knock down of CBFβ reduces the invasive capacity of metastatic breast cancer cells (Mendoza-Villanueva et al., 2010). The second chapter shows that knock down of CBFβ not only reduces invasive capacity but causes metastatic breast cancer cells to undergo phenotypic changes. In 3D Matrigel cell culture, MDA-MB-231 cells knocked down for CBFβ showed clusters of cells formed as opposed to stellate structures. Furthermore, RT-PCR analysis showed shCBFβ MDA-MB-231 cells had an increase in epithelial markers and a decrease in mesenchymal markers, suggesting a mesenchymal to epithelial transition. Thus, shCBFβ MDA-MB-231 cells no longer appeared to express metastatic breast cancer phenotype but instead produced a phenotype which was more similar to a non-metastatic breast cancer cell.

It is already known that metastatic breast cancer cells that colonise to bone secrete factors that result in bone degradation. This degradation releases growth factors that then enable further breast cancer growth and so is termed the ‘vicious cycle’. Breast cancer cells disrupt the normal remodelling process of bone formation by osteoblasts

and degradation by osteoclasts, skewing the balance towards more osteoclast differentiation and thus bone degradation. Factors such as PTHrP and IL11 are secreted from breast cancer cells (Kang et al., 2003). These act on osteoblasts to secrete RANKL which then binds to osteoclasts resulting in degradation or act on osteoclasts directly. Runx2 has already been linked to a role in this process. The presence of a truncated Runx2 lacking the carboxy terminal in breast cancer cells abolishes the ability of these cells to cause osteolystic lesions (Barnes et al., 2004). Mutated Runx2 also causes loss of osteolystic lesions (Javed et al., 2005). Sclerostin is a known factor in the inhibition of osteoblast. This inhibition occurs by preventing ligand mediated wnt signalling (Moester et al., 2010). Runx2 binds to the promoter region of SOST, the gene of sclerostin and regulates its expression (Mendoza-Villanueva et al., 2011). The aim of the third chapter was to investigate possible additional Runx2 targets involved in the 'vicious cycle' of bone remodelling as a consequence of breast cancer interaction. This was achieved by microarray analysis of MDA-MB-231 cells grown in a 3D environment with and without the CBFβ protein. Considering the growth of the MDA-MB-231 cells in a 3D environment, these microarray data were first compared to another microarray previously conducted using 2D MDA-MB-231 cells. The 3D microarray produced multiple possible Runx2/CBFβ targets, of which IL11 was of particular interest due to its known role in bone remodelling. The possible regulation of IL11 by Runx2 in breast cancer cells was further supported by evidence that Runx2 up-regulates IL11 expression in chondrocytes (Enomoto et al., 2004). Considering that the 2D and 3D gene regulation presented in this thesis each contain a very different expression profile, it is important to understand the benefits of the use of 3D cell culture systems.

6.2. Developing a 3D matrigel cell culture system

A key theme throughout this thesis is the importance of a 3D cell culture system. In terms of the structure of mammary glands, the ideal model system would be to work in mice. However, as cells of the mammary differ in architecture and function during different developmental stages, this would be a very time consuming and costly process. In addition, mice models are difficult to manipulate for different conditions such as protein knockdown. For these reasons many experiments have been conducted using traditional 2D cell culture methods. These 2D model systems are very limited in their representations of the environment cells experience *in vivo*. In 2D, both normal and cancer cells lose their tissue specific morphological organisation due to loss of signals from the extracellular environment (Chitcholtan et al., 2013; Harma et al., 2010; Weaver et al., 2002). The 3D cell culture system bridges the gap between 2D and *in vivo* experimentation. It allows the speed and ease of use of a 2D system while recapitulating the structures seen *in vivo*. It is also of particular interest due to its rich extracellular cell matrix proteins (Debnath and Brugge, 2005). For these reasons, 3D cell culture has been used.

Having understood the importance of a 3D cell culture system, the reconstituted basement membrane, commercially known as Matrigel, was used. However, there are many other gel and extracellular cell matrix components that could have been used. Some of these components and their advantages and disadvantages of their use have been shown in Table 6.1. While the reconstituted basement membrane from EHS sarcoma has lot to lot variability, the morphogenetic responses of cells in the matrigel is reproducible (Debnath and Brugge, 2005; Shaw et al., 2004). In terms of morphology, matrigel allows the normal breast cell line MCF10A cells to produce

acini structures (Debnath et al., 2003; Pratap et al., 2009). Cells other than breast and breast cancers have also been tested in 3D matrigel. Endometrial cancers in 2D and 3D matrigel have a change in morphology, producing spherical multicellular structures in 3D (Chitcholtan et al., 2013). Colorectal cancer cell lines in 2D and 3D give different morphology form round, mass and grape-like structures in 3D (Luca et al., 2013).

Component	Advantages	Disadvantages
Reconstituted basement membrane from EHS mouse sarcoma	Successfully applied to many 3D systems	As this is from a mouse tumour xenograft, it has a complex and ill-defined composition Lot to lot variability
Fibrin	Successfully applied 3D system	Easily proteolysed by cellular proteases
Collagen I	Better biologically defined than EHS Can be easily manipulated through changes in concentration, orientation and biochemical modification	Numerous cells fail to form polarised acini Limited range of elastic modulus Lot to lot variability as it is biologically derived
Polyacrylamide gels	Easily manipulated by altering the concentration of acrylamide Large range of elastic moduli	Acrylamide is cytotoxic Not a true 3D system as the cells seeded in polyacrylamide gels are overlaid with reconstituted basement membrane

Table 6.1. Comparison of different 3D cell culture methods available. There are multiple components that can be used to provide a 3D matrigel system. The advantages and disadvantages of each have been listed.

6.3. Knockdown of CBFβ in metastatic breast cancer cells results in a mesenchymal-epithelial transition (MET)

The metastatic breast cancer cells MDA-MB-231 cells are mesenchymal cells that do not show cell-cell adherence and do not have polarity when grown in 3D matrigel. The CBFβ knockdown MDA-MB-231 cells showed an epithelial phenotype in 3D matrigel and epithelial marker expression using RT-PCR analysis.

In order for the epithelial breast cancer cells to move out of the breast, they must acquire the characteristics of mesenchymal cells. This process is termed the epithelial to mesenchymal transition (EMT) (Creighton et al., 2013). Key features of EMT are that the epithelial cells lose polarity, decrease expression of proteins that enable cell-cell adhesion and gain invasive properties (Boyer et al., 2000). EMT is an important process in normal development, particularly in embryogenesis. Here cells from the neural crest undergo EMT to migrate away and differentiate into other cell types such as bone and smooth muscle (Lee et al., 2006). EMT is also important in adults during wound healing, where epithelial cells differentiate into myofibroblasts to rebuild the extracellular matrix (Weber et al., 2012).

In order for EMT to occur, the regulation of many molecular processes must be altered. These include adhesion proteins such as N-Cadherin, E-Cadherin, integrin and occludin (Lee et al., 2006). This loss of cell-cell adhesion and cell junctions, together with loss of cell polarity allows cancer cells to move out of their primary site. For this reason, EMT has been linked to the invasive and metastatic capacity of late stage breast cancer (Hanahan and Weinberg, 2011).

Cancer cells that undergo EMT and invade to other areas of the body must then re-differentiate into epithelial cells in a process termed mesenchymal to epithelial

transition (MET). Invasive mesenchymal cells are growth arrested and must undergo MET in order to colonise and proliferate (Brabletz, 2012; Brabletz et al., 2001; Ocana et al., 2012). EMT inducing transcription factors can directly inhibit proliferation (Thiery et al., 2009). A mouse model for skin cancer shows that the activation of the EMT marker Twist1 increases the number of circulating tumour cells. Using a reversible (MET capable) model and an irreversible Twist1 model showed that there were more colonised metastases in the reversible model. Decreasing Twist1 levels led to increased proliferation and a reversion of MET (Tsai et al., 2012). Therefore, MET is important for metastatic breast cancer cells to colonise bone.

MET is also an important process in healthy tissues. MET is required for the reprogramming required to transform somatic cells into pluripotent stem cells (Esteban et al.; Samavarchi-Tehrani et al., 2010). This has been demonstrated *in vitro* where mouse fibroblasts suppress pro-EMT signals to undergo MET which creates inducible pluripotent stem cells. The transcription factors Sox2/Oct4 suppressed Snail, an EMT mediator and Kif4 induced epithelial genes such as E-Cadherin (Li et al., 2010). Therefore, both EMT and MET are important in reprogramming of cells.

The MET observed following CBFβ knockdown in MDA-MB-231 cells is in keeping with the EMT resulting from Runx2 overexpression in non-metastatic breast cancer cells, MCF7. A doxycycline (dox) inducible Runx2 expression system was used to overexpress Runx2 in MCF7 cells. Dox induction stimulated a decrease in E-Cadherin and an increase in vimentin and invasion consistent with EMT. Runx2 stimulated a known epithelial marker SNAI2 in a WNT and TGFβ dependent manner (Chimge et al., 2011).

6.4. Further work taking shCBFβ cells from the *in vitro* 3D system to *in vivo*

This thesis shows that MDA-MB-231 cells grown in a 3D matrigel system produce an invasive phenotype, spreading throughout the matrigel. Knockdown of CBFβ in these cells causes a change in morphology so that the shCBFβ MDA-MB-231 cells form clusters and in some cases acini type structures. As previously mentioned, matrigel is a basement membrane from mouse EHS sarcoma. This matrigel has a variety of extracellular matrix components to provide an environment for 3D structures to form. The composition however will differ from the environment the breast cancer cells would actually be in within the human bone matrix. To bridge this gap in experimental conditions, the MDA-MB-231 cells were grown in a 3D bone matrix. This experiment was conducted using a specialised bioreactor.

A bioreactor allows the growth of tissues such as bone in a 3D multi-cell layer (Dhurjati et al., 2008; Krishnan et al., 2010; Krishnan et al., 2011; Mastro and Vogler, 2009). Osteoblastic tissue from isolated osteoblast cells was grown. This system was used and MDA-MB-231 cells were grown in co-culture with the mineralised bone. The MDA-MB-231 cells spread throughout the culture in a similar manner to that seen in the 3D matrigel system. The shCBFβ MDA-MB-231 cells were also grown in co-culture. These cells produced clusters of cells as observed in Matrigel and shown in this thesis. Thus, there is evidence that the MDA-MB-231 cells produce similar results in matrigel and on bone *in vitro* (Ayub, Shore and Mastro, unpublished data).

In addition to the investigation of these cells *in vitro*, *in vivo* experiments have also been conducted using immunocompromised mouse models. WT MDA-MB-231 cells

and shCBFβ MDA-MB-231 cells were injected into a mouse heart and the mice were monitored for bone metastases. As expected, the WT MDA-MB-231 cells did have many bone metastases. It was expected that as CBFβ knock down results in loss of invasion *in vitro* and a more epithelial cell phenotype due to MET, as shown in this thesis, that the shCBFβ MDA-MB-231 cells would not metastasis to bone (Mendoza-Villanueva et al., 2010). In contrast to this hypothesis, bone metastases were still observed in these immunocompromised mice. Cells from these bone metastases were used for RNA extraction and subsequently for RT-PCR analysis. Results showed that while cells being injected into the mice showed significantly reduced CBFβ mRNA expression, cells that metastasised to bone showed a rescue of CBFβ mRNA expression.

There are multiple reasons why this CBFβ expression could be increased in bone metastases. One possibility is that there is a mixed population of shCBFβ MDA-MB-231 cells which have differing levels of CBFβ knock down and it is the cells in which there is a higher CBFβ expression that metastasise and proliferate. Another is that the CBFβ suppression is not being maintained by the shRNA. One solution to both these issues and which is currently being investigated in our laboratory is the use of transcription activator-like effector nucleases (TALENs). These would completely remove the CBFβ gene from the MDA-MB-231 cell genome (Sun and Zhao, 2013).

6.5. Disrupting CBFβ interaction with Runx2 as a possible therapeutic target

MDA-MB-231 cells express both Runx2 and CBFβ which form a complex (Mendoza-Villanueva et al., 2010). The Runx2/CBFβ interaction is important for invasion, as shown by knockdown studies of both Runx2 and CBFβ (Mendoza-Villanueva et al., 2010; Pratap et al., 2005). This could be due to the need for CBFβ binding to Runx2 to increase the DNA binding affinity of Runx2. The CBFβ knockdown phenotype in MDA-MB-231 cells suggests that disruption of the Runx2/CBFβ complex interaction results in an MET of the metastatic breast cancer cell.

A drug termed Ro5-3335 has been shown to disrupt the interaction of the Runx1/CBFβ complex (Cunningham et al., 2012). All Runx proteins have the same Runt domain. This domain contains the DNA binding site and also the CBFβ heterodimerisation site (Schroeder et al., 2005). Therefore, this drug could interfere with the interaction between Runx2 and CBFβ also. This drug is currently being investigated in our laboratory. This possibility of interaction of other Runx proteins is worth recognising as other Runx proteins may be of importance in breast development.

6.6. Potential roles of Runx1 and Runx3

Considering all Runx proteins bind to the same DNA binding site, it must be acknowledged that the other Runx proteins, Runx1 and Runx3 could also be involved in mammary development and breast cancer progression. A total RNA extraction of normal mouse mammary gland tissues analysed using RT-PCR showed the presence of all three Runx transcripts. Multiple RT-PCR analyses of mammary glands at different stages of development showed fluctuating levels of Runx expression between virgin, pregnant, lactation and involution stages. In addition, of all Runx genes, Runx1 showed the highest transcript expression in all four stages of mammary development (Blyth et al., 2010). This dynamic expression level suggests that Runx genes may play a role in the different stages of development and that Runx1 may play a larger role than previously expected. The expression of other Runx proteins is further supported by RT-PCR analysis of the normal mammary gland cell line, MCF10A. This showed that Runx1 mRNA is expressed in normal mammary cells and that this expression is 15 fold greater than that of Runx2 mRNA in these same cells. In contrast to the results in whole mammary gland extraction, the MCF10A cells did not express Runx3 mRNA (Wang et al., 2011b). This difference in mRNA expression can be explained by possible contamination from non-epithelial cells in the whole mammary gland extraction, a known issue of RT-PCR analysis (Ferrari et al., 2013). Taken together, this shows that normal mammary gland could express both Runx1 and Runx2.

Having established that Runx1 could also have a role in normal mammary glands, it is important to consider the implications of such an expression. One possible role of Runx1 has already been found. 3D cell culture of the normal breast cell line, MCF10A produces acini structures (Debnath et al., 2003). Overexpression of Runx2

causes disruption of these acini, with loss of polarisation and no hollow lumens forming due to reduction in apoptosis (Pratap et al., 2009). On the other hand, knockdown of Runx1 in these cells also caused loss of acini (Wang et al., 2011b). Thus Runx1 also has a role in acini development. Therefore, any therapeutic target would have to target the downstream effects of Runx1 as well as Runx2. For this reason, the aforementioned drug that disrupts the interaction of the Runx protein with CBFβ could also disrupt the Runx1/CBFβ interaction in the MDA-MB-231 cells (Wang et al., 2011b).

References

Adya N, Castilla LH, Liu PP. 2000. Function of CBFbeta/Bro proteins. Semin Cell Dev Biol 11(5):361-368.

Adya N, Stacy T, Speck NA, Liu PP. 1998. The leukemic protein core binding factor beta (CBFbeta)-smooth-muscle myosin heavy chain sequesters CBFalpha2 into cytoskeletal filaments and aggregates. Mol Cell Biol 18(12):7432-7443.

Aguirre-Ghiso JA. 2007. Models, mechanisms and clinical evidence for cancer dormancy. Nature reviews Cancer 7(11):834-846.

Akhtari M, Mansuri J, Newman KA, Guise TM, Seth P. 2008. Biology of breast cancer bone metastasis. Cancer Biol Ther 7(1):3-9.

Alliston T, Choy L, Ducy P, Karsenty G, Derynck R. 2001. TGF-β-induced repression of CBFA1 by Smad3 decreases cbfa1 and osteocalcin expression and inhibits osteoblast differentiation. EMBO J 20(9):2254-2272.

Backstrom S, Wolf-Watz M, Grundstrom C, Hard T, Grundstrom T, Sauer UH. 2002. The RUNX1 Runt domain at 1.25A resolution: a structural switch and specifically bound chloride ions modulate DNA binding. J Mol Biol 322(2):259-272.

Bae S-C, Takahashi E-i, Zhang YW, Ogawa E, Shigesada K, Namba Y, Satake M, Ito Y. 1995. Cloning, mapping and expression of PEBP2αC, a third gene encoding the mammalian Runt domain Gene 159(2):245-248.

Ball RK, Friis RR, Schoenenberger CA, Doppler W, Groner B. 1988. Prolactin regulation of beta-casein gene expression and of a cytosolic 120-kd protein in a cloned mouse mammary epithelial cell line. EMBO J 7(7):2089-2095.

Banerjee C, Javed A, Choi J-Y, Green J, Rosen V, Wijnen AJv, Stein JL, Lian JB, Stein GS. 2001. Differential regulation of the two principal Runx2/Cbfa1 n-terminal isoforms in response to bone morphogenetic protein-2 during development of the osteoblast phenotype. Endocrinology 142(9):4026-4039.

Barkan D, Green JE, Chambers AF. 2010. Extracellular matrix: a gatekeeper in the transition from dormancy to metastatic growth. Eur J Cancer 46(7):1181-1188.

Barnes GL, Hebert KE, Kamal M, Javed A, Einhorn TA, Lian JB, Stein GS, Gerstenfeld LC. 2004. Fidelity of Runx2 activity in breast cancer cells is required for the generation of metastases-associated osteolytic disease. Cancer Res 64(13):4506-4513.

Barnes GL, Javed A, Waller SM, Kamal MH, Hebert KE, Hassan MQ, Bellahcene A, Van Wijnen AJ, Young MF, Lian JB, Stein GS, Gerstenfeld LC. 2003. Osteoblast-related transcription factors Runx2 (Cbfa1/AML3) and MSX2 mediate the expression of bone sialoprotein in human metastatic breast cancer cells. Cancer Res 63(10):2631-2637.

Bartfeld D, Shimon L, Couture GC, Rabinovich D, Frolow F, Levanon D, Groner Y, Shakked Z. 2002. DNA recognition by the RUNX1 transcription factor is mediated by an allosteric transition in the RUNT domain and by DNA bending. Structure 10(10):1395-1407.

Bi W, Deng JM, Zhang Z, Behringer RR, de Crombrugghe B. 1999. Sox9 is required for cartilage formation. Nat Genet 22(1):85-89.

Bialek P, Kern B, Yang X, Schrock M, Sosic D, Hong N, Wu H, Yu K, Ornitz DM, Olson EN, Justice MJ, Karsenty G. 2004. A Twist Code Determines the Onset of Osteoblast Differentiation Dev Cell 6(3):423-435

Bissell MJ. 2007. Architecture Is the Message: The role of extracellular matrix and 3-D structure in tissue-specific gene expression and breast cancer. Pezcoller Found J 16(29):2-17.

Blyth K, Vaillant F, Jenkins A, McDonald L, Pringle MA, Huser C, Stein T, Neil J, Cameron ER. 2010. Runx2 in normal tissues and cancer cells: A developing story. Blood Cells Mol Dis 45(2):117-123.

Bolstad BM, Irizarry RA, Astrand M, Speed TP. 2003. A comparison of normalization methods for high density oligonucleotide array data based on variance and bias. Bioinformatics 19(2):185-193.

Boyer B, Valles AM, Edme N. 2000. Induction and regulation of epithelial-mesenchymal transitions. Biochemical pharmacology 60(8):1091-1099.

Brabletz T. 2012. EMT and MET in metastasis: where are the cancer stem cells? Cancer Cell 22(6):699-701.

Brabletz T, Jung A, Reu S, Porzner M, Hlubek F, Kunz-Schughart LA, Knuechel R, Kirchner T. 2001. Variable beta-catenin expression in colorectal cancers indicates tumor progression driven by the tumor environment. Proc Natl Acad Sci U S A 98(18):10356-10361.

Braun T, Woollard A. 2009. RUNX factors in development: Lessons from invertebrate model systems. Blood Cells, Molecules, and Diseases 43:43-48.

Brisken C, O'Malley B. 2010. Hormone action in the mammary gland. Cold Spring Harb Perspect Biol 2(12):a003178.

Caruso JA, Laird DW, Batist G. 1999. Role of HSP90 in mediating cross-talk between the estrogen receptor and the Ah receptor signal transduction pathways. Biochemical pharmacology 58(9):1395-1403.

Chang G, Xu S, Dhir R, Chandran U, O'Keefe DS, Greenberg NM, Gingrich JR. 2010. Hypoexpression and epigenetic regulation of candidate tumor suppressor gene CADM-2 in human prostate cancer. Clin Cancer Res 16(22):5390-5401.

Chen YC, Sosnoski DM, Mastro AM. 2010. Breast cancer metastasis to the bone: mechanisms of bone loss. Breast Cancer Res 12(6):215.

Chimge NO, Baniwal SK, Little GH, Chen YB, Kahn M, Tripathy D, Borok Z, Frenkel B. 2011. Regulation of breast cancer metastasis by Runx2 and estrogen signaling: the role of SNAI2. Breast Cancer Res 13(6):R127.

Chimge NO, Frenkel B. 2013. The RUNX family in breast cancer: relationships with estrogen signaling. Oncogene 32(17):2121-2130.

Chitcholtan K, Asselin E, Parent S, Sykes PH, Evans JJ. 2013. Differences in growth properties of endometrial cancer in three dimensional (3D) culture and 2D cell monolayer. Exp Cell Res 319(1):75-87.

Cho KW, Kim JY, Song SJ, Farrell E, Eblaghie MC, Kim HJ, Tickle C, Jung HS. 2006. Molecular interactions between Tbx3 and Bmp4 and a model for dorsoventral positioning of mammary gland development. Proc Natl Acad Sci U S A 103(45):16788-16793.

Chu EY, Hens J, Andl T, Kairo A, Yamaguchi TP, Brisken C, Glick A, Wysolmerski JJ, Millar SE. 2004. Canonical WNT signaling promotes mammary placode development and is essential for initiation of mammary gland morphogenesis. Development 131(19):4819-4829.

Coffman JA. 2003. Runx transcription factors and the developmental balance between cell proliferation and differentiation. Cell Biol Int 27(4):315-324.

Coffman JA, Kirchhamer CV, Harrington MG, Davidson EH. 1996. SpRunt-1, a new member of the runt domain family of transcription factors, is a positive regulator of the aboral ectoderm-specific CyIIIA gene in sea urchin embryos. Dev Biol 174(1):43-54.

Coleman RE. 2001. Should bisphosphonates be the treatment of choice for metastatic bone disease? Seminars in oncology 28(4 Suppl 11):35-41.

Cowin P, Wysolmerski J. 2010. Molecular mechanisms guiding embryonic mammary gland development. Cold Spring Harb Perspect Biol 2(6):a003251.

Creighton CJ, Gibbons DL, Kurie JM. 2013. The role of epithelial-mesenchymal transition programming in invasion and metastasis: a clinical perspective. Cancer Manag Res 5:187-195.

Cunningham L, Finckbeiner S, Hyde RK, Southall N, Marugan J, Yedavalli VR, Dehdashti SJ, Reinhold WC, Alemu L, Zhao L, Yeh JR, Sood R, Pommier Y, Austin CP, Jeang KT, Zheng W, Liu P. 2012. Identification of benzodiazepine Ro5-3335 as an inhibitor of CBF leukemia through quantitative high throughput screen against RUNX1-CBFbeta interaction. Proc Natl Acad Sci U S A 109(36):14592-14597.

Cunningham ML, Seto ML, Hing AV, Bull MJ, Hopkin RJ, Leppig KA. 2006. Birth Defects Cleidocranial dysplasia with severe parietal bone dysplasia: C-terminal RUNX2 mutations. Birth Defects Res A Clin Mol Teratol 76(2):78-85.

Danielson KG, Oborn CJ, Durban EM, Butel JS, Medina D. 1984. Epithelial mouse mammary cell line exhibiting normal morphogenesis in vivo and functional differentiation in vitro. Proc Natl Acad Sci U S A 81(12):3756-3760.

Dauvois S, White R, Parker MG. 1993. The antiestrogen ICI 182780 disrupts estrogen receptor nucleocytoplasmic shuttling. J Cell Sci 106 (Pt 4):1377-1388.

Debnath J, Brugge JS. 2005. Modelling glandular epithelial cancers in three-dimensional cultures. Nature reviews Cancer 5(9):675-688.

Debnath J, Mills KR, Collins NL, Reginato MJ, Muthuswamy SK, Brugge JS. 2002. The role of apoptosis in creating and maintaining luminal space within normal and oncogene-expressing mammary acini. Cell 111(1):29-40.

Debnath J, Muthuswamy SK, Brugge JS. 2003. Morphogenesis and oncogenesis of MCF-10A mammary epithelial acini grown in three-dimensional basement membrane cultures. Methods 30(3):256-268.

Dhurjati R, Krishnan V, Shuman LA, Mastro AM, Vogler EA. 2008. Metastatic breast cancer cells colonize and degrade three-dimensional osteoblastic tissue in vitro. Clin Exp Metastasis 25(7):741-752.

Ducy P, Zhang R, Geoffroy V, Ridall AL, Karsenty G. 1997. Osf2/Cbfa1: a transcriptional activator of osteoblast differentiation. Cell 89(5):747-754.

Enomoto H, Furuichi T, Zanma A, Yamana K, Yoshida C, Sumitani S, Yamamoto H, Enomoto-Iwamoto M, Iwamoto M, Komori T. 2004. Runx2 deficiency in chondrocytes causes adipogenic changes in vitro. J Cell Sci 117(Pt 3):417-425.

Esteban MA, Bao X, Zhuang Q, Zhou T, Qin B, Pei D. 2012. The mesenchymal-to-epithelial transition in somatic cell reprogramming. Curr Opin Genet Dev 22(5):423-428.

Feng Y, Manka D, Wagner KU, Khan SA. 2007. Estrogen receptor-alpha expression in the mammary epithelium is required for ductal and alveolar morphogenesis in mice. Proc Natl Acad Sci U S A 104(37):14718-14723.

Ferrari N, McDonald L, Morris JS, Cameron ER, Blyth K. 2013. RUNX2 in mammary gland development and breast cancer. J Cell Physiol 228(6):1137-1142.

Foley J, Dann P, Hong J, Cosgrove J, Dreyer B, Rimm D, Dunbar M, Philbrick W, Wysolmerski J. 2001. Parathyroid hormone-related protein maintains mammary epithelial fate and triggers nipple skin differentiation during embryonic breast development. Development 128(4):513-525.

Gehrke I, Gandhirajan RK, Kreuzer KA. 2009. Targeting the WNT/beta-catenin/TCF/LEF1 axis in solid and haematological cancers: Multiplicity of therapeutic options. Eur J Cancer 45(16):2759-2767.

Geoffroy V, Kneissel M, Fournier B, Boyde A, Matthias P. 2002. High bone resorption in adult aging transgenic mice overexpressing cbfa1/runx2 in cells of the osteoblastic lineage. Mol Cell Biol 22(17):6222-6233.

Goldman RD, Goldman AE, Shumaker DK. 2005. Nuclear lamins: building blocks of nuclear structure and function. Novartis Found Symp 264:3-16; discussion 16-21, 227-230.

Goyama S, Mulloy JC. 2011. Molecular pathogenesis of core binding factor leukemia: current knowledge and future prospects. International journal of hematology 94(2):126-133.

Guise TA, Yin JJ, Taylor SD, Kumagai Y, Dallas M, Boyce BF, Yoneda T, Mundy GR. 1996. Evidence for a causal role of parathyroid hormone-related protein in the pathogenesis of human breast cancer-mediated osteolysis. J Clin Invest 98(7):1544-1549.

Gupta J, Robbins J, Jilling T, Seth P. 2011. TGFbeta-dependent induction of interleukin-11 and interleukin-8 involves SMAD and p38 MAPK pathways in breast tumor models with varied bone metastases potential. Cancer Biol Ther 11(3):311-316.

Gutierrez S, Javed A, Tennant DK, Rees Mv, Montecino M, Stein GS, Stein JL, Lian JB. 2002. CCAAT/Enhancer-binding Proteins (C/EBP) β and δ Activate Osteocalcin Gene Transcription and Synergize with Runx2 at the C/EBP Element to Regulate Bone-specific Expression. J Biol Chem 277(2):1316-1323.

Hanahan D, Weinberg RA. 2011. Hallmarks of cancer: the next generation. Cell 144(5):646-674.

Hanai J-i, Chen LF, Kanno T, Ohtani-Fujita N, Kim WY, Guo W-H, Imamura T, Ishidou Y, Fukuchi M, Shi M-J, Stavnezer J, Kawabata M, Miyazono K, Ito Y. 1999. Interaction and Functional Cooperation of PEBP2/CBF with Smads. J Biol Chem 274(44):31577-31582.

Harma V, Virtanen J, Makela R, Happonen A, Mpindi JP, Knuuttila M, Kohonen P, Lotjonen J, Kallioniemi O, Nees M. 2010. A comprehensive panel of three-dimensional models for studies of prostate cancer growth, invasion and drug responses. PLoS One 5(5):e10431.

Hart S, Foroni L. 2002. Core binding factor genes and human leukemia. Haematologica 87(12):1307-1323.

Hassiotou F, Geddes D. 2013. Anatomy of the human mammary gland: Current status of knowledge. Clin Anat 26(1):29-48.

Hennighausen L, Robinson GW. 2005. Information networks in the mammary gland. Nat Rev Mol Cell Biol 6(9):715-725.

Hess J, Porte D, Munz C, Angel P. 2001. AP-1 and Cbfa/runt physically interact and regulate parathyroid hormone-dependent MMP13 expression in osteoblasts through a new osteoblast-specific element 2/AP-1 composite element. J Biol Chem 276(23):20029-20038.

Hoeijmakers JH. 2001. Genome maintenance mechanisms for preventing cancer. Nature 411(6835):366-374.

Howard AD, Feighner SD, Cully DF, Arena JP, Liberator PA, Rosenblum CI, Hamelin M, Hreniuk DL, Palyha OC, Anderson J, Paress PS, Diaz C, Chou M, Liu KK, McKee KK, Pong SS, Chaung LY, Elbrecht A, Dashkevicz M, Heavens R, Rigby M, Sirinathsinghji DJ, Dean DC, Melillo DG, Patchett AA, Nargund R, Griffin PR, DeMartino JA, Gupta SK, Schaeffer JM, Smith RG, Van der Ploeg LH. 1996. A receptor in pituitary and hypothalamus that functions in growth hormone release. Science 273(5277):974-977.

Howlin J, McBryan J, Martin F. 2006. Pubertal mammary gland development: insights from mouse models. J Mammary Gland Biol Neoplasia 11(3-4):283-297.

Huang da W, Sherman BT, Lempicki RA. 2009a. Bioinformatics enrichment tools: paths toward the comprehensive functional analysis of large gene lists. Nucleic Acids Res 37(1):1-13.

Huang da W, Sherman BT, Lempicki RA. 2009b. Systematic and integrative analysis of large gene lists using DAVID bioinformatics resources. Nat Protoc 4(1):44-57.

Huang G, Shigesada K, Ito K, Wee H-J, Yokomizo T, Ito Y. 2001. Dimerization with PEBP2β protects RUNX1/AML1 from ubiquitin–proteasome-mediated degradation. EMBO J 20(4):723-733.

Huang X, Peng JW, Speck NA, Bushweller JH. 1999. Solution structure of core binding factor beta and map of the CBF alpha binding site. Nat Struct Biol 6(7):624-627.

Hughes K, Watson CJ. 2012. The spectrum of STAT functions in mammary gland development. Jakstat 1(3):151-158.

Incassati A, Chandramouli A, Eelkema R, Cowin P. 2010. Key signaling nodes in mammary gland development and cancer: beta-catenin. Breast Cancer Res 12(6):213.

Ingeson-Carlsson C, Nilsson M. 2013. Switching from MAPK-dependent to MAPK-independent repression of the sodium-iodide symporter in 2D and 3D cultured normal thyroid cells. Mol Cell Endocrinol 381(1-2):241-254.

Inman CK, Li N, Shore P. 2005. Oct-1 counteracts autoinhibition of Runx2 DNA binding to form a novel Runx2/Oct-1 complex on the promoter of the mammary gland-specific gene beta-casein. Mol Cell Biol 25(8):3182-3193.

Inman CK, Shore P. 2003. The osteoblast transcription factor Runx2 is expressed in mammary epithelial cells and mediates osteopontin expression. J Biol Chem 278(49):48684-48689.

Inoue K, Ozaki S, Ito K, Iseda T, Kawaguchi S, Ogawa M, Bae SC, Yamashita N, Itohara S, Kudo N, Ito Y. 2003. Runx3 is essential for the target-specific axon pathfinding of trkc-expressing dorsal root ganglion neurons. Blood Cells Mol Dis 30(2):157-160.

Ito Y. 2004. Oncogenic potential of the RUNX gene family: 'overview'. Oncogene 23(24):4198-4208.

Jackson AL, Linsley PS. 2004. Noise amidst the silence: off-target effects of siRNAs? Trends in genetics : TIG 20(11):521-524.

Jamieson C, Sharma M, Henderson BR. 2012. Wnt signaling from membrane to nucleus: beta-catenin caught in a loop. The international journal of biochemistry & cell biology 44(6):847-850.

Javed A, Barnes GL, Pratap J, Antkowiak T, Gerstenfeld LC, van Wijnen AJ, Stein JL, Lian JB, Stein GS. 2005. Impaired intranuclear trafficking of Runx2 (AML3/CBFA1) transcription factors in breast cancer cells inhibits osteolysis in vivo. Proc Natl Acad Sci U S A 102(5):1454-1459.

Javed A, Gutierrez S, Montecino M, van Wijnen AJ, Stein JL, Stein GS, Lian JB. 1999. Multiple Cbfa/AML sites in the rat osteocalcin promoter are required for basal and vitamin D-responsive transcription and contribute to chromatin organization. Mol Cell Biol 19(11):7491-7500.

Jensen ED, Schroeder TM, Bailey J, Gopalakrishnan R, Westendorf JJ. 2008. Histone deacetylase 7 associates with Runx2 and represses its activity during osteoblast maturation in a deacetylation-independent manner. J Bone Miner Res 23(3):361-372.

Johansson N, Ahonen M, Kahari VM. 2000. Matrix metalloproteinases in tumor invasion. Cell Mol Life Sci 57(1):5-15.

Jonason JH, Xiao G, Zhang M, Xing L, Chen D. 2009. Post-translational Regulation of Runx2 in Bone and Cartilage. J Dent Res 88(8):693-703.

Kamachi Y, Ogawa E, Asano M, Ishida S, Murakami Y, Satake M, Ito Y, Shigesada K. 1990. Purification of a mouse nuclear factor that binds to both the A and B cores of the polyomavirus enhancer. J Virol 64(10):4808-4819.

Kang Y, Siegel PM, Shu W, Drobnjak M, Kakonen SM, Cordon-Cardo C, Guise TA, Massague J. 2003. A multigenic program mediating breast cancer metastasis to bone. Cancer Cell 3(6):537-549.

Kanno T, Kanno Y, Chen L-F, Ogawa E, Kim W-Y, Ito Y. 1998. Intrinsic transcriptional activation-inhibition domains of the polyomavirus enhancer binding protein 2/core binding factor alpha subunit revealed in the presence of the beta subunit. Moleular Cell Biology 18(5):2444-2454.

Karsenty G. 2008. Transcriptional control of skeletogenesis. Annu Rev Genomics Hum Genet 9:183-196.

Kendrick H, Regan JL, Magnay FA, Grigoriadis A, Mitsopoulos C, Zvelebil M, Smalley MJ. 2008. Transcriptome analysis of mammary epithelial subpopulations identifies novel determinants of lineage commitment and cell fate. BMC Genomics 9:591.

Kim S, Koga T, Isobe M, Kern BE, Yokochi T, Chin YE, Karsenty G, Taniguchi T, Takayanagi H. 2003. Stat1 functions as a cytoplasmic attenuator of Runx2 in the transcriptional program of osteoblast differentiation. Genes Dev 17(16):1979-1991.

Komori T. 2006. Regulation of osteoblast differentiation by transcription factors. J Cell Biochem 99(5):1233-1239.

Komori T. 2011. Signaling networks in RUNX2-dependent bone development. J Cell Biochem 112(3):750-755.

Komori T, Yagi H, Nomura S, Yamaguchi A, Sasaki K, Deguchi K, Shimizu Y, Bronson RT, Gao Y-H, Inada M, Sato M, Okamoto R, Kitamura Y, Yoshiki S, Kishimoto T. 1997. Targeted disruption of Cbfa1 results in a complete lack of bone formation owing to maturational arrest of osteoblasts. Cell 89(5):755-764.

Korach K, Couse J, Curtis S, Washburn T, Lindzey J, Kimbro K, Eddy E, Migliaccio S, Snedeker S, Lubahn D, Schomberg D, Smith E. 1996. Estrogen receptor gene disruption: molecular characterization and experimental and clinical phenotypes. Recent Prog Horm Res 51(1):59-86.

Kouros-Mehr H, Werb Z. 2006. Candidate regulators of mammary branching morphogenesis identified by genome-wide transcript analysis. Dev Dyn 235(12):3404-3412.

Krishnan V, Dhurjati R, Vogler EA, Mastro AM. 2010. Osteogenesis in vitro: from pre-osteoblasts to osteocytes: a contribution from the Osteobiology Research Group, The Pennsylvania State University. In Vitro Cell Dev Biol Anim 46(1):28-35.

Krishnan V, Moore TL, Ma YL, Helvering LM, Frolik CA, Valasek KM, Ducy P, Geiser AG. 2003. Parathyroid hormone bone anabolic action requires Cbfa1/Runx2-dependent signaling. Mol Endocrinol 17(3):423-435.

Krishnan V, Shuman LA, Sosnoski DM, Dhurjati R, Vogler EA, Mastro AM. 2011. Dynamic interaction between breast cancer cells and osteoblastic tissue: comparison of two- and three-dimensional cultures. J Cell Physiol 226(8):2150-2158.

Kritikou EA, Sharkey A, Abell K, Came PJ, Anderson E, Clarkson RW, Watson CJ. 2003. A dual, non-redundant, role for LIF as a regulator of development and STAT3-mediated cell death in mammary gland. Development 130(15):3459-3468.

Kugimiya F, Kawaguchi H, Ohba S, Kawamura N, Hirata M, Chikuda H, Azuma Y, Woodgett JR, Nakamura K, Chung UI. 2007. GSK-3beta controls osteogenesis through regulating Runx2 activity. PLoS One 2(9):e837.

Kundu M, Javed A, Jeon JP, Horner A, Shum L, Eckhaus M, Muenke M, Lian JB, Yang Y, Nuckolls GH, Stein GS, Liu PP. 2002. Cbfbeta interacts with Runx2 and has a critical role in bone development. Nat Genet 32(4):639-644.

Lacroix M, Siwek B, Marie PJ, Body JJ. 1998. Production and regulation of interleukin-11 by breast cancer cells. Cancer Lett 127(1-2):29-35.

Lakhani SR, Audretsch W, Cleton-Jensen AM, Cutuli B, Ellis I, Eusebi V, Greco M, Houslton RS, Kuhl CK, Kurtz J, Palacios J, Peterse H, Rochard F, Rutgers E. 2006. The management of lobular carcinoma in situ (LCIS). Is LCIS the same as ductal carcinoma in situ (DCIS)? Eur J Cancer 42(14):2205-2211.

Lau QC, Raja E, Salto-Tellez M, Liu Q, Ito K, Inoue M, Putti TC, Loh M, Ko TK, Huang C, Bhalla KN, Zhu T, Ito Y, Sukumar S. 2006. RUNX3 is frequently inactivated by dual mechanisms of protein mislocalization and promoter hypermethylation in breast cancer. Cancer Res 66(13):6512-6520.

Le Beau MM, Larson RA, Bitter MA, Vardiman JW, Golomb HM, Rowley JD. 1983. Association of an inversion of chromosome 16 with abnormal marrow eosinophils in acute myelomonocytic leukemia. A unique cytogenetic-clinicopathological association. The New England journal of medicine 309(11):630-636.

Lee B, Thirunavukkarasu K, Zhou L, Pastore L, Baldini A, Hecht J, Geoffrey V, Ducy P, Karsenty G. 1997. Missense mutations abolishing DNA binding of the osteoblast-specific transcription factor OSF2/CBFA1 in cleidocranial dysplasia. Nature Genetics 16:307-310.

Lee GY, Kenny PA, Lee EH, Bissell MJ. 2007. Three-dimensional culture models of normal and malignant breast epithelial cells. Nat Methods 4(4):359-365.

Lee JM, Dedhar S, Kalluri R, Thompson EW. 2006. The epithelial-mesenchymal transition: new insights in signaling, development, and disease. J Cell Biol 172(7):973-981.

Lehtinen L, Vainio P, Wikman H, Reemts J, Hilvo M, Issa R, Pollari S, Brandt B, Oresic M, Pantel K, Kallioniemi O, Iljin K. 2012. 15-Hydroxyprostaglandin dehydrogenase associates with poor prognosis in breast cancer, induces epithelial-mesenchymal transition, and promotes cell migration in cultured breast cancer cells. J Pathol 226(4):674-686.

Lejen T, Pene TD, Rose SD, Trifaro JM. 2002. The role of different Scinderin domains in the control of F-actin cytoskeleton during exocytosis. Ann N Y Acad Sci 971:248-250.

Levanon D, Bettoun D, Harris-Cerruti C, Woolf E, Negreanu V, Eilam R, Bernstein Y, Goldenberg D, Xiao C, Fliegauf M, Kremer E, Otto F, Brenner O, Lev-Tov A, Groner Y. 2002. The Runx3 transcription factor regulates development and survival of TrkC dorsal root ganglia neurons. EMBO J 21(13):3454-3463.

Levanon D, Groner Y. 2004. Structure and regulated expression of mammalian RUNX genes. Oncogene 23(24):4211-4219.

Levanon D, Negreanu V, Bernstein Y, Bar-Am I, Avivi L, Groner Y. 1994. AML1, AML2, and AML3, the Human Members of the runt domain Gene-Family: cDNA Structure, Expression, and Chromosomal Localization Genomics 23(2):425-432.

Li C, Wong WH. 2001. Model-based analysis of oligonucleotide arrays: expression index computation and outlier detection. Proc Natl Acad Sci U S A 98(1):31-36.

Li Q, Ito K, Sakakura C, Fukamachi H, Inoue K, Chi X, Lee K, Nomura S, Lee C, Han S, Kim H, Kim W, Yamamoto H, Yamashita N, Yano T, Ikeda T, Itohara S, Inazawa J, Abe T, Hagiwara A, Yamagishi H, Ooe A, Kaneda A, Sugimura T, Ushijima T, Bae S, to I. 2002. Causal relationship between the loss of RUNX3 expression and gastric cancer. Cell 109(1):113-124.

Li R, Liang J, Ni S, Zhou T, Qing X, Li H, He W, Chen J, Li F, Zhuang Q, Qin B, Xu J, Li W, Yang J, Gan Y, Qin D, Feng S, Song H, Yang D, Zhang B, Zeng L, Lai L, Esteban MA, Pei D. 2010. A mesenchymal-to-epithelial transition initiates and is required for the nuclear reprogramming of mouse fibroblasts. Cell Stem Cell 7(1):51-63.

Lipton A, Uzzo R, Amato RJ, Ellis GK, Hakimian B, Roodman GD, Smith MR. 2009. The science and practice of bone health in oncology: managing bone loss and metastasis in patients with solid tumors. Journal of the National Comprehensive Cancer Network : JNCCN 7 Suppl 7:S1-29; quiz S30.

Liu NK, Xu XM. 2006. beta-tubulin is a more suitable internal control than beta-actin in western blot analysis of spinal cord tissues after traumatic injury. J Neurotrauma 23(12):1794-1801.

Liu P, Tarle SA, Hajra A, Claxton DF, Mariton P, Freedman M, Siciliano MJ, Collins FS. 1993. Fusion between transcription factor CBF beta/PEBP2 beta and a myosin heavy chain in acute myeloid leukemia. Science 261(5124):1041-1044.

Liu W, Toyosawa S, Furuichi T, Kanatani N, Yoshida C, Liu Y, Himeno M, Narai S, Yamaguchi A, Komori T. 2001. Overexpression of Cbfa1 in osteoblasts inhibits osteoblast maturation and causes osteopenia with multiple fractures. J Cell Biol 155(1):157-166.

Livak KJ, Schmittgen TD. 2001. Analysis of relative gene expression data using real-time quantitative PCR and the 2(-Delta Delta C(T)) Method. Methods 25(4):402-408.

Luca AC, Mersch S, Deenen R, Schmidt S, Messner I, Schafer KL, Baldus SE, Huckenbeck W, Piekorz RP, Knoefel WT, Krieg A, Stoecklein NH. 2013. Impact of the 3D microenvironment on phenotype, gene expression, and EGFR inhibition of colorectal cancer cell lines. PLoS One 8(3):e59689.

Macias H, Hinck L. 2012. Mammary gland development. Wiley Interdiscip Rev Dev Biol 1(4):533-557.

Mancino AT, Klimberg VS, Yamamoto M, Manolagas SC, Abe E. 2001. Breast cancer increases osteoclastogenesis by secreting M-CSF and upregulating RANKL in stromal cells. J Surg Res 100(1):18-24.

Marie PJ. 2008. Transcription factors controlling osteoblastogenesis. Science 473:98-105.

Mastro AM, Vogler EA. 2009. A three-dimensional osteogenic tissue model for the study of metastatic tumor cell interactions with bone. Cancer Res 69(10):4097-4100.

McCarthy TL, Changhua, Chen Y, Kim KK, Imagawa M, Ito Y, Centrella M. 2000. Runt domain factor (Runx)-dependent effects on CCAAT/ enhancer-binding protein delta expression and activity in osteoblasts. J Biol Chem 275(8):21746-21753.

McCave EJ, Cass CA, Burg KJ, Booth BW. 2010. The normal microenvironment directs mammary gland development. J Mammary Gland Biol Neoplasia 15(3):291-299.

McLarren KW, Lo R, Grbavec D, Thirunavukkarasu K, Karsenty G, Stifani S. 2000. The mammalian basic helix loop helix protein HES-1 binds to and modulates the transactivating function of the runt-related factor Cbfa1. J Biol Chem 275(1):530-538.

Mendoza-Villanueva D, Deng W, Lopez-Camacho C, Shore P. 2010. The Runx transcriptional co-activator, CBFbeta, is essential for invasion of breast cancer cells. Mol Cancer 9:171.

Mendoza-Villanueva D, Zeef L, Shore P. 2011. Metastatic breast cancer cells inhibit osteoblast differentiation through the Runx2/CBFbeta-dependent expression of the Wnt antagonist, sclerostin. Breast Cancer Res 13(5):R106.

Moester MJ, Papapoulos SE, Lowik CW, van Bezooijen RL. 2010. Sclerostin: current knowledge and future perspectives. Calcified tissue international 87(2):99-107.

Molyneux G, Geyer FC, Magnay FA, McCarthy A, Kendrick H, Natrajan R, Mackay A, Grigoriadis A, Tutt A, Ashworth A, Reis-Filho JS, Smalley MJ. 2010. BRCA1 basal-like breast cancers originate from luminal epithelial progenitors and not from basal stem cells. Cell Stem Cell 7(3):403-417.

Mundlos S. 1999. Cleidocranial dysplasia: clinical and molecular genetics. J Med Genet 36(3):177-182.

Nagaraja GM, Othman M, Fox BP, Alsaber R, Pellegrino CM, Zeng Y, Khanna R, Tamburini P, Swaroop A, Kandpal RP. 2006. Gene expression signatures and biomarkers of noninvasive and invasive breast cancer cells: comprehensive profiles by representational difference analysis, microarrays and proteomics. Oncogene 25(16):2328-2338.

Nakashima K, Zhou X, Kunkel G, Zhang Z, Deng JM, Behringer RR, de Crombrugghe B. 2002. The novel zinc finger-containing transcription factor

osterix is required for osteoblast differentiation and bone formation. Cell 108(1):17-29.
Nemir M, Bhattacharyya D, Li X, Singh K, Mukherjee AB, Mukherjee BB. 2000. Targeted inhibition of osteopontin expression in the mammary gland causes abnormal morphogenesis and lactation deficiency. J Biol Chem 275(2):969-976.
Ning Y-M, Robins DM. 1999. AML3/CBFalpha1 is required for androgen-specific activation of the enhancer of the mouse sex-limited protein (Slp) gene. J Biol Chem 274(43):30624-30630.
Niu DF, Kondo T, Nakazawa T, Oishi N, Kawasaki T, Mochizuki K, Yamane T, Katoh R. 2012. Transcription factor Runx2 is a regulator of epithelial-mesenchymal transition and invasion in thyroid carcinomas. Lab Invest 92(8):1181-1190.
North T, Gu T-L, Stacy T, Wang Q, Howard L, Binder M, Marín-Padilla M, Speck NA. 1999. Cbfa2 is required for the formation of intra-aortic hematopoietic clusters. Development 126(11):2563-2575.
Oakes SR, Hilton HN, Ormandy CJ. 2006. The alveolar switch: coordinating the proliferative cues and cell fate decisions that drive the formation of lobuloalveoli from ductal epithelium. Breast Cancer Res 8(2):207.
Ocana OH, Corcoles R, Fabra A, Moreno-Bueno G, Acloque H, Vega S, Barrallo-Gimeno A, Cano A, Nieto MA. 2012. Metastatic colonization requires the repression of the epithelial-mesenchymal transition inducer Prrx1. Cancer Cell 22(6):709-724.
Okuda T, Deursen Jv, Hiebert SW, Grosveld G, Downing JR. 1996. AML1, the target of multiple chromosomal translocations in human leukemia, is essential for normal fetal liver hematopoiesis. Cell 84(2):321-330.
Otero M, Plumb DA, Tsuchimochi K, Dragomir CL, Hashimoto K, Peng H, Olivotto E, Bevilacqua M, Tan L, Yang Z, Zhan Y, Oettgen P, Li Y, Marcu KB, Goldring MB. 2012. E74-like factor 3 (ELF3) impacts on matrix metalloproteinase 13 (MMP13) transcriptional control in articular chondrocytes under proinflammatory stress. J Biol Chem 287(5):3559-3572.
Otto F, Kanegane H, Mundlos S. 2002. Mutations in the RUNX2 gene in patients with cleidocranial dysplasia. Human mutation 19(3):209-216.
Otto F, Thornell AP, Crompton T, Denzel A, Gilmour KC, Rosewell IR, Stamp GW, Beddington RS, Mundlos S, Olsen BR, Selby PB, Owen MJ. 1997. Cbfa1, a candidate gene for cleidocranial dysplasia syndrome, is essential for osteoblast differentiation and bone development. Cell 89(5):765-771.
Paget S. 1889. The distribution of secondary growths in cancer of the breast. 1889. Cancer Metastasis Rev 8(2):98-101.
Patel LR, Camacho DF, Shiozawa Y, Pienta KJ, Taichman RS. 2011. Mechanisms of cancer cell metastasis to the bone: a multistep process. Future Oncol 7(11):1285-1297.
Pelletier N, Champagne N, Stifani S, Yang X-J. 2002. MOZ and MORF histone acetyltransferases interact with the Runt-domain transcription factor Runx2. Oncogene 21(17):2729-2740.
Pensa S, Watson CJ, Poli V. 2009. Stat3 and the inflammation/acute phase response in involution and breast cancer. J Mammary Gland Biol Neoplasia 14(2):121-129.

Pinto MP, Jacobsen BM, Horwitz KB. 2011. An immunohistochemical method to study breast cancer cell subpopulations and their growth regulation by hormones in three-dimensional cultures. Frontiers in endocrinology 2:15.

Pratap J, Imbalzano KM, Underwood JM, Cohet N, Gokul K, Akech J, van Wijnen AJ, Stein JL, Imbalzano AN, Nickerson JA, Lian JB, Stein GS. 2009. Ectopic runx2 expression in mammary epithelial cells disrupts formation of normal acini structure: implications for breast cancer progression. Cancer Res 69(17):6807-6814.

Pratap J, Javed A, Languino LR, van Wijnen AJ, Stein JL, Stein GS, Lian JB. 2005. The Runx2 osteogenic transcription factor regulates matrix metalloproteinase 9 in bone metastatic cancer cells and controls cell invasion. Mol Cell Biol 25(19):8581-8591.

Pratap J, Wixted JJ, Gaur T, Zaidi SK, Dobson J, Gokul KD, Hussain S, van Wijnen AJ, Stein JL, Stein GS, Lian JB. 2008. Runx2 transcriptional activation of Indian Hedgehog and a downstream bone metastatic pathway in breast cancer cells. Cancer Res 68(19):7795-7802.

Proff P, Romer P. 2009. The molecular mechanism behind bone remodelling: a review. Clinical oral investigations 13(4):355-362.

Quackenbush J. 2001. Computational analysis of microarray data. Nature reviews Genetics 2(6):418-427.

Richert MM, Schwertfeger KL, Ryder JW, Anderson SM. 2000. An atlas of mouse mammary gland development. J Mammary Gland Biol Neoplasia 5(2):227-241.

Robertson AJ, Dickey-Sims C, Ransick A, Rupp DE, McCarthy JJ, Coffman JA. 2006. CBFbeta is a facultative Runx partner in the sea urchin embryo. BMC Biol 4:4.

Russo IH, Russo J. 1996. Mammary gland neoplasia in long-term rodent studies. Environ Health Perspect 104(9):938-967.

Saito H, Oka T. 1996. Hormonally regulated double- and single-stranded DNA-binding complexes involved in mouse beta-casein gene transcription. J Biol Chem 271(15):8911-8918.

Saleem M, Qadir MI, Perveen N, Ahmad B, Saleem U, Irshad T, Ahmad B. 2013. Inhibitors of apoptotic proteins: new targets for anticancer therapy. Chem Biol Drug Des 82(3):243-251.

Samavarchi-Tehrani P, Golipour A, David L, Sung HK, Beyer TA, Datti A, Woltjen K, Nagy A, Wrana JL. 2010. Functional genomics reveals a BMP-driven mesenchymal-to-epithelial transition in the initiation of somatic cell reprogramming. Cell Stem Cell 7(1):64-77.

Sasaki A, Yoneda T, Terakado N, Alcalde RE, Suzuki A, Matsumura T. 1998. Experimental bone metastasis model of the oral and maxillofacial region. Anticancer Res 18(3A):1579-1584.

Sasaki K, Yagi H, Bronson RT, Tominaga K, Matsunashi T, Deguchi K, Tani Y, Kishimoto T, Komori T. 1996. Absence of fetal liver hematopoiesis in mice deficient in transcriptional coactivator core binding factor beta. Proc Natl Acad Sci U S A 93(22):12359-12363.

Sato M, Morii E, Komori T, Kawahata H, Sugimoto M, Terai K, Shimizu H, Yasui T, Ogihara H, Yasui N, Ochi T, Kitamura Y, Ito Y, Nomura S. 1998a. Transcriptional regulation of osteopontin gene in vivo by PEBP2 A/CBFA1 and ETS1 in the skeletal tissues. Oncogene 17(12):1517-1525.

Schroeder TM, Jensen ED, Westendorf JJ. 2005. Runx2: a master organizer of gene transcription in developing and maturing osteoblasts. Birth Defects Res C Embryo Today 75(3):213-225.

Schroeder TM, Kahler RA, Li X, Westendorf JJ. 2004. Histone deacetylase 3 interacts with runx2 to repress the osteocalcin promoter and regulate osteoblast differentiation. J Biol Chem 279(40):41998-42007.

Selvamurugan N, Kwok S, Partridge NC. 2004. Smad3 interacts with JunB and Cbfa1/Runx2 for transforming growth factor-beta1-stimulated collagenase-3 expression in human breast cancer cells. J Biol Chem 279(26):27764-27773.

Selvamurugan N, Pulumati MR, Tyson DR, Partridge NC. 2000. Parathyroid hormone regulation of the rat collagenase-3 promoter by protein kinase A-dependent transactivation of core binding factor alpha1. J Biol Chem 275(7):5037-5042.

Shackleton M, Vaillant F, Simpson KJ, Stingl J, Smyth GK, Asselin-Labat ML, Wu L, Lindeman GJ, Visvader JE. 2006. Generation of a functional mammary gland from a single stem cell. Nature 439(7072):84-88.

Shaw KR, Wrobel CN, Brugge JS. 2004. Use of three-dimensional basement membrane cultures to model oncogene-induced changes in mammary epithelial morphogenesis. J Mammary Gland Biol Neoplasia 9(4):297-310.

Shen FH, Werner BC, Liang H, Shang H, Yang N, Li X, Shimer AL, Balian G, Katz AJ. 2013. Implications of adipose-derived stromal cells in a 3D culture system for osteogenic differentiation: an in vitro and in vivo investigation. Spine J 13(1):32-43.

Shen R, Wang X, Drissi H, Liu F, O'Keefe RJ, Chen D. 2006. Cyclin D1-cdk4 induce runx2 ubiquitination and degradation. J Biol Chem 281(24):16347-16353.

Shiau AK, Barstad D, Loria PM, Cheng L, Kushner PJ, Agard DA, Greene GL. 1998. The structural basis of estrogen receptor/coactivator recognition and the antagonism of this interaction by tamoxifen. Cell 95(7):927-937.

Shigesada K, van de Sluis B, Liu PP. 2004. Mechanism of leukemogenesis by the inv(16) chimeric gene CBFB/PEBP2B-MHY11. Oncogene 23(24):4297-4307.

Shirakabe K, Terasawa K, Miyama K, Shibuya H, Nishida E. 2001. Regulation of the activity of the transcription factor Runx2 by two homeobox proteins, Msx2 and Dlx5. Genes Cells 6(10):851-856.

Shui C, Spelsberg TC, Riggs BL, Khosla S. 2003. Changes in Runx2/Cbfa1 expression and activity during osteoblastic differentiation of human bone marrow stromal cells. J Bone Miner Res 18(2):213-221.

Sierra J, Villagra A, Paredes R, Cruzat F, Gutierrez S, Javed A, Arriagada G, Olate J, Imschenetzky M, Van Wijnen AJ, Lian JB, Stein GS, Stein JL, Montecino M. 2003a. Regulation of the bone-specific osteocalcin gene by p300 requires Runx2/Cbfa1 and the vitamin D3 receptor but not p300 intrinsic histone acetyltransferase activity. Mol Cell Biol 23(9):3339-3351.

Smyth GK. 2004. Linear models and empirical bayes methods for assessing differential expression in microarray experiments. Statistical applications in genetics and molecular biology 3:Article3.

Stock M, Otto F. 2005. Control of RUNX2 isoform expression: the role of promoters and enhancers. J Biol Chem 95(3):506-517.

Storey JD, Tibshirani R. 2003. Statistical significance for genomewide studies. Proc Natl Acad Sci U S A 100(16):9440-9445.

Sun N, Zhao H. 2013. Transcription activator-like effector nucleases (TALENs): a highly efficient and versatile tool for genome editing. Biotechnol Bioeng 110(7):1811-1821.

Tahirov TH, Inoue-Bungo T, Morii H, Fujikawa A, Sasaki M, Kimura K, Shiina M, Sato K, Kumasaka T, Yamamoto M, Ishii S, Ogata K. 2001. Structural analyses of DNA recognition by the AML1/Runx-1 Runt domain and its allosteric control by CBFbeta. Cell 104(5):755-767.

Takeda S, Bonnamy J-P, Owen MJ, Ducy P, Karsenty G. 2001. Continuous expression of Cbfa1 in nonhypertrophic chondrocytes uncovers its ability to induce hypertrophic chondrocyte differentiation and partially rescues Cbfa1-deficient mice. Genes Dev 15(4):467-481.

Tanaka Y, Watanabe T, Chiba N, Niki M, Kuroiwa Y, Nishihira T, Satomi S, Ito Y, Satake M. 1997. The protooncogene product, PEBP2beta/CBFbeta, is mainly located in the cytoplasm and has an affinity with cytoskeletal structures. Oncogene 15(6):677-683.

Tang W, Yang L, Yang YC, Leng SX, Elias JA. 1998. Transforming growth factor-beta stimulates interleukin-11 transcription via complex activating protein-1-dependent pathways. J Biol Chem 273(10):5506-5513.

Tanga Y-Y, Crutea BE, IIIb JJK, Huangb X, Yanb J, Shib J, Hartmanc KL, Lauec TM, Specka NA, Bushwellerb JH. 2000. Biophysical characterization of interactions between the core binding factor alpha and beta subunits and DNA. FEBS Lett 470(2):167-172.

Taniuchi I, Osato M, Egawa T, Sunshine MJ, Bae S-C, Komori o, Itp Y, Littman DR. 2002. Differential requirements for Runx proteins in CD4 repression and epigenetic silencing during T lymphocyte development. Cell 111(5):621-633.

Taverna D, Groner B, Hynes NE. 1991. Epidermal growth factor receptor, platelet-derived growth factor receptor, and c-erbB-2 receptor activation all promote growth but have distinctive effects upon mouse mammary epithelial cell differentiation. Cell Growth Differ 2(3):145-154.

Thiery JP, Acloque H, Huang RY, Nieto MA. 2009. Epithelial-mesenchymal transitions in development and disease. Cell 139(5):871-890.

Thirunavukkarasu K, Mahajan M, McLarren KW, Stifani S, Karsenty G. 1998. Two domains unique to osteoblast-specific transcription factor Osf2/Cbfa1 contribute to its transactivation function and its inability to heterodimerize with Cbfbeta. Mol Cell Biol 18(7):4197-4208.

Thomas RJ, Guise TA, Yin JJ, Elliott J, Horwood NJ, Martin TJ, Gillespie MT. 1999. Breast cancer cells interact with osteoblasts to support osteoclast formation. Endocrinology 140(10):4451-4458.

Tsai JH, Donaher JL, Murphy DA, Chau S, Yang J. 2012. Spatiotemporal regulation of epithelial-mesenchymal transition is essential for squamous cell carcinoma metastasis. Cancer Cell 22(6):725-736.

Vega RB, Matsuda K, Oh J, Barbosa AC, Yang X, Meadows E, McAnally J, Pomajzl C, Shelton JM, Richardson JA, Karsenty G, Olson EN. 2004. Histone deacetylase 4 controls chondrocyte hypertrophy during skeletogenesis. Cell 119(4):555-566.

Veltmaat JM, Van Veelen W, Thiery JP, Bellusci S. 2004. Identification of the mammary line in mouse by Wnt10b expression. Dev Dyn 229(2):349-356.

Wang CQ, Jacob B, Nah GS, Osato M. 2010. Runx family genes, niche, and stem cell quiescence. Blood Cells Mol Dis 44(4):275-286.

Wang JF, She L, Su BH, Ding LC, Zheng FF, Zheng DL, Lu YG. 2011a. CDH12 promotes the invasion of salivary adenoid cystic carcinoma. Oncol Rep 26(1):101-108.

Wang L, Brugge JS, Janes KA. 2011b. Intersection of FOXO- and RUNX1-mediated gene expression programs in single breast epithelial cells during morphogenesis and tumor progression. Proc Natl Acad Sci U S A 108(40):E803-812.

Wang Q, Stac T, Binder M, Marin-Padilla M, Sharpe AH, Speck NA. 1996a. Disruption of the Cbfa2 gene causes necrosis and hemorrhaging in the central nervous system and blocks definitive hematopoiesis. Proc Natl Acad Sci U S A 93(8):3444-3449.

Wang Q, Stacy T, Miller JD, Lewis AF, Gu T-L, Huang X, Bushweller JH, Bories J-C, Alt FW, Ryan G, Liu PP, Wynshaw-Boris A, Binder M, Marín-Padilla M, Sharpe AH, Speck NA. 1996b. The CBFbeta subunit is essential for CBFalpha2 (AML1) function in vivo. Cell 87(4):697-708.

Wang S, Wang Q, Crute BE, Melnikova IN, Keller SR, Speck NA. 1993. Cloning and characterization of subunits of the T-cell receptor and murine leukemia virus enhancer core-binding factor. Mol Cell Biol 13(6):3324-3339.

Watson CJ, Khaled WT. 2008. Mammary development in the embryo and adult: a journey of morphogenesis and commitment. Development 135(6):995-1003.

Watson CJ, Kreuzaler PA. 2011. Remodeling mechanisms of the mammary gland during involution. Int J Dev Biol 55(7-9):757-762.

Weaver VM, Lelievre S, Lakins JN, Chrenek MA, Jones JC, Giancotti F, Werb Z, Bissell MJ. 2002. beta4 integrin-dependent formation of polarized three-dimensional architecture confers resistance to apoptosis in normal and malignant mammary epithelium. Cancer Cell 2(3):205-216.

Weber CE, Li NY, Wai PY, Kuo PC. 2012. Epithelial-mesenchymal transition, TGF-beta, and osteopontin in wound healing and tissue remodeling after injury. Journal of burn care & research : official publication of the American Burn Association 33(3):311-318.

Wee HJ, Huang G, Shigesada K, Ito Y. 2002. Serine phosphorylation of RUNX2 with novel potential functions as negative regulatory mechanisms. EMBO Rep 3(10):967-974.

Weigelt B, Bissell MJ. 2008. Unraveling the microenvironmental influences on the normal mammary gland and breast cancer. Seminars in cancer biology 18(5):311-321.

Westendorf JJ, Zaidi SK, Cascino JE, Kahler R, Wijnen AJv, Lian JB, Yoshida M, Stein GS, Li X. 2002. Runx2 (Cbfa1, AML-3) interacts with histone deacetylase 6 and represses the p21(CIP1/WAF1) promoter. Mol Cell Biol 22(22):7982-7992.

Williams C, Helguero L, Edvardsson K, Haldosen LA, Gustafsson JA. 2009. Gene expression in murine mammary epithelial stem cell-like cells shows similarities to human breast cancer gene expression. Breast Cancer Res 11(3):R26.

Woolf E, Xiao C, Fainaru O, Lotem J, Rosen D, Negreanu V, Bernstein Y, Goldenberg D, Brenner O, Berke G, Levanon D, Groner Y. 2003. Runx3 and Runx1 are required for CD8 T cell development during thymopoiesis. Proc Natl Acad Sci U S A 100(13):7731-7736.

Wysolmerski JJ, McCaughern-Carucci JF, Daifotis AG, Broadus AE, Philbrick WM. 1995. Overexpression of parathyroid hormone-related protein or parathyroid

hormone in transgenic mice impairs branching morphogenesis during mammary gland development. Development 121(11):3539-3547.

Xian W, Schwertfeger KL, Vargo-Gogola T, Rosen JM. 2005. Pleiotropic effects of FGFR1 on cell proliferation, survival, and migration in a 3D mammary epithelial cell model. J Cell Biol 171(4):663-673.

Xiao G, Jiang D, Ge C, Zhao Z, Lai Y, Boules H, Phimphilai M, Yang X, Karsenty G, Franceschi RT. 2005. Cooperative interactions between activating transcription factor 4 and Runx2/Cbfa1 stimulate osteoblast-specific osteocalcin gene expression. J Biol Chem 280(35):30689-30696.

Yamagata T, Maki K, Mitani K. 2005. Runx1/AML1 in normal and abnormal hematopoiesis. Int J Hematol 82(1):1-8.

Yang X, Matsuda K, Bialek P, Jacquot S, Masuoka HC, Schinke T, Li L, Brancorsini S, Sassone-Corsi P, Townes TM, Hanauer A, Karsenty G. 2004. ATF4 is a substrate of RSK2 and an essential regulator of osteoblast biology; implication for Coffin-Lowry Syndrome. Cell 117(3):387-398.

Yang Y, Li Z. 2005. Roles of heat shock protein gp96 in the ER quality control: redundant or unique function? Molecules and cells 20(2):173-182.

Yin JJ, Pollock CB, Kelly K. 2005. Mechanisms of cancer metastasis to the bone. Cell Res 15(1):57-62.

Yin JJ, Selander K, Chirgwin JM, Dallas M, Grubbs BG, Wieser R, Massague J, Mundy GR, Guise TA. 1999. TGF-beta signaling blockade inhibits PTHrP secretion by breast cancer cells and bone metastases development. J Clin Invest 103(2):197-206.

Yoshida CA, Furuichi T, Fujita T, Fukuyama R, Kanatani N, Kobayashi S, Satake M, Takada K, Komori T. 2002. Core-binding factor beta interacts with Runx2 and is required for skeletal development. Nat Genet 32(4):633-638.

Yoshida N, Ogata T, Tanabe K, Li S, Nakazato M, Kohu K, Takafuta T, Shapiro S, Ohta Y, Satake M, Watanabe T. 2005. Filamin A-bound PEBP2beta/CBFbeta is retained in the cytoplasm and prevented from functioning as a partner of the Runx1 transcription factor. Mol Cell Biol 25(3):1003-1012.

Zaidi SK, Javed A, Choi JY, van Wijnen AJ, Stein JL, Lian JB, Stein GS. 2001. A specific targeting signal directs Runx2/Cbfa1 to subnuclear domains and contributes to transactivation of the osteocalcin gene. J Cell Sci 114(Pt 17):3093-3102.

Zeng C, McNeil S, Pockwinse S, Nickerson J, Shopland L, Lawrence JB, Penman S, Hiebert S, Lian JB, Wijnen AJv, Stein JL, Stein GS. 1998. Intranuclear targeting of AML/CBFalpha regulatory factors to nuclear matrix-associated transcriptional domains. Proc Natl Acad Sci U S A 95(4):1585-1589.

Zeng C, Wijnen AJv, Stein JL, Meyers S, Sun W, Shopland L, Lawrence JB, Penman S, Lian JB, Stein GS, Hiebert SW. 1997. Identification of a nuclear matrix targeting signal in the leukemia and bone-related AML/CBF-alpha transcription factors. Proc Natl Acad Sci U S A 94(13):6746-6751.

Zhang Y, Ma B, Fan Q. 2010. Mechanisms of breast cancer bone metastasis. Cancer Lett 292(1):1-7.

Appendix

Probe Set ID	Gene Symbol	core-binding factor, beta subunit	Fold-Change(CBFb vs. NS)	q-value
1552365_at	SCIN	scinderin	16.8834	0.000138892
203913_s_at	HPGD	hydroxyprostaglandin dehydrogenase 15-(NAD)	15.9149	0.000138892
39248_at	AQP3	aquaporin 3 (Gill blood group)	14.0119	0.000138892
203914_x_at	HPGD	hydroxyprostaglandin dehydrogenase 15-(NAD)	13.9093	0.000152852
211548_s_at	HPGD	hydroxyprostaglandin dehydrogenase 15-(NAD)	13.9012	0.000138892
1552367_a_at	SCIN	scinderin	12.2981	0.000138892
1569582_at	LOC201651	arylacetamide deacetylase (esterase) pseudogene	11.3667	0.000215749
230135_at	HHIP	hedgehog interacting protein	11.2293	0.000138892
231628_s_at	SERPINB6	Serpin peptidase inhibitor, clade B (ovalbumin), member 6	10.7613	0.001478334
228241_at	AGR3	anterior gradient 3 homolog (Xenopus laevis)	9.75997	0.000220658
232056_at	SCEL	sciellin	9.23629	0.000242121
211549_s_at	HPGD	hydroxyprostaglandin dehydrogenase 15-(NAD)	8.88719	0.000138892
222043_at	CLU	clusterin	8.64751	0.000155442
229177_at	C16orf89	chromosome 16 open reading frame 89	8.60882	0.000138892
206884_s_at	SCEL	sciellin	7.91897	0.000306095
207996_s_at	C18orf1	chromosome 18 open reading frame 1	7.44068	0.000145333
226534_at	KITLG	KIT ligand	7.13176	0.000138892
230061_at	TM4SF18	transmembrane 4 L six family member 18	6.49088	0.000209034
229242_at	TNFSF15	tumor necrosis factor (ligand) superfamily, member 15	6.41132	0.000138892
221085_at	TNFSF15	tumor necrosis factor (ligand) superfamily, member 15	6.10539	0.000752473
219316_s_at	FLVCR2	feline leukemia virus subgroup C cellular receptor family, member 2	6.02876	0.000209034
229839_at	SCARA5	scavenger receptor class A, member 5 (putative)	5.94598	0.000154888
219572_at	CADPS2	Ca++-dependent secretion activator 2	5.68966	0.000138892
229377_at	GRTP1	growth hormone regulated TBC protein 1	5.63919	0.000241766
204378_at	BCAS1	breast carcinoma amplified sequence 1	5.62616	0.000138892
228489_at	TM4SF18	transmembrane 4 L six family member 18	5.54706	0.000138892
208792_s_at	CLU	clusterin	5.47382	0.000220658
232054_at	PCDH20	protocadherin 20	5.39725	0.000144985
223775_at	HHIP	hedgehog interacting protein	5.3732	0.000569353
208791_at	CLU	clusterin	5.0936	0.000188403
227812_at	TNFRSF19	tumor necrosis factor receptor superfamily, member 19	5.05845	0.0038148
212950_at	GPR116	G protein-coupled receptor 116	4.96344	0.000152852
209277_at	TFPI2	tissue factor pathway inhibitor 2	4.73129	0.000306095
212951_at	GPR116	G protein-coupled receptor 116	4.71141	0.000154888
201842_s_at	EFEMP1	EGF containing fibulin-like extracellular matrix protein 1	4.53909	0.000538787
242943_at	ST8SIA4	ST8 alpha-N-acetyl-neuraminide alpha-2,8-sialyltransferase 4	4.50166	0.000188403
209278_s_at	TFPI2	tissue factor pathway inhibitor 2	4.47727	0.000154888
206224_at	CST1	cystatin SN	4.42952	0.000252053
205014_at	FGFBP1	fibroblast growth factor binding protein 1	4.32535	0.000209034
243681_at	SHANK2	SH3 and multiple ankyrin repeat domains 2	4.28429	0.000220658
213800_at	CFH	complement factor H	4.21338	0.000207137
1568868_at	CYP27C1	cytochrome P450, family 27, subfamily C, polypeptide 1	4.12748	0.000220658
203780_at	MPZL2	myelin protein zero-like 2	4.10762	0.000251704
205569_at	LAMP3	lysosomal-associated membrane protein 3	4.09147	0.000197255
1555120_at	CD96	CD96 molecule	4.04548	0.00134851
236489_at	GPR110	G protein-coupled receptor 110	4.04388	0.000188403
218858_at	DEPTOR	DEP domain containing MTOR-interacting protein	4.01756	0.000242121
1564150_a_at	LOC256021	uncharacterized LOC256021	4.00367	0.000220658
203908_at	SLC4A4	solute carrier family 4, sodium bicarbonate cotransporter, member 4	3.99189	0.000453496
228969_at	AGR2	anterior gradient 2 homolog (Xenopus laevis)	3.96249	0.000458526
223204_at	FAM198B	family with sequence similarity 198, member B	3.95401	0.000306095
209909_s_at	TGFB2	transforming growth factor, beta 2	3.94075	0.000192985
230261_at	ST8SIA4	ST8 alpha-N-acetyl-neuraminide alpha-2,8-sialyltransferase 4	3.9386	0.000197255
237466_s_at	HHIP	hedgehog interacting protein	3.77858	0.000209034
206761_at	CD96	CD96 molecule	3.7741	0.000220658
207018_s_at	RAB27B	RAB27B, member RAS oncogene family	3.7519	0.000220658
238178_at	---	---	3.7435	0.000982457
230836_at	ST8SIA4	ST8 alpha-N-acetyl-neuraminide alpha-2,8-	3.69056	0.000215749

		sialyltransferase 4		
204273_at	EDNRB	endothelin receptor type B	3.62364	0.000209034
225817_at	CGNL1	cingulin-like 1	3.57993	0.000339946
220180_at	CCDC68	coiled-coil domain containing 68	3.54098	0.000220658
223599_at	TRIM6	tripartite motif containing 6	3.49269	0.000242121
204897_at	PTGER4	prostaglandin E receptor 4 (subtype EP4)	3.43697	0.000251704
229041_s_at	LOC100505746	uncharacterized LOC100505746	3.4344	0.000220658
225671_at	SPNS2	spinster homolog 2 (Drosophila)	3.42704	0.000257471
214433_s_at	SELENBP1	selenium binding protein 1	3.42523	0.000946212
1569344_a_at	---	---	3.34496	0.000258774
213122_at	TSPYL5	TSPY-like 5	3.31824	0.000551009
244121_at	UBR3	Ubiquitin protein ligase E3 component n-recognin 3 (putative)	3.31465	0.00082485
209173_at	AGR2	anterior gradient 2 homolog (Xenopus laevis)	3.26213	0.000241766
204404_at	SLC12A2	solute carrier family 12 (sodium/potassium/chloride transporters), member 2	3.24637	0.000313377
229170_s_at	TTC18	tetratricopeptide repeat domain 18	3.18183	0.000946212
235988_at	GPR110	G protein-coupled receptor 110	3.18085	0.000943254
201939_at	PLK2	polo-like kinase 2	3.16476	0.000241766
229720_at	BAG1	BCL2-associated athanogene	3.16037	0.000313377
213307_at	SHANK2	SH3 and multiple ankyrin repeat domains 2	3.15694	0.000323699
209735_at	ABCG2	ATP-binding cassette, sub-family G (WHITE), member 2	3.15378	0.000294926
213308_at	SHANK2	SH3 and multiple ankyrin repeat domains 2	3.12957	0.000313377
229030_at	CAPN8	calpain 8	3.12805	0.000430852
226869_at	MEGF6	multiple EGF-like-domains 6	3.09921	0.00052489
228834_at	---	---	3.09651	0.000242121
1552754_a_at	CADM2	cell adhesion molecule 2	3.09248	0.000220658
212230_at	PPAP2B	phosphatidic acid phosphatase type 2B	3.08083	0.000241766
207761_s_at	METTL7A	methyltransferase like 7A	3.07628	0.000313775
244835_at	C16orf52	Chromosome 16 open reading frame 52	3.02492	0.000766822
226811_at	FAM46C	family with sequence similarity 46, member C	3.00563	0.000288439
215076_s_at	COL3A1	collagen, type III, alpha 1	2.9298	0.000964406
212183_at	NUDT4	nudix (nucleoside diphosphate linked moiety X)-type motif 4	2.92604	0.000752473
230729_at	---	---	2.90459	0.000752473
228325_at	KIAA0146	KIAA0146	2.90414	0.000242121
239751_at	LOC100506860	uncharacterized LOC100506860	2.87691	0.000242121
213006_at	CEBPD	CCAAT/enhancer binding protein (C/EBP), delta	2.86482	0.000465139
201843_s_at	EFEMP1	EGF containing fibulin-like extracellular matrix protein 1	2.84323	0.001068327
233677_at	---	---	2.83126	0.000662968
234982_at	UBR3	ubiquitin protein ligase E3 component n-recognin 3 (putative)	2.82775	0.000328693
209392_at	ENPP2	ectonucleotide pyrophosphatase/phosphodiesterase 2	2.82567	0.000662968
235849_at	SCARA5	scavenger receptor class A, member 5 (putative)	2.82043	0.000323652
230029_x_at	UBR3	ubiquitin protein ligase E3 component n-recognin 3 (putative)	2.79932	0.000770346
214920_at	THSD7A	thrombospondin, type I, domain containing 7A	2.79004	0.000447932
1555854_at	AKR1C1 /// AKR1C2 /// LOC100653286	aldo-keto reductase family 1, member C1 (dihydrodiol dehydrogenase 1; 20-alpha (3-alpha)-hydroxysteroid dehydrogenase) /// aldo-keto reductase family 1, member C2 (dihydrodiol dehydrogenase 2; bile acid binding protein; 3-alpha hydroxysteroid dehydrogenase, type III) /// aldo-keto reductase family 1 member C2-like	2.78901	0.000313775
207826_s_at	ID3	inhibitor of DNA binding 3, dominant negative helix-loop-helix protein	2.78462	0.000467368
227503_at	---	---	2.74272	0.000447063
220407_s_at	TGFB2	transforming growth factor, beta 2	2.73219	0.002391263
227475_at	FOXQ1	forkhead box Q1	2.72772	0.000275718
212830_at	MEGF9	multiple EGF-like-domains 9	2.70677	0.000281165
213059_at	CREB3L1	cAMP responsive element binding protein 3-like 1	2.70235	0.000545787
204790_at	SMAD7	SMAD family member 7	2.69839	0.000447063
226865_at	LOC100509635	uncharacterized LOC100509635	2.69834	0.000339946
202743_at	PIK3R3	phosphoinositide-3-kinase, regulatory subunit 3 (gamma)	2.69646	0.000313775
229842_at	ELF3	E74-like factor 3 (ets domain transcription factor, epithelial-specific)	2.69226	0.000586042
203824_at	TSPAN8	tetraspanin 8	2.69147	0.00077036
213325_at	PVRL3	poliovirus receptor-related 3	2.68578	0.000313377
1554921_a_at	SCEL	sciellin	2.67561	0.000676959
217761_at	ADI1	acireductone dioxygenase 1	2.67118	0.00043977
208451_s_at	C4A /// C4B /// LOC100293534	complement component 4A (Rodgers blood group) /// complement component 4B (Chido blood group) /// complement C4-B-like	2.66177	0.000413101
205259_at	NR3C2	nuclear receptor subfamily 3, group C, member 2	2.65833	0.001605263
215071_s_at	HIST1H2AC	histone cluster 1, H2ac	2.64797	0.000555175
208653_s_at	CD164	CD164 molecule, sialomucin	2.64629	0.001268992

228121_at	TGFB2	transforming growth factor, beta 2	2.64199	0.000425055
1568597_at	LOC646762	uncharacterized LOC646762	2.64035	0.000345356
209355_s_at	PPAP2B	phosphatidic acid phosphatase type 2B	2.62199	0.000762157
215388_s_at	CFH /// CFHR1	complement factor H /// complement factor H-related 1	2.58528	0.00043977
203372_s_at	SOCS2	suppressor of cytokine signaling 2	2.57187	0.000430852
217771_at	GOLM1	golgi membrane protein 1	2.56977	0.000339946
212226_s_at	PPAP2B	phosphatidic acid phosphatase type 2B	2.56119	0.00033878
212636_at	QKI	QKI, KH domain containing, RNA binding	2.55975	0.001362669
209574_s_at	C18orf1	chromosome 18 open reading frame 1	2.55486	0.000828827
202291_s_at	MGP	matrix Gla protein	2.55467	0.0014428
229169_at	TTC18	tetratricopeptide repeat domain 18	2.55254	0.000413101
229199_at	SCN9A	sodium channel, voltage-gated, type IX, alpha subunit	2.55135	0.000308335
212181_s_at	NUDT4 /// NUDT4P1	nudix (nucleoside diphosphate linked moiety X)-type motif 4 /// nudix (nucleoside diphosphate linked moiety X)-type motif 4 pseudogene 1	2.5384	0.000308335
225731_at	ANKRD50	ankyrin repeat domain 50	2.52961	0.000317735
235944_at	HMCN1	hemicentin 1	2.51957	0.000775365
214455_at	HIST1H2BC /// HIST1H2BE /// HIST1H2BF /// HIST1H2BG /// HIST1H2BI	histone cluster 1, H2bc /// histone cluster 1, H2be /// histone cluster 1, H2bf /// histone cluster 1, H2bg /// histone cluster 1, H2bi	2.51826	0.000714308
206994_at	CST4	cystatin S	2.51273	0.000579943
214954_at	SUSD5	sushi domain containing 5	2.50781	0.003043351
228708_at	RAB27B	RAB27B, member RAS oncogene family	2.50634	0.000374511
1556037_s_at	HHIP	hedgehog interacting protein	2.50311	0.003023417
219106_s_at	KBTBD10	kelch repeat and BTB (POZ) domain containing 10	2.49394	0.000574389
200878_at	EPAS1 /// LOC100652809	endothelial PAS domain protein 1 /// uncharacterized LOC100652809	2.49221	0.000313377
225835_at	SLC12A2	solute carrier family 12 (sodium/potassium/chloride transporters), member 2	2.47125	0.000764734
40093_at	BCAM	basal cell adhesion molecule (Lutheran blood group)	2.44252	0.000328347
225987_at	STEAP4	STEAP family member 4	2.44037	0.001382881
209488_s_at	RBPMS	RNA binding protein with multiple splicing	2.4387	0.000328347
201468_s_at	NQO1	NAD(P)H dehydrogenase, quinone 1	2.42758	0.00038313
225975_at	PCDH18	protocadherin 18	2.42497	0.005421818
200670_at	XBP1	X-box binding protein 1	2.42399	0.000541931
239814_at	LOC100506860	uncharacterized LOC100506860	2.41469	0.00038313
224558_s_at	LOC100507645 /// MALAT1	uncharacterized LOC100507645 /// metastasis associated lung adenocarcinoma transcript 1 (non-protein coding)	2.41464	0.00061957
239336_at	THBS1	thrombospondin 1	2.4138	0.000472706
211475_s_at	BAG1	BCL2-associated athanogene	2.41005	0.00042093
209487_at	RBPMS	RNA binding protein with multiple splicing	2.40666	0.000541931
208555_x_at	CST2	cystatin SA	2.4014	0.002862077
202704_at	TOB1	transducer of ERBB2, 1	2.39696	0.000735629
228058_at	ZG16B	zymogen granule protein 16 homolog B (rat)	2.39131	0.000339946
206302_s_at	NUDT4 /// NUDT4P1	nudix (nucleoside diphosphate linked moiety X)-type motif 4 /// nudix (nucleoside diphosphate linked moiety X)-type motif 4 pseudogene 1	2.38942	0.000756546
201565_s_at	ID2	inhibitor of DNA binding 2, dominant negative helix-loop-helix protein	2.38082	0.000725897
236129_at	GALNT5	UDP-N-acetyl-alpha-D-galactosamine:polypeptide N-acetylgalactosaminyltransferase 5 (GalNAc-T5)	2.37619	0.000345356
202387_at	BAG1	BCL2-associated athanogene	2.37088	0.000447063
230112_at	MARCH4	membrane-associated ring finger (C3HC4) 4, E3 ubiquitin protein ligase	2.36311	0.003128666
203561_at	FCGR2A	Fc fragment of IgG, low affinity IIa, receptor (CD32)	2.35446	0.000835181
1566166_at	---	---	2.35273	0.001285794
228827_at	RUNX1T1	runt-related transcription factor 1; translocated to, 1 (cyclin D-related)	2.35005	0.000840238
228850_s_at	SLIT2	slit homolog 2 (Drosophila)	2.34607	0.001957628
235342_at	SPOCK3	sparc/osteonectin, cwcv and kazal-like domains proteoglycan (testican) 3	2.34597	0.00310283
204731_at	TGFBR3	transforming growth factor, beta receptor III	2.34469	0.000553311
203747_at	AQP3	aquaporin 3 (Gill blood group)	2.3392	0.00117349
227276_at	PLXDC2	plexin domain containing 2	2.33404	0.001700976
218918_at	MAN1C1	mannosidase, alpha, class 1C, member 1	2.33276	0.003037853
202350_s_at	LOC100506558 /// MATN2	uncharacterized LOC100506558 /// matrilin 2	2.31309	0.001354196
230130_at	SLIT2	Slit homolog 2 (Drosophila)	2.30808	0.000792662
207144_s_at	CITED1	Cbp/p300-interacting transactivator, with Glu/Asp-rich carboxy-terminal domain, 1	2.30654	0.000886281
1564220_a_at	LOC100506465	uncharacterized LOC100506465	2.30385	0.001759064
243563_at	---	---	2.30176	0.000752473
207149_at	CDH12	cadherin 12, type 2 (N-cadherin 2)	2.30107	0.001442548
204151_x_at	AKR1C1	aldo-keto reductase family 1, member C1 (dihydrodiol dehydrogenase 1; 20-alpha (3-alpha)-hydroxysteroid dehydrogenase)	2.30095	0.000909799
229040_at	LOC100505746	uncharacterized LOC100505746	2.27594	0.000553311

227741_at	PTPLB	protein tyrosine phosphatase-like (proline instead of catalytic arginine), member b	2.27527	0.002715802
212096_s_at	MTUS1	microtubule associated tumor suppressor 1	2.27229	0.000968413
222400_s_at	ADI1	acireductone dioxygenase 1	2.26993	0.000410661
229569_at	---	---	2.26892	0.000699741
214428_x_at	C4A /// C4B /// LOC100293534	complement component 4A (Rodgers blood group) /// complement component 4B (Chido blood group) /// complement C4-B-like	2.25945	0.000538787
238455_at	---	---	2.25932	0.00776382
201510_at	ELF3	E74-like factor 3 (ets domain transcription factor, epithelial-specific)	2.25468	0.000447063
217979_at	TSPAN13	tetraspanin 13	2.23928	0.000513103
222877_at	---	---	2.23781	0.002163423
235976_at	SLITRK6	SLIT and NTRK-like family, member 6	2.23287	0.000467368
206925_at	ST8SIA4	ST8 alpha-N-acetyl-neuraminide alpha-2,8-sialyltransferase 4	2.23127	0.001663607
225735_at	ANKRD50	ankyrin repeat domain 50	2.23111	0.00043977
203221_at	TLE1	transducin-like enhancer of split 1 (E(sp1) homolog, Drosophila)	2.22727	0.000523113
217599_s_at	MDFIC	MyoD family inhibitor domain containing	2.22714	0.003341787
213894_at	THSD7A	thrombospondin, type I, domain containing 7A	2.22654	0.000938425
207723_s_at	KLRC3	killer cell lectin-like receptor subfamily C, member 3	2.22628	0.000421555
212831_at	MEGF9	multiple EGF-like-domains 9	2.21774	0.002053883
237183_at	GALNT5	UDP-N-acetyl-alpha-D-galactosamine:polypeptide N-acetylgalactosaminyltransferase 5 (GalNAc-T5)	2.20636	0.000447063
214748_at	N4BP2L2	NEDD4 binding protein 2-like 2	2.1928	0.001647732
204990_s_at	ITGB4	integrin, beta 4	2.18627	0.000550179
230250_at	PTPRB	protein tyrosine phosphatase, receptor type, B	2.17992	0.001759064
225912_at	TP53INP1	tumor protein p53 inducible nuclear protein 1	2.17781	0.000451332
201349_at	SLC9A3R1	solute carrier family 9, subfamily A (NHE3, cation proton antiporter 3), member 3 regulator 1	2.17508	0.000762157
1558508_a_at	C1orf53	chromosome 1 open reading frame 53	2.15385	0.000676959
206950_at	SCN9A	sodium channel, voltage-gated, type IX, alpha subunit	2.14205	0.002086606
220474_at	SLC25A21	solute carrier family 25 (mitochondrial oxoadipate carrier), member 21	2.14179	0.001404185
221245_s_at	FZD5	frizzled family receptor 5	2.13805	0.000671183
226625_at	TGFBR3	transforming growth factor, beta receptor III	2.13451	0.000600148
236193_at	HIST1H2BC	histone cluster 1, H2bc	2.13117	0.000677138
236330_at	---	---	2.13029	0.000544873
215146_s_at	TTC28	tetratricopeptide repeat domain 28	2.12285	0.000762157
222912_at	ARRB1	arrestin, beta 1	2.12275	0.000777033
209357_at	CITED2	Cbp/p300-interacting transactivator, with Glu/Asp-rich carboxy-terminal domain, 2	2.11888	0.000475891
203222_s_at	TLE1	transducin-like enhancer of split 1 (E(sp1) homolog, Drosophila)	2.1177	0.001222782
207980_s_at	CITED2	Cbp/p300-interacting transactivator, with Glu/Asp-rich carboxy-terminal domain, 2	2.11406	0.000886281
214022_s_at	IFITM1	interferon induced transmembrane protein 1	2.1106	0.000503863
229309_at	ADRB1	adrenoceptor beta 1	2.10713	0.001696266
228979_at	SFTA3	surfactant associated 3	2.10659	0.00085435
208405_s_at	CD164	CD164 molecule, sialomucin	2.10631	0.000676087
239942_at	---	---	2.1039	0.001553908
237329_at	LOC100509621	uncharacterized LOC100509621	2.1031	0.001447466
229975_at	BMPR1B	bone morphogenetic protein receptor, type IB	2.0955	0.001557117
211538_s_at	HSPA2	heat shock 70kDa protein 2	2.0919	0.000628992
232298_at	LOC401093	uncharacterized LOC401093	2.08558	0.000567025
240806_at	RPL15	Ribosomal protein L15	2.07925	0.001212343
205226_at	PDGFRL	platelet-derived growth factor receptor-like	2.07697	0.002737095
205698_s_at	MAP2K6	mitogen-activated protein kinase kinase 6	2.07536	0.003195058
238116_at	DYNLRB2	dynein, light chain, roadblock-type 2	2.07285	0.009194123
205552_s_at	OAS1	2'-5'-oligoadenylate synthetase 1, 40/46kDa	2.07232	0.000589751
235173_at	LOC401093	uncharacterized LOC401093	2.07142	0.000582811
202708_s_at	HIST2H2BE	histone cluster 2, H2be	2.06424	0.000625354
201601_x_at	IFITM1 /// IFITM2	interferon induced transmembrane protein 1 /// interferon induced transmembrane protein 2	2.0596	0.000553311
208654_s_at	CD164	CD164 molecule, sialomucin	2.05892	0.000545149
221011_s_at	LBH	limb bud and heart development homolog (mouse)	2.05821	0.000956883
241933_at	QRSL1	glutaminyl-tRNA synthase (glutamine-hydrolyzing)-like 1	2.05739	0.003243091
201467_s_at	NQO1	NAD(P)H dehydrogenase, quinone 1	2.05677	0.000670772
206382_s_at	BDNF	brain-derived neurotrophic factor	2.05168	0.00070608
225354_s_at	SH3BGRL2	SH3 domain binding glutamic acid-rich protein like 2	2.05125	0.000676087
238919_at	---	---	2.05095	0.001067818
204271_s_at	EDNRB	endothelin receptor type B	2.04354	0.005421587
220321_s_at	CCDC121	coiled-coil domain containing 121	2.04275	0.001010145
218901_at	PLSCR4	phospholipid scramblase 4	2.04272	0.001012945
232270_at	C9orf3 /// LOC100507319	chromosome 9 open reading frame 3 /// uncharacterized LOC100507319	2.0416	0.000677138

200696_s_at	GSN	gelsolin	2.03942	0.00070608
212400_at	FAM102A	family with sequence similarity 102, member A	2.03236	0.000676959
214807_at	---	---	2.02982	0.001177466
202869_at	OAS1	2'-5'-oligoadenylate synthetase 1, 40/46kDa	2.02919	0.002189372
202283_at	SERPINF1	serpin peptidase inhibitor, clade F (alpha-2 antiplasmin, pigment epithelium derived factor), member 1	2.02847	0.001004671
224973_at	FAM46A	family with sequence similarity 46, member A	2.02529	0.000840238
236297_at	---	---	2.02353	0.00085435
229555_at	GALNT5	UDP-N-acetyl-alpha-D-galactosamine:polypeptide N-acetylgalactosaminyltransferase 5 (GalNAc-T5)	2.02117	0.001159234
213058_at	TTC28	tetratricopeptide repeat domain 28	2.01696	0.000889114
223044_at	SLC40A1	solute carrier family 40 (iron-regulated transporter), member 1	2.01568	0.000609998
242052_at	---	---	-2.00115	0.001632297
233675_s_at	TPTE2P6	transmembrane phosphoinositide 3-phosphatase and tensin homolog 2 pseudogene 6	-2.0018	0.000939529
205691_at	SYNGR3	synaptogyrin 3	-2.00231	0.01504285
208241_at	NRG1	neuregulin 1	-2.00539	0.001034045
219155_at	PITPNC1	phosphatidylinositol transfer protein, cytoplasmic 1	-2.00728	0.001050381
1564485_at	LOC100131551	uncharacterized LOC100131551	-2.00804	0.004577766
241425_at	NUPL1	nucleoporin like 1	-2.00815	0.000633348
1557389_at	LOC100505839	uncharacterized LOC100505839	-2.0083	0.001605834
209627_s_at	OSBPL3	oxysterol binding protein-like 3	-2.0085	0.000968413
242894_at	---	---	-2.00953	0.001061713
240991_at	---	---	-2.00966	0.00316504
1557580_at	---	---	-2.00971	0.000826357
207196_s_at	TNIP1	TNFAIP3 interacting protein 1	-2.01071	0.000770346
225034_at	ST3GAL1	ST3 beta-galactoside alpha-2,3-sialyltransferase 1	-2.01196	0.002725361
244292_at	---	---	-2.01321	0.001692628
236404_at	---	---	-2.0145	0.003190554
1565701_at	---	---	-2.015	0.00085435
225759_x_at	CLMN	calmin (calponin-like, transmembrane)	-2.01774	0.000677883
222186_at	---	---	-2.01931	0.003805284
207463_x_at	PRSS3	protease, serine, 3	-2.01936	0.001712065
1561167_at	---	---	-2.01938	0.002966343
235912_at	---	---	-2.02028	0.000762343
239655_at	---	---	-2.02068	0.000620619
201889_at	FAM3C	family with sequence similarity 3, member C	-2.0207	0.000817813
213700_s_at	---	---	-2.02185	0.001597749
222372_at	---	---	-2.02213	0.000762157
219926_at	POPDC3	popeye domain containing 3	-2.02265	0.000840238
243462_s_at	---	---	-2.0236	0.001008788
209946_at	VEGFC	vascular endothelial growth factor C	-2.02424	0.000692374
236879_at	---	---	-2.02434	0.000770346
200982_s_at	ANXA6	annexin A6	-2.02616	0.000607412
228007_at	CEP85L	centrosomal protein 85kDa-like	-2.02669	0.000553311
242448_at	---	---	-2.02746	0.002305485
237028_at	ENO1-AS1	ENO1 antisense RNA 1 (non-protein coding)	-2.02781	0.001191573
213234_at	KIAA1467	KIAA1467	-2.0316	0.001234285
220921_at	SPANXB1 /// SPANXB2 /// SPANXF1	SPANX family, member B1 /// SPANX family, member B2 /// SPANX family, member F1	-2.03161	0.001073285
1556318_s_at	CAND1	cullin-associated and neddylation-dissociated 1	-2.03192	0.008278406
229389_at	ATG16L2	autophagy related 16-like 2 (S. cerevisiae)	-2.03447	0.001818143
237194_at	---	---	-2.03547	0.001287515
205651_x_at	RAPGEF4	Rap guanine nucleotide exchange factor (GEF) 4	-2.03617	0.000634703
242108_at	---	---	-2.03646	0.0022507
209291_at	ID4	inhibitor of DNA binding 4, dominant negative helix-loop-helix protein	-2.03831	0.000880527
210587_at	INHBE	inhibin, beta E	-2.03904	0.008535191
1559072_a_at	ELFN2	extracellular leucine-rich repeat and fibronectin type III domain containing 2	-2.03944	0.004796599
1555167_s_at	NAMPT	nicotinamide phosphoribosyltransferase	-2.04052	0.001108854
223423_at	GPR160	G protein-coupled receptor 160	-2.04134	0.000545787
217482_at	---	---	-2.04537	0.003766877
213742_at	SRSF11	serine/arginine-rich splicing factor 11	-2.04556	0.008529868
238587_at	UBASH3B	ubiquitin associated and SH3 domain containing B	-2.04768	0.00085435
1566698_at	---	---	-2.05137	0.01550072
243589_at	KANSL1	KAT8 regulatory NSL complex subunit 1	-2.05171	0.001696266
234196_at	---	---	-2.05179	0.02517368
244424_at	LOC439938	uncharacterized LOC439938	-2.05343	0.000938004
217739_s_at	NAMPT	nicotinamide phosphoribosyltransferase	-2.05454	0.000775678
228737_at	TOX2	TOX high mobility group box family member 2	-2.05595	0.000544873
232744_x_at	---	---	-2.05615	0.004417666
243149_at	---	---	-2.05695	0.005604194

203185_at	RASSF2	Ras association (RalGDS/AF-6) domain family member 2	-2.05836	0.00111488
230710_at	MIR210HG	MIR210 host gene (non-protein coding)	-2.0598	0.00070608
220668_s_at	DNMT3B	DNA (cytosine-5-)-methyltransferase 3 beta	-2.06178	0.000544873
226382_at	CAMK1D /// LOC283070	calcium/calmodulin-dependent protein kinase ID /// uncharacterized LOC283070	-2.06247	0.00232165
243315_at	---	---	-2.06316	0.001073285
1558649_at	LOC145757	uncharacterized LOC145757	-2.06443	0.000972414
205893_at	NLGN1	neuroligin 1	-2.06546	0.004159108
215066_at	PTPRF	protein tyrosine phosphatase, receptor type, F	-2.06586	0.00157251
219983_at	HRASLS	HRAS-like suppressor	-2.0678	0.001106547
202619_s_at	PLOD2	procollagen-lysine, 2-oxoglutarate 5-dioxygenase 2	-2.06869	0.001442548
233630_at	CDS2	CDP-diacylglycerol synthase (phosphatidate cytidylyltransferase) 2	-2.0692	0.004487754
232122_s_at	VEPH1	ventricular zone expressed PH domain homolog 1 (zebrafish)	-2.06957	0.00117349
1559147_at	---	---	-2.07021	0.00084561
224733_at	CMTM3	CKLF-like MARVEL transmembrane domain containing 3	-2.0705	0.000589751
201170_s_at	BHLHE40	basic helix-loop-helix family, member e40	-2.07058	0.000550797
230229_at	DLG1	Discs, large homolog 1 (Drosophila)	-2.07075	0.000909799
239227_at	---	---	-2.07122	0.001177466
217655_at	LOC100127972	uncharacterized LOC100127972	-2.07184	0.001608124
229656_s_at	EML6	echinoderm microtubule associated protein like 6	-2.07197	0.000633348
241692_at	---	---	-2.07314	0.00190881
202790_at	CLDN7	claudin 7	-2.07387	0.001695108
242467_at	---	---	-2.07479	0.000958233
236696_at	U2SURP	U2 snRNP-associated SURP domain containing	-2.07542	0.002979017
225097_at	HIPK2	homeodomain interacting protein kinase 2	-2.07707	0.000933921
218507_at	HILPDA	hypoxia inducible lipid droplet-associated	-2.07738	0.000670772
236379_at	---	---	-2.0801	0.002664721
242827_x_at	---	---	-2.08017	0.004492459
203543_s_at	KLF9	Kruppel-like factor 9	-2.08035	0.001221263
243808_at	---	---	-2.0807	0.00232165
205925_s_at	RAB3B	RAB3B, member RAS oncogene family	-2.0834	0.003431397
231361_at	NLGN1	neuroligin 1	-2.08436	0.001793447
202628_s_at	SERPINE1	serpin peptidase inhibitor, clade E (nexin, plasminogen activator inhibitor type 1), member 1	-2.08468	0.000609998
224774_s_at	NAV1	neuron navigator 1	-2.08511	0.000655001
208581_x_at	MT1X	metallothionein 1X	-2.08522	0.001173759
1556183_at	ANKRD36BP2	ankyrin repeat domain 36B pseudogene 2	-2.088	0.001742423
215392_at	---	---	-2.08814	0.002249313
222071_s_at	SLCO4C1	solute carrier organic anion transporter family, member 4C1	-2.08962	0.002378681
204451_at	FZD1	frizzled family receptor 1	-2.09109	0.000747375
1566539_at	---	---	-2.09185	0.002789177
237585_at	C4orf47	chromosome 4 open reading frame 47	-2.09463	0.005988592
233914_s_at	SBF2	SET binding factor 2	-2.09768	0.001229334
242279_at	---	---	-2.10446	0.008397651
225803_at	FBXO32	F-box protein 32	-2.10489	0.000500124
241569_at	---	---	-2.10537	0.002219033
214577_at	MAP1B	microtubule-associated protein 1B	-2.10554	0.001632979
204730_at	RIMS3	regulating synaptic membrane exocytosis 3	-2.10573	0.000506128
228935_at	SLC4A8	solute carrier family 4, sodium bicarbonate cotransporter, member 8	-2.10574	0.001632979
1560926_at	---	---	-2.1059	0.001696266
1552690_a_at	CACNA2D4	calcium channel, voltage-dependent, alpha 2/delta subunit 4	-2.10678	0.000589072
207797_s_at	LRP2BP	LRP2 binding protein	-2.1071	0.000475356
236327_at	---	---	-2.1073	0.02407484
205158_at	RNASE4	ribonuclease, RNase A family, 4	-2.10794	0.000549499
227749_at	POU2F2	POU class 2 homeobox 2	-2.1081	0.003910593
236475_at	MICAL2	Microtubule associated monoxygenase, calponin and LIM domain containing 2	-2.1088	0.01255971
232216_at	YME1L1	YME1-like 1 (S. cerevisiae)	-2.10941	0.001034045
201720_s_at	LAPTM5	lysosomal protein transmembrane 5	-2.10962	0.000766104
240656_at	---	---	-2.11003	0.000670227
236480_at	MIR210HG	MIR210 host gene (non-protein coding)	-2.11006	0.000938004
209270_at	LAMB3	laminin, beta 3	-2.11038	0.001452223
238049_at	GRAMD3	GRAM domain containing 3	-2.1117	0.001048879
204519_s_at	PLLP	plasmolipin	-2.11379	0.000938004
235107_at	---	---	-2.11418	0.00178524
209652_s_at	PGF	placental growth factor	-2.11626	0.000620282
230681_at	TBRG1	transforming growth factor beta regulator 1	-2.11693	0.007308493
204933_s_at	TNFRSF11B	tumor necrosis factor receptor superfamily, member 11b	-2.11772	0.001220633
230319_at	---	---	-2.11842	0.000817463
203980_at	FABP4	fatty acid binding protein 4, adipocyte	-2.11885	0.001594159

243233_at	---	---	-2.11904	0.001957628
225407_at	MBP	myelin basic protein	-2.12019	0.000549499
208811_s_at	DNAJB6 /// TMEM135	DnaJ (Hsp40) homolog, subfamily B, member 6 /// transmembrane protein 135	-2.12028	0.000538787
239243_at	ZNF638	zinc finger protein 638	-2.12076	0.000867583
237689_at	---	---	-2.12083	0.001504749
235927_at	XPO1	exportin 1 (CRM1 homolog, yeast)	-2.12179	0.000817813
238462_at	UBASH3B	ubiquitin associated and SH3 domain containing B	-2.1224	0.000543877
243003_at	---	---	-2.12273	0.001664319
229497_at	ANKDD1A	ankyrin repeat and death domain containing 1A	-2.12372	0.00220827
204348_s_at	AK4 /// LOC100507855	adenylate kinase 4 /// adenylate kinase isoenzyme 4, mitochondrial-like	-2.12382	0.000677138
239846_at	LOC100506245	uncharacterized LOC100506245	-2.12394	0.000591232
203485_at	RTN1	reticulon 1	-2.12437	0.003071089
235419_at	---	---	-2.12669	0.000903681
223185_s_at	BHLHE41	basic helix-loop-helix family, member e41	-2.12951	0.001004671
213135_at	TIAM1	T-cell lymphoma invasion and metastasis 1	-2.13065	0.000645258
227462_at	ERAP2	endoplasmic reticulum aminopeptidase 2	-2.13436	0.000762157
240939_x_at	---	---	-2.13812	0.001081671
221583_s_at	KCNMA1	potassium large conductance calcium-activated channel, subfamily M, alpha member 1	-2.13862	0.001396281
1556210_at	---	---	-2.13899	0.01119804
236417_at	---	---	-2.14162	0.003873305
1559038_at	SEPT2	septin 2	-2.14309	0.004504787
223710_at	CCL26	chemokine (C-C motif) ligand 26	-2.14459	0.003579222
227223_at	RBM39	RNA binding motif protein 39	-2.14477	0.000482416
242068_at	---	---	-2.14492	0.001173759
227742_at	CLIC6	chloride intracellular channel 6	-2.1451	0.000734344
222306_at	---	---	-2.14515	0.00254854
244464_at	---	---	-2.1466	0.002206542
240625_at	---	---	-2.14663	0.000968413
239646_at	---	---	-2.14791	0.001924443
244533_at	PTPN14	protein tyrosine phosphatase, non-receptor type 14	-2.14815	0.00052489
236571_at	---	---	-2.14847	0.003252083
203769_s_at	STS	steroid sulfatase (microsomal), isozyme S	-2.15116	0.001042081
238619_at	---	---	-2.15159	0.000714308
236552_at	---	---	-2.15186	0.004742754
208475_at	FRMD4A	FERM domain containing 4A	-2.15274	0.002465051
219383_at	PRR5L	proline rich 5 like	-2.15303	0.001821295
230505_at	LOC145474	uncharacterized LOC145474	-2.15613	0.003367069
207339_s_at	LTB	lymphotoxin beta (TNF superfamily, member 3)	-2.15864	0.000961225
209708_at	MOXD1	monooxygenase, DBH-like 1	-2.16172	0.002663094
200635_s_at	PTPRF	protein tyrosine phosphatase, receptor type, F	-2.16315	0.002876895
227618_at	---	---	-2.16491	0.00808384
230375_at	PNISR	PNN-interacting serine/arginine-rich protein	-2.16531	0.000709998
239908_at	---	---	-2.16684	0.00077636
201325_s_at	EMP1	epithelial membrane protein 1	-2.16707	0.000555175
1554997_a_at	PTGS2	prostaglandin-endoperoxide synthase 2 (prostaglandin G/H synthase and cyclooxygenase)	-2.1692	0.008299504
239201_at	CDK15	cyclin-dependent kinase 15	-2.17052	0.002553877
218181_s_at	MAP4K4	mitogen-activated protein kinase kinase kinase kinase 4	-2.17121	0.001313325
223434_at	GBP3	guanylate binding protein 3	-2.17258	0.000453496
225262_at	FOSL2	FOS-like antigen 2	-2.17289	0.000447063
236685_at	---	---	-2.17322	0.003042288
209445_x_at	COA1	cytochrome C oxidase assembly factor 1 homolog (S. cerevisiae)	-2.17325	0.000775365
242871_at	PAQR5	progestin and adipoQ receptor family member V	-2.17361	0.000810506
230085_at	PDK3	pyruvate dehydrogenase kinase, isozyme 3	-2.1738	0.002392788
1552626_a_at	TMEM163	transmembrane protein 163	-2.17398	0.01790303
1557852_at	---	---	-2.17633	0.002443911
244026_at	---	---	-2.18212	0.000842051
204073_s_at	C11orf9	chromosome 11 open reading frame 9	-2.18401	0.000544873
231205_at	---	---	-2.1857	0.000447063
1555705_a_at	CMTM3	CKLF-like MARVEL transmembrane domain containing 3	-2.18598	0.001605263
219338_s_at	LRRC49	leucine rich repeat containing 49	-2.18724	0.000895648
1561969_at	ZPLD1	zona pellucida-like domain containing 1	-2.19011	0.003244051
233405_at	---	---	-2.19174	0.001903363
223698_at	SLC25A36	solute carrier family 25 (pyrimidine nucleotide carrier), member 36	-2.19223	0.002283327
226641_at	ANKRD44	ankyrin repeat domain 44	-2.19405	0.00043977
233857_s_at	ASB2	ankyrin repeat and SOCS box containing 2	-2.1941	0.001081671
202388_at	RGS2	regulator of G-protein signaling 2, 24kDa	-2.1945	0.000439789
228188_at	FOSL2	FOS-like antigen 2	-2.19557	0.000472706
242343_x_at	---	---	-2.19562	0.001096062

203542_s_at	KLF9	Kruppel-like factor 9	-2.19709	0.000609998
220675_s_at	PNPLA3	patatin-like phospholipase domain containing 3	-2.19926	0.002019811
201162_at	IGFBP7	insulin-like growth factor binding protein 7	-2.20041	0.000472706
208810_at	DNAJB6 /// TMEM135	DnaJ (Hsp40) homolog, subfamily B, member 6 /// transmembrane protein 135	-2.20576	0.000620619
231165_at	---	---	-2.20893	0.000761415
241435_at	---	---	-2.20943	0.002311403
229872_s_at	LOC100132999 /// LOC642441 /// LOC730256	uncharacterized LOC100132999 /// uncharacterized LOC642441 /// uncharacterized LOC730256	-2.21022	0.000472706
233884_at	HIVEP3	human immunodeficiency virus type I enhancer binding protein 3	-2.21116	0.003384424
39402_at	IL1B	interleukin 1, beta	-2.21385	0.008782276
206548_at	---	---	-2.21659	0.003829458
210281_s_at	ZMYM2	zinc finger, MYM-type 2	-2.21725	0.001285794
1554452_a_at	HILPDA	hypoxia inducible lipid droplet-associated	-2.21776	0.000520157
219710_at	SH3TC2	SH3 domain and tetratricopeptide repeats 2	-2.21841	0.001984263
240263_at	---	---	-2.22029	0.000426608
229540_at	RBPJ	recombination signal binding protein for immunoglobulin kappa J region	-2.22066	0.000549499
212390_at	LOC728802 /// PDE4DIP	myomegalin-like /// phosphodiesterase 4D interacting protein	-2.2218	0.000625354
1557895_at	FLJ35934	FLJ35934	-2.22183	0.001028763
229765_at	ZNF207	zinc finger protein 207	-2.22223	0.002508616
1553299_at	DUSP5P	dual specificity phosphatase 5 pseudogene	-2.22337	0.002804188
206580_s_at	EFEMP2	EGF containing fibulin-like extracellular matrix protein 2	-2.22351	0.000553311
213839_at	CLMN	calmin (calponin-like, transmembrane)	-2.22389	0.000472706
240370_at	---	---	-2.22514	0.002760486
1559663_at	---	---	-2.22597	0.002305485
238970_at	---	---	-2.227	0.000677883
202948_at	IL1R1	interleukin 1 receptor, type I	-2.22812	0.000453496
206380_s_at	CFP	complement factor properdin	-2.22843	0.000611614
1557419_a_at	ACSL4	Acyl-CoA synthetase long-chain family member 4	-2.22865	0.000541931
234088_at	---	---	-2.22876	0.004553593
1561079_at	ANKRD28	ankyrin repeat domain 28	-2.22997	0.002026328
215206_at	---	---	-2.23065	0.001042055
233404_at	---	---	-2.23164	0.001846352
1565999_at	LOC286299	uncharacterized LOC286299	-2.23345	0.02553122
200637_s_at	PTPRF	protein tyrosine phosphatase, receptor type, F	-2.23378	0.002791874
232726_at	---	---	-2.23948	0.000545149
239451_at	---	---	-2.23965	0.001866879
205462_s_at	HPCAL1	hippocalcin-like 1	-2.24058	0.000817813
228471_at	ANKRD44	ankyrin repeat domain 44	-2.24135	0.000840238
1557239_at	BBX	bobby sox homolog (Drosophila)	-2.24207	0.00056094
208535_x_at	COL13A1	collagen, type XIII, alpha 1	-2.24371	0.000734325
244075_at	---	---	-2.25506	0.000662968
203570_at	LOXL1	lysyl oxidase-like 1	-2.25716	0.000514634
202828_s_at	MMP14	matrix metallopeptidase 14 (membrane-inserted)	-2.25749	0.000943254
242321_at	PTPN14	protein tyrosine phosphatase, non-receptor type 14	-2.25972	0.001866879
210612_s_at	SYNJ2	synaptojanin 2	-2.25975	0.000485821
230127_at	---	---	-2.2603	0.001759064
209040_s_at	PSMB8	proteasome (prosome, macropain) subunit, beta type, 8 (large multifunctional peptidase 7)	-2.26032	0.000457783
242710_at	---	---	-2.26125	0.000938004
225116_at	HIPK2	homeodomain interacting protein kinase 2	-2.26275	0.00043977
239559_at	---	---	-2.26352	0.002070847
209721_s_at	IFFO1	intermediate filament family orphan 1	-2.26492	0.00093995
235850_at	FAM162A	family with sequence similarity 162, member A	-2.26528	0.000472706
232000_at	---	---	-2.26662	0.000567631
205076_s_at	MTMR11	myotubularin related protein 11	-2.2746	0.000407998
226084_at	MAP1B	microtubule-associated protein 1B	-2.27655	0.0022507
235238_at	SHC4	SHC (Src homology 2 domain containing) family, member 4	-2.28372	0.000453496
219523_s_at	ODZ3	odz, odd Oz/ten-m homolog 3 (Drosophila)	-2.28473	0.000501177
1568611_at	---	---	-2.28648	0.000467368
228959_at	PDK3	pyruvate dehydrogenase kinase, isozyme 3	-2.28767	0.000453496
203726_s_at	LAMA3	laminin, alpha 3	-2.29237	0.000541931
204682_at	LTBP2	latent transforming growth factor beta binding protein 2	-2.29343	0.000590294
219936_s_at	GPR87	G protein-coupled receptor 87	-2.29456	0.000475783
214967_at	---	---	-2.29931	0.001190813
235626_at	CAMK1D	calcium/calmodulin-dependent protein kinase ID	-2.30002	0.000770346
205681_at	BCL2A1	BCL2-related protein A1	-2.30141	0.005075028
232528_at	---	---	-2.30149	0.001089487
217388_s_at	KYNU	kynureninase	-2.30218	0.000932828
239965_at	---	---	-2.30436	0.000541931

227051_at	---	---	-2.30704	0.000903681
219028_at	HIPK2	homeodomain interacting protein kinase 2	-2.31131	0.000921975
237335_at	ZP1	zona pellucida glycoprotein 1 (sperm receptor)	-2.31256	0.01148172
1557418_at	ACSL4	Acyl-CoA synthetase long-chain family member 4	-2.31283	0.001050381
218980_at	FHOD3	formin homology 2 domain containing 3	-2.31414	0.000384489
228083_at	CACNA2D4	calcium channel, voltage-dependent, alpha 2/delta subunit 4	-2.31464	0.000406379
244427_at	KIF23	Kinesin family member 23	-2.31701	0.000611614
229307_at	ANKRD28	ankyrin repeat domain 28	-2.31877	0.000739451
1564358_at	---	---	-2.31945	0.000447063
230387_at	---	---	-2.32	0.000500073
221581_s_at	LAT2	linker for activation of T cells family, member 2	-2.32188	0.000392185
211828_s_at	TNIK	TRAF2 and NCK interacting kinase	-2.3229	0.000398642
210136_at	MBP	myelin basic protein	-2.32658	0.000821759
238563_at	---	---	-2.33609	0.007739101
1562516_at	WDR60	WD repeat domain 60	-2.33745	0.006251263
1567224_at	HMGA2	high mobility group AT-hook 2	-2.3394	0.001377802
211809_x_at	COL13A1	collagen, type XIII, alpha 1	-2.34016	0.000458526
1556212_x_at	---	---	-2.34116	0.000444666
203741_s_at	ADCY7	adenylate cyclase 7	-2.34148	0.00043977
1555009_a_at	SYNJ2	synaptojanin 2	-2.34162	0.000553311
225168_at	FRMD4A	FERM domain containing 4A	-2.34523	0.001503487
237883_at	---	---	-2.34587	0.004658713
212828_at	SYNJ2	synaptojanin 2	-2.34752	0.000447063
229520_s_at	C14orf118	chromosome 14 open reading frame 118	-2.36474	0.001579286
236930_at	NUMB	numb homolog (Drosophila)	-2.36534	0.000440817
1556203_a_at	SRGAP2	SLIT-ROBO Rho GTPase activating protein 2	-2.36593	0.005051419
222061_at	CD58	CD58 molecule	-2.37381	0.001605834
219313_at	GRAMD1C	GRAM domain containing 1C	-2.37551	0.001199448
225842_at	PHLDA1	pleckstrin homology-like domain, family A, member 1	-2.37686	0.000430852
239798_at	---	---	-2.38327	0.001073285
210621_s_at	RASA1	RAS p21 protein activator (GTPase activating protein) 1	-2.38655	0.000378121
216236_s_at	SLC2A14 /// SLC2A3	solute carrier family 2 (facilitated glucose transporter), member 14 /// solute carrier family 2 (facilitated glucose transporter), member 3	-2.38935	0.001139517
209670_at	TRAC	T cell receptor alpha constant	-2.39497	0.000611614
206343_s_at	NRG1	neuregulin 1	-2.40101	0.001810913
1559410_at	---	---	-2.40281	0.009449629
204158_s_at	TCIRG1	T-cell, immune regulator 1, ATPase, H+ transporting, lysosomal V0 subunit A3	-2.41395	0.000453496
232094_at	C15orf29	chromosome 15 open reading frame 29	-2.41551	0.001605263
227870_at	IGDCC4	immunoglobulin superfamily, DCC subclass, member 4	-2.41733	0.000330757
241060_x_at	---	---	-2.4219	0.00038313
243745_at	---	---	-2.42234	0.000538787
202555_s_at	MYLK	myosin light chain kinase	-2.42773	0.000909799
1564424_at	---	---	-2.43095	0.000388443
160020_at	MMP14	matrix metallopeptidase 14 (membrane-inserted)	-2.43404	0.000714308
205207_at	IL6	interleukin 6 (interferon, beta 2)	-2.43497	0.005075028
232958_at	---	---	-2.43936	0.00126075
214782_at	CTTN	cortactin	-2.44504	0.003369573
235811_at	---	---	-2.44983	0.00323828
239005_at	---	---	-2.45374	0.001285794
206924_at	IL11	interleukin 11	-2.45542	0.001073285
202254_at	SIPA1L1	signal-induced proliferation-associated 1 like 1	-2.45926	0.000337484
227396_at	LOC100287223 /// PTPRJ	uncharacterized LOC100287223 /// protein tyrosine phosphatase, receptor type, J	-2.46256	0.000331553
203305_at	F13A1	coagulation factor XIII, A1 polypeptide	-2.47011	0.000590294
229585_at	ADAMTSL1	ADAMTS-like 1	-2.47013	0.000588917
233030_at	PNPLA3	patatin-like phospholipase domain containing 3	-2.47189	0.000320084
204401_at	KCNN4	potassium intermediate/small conductance calcium-activated channel, subfamily N, member 4	-2.47573	0.000453496
236561_at	TGFBR1	transforming growth factor, beta receptor 1	-2.48295	0.000447063
217513_at	MILR1	mast cell immunoglobulin-like receptor 1	-2.48399	0.000662968
243296_at	NAMPT	Nicotinamide phosphoribosyltransferase	-2.4897	0.000328347
241769_at	---	---	-2.49032	0.000550879
1562415_a_at	SPOCD1	SPOC domain containing 1	-2.49528	0.00043977
206091_at	MATN3	matrilin 3	-2.49784	0.000549499
207992_s_at	AMPD3	adenosine monophosphate deaminase 3	-2.50108	0.000313775
233358_at	---	---	-2.50222	0.001133536
218559_s_at	MAFB	v-maf musculoaponeurotic fibrosarcoma oncogene homolog B (avian)	-2.50224	0.000345356
240038_at	---	---	-2.50709	0.000773999
1558199_at	FN1	fibronectin 1	-2.51179	0.000328693
231798_at	NOG	noggin	-2.51377	0.000545787

222835_at	THSD4	thrombospondin, type I, domain containing 4	-2.5154	0.00033878
239757_at	ZFAND6	Zinc finger, AN1-type domain 6	-2.52273	0.000545149
240326_at	---	---	-2.52697	0.001632979
232473_at	---	---	-2.5271	0.000339946
236471_at	NFE2L3	nuclear factor (erythroid-derived 2)-like 3	-2.52864	0.000433781
228499_at	PFKFB4	6-phosphofructo-2-kinase/fructose-2,6-biphosphatase 4	-2.52892	0.000425055
240307_at	---	---	-2.53332	0.000979956
229538_s_at	IQGAP3	IQ motif containing GTPase activating protein 3	-2.53338	0.000399537
235805_at	---	---	-2.53514	0.00077036
209292_at	ID4	inhibitor of DNA binding 4, dominant negative helix-loop-helix protein	-2.53783	0.000337048
204702_s_at	NFE2L3	nuclear factor (erythroid-derived 2)-like 3	-2.53802	0.000424442
1552999_a_at	WFDC10B	WAP four-disulfide core domain 10B	-2.53934	0.000467368
229302_at	TMEM178A	transmembrane protein 178A	-2.54104	0.001247301
244633_at	---	---	-2.54728	0.000502004
232615_at	---	---	-2.54886	0.000377184
229778_at	C12orf39	chromosome 12 open reading frame 39	-2.55047	0.000486989
202855_s_at	SLC16A3	solute carrier family 16, member 3 (monocarboxylic acid transporter 4)	-2.55088	0.000618135
208296_x_at	TNFAIP8	tumor necrosis factor, alpha-induced protein 8	-2.55195	0.000320084
232797_at	---	---	-2.55255	0.000453273
204932_at	TNFRSF11B	tumor necrosis factor receptor superfamily, member 11b	-2.55308	0.002305485
239274_at	---	---	-2.55734	0.000676959
227584_at	NAV1	neuron navigator 1	-2.56035	0.000687033
202827_s_at	MMP14	matrix metallopeptidase 14 (membrane-inserted)	-2.5605	0.00043977
240257_at	SYNJ2	synaptojanin 2	-2.56061	0.000544873
202421_at	IGSF3	immunoglobulin superfamily, member 3	-2.56301	0.000328347
210260_s_at	TNFAIP8	tumor necrosis factor, alpha-induced protein 8	-2.56645	0.000339946
241762_at	FBXO32	F-box protein 32	-2.57206	0.00043977
211071_s_at	MLLT11	myeloid/lymphoid or mixed-lineage leukemia (trithorax homolog, Drosophila); translocated to, 11	-2.57779	0.000345356
236251_at	---	---	-2.584	0.000671183
235629_at	---	---	-2.58805	0.000413101
205349_at	GNA15	guanine nucleotide binding protein (G protein), alpha 15 (Gq class)	-2.58916	0.00038313
236462_at	---	---	-2.58967	0.000762343
244846_at	---	---	-2.58971	0.000655001
232264_at	---	---	-2.59258	0.004221507
210367_s_at	PTGES	prostaglandin E synthase	-2.59522	0.000621208
241860_at	---	---	-2.59696	0.00126075
204955_at	SRPX	sushi-repeat containing protein, X-linked	-2.60035	0.000330757
236962_at	---	---	-2.60044	0.000553311
215248_at	GRB10	growth factor receptor-bound protein 10	-2.60171	0.000313775
1560622_at	---	---	-2.60374	0.000447063
227084_at	DTNA	dystrobrevin, alpha	-2.61603	0.000313377
237469_at	TOP2A	Topoisomerase (DNA) II alpha 170kDa	-2.61699	0.00070608
236963_at	---	---	-2.62058	0.000589889
229006_at	LOC100507487	uncharacterized LOC100507487	-2.62475	0.000643658
231956_at	RNF213	ring finger protein 213	-2.62502	0.000967392
241824_at	---	---	-2.62725	0.005456121
210282_at	ZMYM2	zinc finger, MYM-type 2	-2.62834	0.000662968
242835_s_at	LOC728730	uncharacterized LOC728730	-2.63046	0.000306095
220014_at	PRR16	proline rich 16	-2.63181	0.000725846
236915_at	C4orf47	chromosome 4 open reading frame 47	-2.63506	0.001946204
215231_at	PRKAG2	Protein kinase, AMP-activated, gamma 2 non-catalytic subunit	-2.63569	0.000676087
202856_s_at	SLC16A3	solute carrier family 16, member 3 (monocarboxylic acid transporter 4)	-2.63895	0.000365688
226122_at	PLEKHG1	pleckstrin homology domain containing, family G (with RhoGef domain) member 1	-2.65231	0.000938004
211518_s_at	BMP4	bone morphogenetic protein 4	-2.65292	0.000337048
204597_x_at	STC1	stanniocalcin 1	-2.65715	0.002396147
230746_s_at	---	---	-2.66224	0.000467368
203409_at	DDB2	damage-specific DNA binding protein 2, 48kDa	-2.66322	0.000308335
238593_at	C11orf80	chromosome 11 open reading frame 80	-2.66698	0.001632979
240859_at	ZFYVE16	zinc finger, FYVE domain containing 16	-2.66839	0.00073385
237741_at	SLC25A36	Solute carrier family 25 (pyrimidine nucleotide carrier), member 36	-2.67067	0.000555175
201858_s_at	SRGN	serglycin	-2.67133	0.000313377
242457_at	---	---	-2.67172	0.001557922
1556211_a_at	---	---	-2.67515	0.000486346
210513_s_at	VEGFA	vascular endothelial growth factor A	-2.69164	0.000909799
238769_at	---	---	-2.69294	0.002833221
202643_s_at	TNFAIP3	tumor necrosis factor, alpha-induced protein 3	-2.69521	0.000579943
239568_at	PLEKHH2	pleckstrin homology domain containing, family H (with MyTH4 domain) member 2	-2.70089	0.000453496

239808_at	---	---	-2.70945	0.001073285
224771_at	NAV1	neuron navigator 1	-2.71322	0.002428308
1555538_s_at	FAM9B	family with sequence similarity 9, member B	-2.71437	0.001664319
231403_at	TRIO	triple functional domain (PTPRF interacting)	-2.723	0.000662968
214375_at	PPFIBP1	PTPRF interacting protein, binding protein 1 (liprin beta 1)	-2.7239	0.000466932
240152_at	---	---	-2.73066	0.000374511
204279_at	PSMB9	proteasome (prosome, macropain) subunit, beta type, 9 (large multifunctional peptidase 2)	-2.73538	0.001918996
244511_at	---	---	-2.75144	0.000887639
242313_at	LOC728730	Uncharacterized LOC728730	-2.76906	0.000281165
239448_at	---	---	-2.77141	0.000545149
1555675_at	BLID	BH3-like motif containing, cell death inducer	-2.77986	0.000258774
232451_at	---	---	-2.81352	0.000313377
228303_at	GALNT6	UDP-N-acetyl-alpha-D-galactosamine:polypeptide N-acetylgalactosaminyltransferase 6 (GalNAc-T6)	-2.81381	0.000460556
225115_at	HIPK2	homeodomain interacting protein kinase 2	-2.81658	0.000345356
204595_s_at	STC1	stanniocalcin 1	-2.81866	0.000308335
1555400_at	LOC645261	PP565	-2.82468	0.000817813
224480_s_at	AGPAT9	1-acylglycerol-3-phosphate O-acyltransferase 9	-2.84103	0.00024326
206157_at	PTX3	pentraxin 3, long	-2.84986	0.000306095
215395_x_at	PRSS3P2	protease, serine, 3 pseudogene 2	-2.85691	0.000249885
202269_x_at	GBP1	guanylate binding protein 1, interferon-inducible	-2.85743	0.001382881
1558404_at	LOC644242	uncharacterized LOC644242	-2.86889	0.002152276
202644_s_at	TNFAIP3	tumor necrosis factor, alpha-induced protein 3	-2.86967	0.000488293
206070_s_at	EPHA3	EPH receptor A3	-2.87661	0.000242121
241036_at	---	---	-2.89324	0.000467368
204326_x_at	MT1X	metallothionein 1X	-2.90164	0.000313775
227383_at	LOC727820	uncharacterized LOC727820	-2.90414	0.000242121
231577_s_at	GBP1	guanylate binding protein 1, interferon-inducible	-2.90491	0.000313377
209765_at	ADAM19	ADAM metallopeptidase domain 19	-2.90973	0.000288439
230720_at	RNF182	ring finger protein 182	-2.9138	0.000242121
1554640_at	PALM2	paralemmin 2	-2.92623	0.004318455
213113_s_at	SLC43A3	solute carrier family 43, member 3	-2.93472	0.000251704
219956_at	GALNT6	UDP-N-acetyl-alpha-D-galactosamine:polypeptide N-acetylgalactosaminyltransferase 6 (GalNAc-T6)	-2.94723	0.000323652
202477_s_at	LOC100506167 /// TUBGCP2	uncharacterized LOC100506167 /// tubulin, gamma complex associated protein 2	-2.9505	0.000506128
213895_at	EMP1	epithelial membrane protein 1	-2.97153	0.00024326
210512_s_at	VEGFA	vascular endothelial growth factor A	-2.97572	0.00044709
1562528_at	---	---	-2.97868	0.000242121
209822_s_at	VLDLR	very low density lipoprotein receptor	-2.98254	0.00033878
204220_at	GMFG	glia maturation factor, gamma	-2.98823	0.000258774
213524_s_at	G0S2	G0/G1switch 2	-2.99276	0.000313377
201313_at	ENO2	enolase 2 (gamma, neuronal)	-3.00186	0.000242121
1558683_a_at	HMGA2	high mobility group AT-hook 2	-3.01055	0.000903681
1566959_at	---	---	-3.01904	0.000775365
1562529_s_at	---	---	-3.01914	0.000671183
232544_at	---	---	-3.02392	0.000600238
233811_at	RIN2	Ras and Rab interactor 2	-3.03372	0.000678583
222878_s_at	OTUB2	OTU domain, ubiquitin aldehyde binding 2	-3.03587	0.000313775
202270_at	GBP1	guanylate binding protein 1, interferon-inducible	-3.03609	0.000272699
234234_at	---	---	-3.03893	0.000805302
225381_at	MIR100HG	mir-100-let-7a-2 cluster host gene (non-protein coding)	-3.04017	0.00033878
227384_s_at	LOC727820 /// LOC728855 /// LOC728875	uncharacterized LOC727820 /// uncharacterized LOC728855 /// uncharacterized LOC728875	-3.05173	0.000242121
205199_at	CA9	carbonic anhydrase IX	-3.05487	0.002003491
236304_at	---	---	-3.06149	0.000762157
1564796_at	EMP1	epithelial membrane protein 1	-3.06152	0.001087948
207080_s_at	PYY	peptide YY	-3.06911	0.000257471
213142_x_at	PION	pigeon homolog (Drosophila)	-3.07435	0.00022692
234932_s_at	CDCP1	CUB domain containing protein 1	-3.07545	0.000287977
207850_at	CXCL3	chemokine (C-X-C motif) ligand 3	-3.09712	0.001353326
201294_s_at	WSB1	WD repeat and SOCS box containing 1	-3.10035	0.000313377
206497_at	COA1	cytochrome C oxidase assembly factor 1 homolog (S. cerevisiae)	-3.10464	0.000288439
36030_at	IFFO1	intermediate filament family orphan 1	-3.11063	0.00042313
205100_at	GFPT2	glutamine-fructose-6-phosphate transaminase 2	-3.11868	0.000257471
238608_at	---	---	-3.11869	0.002966343
1558732_at	MAP4K4	mitogen-activated protein kinase kinase kinase kinase 4	-3.12227	0.000447063
220882_at	---	---	-3.13277	0.006260766
221538_s_at	PLXNA1	plexin A1	-3.15118	0.000328347
1563745_a_at	LOC283050	uncharacterized LOC283050	-3.16418	0.001478525
228483_s_at	TAF9B	TAF9B RNA polymerase II, TATA box binding protein (TBP)-associated factor, 31kDa	-3.17042	0.000288439

219965_s_at	MAGIX	MAGI family member, X-linked	-3.18573	0.000313775
222150_s_at	PION	pigeon homolog (Drosophila)	-3.19146	0.000242121
1558365_at	LOC100652805 /// LOC100653302 /// PGK1	uncharacterized LOC100652805 /// uncharacterized LOC100653302 /// phosphoglycerate kinase 1	-3.19338	0.000323652
202497_x_at	SLC2A3	solute carrier family 2 (facilitated glucose transporter), member 3	-3.19967	0.000257471
225167_at	FRMD4A	FERM domain containing 4A	-3.20357	0.000586941
238706_at	PAPD4	PAP associated domain containing 4	-3.21569	0.001775613
223690_at	LTBP2	latent transforming growth factor beta binding protein 2	-3.25109	0.000220658
1556209_at	CLEC2B	C-type lectin domain family 2, member B	-3.27435	0.000475891
219888_at	SPAG4	sperm associated antigen 4	-3.2936	0.000220658
1563881_at	MAGI1	Membrane associated guanylate kinase, WW and PDZ domain containing 1	-3.29987	0.001198393
1561775_at	---	---	-3.32017	0.000399537
224772_at	NAV1	neuron navigator 1	-3.33706	0.000241766
229695_at	---	---	-3.33881	0.000397966
236316_at	FAM3C	family with sequence similarity 3, member C	-3.34002	0.000309075
219410_at	TMEM45A	transmembrane protein 45A	-3.34971	0.000242121
224823_at	MYLK	myosin light chain kinase	-3.3677	0.000551009
205501_at	PDE10A	phosphodiesterase 10A	-3.37623	0.00024326
229435_at	GLIS3	GLIS family zinc finger 3	-3.41693	0.000220658
238243_at	---	---	-3.41808	0.000609998
226028_at	ROBO4	roundabout, axon guidance receptor, homolog 4 (Drosophila)	-3.45158	0.000968413
230015_at	PRCD	progressive rod-cone degeneration	-3.46178	0.001028763
209732_at	CLEC2B	C-type lectin domain family 2, member B	-3.47174	0.000424442
234432_at	---	---	-3.48508	0.000272699
235661_at	POU2F2	POU class 2 homeobox 2	-3.49339	0.000257471
218451_at	CDCP1	CUB domain containing protein 1	-3.51964	0.000220658
1562048_at	LOC152225	uncharacterized LOC152225	-3.53795	0.000313377
1563057_at	---	---	-3.58677	0.000460024
214841_at	CNIH3 /// LOC100506354	cornichon homolog 3 (Drosophila) /// uncharacterized LOC100506354	-3.61416	0.000221526
229105_at	GPR39	G protein-coupled receptor 39	-3.65043	0.000220658
212171_x_at	VEGFA	vascular endothelial growth factor A	-3.6691	0.000302686
201295_s_at	WSB1	WD repeat and SOCS box containing 1	-3.69262	0.00130893
213338_at	TMEM158	transmembrane protein 158 (gene/pseudogene)	-3.69291	0.000220658
211527_x_at	VEGFA	vascular endothelial growth factor A	-3.70281	0.000241766
1569257_at	FMNL1	formin-like 1	-3.71975	0.000444666
232344_at	---	---	-3.73972	0.000330757
1560031_at	FRMD4A	FERM domain containing 4A	-3.74448	0.000288439
230258_at	GLIS3	GLIS family zinc finger 3	-3.75463	0.000544873
214978_s_at	PPFIA4	protein tyrosine phosphatase, receptor type, f polypeptide (PTPRF), interacting protein (liprin), alpha 4	-3.77116	0.000345356
225163_at	FRMD4A	FERM domain containing 4A	-3.79233	0.000197255
201721_s_at	LAPTM5	lysosomal protein transmembrane 5	-3.81503	0.000202417
216250_s_at	LPXN	leupaxin	-3.82761	0.000241766
205924_at	RAB3B	RAB3B, member RAS oncogene family	-3.84747	0.00126075
205899_at	CCNA1	cyclin A1	-3.88827	0.000444666
207056_s_at	SLC4A8	solute carrier family 4, sodium bicarbonate cotransporter, member 8	-3.9123	0.000670772
1564158_a_at	LOC100130894	uncharacterized LOC100130894	-3.91535	0.000220658
219263_at	RNF128	ring finger protein 128, E3 ubiquitin protein ligase	-3.9226	0.000209034
226436_at	RASSF4	Ras association (RalGDS/AF-6) domain family member 4	-3.92351	0.000215749
230494_at	SLC20A1	solute carrier family 20 (phosphate transporter), member 1	-3.9499	0.000541931
238332_at	ANKRD29	ankyrin repeat domain 29	-3.9655	0.000242121
230372_at	HAS2	hyaluronan synthase 2	-4.01056	0.000188403
227971_at	NRK	Nik related kinase	-4.02198	0.000347108
239202_at	RAB3B	RAB3B, member RAS oncogene family	-4.0854	0.000220658
204475_at	MMP1	matrix metallopeptidase 1 (interstitial collagenase)	-4.12586	0.001602745
227478_at	SETBP1	SET binding protein 1	-4.14255	0.000220658
227123_at	RAB3B	RAB3B, member RAS oncogene family	-4.17164	0.000241766
240061_at	---	---	-4.19718	0.000600238
239672_at	---	---	-4.30635	0.001603502
220641_at	NOX5	NADPH oxidase, EF-hand calcium binding domain 5	-4.32494	0.000313377
232113_at	---	---	-4.33647	0.000444666
204774_at	EVI2A	ecotropic viral integration site 2A	-4.37709	0.000220658
233364_s_at	---	---	-4.39467	0.000538787
49306_at	RASSF4	Ras association (RalGDS/AF-6) domain family member 4	-4.41001	0.000308335
202370_s_at	CBFB	core-binding factor, beta subunit	-4.42171	0.000157587
219369_s_at	OTUB2	OTU domain, ubiquitin aldehyde binding 2	-4.44681	0.000313377
229011_at	---	---	-4.51481	0.000152852
206432_at	HAS2	hyaluronan synthase 2	-4.51521	0.000155442

229308_at	ANKRD29	ankyrin repeat domain 29	-4.53586	0.000220658
202498_s_at	SLC2A3	solute carrier family 2 (facilitated glucose transporter), member 3	-4.65055	0.001020404
216470_x_at	PRSS2	protease, serine, 2 (trypsin 2)	-4.75045	0.000152852
242629_at	RAB3B	RAB3B, member RAS oncogene family	-4.93729	0.000152852
205968_at	KCNS3	potassium voltage-gated channel, delayed-rectifier, subfamily S, member 3	-5.10363	0.000154888
223484_at	C15orf48	chromosome 15 open reading frame 48	-5.14489	0.000155442
209774_x_at	CXCL2	chemokine (C-X-C motif) ligand 2	-5.16444	0.000220658
232504_at	LOC285628 /// MIR146A	uncharacterized LOC285628 /// microRNA 146a	-5.47023	0.000522002
223503_at	TMEM163	transmembrane protein 163	-5.48733	0.000257471
222088_s_at	SLC2A14 /// SLC2A3	solute carrier family 2 (facilitated glucose transporter), member 14 /// solute carrier family 2 (facilitated glucose transporter), member 3	-5.50855	0.000138892
205402_x_at	PRSS2	protease, serine, 2 (trypsin 2)	-5.5234	0.000152852
202499_s_at	SLC2A3	solute carrier family 2 (facilitated glucose transporter), member 3	-5.54592	0.000197255
211506_s_at	IL8	interleukin 8	-5.99335	0.000209034
211742_s_at	EVI2B	ecotropic viral integration site 2B	-6.75714	0.000138892
1553023_a_at	NOX5	NADPH oxidase, EF-hand calcium binding domain 5	-7.2996	0.000154888
205476_at	CCL20	chemokine (C-C motif) ligand 20	-7.38592	0.000467368
224964_s_at	GNG2	guanine nucleotide binding protein (G protein), gamma 2	-7.65705	0.000138892
202859_x_at	IL8	interleukin 8	-7.90774	0.000138892
210538_s_at	BIRC3	baculoviral IAP repeat containing 3	-8.07911	0.000251704
227915_at	ASB2	ankyrin repeat and SOCS box containing 2	-9.473	0.000543877
210229_s_at	CSF2	colony stimulating factor 2 (granulocyte-macrophage)	-10.1452	0.000938425
234623_x_at	---	---	-13.7195	0.000220658
204470_at	CXCL1	chemokine (C-X-C motif) ligand 1 (melanoma growth stimulating activity, alpha)	-14.9636	0.000138892
233847_x_at	---	---	-69.7468	0.000209034
224354_at	---	---	-104.431	0.000306095
1555623_at	---	---	-148.407	0.000313775